UNIVERSITEIT VAN PRETORIA
UNIVERSITY OF PRETORIA
YUNIBESITHI YA PRETORIA

Investigation into the effect of cooling conditions on the particle size distribution of titania slag

Hanlie Kotzé

A thesis submitted in partial fulfilment of the requirements for the degree

PhD (Metallurgical Engineering)

In the Department of Materials Science and Metallurgical Engineering, Faculty of Engineering, University of Pretoria

Promoter: Professor P.C. Pistorius

June 2007

Acknowledgements

Several people over the years contributed to this work. It was, and still is, a privilege to work with all of you.

My appreciation goes to the staff of Exxaro R&D and Exxaro KZN Sands. The block cooling trials during campaigns 9 and 10 and the subsequent plant trials were characterised by intensive preparations, sampling and monitoring. My gratitude to all those involved in these activities for their unselfish contributions and time. My sincere appreciation to Exxaro KZN Sands for financially supporting this work.

My gratitude goes to all official and unofficial mentors who guided my growing process over the years: Dr. Willem van Niekerk, Matie von Wielligh, Geoff Randall, Johan Meyer, Gerrit van Zyl, Jeremy Bosman and Rob Hattingh. I learned immensely from you. May I bless others with the same dedication you have afforded me.

My deep gratitude to the staff of the University of Pretoria - Professor Chris Pistorius, Professor Johan de Villiers and Jeremy Bosman: thank you for your dedicated time, patience, contributions and support. Thank you Dr. Johan Zietsman for coding the block cooling model!

To my parents who somehow, through loving me unconditionally, taught me tenacity: thank you. May I be a mirror of your values.

To Manie and Willemien: thank you for showing me the balance in life. It seems appropriate that I had to understand this, before I could complete this work. Thank you for your motivation during the completion stages (which seemed never ending) of this thesis.

Thank You for the opportunities You are giving to me throughout my whole life. Thank You for your immensely beautiful and interesting creation. May I never cease to wonder at it’s intricate, yet unadorned, interactions.

Abstract

Titania slag is a feedstock to the pigment industry, which in turn provides titania pigment to producers of everyday products like paper, cosmetics and toothpaste. Titania slag is the primary product of the pyrometallurgical process of ilmenite smelting – the other products being iron and CO gas. Titania slag is typically tapped from the furnace into blocks of approximately 20 tons. After cooling these blocks are crushed and milled to size fractions suitable for the processes of the pigment producers. These processes are broadly grouped into two types of technology: the chloride route (during which titania slag is reacted with chlorine and subsequently re-oxidised thereby removing the impurities) and the sulphate route (in this process the titania slag is purified after dissolving the slag in sulphuric acid). Due to the nature of these two processes, several specifications are imposed on the quality of the titania slags.

The fluidised-bed technology used in the chloride process limits the size distribution of the slag to between 106 µm and 850 µm. Ilmenite smelting industries consequently crush and mill the titania slag to below 850 µm. The fraction below 106 µm is then sold to the sulphate market. Since the coarser chloride grade product is the more valuable product, slag producers continuously strive to improve the ratio between the coarser and finer fractions.

This study reports on parameters which influence the particle size distribution of titania slags and therefore the split between the coarser (more valuable) and finer (less valuable) products. Pilot-scale slag ingots were used to identify chemical and process variables which influence the yield of coarser material. The microstructure of as-cast and milled slag was examined, and indicated a role of silicate phases in the crushing behaviour. Industrial-scale slag ingots were used to test whether the roles of tapping rate and water cooling (as identified from the pilot-scale ingots) also applied under industrial conditions. A numerical method was applied to estimate the thermal conductivity of the solidified slag (from measurements on pilot-scale ingots), and to predict the cooling and solidification behaviour of industrial-scale ingots.

The study concludes that the chemical composition and cooling conditions of the slag block play central roles in the final particle size distribution of the slag.

Key words: titania slag; pseudobrookite; solidification; ilmenite smelting

Table of Contents

1 Introduction 15

1.1 TiO_2 pigment feedstock 16

1.2 The origin of Exxaro KZN Sands 16

1.3 Ilmenite smelting and slag processing 17

1.4 Problem statement 19

1.5 Research approach 22

2 Part 1: Pilot Plant Trials 23

2.1.1 Background 24

2.2 Slag block cooling 25

2.2.1 Experimental procedure 25

2.2.2 Results 26

2.2.3 Conclusions 30

2.3 Crushing and Milling 33

2.3.1 Experimental procedure 33

2.3.2 Results 36

2.3.3 Conclusions 45

3 Part 2: Plant Trials 48

3.1 Background 49

3.2 Block selection 49

3.3 Tumbling tests 52

3.3.1 Method 53

3.3.2 Results 54

3.4 Compression tests 59

3.4.1 Method 59

3.4.2 Results 62

3.5 Slag chemistry and mineralogy 65

  3.5.1 Method 65

  3.5.2 Results 67

3.6 Tapping rate 74

  3.6.1 Method 75

  3.6.2 Results 76

3.7 Surface temperatures 80

  3.7.1 Method 81

  3.7.2 Results 81

3.8 Conclusions 82

4 Part 3: Cooling Model 84

4.1 Background 85

4.2 Comparison of analytical and numerical solutions 85

4.3 Model formulation 87

  4.3.1 Requirements 88

  4.3.2 Simplifications 88

4.4 Energy balance 89

4.5 Shape notations, dimensions and calculations 90

4.6 Material definitions 93

  4.6.1 Slag thermodynamic properties 93

  4.6.2 Pot thermodynamic properties 96

4.7 Boundary conditions 98

  4.7.1 Contact coefficient between the block and pot surfaces 98

  4.7.2 Contact coefficient between the block and ground surface 102

  4.7.3 Natural convection in air 103

  4.7.4 Forced spray water cooling 105

4.8 Model calibration 108

4.9 Model verification 115

4.9.1 Crust thickness 115

4.9.2 Surface temperatures 117

4.10 Implication for large scale operations 119

4.10.1 Solidification 119

4.10.2 Surface temperatures 123

4.10.3 Internal temperatures 127

4.11 Conclusions 128

4.11.1 Proposed further research 129

5 Appendices 131

5.1 Determination of tri-valent titanium (Ti^{3+}) in titania slag 131

5.2 List of parameters evaluated in the search for parameters correlating with the -106 µm fraction. 144

5.3 SEM examples of SiO_2 on particle surfaces 145

5.4 FlexPDE code for the one dimensional example 149

5.5 Flex PDE code for the slag block model 151

5.6 List of expressions used to calculate the heat transfer coefficient in spray cooling. [37,38] 164

5.7 Nomenclature 164

5.8 Tap information and composition of the two thermocouple blocks 167

5.9 Cross sections water vs. air cooling 168

6 References 172

List of Figures

Figure 1 Block diagram depicting the process flow of the Exxaro KZN Sands Slag Processing Plant. 18

Figure 2 Aerial photograph of the furnace and metal treatment building (upper left hand corner) and slag processing building (lower right hand corner). The block yard is located between these two buildings. 19

Figure 3 Calculated partial pseudobinary section through the $FeO-Ti_2O_3-TiO_2$ system, at an FeO mole fraction of 0.13.[22] 21

Figure 4 Slag pot with 1.5 t capacity used during the Campaign 9 slag block cooling trials. 24

Figure 5 Grid and tray stand on which slag blocks were placed to cool 27

Figure 6 Slag block under water cooling during Campaign 9....27

Figure 7 Average surface temperature of slag blocks cooled in air. 27

Figure 8 Average surface and subsurface temperatures of tap 59 (isolating block). 28

Figure 9 Example of decrepitated material showing the flake-like structure which captures air to form an isolating layer round the block when left to accumulate. 28

Figure 10 Average surface temperature of blocks cooled continuously with water....29

Figure 11 Average surface temperature of blocks cooled intermittently with water. 29

Figure 12 Average surface temperature of blocks after submersion in water. 30

Figure 13 Block diagram showing the breaking and crushing procedure of the Campaign 9 blocks. 34

Figure 14 Correlation between FeO and Ti_2O_3 as analysed during the Campaign 9 trials. .36

Figure 15 Particle size distributions of the screen series in the crushing & milling trials: (a) air cooled block; (b) intermittent water cooling, and (c) continuous water cooling. Tap numbers are indicated in brackets in graph headings. Numbers 1 to 4 indicate the change in size distribution following initial crushing (nr 1), and three subsequent steps of recirculating oversize (nr 2 to 4). 36

Figure 16 -106µm vs. +850µm mass percentages of the Campaign 9 crushed blocks....37

Figure 17 Mass percentage fines generated (-106 µm fraction) per milling step 1 to 4, shown per cooling method (tap numbers are shown in brackets), arranged from worst to least fines generation....38

Figure 18 Mass percentage fines generated (-106 µm) ordered with increasing ($\%SiO_2+Al_2O_{3(glass)}+CaO$). 39

Figure 19 Mass percentage -106µm generated shown against increasing tapping rate. 39

Figure 20 Mass percentage residual coarse fraction (+850µm) ordered from worst to best. 41

Figure 21 Residual coarse fractions arranged in order of increasing specific surface area of the blocks – after cooling..42

Figure 22 Residual +850 µm with increasing block mass yield...43

Figure 23 Residual coarse fraction arranged in order of increasing (SiO_2+$Al_2O_{3(glass)}$+CaO).. 43

Figure 24 Residual coarse fraction arranged in order of increasing tapping rate................44

Figure 25 Residual coarse fraction arranged in order of increasing equivalent Ti_2O_3..........44

Figure 26 Correlation between %FeO and %Ti_2O_3 for pilot plant slags (solid squares and line; equation on right hand side) and plant slags (open circles and dotted line; equation on left hand side). 50

Figure 27 Average surface temperature of blocks L1R9 and L1R11 after closure of the cooling water. 51

Figure 28 Photograph of a plant size block showing fine decrepitated material and large chunks breaking off from the block corners. As an indication of scale, the bottom diameter of the block is approximately 1.8 to 2 m. 51

Figure 29 Particle size distribution of the block yard remains – decrepitated material and coarser sections. 52

Figure 30 Particle size distribution of the feed to and product material from the tumbling testwork done on block L1R11 (slow, 10 days). 53

Figure 31 Average particle size distribution of the four blocks (90% confidence intervals shown). Triangles represent higher tapping rates, while circles represent lower tapping rates. Open symbols of 3 days water cooling; solid symbols for 10 days water cooling.....................54

Figure 32 Particle size distributions of the tumble test feed and products. 55

Figure 33 -106µm fraction (fines) generated with each tumbling test (solid markers). The fines present in the feed are shown by the open markers. 56

Figure 34 Ratio of -106 µm in the product to that in the feed of the tumbling tests. Circles denote low tapping rates and triangles high tapping rates. Solid symbols denote 10 days of water cooling while open symbols represent 3 days of water cooling. 56

Figure 35 The +850 µm fraction (residual coarse) remaining after each tumbling test (solid symbols). The coarse material present in the feed is shown by the open symbols. 57

Figure 36 Ratio of the +850 µm in the product to that in the feed of the tumbling tests. Circles denote low tapping rates and triangles high tapping rates. Solid symbols denote 10 days of water cooling while open symbols represent 3 days of water cooling. 58

Figure 37 Sketch of a typical Loesche mill. 59

Figure 38 Schematic depiction of the experimental set-up for the compression testwork. ..60

Figure 39 Example of distance and force against (a) time and (b) compression energy as recorded and calculated respectively during the compression tests...61

Figure 40. Distance (a) and maximum force (b) per test as recorded during the compression tests. 61

Figure 41. Specific energy exerted on the samples during the compression tests. 62

Figure 42 (a) Amount of fines generated with the 1st to 6th run of the compression test series for the four blocks. (b) Specific energy (kJ per mass% -106 µm) per compression run for the four blocks. 62

Figure 43 (a) Residual +850 µm mass% from the 1st to 6th test of the compression test series for the four blocks; (b) Specific energy (kJ per mass% +850 µm) per compression run for the four blocks. 63

Figure 44 Average % -106 µm and specific energy in kJ/% -106 µm per compression test for each of the four blocks. (Error bars showing a 95% confidence interval). 64

Figure 45 Average % +850 µm per compression test for each of the four blocks. (Error bars showing a 95% confidence interval). 64

Figure 46 Cross section of block 60 showing the horizontal groove where the drill core was removed. The block surface is apparent from the rusty coloured area in the upper left hand corner of the photo. 66

Figure 47 Microstructure of the chill zone in the pilot-plant slag block, next to the mould. The outer surface is at the bottom of both images. The higher-magnification image at right shows that this region largely consists of two phases; the darker phase (marked "R") was found to be TiO_2 (rutile or anatase). 67

Figure 48 Typical microstructures found within the pilot-plant slag block, near the surface of the slag block, but outside the oxidised zone (top two images), halfway between the surface and the centre (middle two images), and at the centre (bottom two images). The light-gray matrix phase is karrooite (M_3O_5), the black lines are cracks, larger black areas are pores, dark grey areas are silicate phases (S_1 and S_2), and the phase with intermediate brightness is TiO_2 (likely rutile; indicated with R). 68

Figure 49 Typical microstructures found within the industrial-plant slag block, near the surface of the slag block, (top two images), within the body of the slag block (middle two images), and at the centre (bottom two images). Phase identification is as for the images of the pilot-plant slag block. 69

Figure 50 Pairs of images of the same particles of chloride-grade crushed slag. Arrowed black patches in the back-scattered electron images (BEI) at left indicate silicates. The secondary electron images (SEI) at right show the particle morphologies. 72

Figure 51 Pairs of images of the same particles of fine-grade crushed slag. Arrowed darker particles in the back-scattered electron images (BEI) at left indicate silicates. The secondary electron images (SEI) at right show the particle morphologies...73

Figure 52 %Oxide per average particle size fraction (a) SiO_2, Al_2O_3 and CaO, and (b) Cr_2O_3, MgO, MnO and V_2O_3...74

Figure 53 Relationship between equivalent %FeO, equivalent $\%Ti_2O_3$ and $\%TiO_2$ of slags produced at the pilot facility during campaign 9 and at the industrial scale plant. 75

Figure 54 Sketch of the tapping system layout..76

Figure 55 Photographs of the tapstream of (a) fast and (b) slow flowing tapstreams. 76

Figure 56 Tapping rate vs. $\%Ti_2O_3$. 77

Figure 57 Tapping rate vs. superheat...77

Figure 58 Superheat vs. %Ti2O3. 77

Figure 59 Equivalent %FeO vs. equivalent $\%Ti_2O_3$ grouped for high, medium and low tapping rates. Also shown is the ratio for samples taken from the blocks following cooling in the block yard. The order of the correlations in the upper right corner corresponds with the order of the legend. 78

Figure 60 Calculated section through the TiO_2-Ti_2O_3-FeO phase diagram, at a constant FeO mole fraction of 0.13 (assuming that Magnéli phases are absent). Phases are identified as follows: "sl" is the molten oxide (slag), "psb" is the M_3O_5 phase, "rut" is the rutile-based solid solution (TiO_2 with some Ti_2O_3 in solution), and "Fe" is metallic iron[4]. 79

Figure 61 Change in phase relationships in high-titanium slag during solid-state oxidation above 550°C[4]...79

Figure 62 Tapping rate vs. $\%SiO_2$. 80

Figure 63 %FeO vs. $\%SiO_2$. 80

Figure 64 %FeO vs. %SiO2 from campaign 9 data. 80

Figure 65 Mineralogy of blocks (a) L2R9 and (b) L1R11 when exposed to air at 100 ºC. ...82

Figure 66 Temperature of the one dimensional shape as a function of its distance. Solid lines represent the results of the analytical solution, while broken lines represent the numerical results. The unit of the numbers is in hours...87

Figure 67 The shell thickness of a one dimensional shape cooling from 1550 ˚C. The solid line represent the solution from the analytical method described above, while the triangles represent that of the numerical model as calculated by FlexPDE. 87

Figure 68 Results of an energy balance check conducted over a pilot scale size slag block. 90

Figure 69 A sketch of the block illustrating the important shape notations. 91

Figure 70 Example of the mesh configuration for the slag block (Z and R are in metre). Areas of denser node configurations are shown where FlexPDE reduced the node size to remain within the accuracy tolerance of 0.1%. 93

Figure 71 Analyses (mass%) of industrial plant slags. 94

Figure 72 Predicted effect of temperature on (a) the fraction liquid and (b) the enthalpy (relative to that of solid slag at 298 K) of slag no. 4. The broken line gives the linear approximation which was used as model input. 95

Figure 73 Heat losses from the vertical surface of a 1,365 kg block. The black line represents model results with constant heat capacity of the block; while the brown line represents model results where the pot heat capacity is equivalent to that of pure iron. 97

Figure 74 Heat capacity of pure iron. 98

Figure 75 Simplified conical pot and block, which was used to estimate the thermal contact resistance. 101

Figure 76 Pot surface temperatures as predicted by the cooling model (lines). Symbols indicate surface measurements derived from actual temperature measurements within the pot shell. 102

Figure 77 Heat losses from the horizontal surface of the block during secondary cooling. The different lines show the sensitivity of heat losses to the assumed height of the air gap between the block surface and ground. 103

Figure 78 Heat transfer coefficients for natural cooling in air. 105

Figure 79 Boiling curve associated with quenching of a hot surface in a stagnant pool.[17,18] 106

Figure 80 Heat transfer coefficients for cooling in water with varying (a) volumetric water flows (b) drop speeds and (c) drop diameters. Surface temperatures are in °C. 107

Figure 81 Model-predicted results for block surface temperatures for different of water volumetric flow rates and drop speeds. 107

Figure 82 Surface temperature and heat transfer coefficients for intermittent water cooling at four positions on the block. “Flat centre” is the centre of the horizontal surface, “corner” is the corner between the horizontal and inclined surfaces of the block, “$r_t : z_t$” is the join on the surface of the spherical and conical block volumes, and “round end” is the centre of the round end of the block. 108

Figure 83 Photograph of a slag block and pot directly after thermocouples were inserted into the block. For support the refractory tubes were inserted into the slag through slots in a steel channel which was placed horizontally over the pot edge. 109

Figure 84 Photograph showing the configuration of the thermocouples which were inserted into the slag blocks. 110

Figure 85 Thermocouple positions for blocks 37 and 38 tapped during Campaign 10. Alphabetic subscripts denote thermocouple positions inserted into the slag, while numeric subscripts denote positions of thermocouples inserted into the pot shell. 110

Figure 86 RMS error (in ˚C) of actual vs. model predictions for slag temperatures within tap 37. 111

Figure 87 RMS error (in ˚C) between actual temperature measurements and model predictions for tap 38. 112

Figure 88 RMS errors (in ˚C) between the actual and model predicted slag temperatures with $k_{slag} = 0.00175T + 0.3$. (a) Liquidus and (b) solidus temperatures were varied with ± 2% and ± 5%. 112

Figure 89 Internal slag temperatures for (a) tap 37 and (b) tap 38. Lines indicate model predictions, while symbols represent actual temperature measurements (k=0.00175T+0.3). ..113

Figure 90 Best fit k-values for taps 37 and 38. For modelling purposes the k-value was expressed as given by the solid black line. 114

Figure 91 Comparison of the fitted thermal conductivity of the solidified slag (heavy line), with literature data on the range of thermal conductivity of natural rocks[1] (broken line), and synthetic karrooite ($MgTi_2O_5$) and pseudobrookite (Fe_2TiO_5). For the M_3O_5 materials, the arrows indicate the direction of temperature change during the measurements. 115

Figure 92 Internal structure of a partially solidified block, as revealed by failure during tipping after primary cooling in the pot. 116

Figure 93 Temperature contours (scale in thousands of ˚C) of an 18 t block after 18 hours primary cooling (in pot). 116

Figure 94 Internal macro structure of solidified blocks showing the shell formation during primary cooling and the ball formation in the centre of the block: (a) and (b) approximate 18 ton blocks; (c) sketch illustrating the ball and dome macro structures which are displayed in (a) and (b). 117

Figure 95 Surface temperatures of two 18 ton blocks. Symbols represent actual measurements while lines represent model predictions. 118

Figure 96 Surface temperatures of an 18 ton block; times are expressed relative to the time of closing the taphole. 118

Figure 97 Remaining liquid core and shell thicknesses of a slag block cooling in a pot up to complete solidification. 120

Figure 98 Comparison of the remaining liquid and mushy cores, for slag blocks cooled in the pot, in air and with water cooling. 120

Figure 99 Shell growth of the slag block for the first half hour of cooling in a pot. 121

Figure 100 Thermal conductance for horizontal and inclined (vertical) surfaces. The units of the values within the above graphs are in seconds, counting from closing of the taphole. Time increments run according to the series 0, 2, 4, 8, 16, 32, 64, 100, 200, 400, 800, 1600, 3200 122

Figure 101 Surface temperatures along the inclined surface of the block for (a) cooling in water and (b) cooling in air. 0 denotes the block centre at the round end of the block, with the corner between the horizontal and inclined surface the furthest point......123

Figure 102 Photograph of a 17-18 ton slag block showing typical breaking off of the corner between the horizontal and inclined surfaces. To the left of the broken-off corner decrepitated material has formed. 124

Figure 103 Average surface temperatures of (a) air and (b) water cooled blocks. Maximum and minimum surface temperatures are shown with dotted lines......125

Figure 104 Internal temperature gradient of an air and water cooled block along the line from the centre point of the block to the transition point between the spherical and conical section of the block – points (0;0) and $(r_t; z_t)$ respectively on Figure 93. Solid lines indicate air cooling while dotted lines indicate water cooling. 126

Figure 105 Surface temperatures of a slag block cooled between 1 and 10 days under water and allowed to re-heat for 1 hour. 127

List of Tables

Table 1 Summary of the cooling methods used during the pilot plant trials of Campaign 9. .26

Table 2 Blocks produced during campaign 9 which were used for the crushing trials. 33

Table 3 Correlation coefficients of parameters affecting the fines generation during crushing & milling. 38

Table 4 Comparison of the experimental worst to best ranking and that predicted by the regression model including the $(SiO_2+Al_2O_{3(glass)}+CaO)$, tapping rate, block yield, specific surface area after cooling and equivalent $\%Ti_2O_3$. 40

Table 5 Correlation coefficients of independent variables affecting the residual coarse fractions during crushing. The best correlation coefficients were obtained by excluding the blocks named in the right hand column. 42

Table 6 Comparison between the actual worst to best order and the predicted order (including the block yield, specific surface area after cooling and glass phase variables).........45

Table 7 Details of the four blocks selected for the plant trials. 50

Table 8 Absolute values of the residual coarse fraction (+850 µm) of the tumbling products. 58

Table 9 Average numbers for the last 3 compression tests ran for each block, including 95% confidence intervals. 63

Table 10 Tap chemistry of block 60 (mass percentages; XRF) 66

Table 11 Average compositions (with 95% confidence intervals on average values), as found by EDS. Compositions are in mass percentages. For the karrooite phase, the Ti_2O_3 content was calculated by assuming that M_3O_5 stoichiometry holds. For the area analyses and silicate analyses, all titanium is expressed as TiO_2. 70

Table 12 Micro-analyses of dark regions (silicates) identified in crushed slag (mass percentages) 72

Table 13 List of shape notations and their meaning used in describing the block shape. ..91

Table 14 Average compositions of eight groups of slags from the full plant dataset; each group spans a specific range of FeO contents. 95

Table 15 Parameters of linear approximations to thermodynamic properties, and fitted relationships. 96

Table 16 Input data used to estimate contact resistance for pilot-scale block, with estimated resistances. 101

Table 17 Constants used for calculation of the heat transfer coefficient as per equation (18) 104

Table 18 Best-fit values for coefficients a and b for each of the thermocouples inserted into the slag blocks (expression: $k_{slag} = aT + b$)..111

1 Introduction

1.1 TiO_2 pigment feedstock

Titanium dioxide (TiO_2) is used as pigment in amongst others paints, coatings, plastics, paper, inks, foods, toothpaste and cosmetics due to its brightness, high refractive index, whiteness, opacity and resistance to discolouration under ultraviolet light[1].

The value chain of the titanium dioxide (TiO_2) pigment industry starts with the mining of a group of minerals collectively referred to as heavy minerals. This group of minerals includes ilmenite ($FeTiO_3$), zircon ($ZrSiO_4$), rutile (TiO_2), leucoxene (a weathered form of ilmenite) and monazite ((Ce, La, Pr, Nd, Th, Y)PO_4). When of sufficiently high grade, ilmenite can be used directly as feedstock in the TiO_2 pigment manufacturing processes. Alternatively, it can be upgraded to feedstock quality through reduction in rotary kilns to manufacture synthetic rutile, or reductive smelting in electric arc furnaces to produce TiO_2 slag.

The required feedstock quality (TiO_2 content and impurity level of individual oxides) depends on the pigment manufacturing process: chloride process or sulphate process. With the chloride process the feedstock is converted from TiO_2 to $TiCl_4$ in a fluidised bed after which the $TiCl_4$ is oxidised back into a pure TiO_2 crystal which is further surface treated to yield a pigment with the desired properties[2]. During the sulphate process, the feedstock is dissolved in sulphuric acid before controlled crystallisation of the titanium units to yield TiO_2 pigment[2]. Due to the different processing routes, the chemical specifications differ for the two products.

The two pigment manufacturing processes furthermore impose a specification on the particle size distribution of the feedstock. The fluidised bed technology used in the chloride process necessitates an upper and lower limit on the particle size distribution (in some instances also a d_{50} constraint). This is the origin of the very specific particle size range specification of -850 µm +106 µm for feedstock intended for the chloride route. The sulphate process requires a large surface area and feedstock is milled to very fine particle sizes. The -106 µm fraction is therefore sold as feedstock in the sulphate process market.

At Exxaro KZN Sands, TiO_2 slag produced via reductive smelting of ilmenite is crushed and milled to -850 µm. The milled slag is classified into the coarser -850 µm +106 µm fraction intended as feedstock in the chloride pigment manufacturing processes and referred to as "chloride slag". The finer -106 µm fraction is sold as feedstock for the sulphate pigment manufacturing route, and is referred to as "sulphate slag" or "fine slag". However, since chloride slag has a higher market value than fine slag, a primary key performance indicator of plant production is the ratio of chloride to fine slag; a high ratio indicates that size reduction of the slag to below -850 µm is achieved, while avoiding formation of -106 µm material.

1.2 The origin of Exxaro KZN Sands

During the mid 1990's Iscor (then a steel producer and mining company) identified the opportunity to invest in the heavy minerals industry. The Iscor Heavy Minerals project (IHM Heavy Minerals) commenced with a feasibility study flowing into an engineering and design phase. These started in 1996 and concluded in 2000 with Board approval of phase 1 of the project – Hillendale Mine and the Mineral Beneficiation Plant. Construction of the two Smelters and Slag Processing Plant – phase 2 – was subsequently announced in August 2001. Commissioning of the Smelters commenced during the last quarter of 2003 followed by that of the Slag Processing Plant in March 2004.

Between 1995 and 2001 Exxaro KZN Sands (then IHM Heavy Minerals) conducted 12 ilmenite smelting campaigns on the 3MVA DC pilot furnace at Exxaro's Research and Development facilities. These campaigns varied in length from one week to six weeks, with the majority running for two weeks. Technical objectives for these campaigns included testing of different ilmenite and reductant sources, production of TiO_2 slag market samples and formulating operating philosophies for the smelting process[3].

During these smelting campaigns it became clear that the TiO_2 slag as tapped from the furnace showed characteristics different from typical slags encountered in other metallurgical operations, e.g. iron and steelmaking[4]. One pronounced difference was the tendency of these slags to decrepitate from a solid block into a powder with particle sizes finer than 100 µm. This phenomenon was intensively investigated in the subsequent years[5, 6, 7].

In addition to these studies which focused primarily on the decrepitation of TiO_2 slag, experimental work was initiated during the 9th 3MVA ilmenite smelting campaign to investigate the effect of various cooling conditions on the decrepitation behaviour of the slag, as well as the possible effect of such cooling conditions on the particle size distribution of the final products (and hence on the ratio of chloride to fine slag). This testwork and the results thereof are discussed in Part 1 of this thesis. Part 2 of this document presents the results of subsequent plant trials. Part 3 describes a cooling model, based on finite element principles, to calculate the internal and surface temperatures of TiO_2 slag blocks as functions of time.

While Campaign 9 was performed during June 2001, the plant trials were only conducted during January 2005. The four-year lapse between the experimental work of Parts 1 and 2 was mainly due to the industrial-scale plant only being commissioned during the first quarter of 2003. This time lapse created the opportunity for lessons learned during the pilot plant campaigns to be implemented already during the design and construction phases of the Slag Processing Plant.

1.3 Ilmenite smelting and slag processing

To enable the context of this work be seen in perspective, a brief process description of the ilmenite smelting and slag processing processes is required[8].

During the smelting process as applied in a DC electric arc furnace, ilmenite is continuously fed together with anthracite in a tightly controlled ratio through a hollow electrode into the operating furnace. The primary reduction reaction can be simplified and written as in equation (1) (equation not balanced):

$$FeTiO_{3\,(s)} + C_{(s)} \rightarrow M_3O_{5(\ell)} + Fe_{(\ell)} + CO_{(g)}\text{; where } M = Ti,\ Fe \qquad (1)$$

The primary product - titanium oxide slag, written as M_3O_5 - contains an average of 85% TiO_2[*]. In addition the slag also contains approximately 10% FeO. Also present are impurities such as SiO_2, Al_2O_3, MgO, MnO, CaO, Cr_2O_3, V_2O_3 and ZrO_2. The slag contains titanium in both the +3 and +4 oxidation states. Substitution of the Ti^{3+} ions by Cr^{3+}, V^{3+} and Al^{3+}, and that of Fe^{2+} by Mg^{2+} and Mn^{2+} also occur. The oxides SiO_2, CaO and in part Al_2O_3 separate into silicate phases (including a glass phase).

---

[*] Total Ti expressed as TiO_2 (Ti in slag is present in both the +3 and +4 oxidation states).

Due to the reducing conditions in ilmenite smelting titanium units and some of the impurities are partially reduced to report to the metal phase. The maximum limits of impurities in both the slag and iron are fixed in supplier-customer contractual agreements.

The smelting and reduction processes are conducted within a crucible of a solidified, high titanium content slag (known as the freeze lining), contained within the furnace refractory walls. This freeze lining protects the magnesia refractory from chemical attack by the slag (chemical attack will not only reduce the refractory life, but will also contaminate the slag).

The slag has a lower density than the iron and separation of the two liquid products occurs within the furnace. Slag and iron are tapped periodically from separate sets of tapholes located around the circumference of the furnace – the slag tapholes are at a higher elevation than those of the iron. Slag is tapped into 20 t steel pots and cooled for several hours within these pots before being tipped out. These blocks are subsequently transported to the block yard where they are cooled under water sprays for a number of days. They are then crushed, milled and classified according to particle size into the chloride and fine slag products. A block flow diagram of the Slag Processing Plant is given in Figure 1 .

The tapped pig iron is re-carburised and desulphurised and cast into 7 kg pigs for use in among others, the automotive industry.

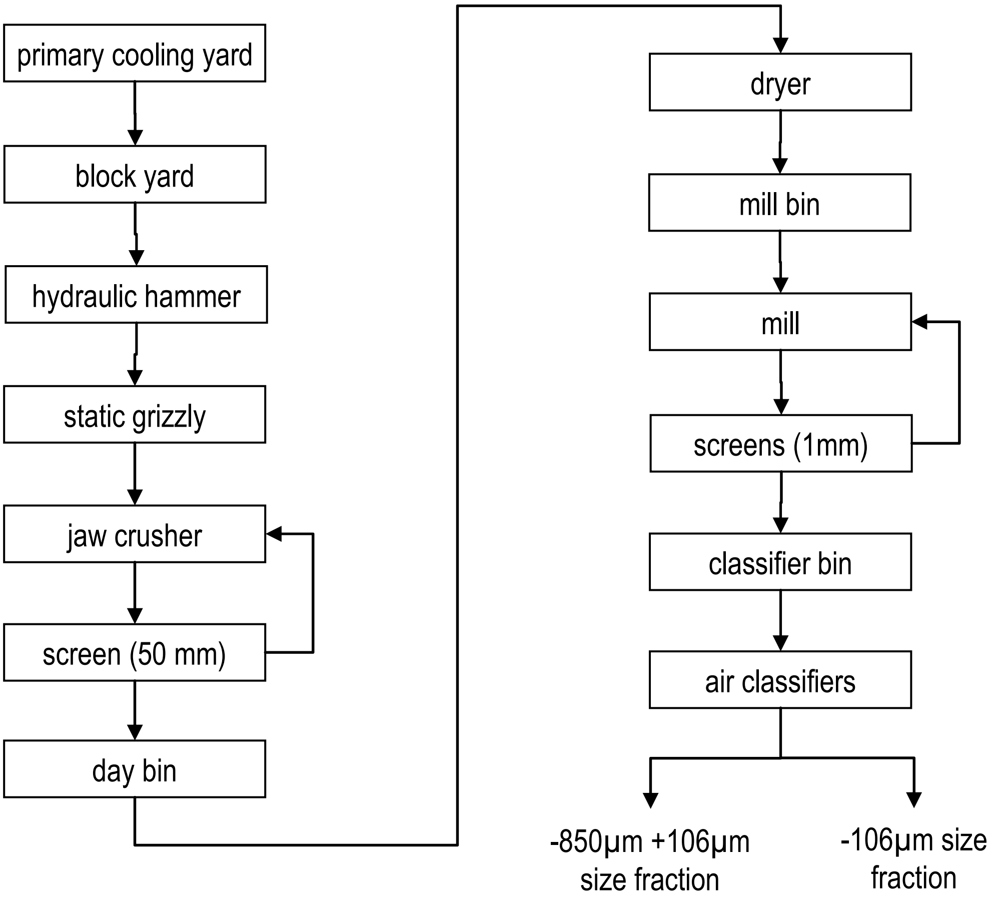

Figure 1 Block diagram depicting the process flow of the Exxaro KZN Sands Slag Processing Plant.

The layout of the Exxaro KZN Sands furnace and metal treatment buildings, slag block yard and slag processing plant is shown in Figure 2.

Figure 2 Aerial photograph of the furnace and metal treatment building (upper left hand corner) and slag processing building (lower right hand corner). The block yard is located between these two buildings.

1.4 Problem statement

The relatively young process of titania slag production and the closed nature of the industry led the present situation where little information regarding the characteristics of titania slags is available in the open literature. Although useful information was published from research work conducted by the Canadian QIT research laboratories during the 1970s, these slags contained approximately 70% TiO_2 whereas titania slags produced by South-African producers typically contain around 85% TiO_2. From the available information, this difference is composition was expected to have a considerable influence on the slag properties and behaviour. Only fairly recently was more information published regarding the properties of these relatively higher grade titania slags. These publications focused on mineralogy of the solid phases, decrepitation behaviour and in some instances even included smelting behaviour, and are summarised later in this section.

During the ilmenite smelting campaigns conducted by IHM Heavy Minerals (as the forerunner of Exxaro KZN Sands was known at the time), it became evident that the final particle size of the slag is a strong function of the cooling environment. This initiated various studies into decrepitation behaviour (discussed below). It soon became evident, however, that the final slag product size distribution was the consequence of parameters other than just decrepitation.

This study therefore focused on testing the hypothesis that various aspects of the cooling environment influence the particle size distribution of the final product. This was in contrast with the general concept of the time (prevalent within IHM Heavy Minerals) that crushing and milling are the primary factors determining the particle size distribution.

General mineralogy of titania slags

The ilmenite smelting process[9,10] and slag structure[4,11,12] have been reviewed recently, and hence only a brief summary is given here (based on these references), focusing on the factors which can affect the phases which are present in the slag (since these phases are expected to influence the crushing behaviour of the solidified slag).

The most striking feature of the solidified slag is that it largely consists of a single phase, which is a solid solution which follows M_3O_5 stoichiometry.[4] This phase can be viewed as a solid solution of the end members $FeTi_2O_5$, Ti_3O_5, $MnTi_2O_5$, $MgTi_2O_5$, Cr_2TiO_5, Al_2TiO_5 and V_2TiO_5, and incorporates all or nearly all of the iron, titanium, manganese, magnesium, aluminium and vanadium which are present in the product. The major elements which are not incorporated in the M_3O_5 ("pseudobrookite" or "karrooite") solid solution are silicon and calcium; these report as separate silicate phases (both crystalline and glassy), which also contain aluminium, and some titanium (all of these in the form of oxides). The silicate phases are present between the M_3O_5 grains, and appear to form during the latest stages of solidification. Some rutile (TiO_2) is generally present in the solidified slag, also at the positions of final solidification. This is in agreement with the predicted solidification behaviour of the slag, as reviewed below.

The tendency of SiO_2 and CaO to form separate silicate phases between the M_3O_5 grains may well contribute to the crushing behaviour of the slag; this possibility was studied in this project.

The reason why the slag composition remains close to M_3O_5 stoichiometry is not clear; suggested reasons include chemical equilibrium[13] (of the reaction $FeO+Ti_2O_3=Fe+2TiO_2$), and phase equilibrium[10] (involving transient solidification and remelting, driven by the temperature difference between the slag and the metal). The main reason for this uncertainty is that the calculated activities in the liquid slag and solid phases are based on extrapolations from the binary systems[14] (mainly FeO-TiO_2 and Ti_2O_3-TiO_2), measurements of sub-solidus equilibria,[15] and a few measurements involving melts in the FeO-TiO_2-Ti_2O_3 system.[16] The available data as evaluated in references 14 and 15 have been incorporated in the FactSage database.[17] Given the limited and uncertain experimental data, it is not surprising that predicted phase equilibria differ. For example, the "Multi-Phase Equilibrium" (MPE) package of the CSIRO[18] appears to predict a much wider liquidus-solidus gap than FactSage predicts; a cell model predicts a smaller liquidus region at temperatures of 1500°C, 1600°C and 1700°C (hence higher melting points overall) than does FactSage.[19]

While it is realised that there are uncertainties in the reaction and phase equilibria as predicted by FactSage, this package was used to provide much of fundamental thermodynamic data which were used in this work, since the package was the most comprehensive and convenient data source available to the author.

Reactions during solidification

Figure 3 gives a calculated pseudo-binary section through the FeO-Ti_2O_3-TiO_2 system, at a constant mole fraction of FeO; the section was calculated using FactSage, suppressing the Magnéli phases.[20] As mentioned before, the slag compositions are close to M_3O_5, but solidified slags contain a small but significant fraction of rutile.[4] The presence of rutile indicates that the slag contains more TiO_2 (and hence less Ti_2O_3) than M_3O_5 stoichiometry would require; that is, the slag composition lies between M_3O_5 stoichiometry and point A on the diagram (there is no evidence that the slag composition lies beyond point A, which would imply rutile forming as primary phase upon solidification, and the presence of a large fraction of rutile in the solidified slag.) The implication of the presence of rutile in the solidified slag is hence that the titanium in the slag is less strongly reduced (containing more TiO_2 and less Ti_2O_3) than M_3O_5 stoichiometry would require. One way in which this can arise, is for the slag to conform to M_3O_5 stoichiometry within the furnace (whether for reasons of chemical equilibrium or phase equilibrium, as discussed above), but that some of the Ti_2O_3 can be oxidised to TiO_2 during tapping, when the slag stream is exposed to air. This is certainly thermodynamically possible, since the calculated partial pressure of oxygen for equilibrium between TiO_2 and Ti_2O_3 in the slag is approximately 10^{-9} atm,[21] much lower than the partial pressure of oxygen in air.

The possibility that oxidation of slag during tapping can change the crushing behaviour of the slag (by changing the solidified microstructure, mainly by increasing the volume fraction of rutile in the structure) is one which was investigated in this work.

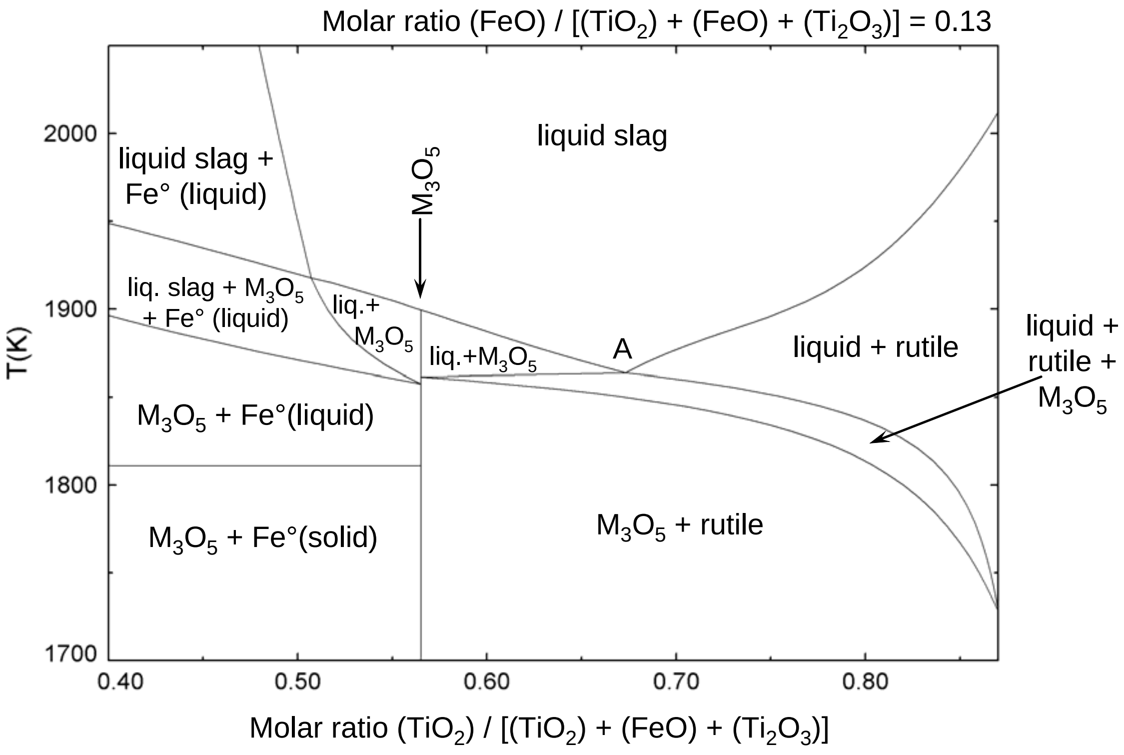

Figure 3 Calculated partial pseudobinary section through the $FeO-Ti_2O_3-TiO_2$ system, at an FeO mole fraction of 0.13.[20]

Reactions after solidification

Changes in microstructure can occur through phase transformations below the solidus temperature. One possible reaction is the decomposition of M_3O_5 into rutile and metallic iron; M_3O_5 tends to undergo this reaction below approximately 1100°C (depending on composition).[15] However, this reaction is generally not observed in solidified slags during practical cooling, and the M_3O_5 structure persists (metastably) down to room temperature. A small degree of oxidation of slag can trigger this transformation of M_3O_5 to rutile (or anatase) and metallic iron, though.[22] If such a transformation does occur, it could influence crushing, but there is no evidence from any of the microstructural studies on these slags that this decomposition reaction normally occurs to any significant extent.

What is expected to play a significant role is the formation of the "M_6O_{11}" phase by low-temperature oxidation (that is, at 400°C or below).[7,23] As indicated by its stoichiometry, formation of M_6O_{11} involves only a small degree of oxidation of M_3O_5, yet it has been shown to cause severe decrepitation of the material: the solidified slag breaks up into small flakelike particles.[5,6] Suppression of this low-temperature oxidation reaction is one of the main reasons why water cooling is applied to the surfaces of the slag blocks in the "block yard" of the plant. Possible effects of low-temperature oxidation were hence also studied in this project.

Higher-temperature oxidation reactions lead to different reaction products, and can also give substantial changes in the microstructure.[6] However, such reaction products are not evident in the slag microstructures. Such higher-temperature oxidation of the slag (typically in the temperature range 900-1100°C) was hence not expected to be relevant to this project; such oxidation reactions play a central role in processes which upgrade solidified slags to higher-TiO_2 products, though.[12,24]

1.5 Research approach

Based on the background information (as summarised above), the investigation into the influence of the cooling environment on the final particle size distribution was conducted in three parts:

Part 1 was conducted on pilot scale; given the flexibility of a pilot plant this afforded the opportunity to investigate the effects of several cooling methods. Although this work touched on the decrepitation behaviour of titania slags, the primary objective of this part was to determine whether a correlation exists between the cooling environment and cooling history, and the particle size distribution of the slag blocks which remain intact after cooling – in other words that portion of the block which appears to be untouched by decrepitation.

Part 2 built on the information obtained in Part 1. Part 2 sought to test the influence of those parameters (as identified in Part 1 as factors determining the crushing behaviour of the slag) which can be manipulated at the industrial scale plant of Exxaro KZN Sands.

Part 3 was a logical follow-up on the preceding parts, in predicting cooling. Since temperature is a predominant driver in the processes and factors influencing the slag particle size distribution, knowledge of the temperature profiles along the slag block surface and within the slag block over time is essential to understanding the problem, and to enabling the formulation of potential improvements in titania slag processing. Part 3 therefore describes the construction and results obtained from a finite element model of a cooling slag block. The predictions by this model provide insight into the temperature-time profiles of a slag block.

2 Part 1: Pilot Plant Trials

2.1.1 Background

Studies into the decrepitation behaviour of TiO_2 slags showed the phenomenon to occur due to oxidation of the M_3O_5 phase to M_6O_{11}.[5,6,7] The accompanying volume change of the crystal appears to initiate the physical breakdown of the material to particles smaller than 100 µm. This reaction was found to occur readily at temperatures between 200 and 600 ºC. (Above 600 ºC oxidation of the M_3O_5 phase results in anatase; at temperatures below 200 ºC, the reaction kinetics was considered to be too slow for the M_3O_5 to M_6O_{11} reaction to proceed.)

As a continuation of this work the objectives of the slag block cooling trials conducted during the 9th 3MVA ilmenite smelting campaign were:

- To quantify the impact of different cooling methods on block decrepitation;
- To investigate the possible impact of the cooling method on the crushing and milling behaviour of those blocks which remained fully or partially intact during cooling.

Slag taps were made from the 3MVA pilot furnace into slag pots with a 1.5 tons TiO_2 slag capacity. The shape of these cast steel bowls resembled that of the 20 t slag bowls intended for the industrial scale plant (Figure 4).

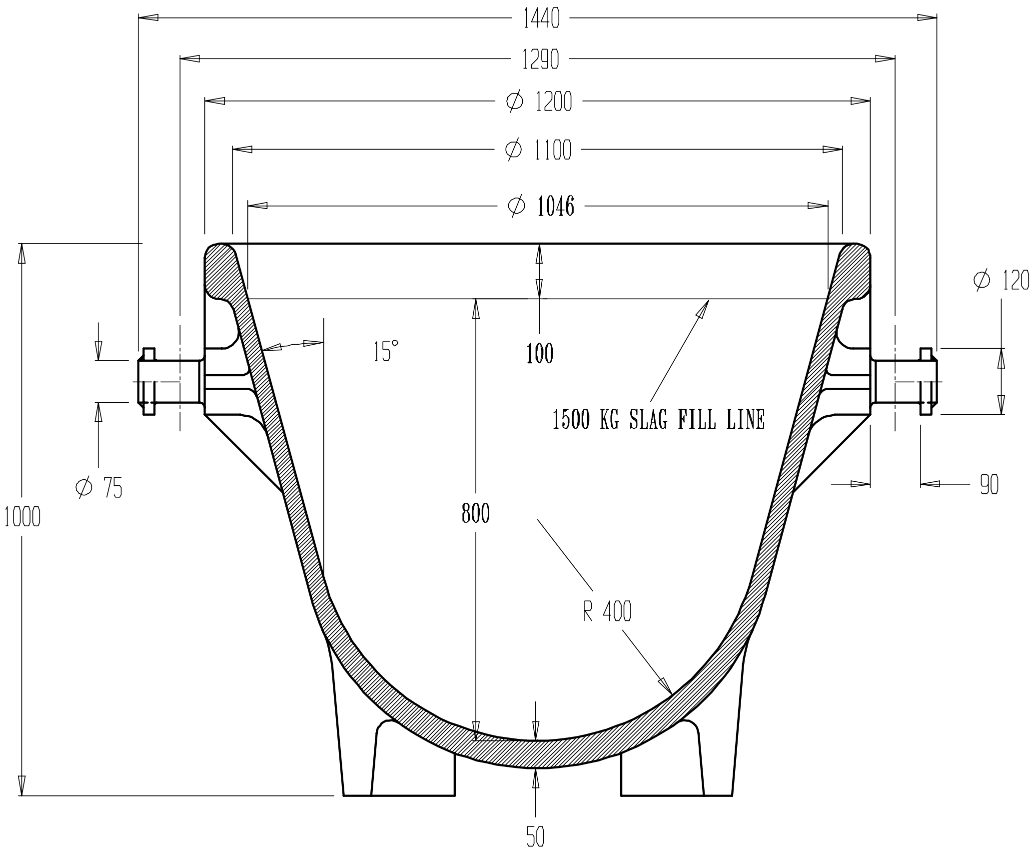

Figure 4 Slag pot with 1.5 t capacity used during the Campaign 9 slag block cooling trials.

2.2 Slag block cooling

2.2.1 Experimental procedure

Following tapping, the slag blocks were left to cool in the pots for 6 to 8 hours. After this period of primary cooling the blocks were tipped out of the pots and cooled under various cooling conditions:

- Air cooling. Apart from one block, each of the blocks cooled in air was tipped onto a 1.2 x 1.2 m steel grid positioned above an steel tray (Figure 5). Any material losses from the block (e.g. due to decrepitation) fell through the grid into the tray enabling the measurement of mass loss over time. One air cooled block was placed on a solid concrete base. All decrepitated material was left to accumulate on and around this block. All the air cooled blocks were left to cool undisturbed, under conditions of natural air cooling.

- Water cooling. These blocks were tipped from the pots onto the grid and tray stands. To enable continuous water cooling over the full block surface, a pipe cage with water sprays was positioned over each block (Figure 6). Apart from the short intervals when surface temperatures of the blocks were measured, these blocks were cooled continuously under water. Surface temperatures were measured using an optical pyrometer with an emissivity setting of 0.8 (during those short periods when the water sprays were turned off).

- Intermittent water cooling. These blocks were tipped onto the grid and tray stands and covered with a water spray cage. As in the case of the water cooled blocks, the water supply was closed when surface temperatures were measured. When such surface temperatures were below 200 ºC, the water supply remained closed. In instances were the surface temperature was above 200 ˚C during follow-up measurements, the water supply was immediately opened. The surface temperatures of these blocks were measured with a handheld pyrometer with an emissivity setting of 0.8. The surface temperatures of one of these blocks during the water-off periods were recorded with a thermographic camera.

- Submerged cooling. Several blocks were submerged directly after tipping into a water tank, through which water was circulated continuously. The period of submersion varied from 1 to 16 hours, with one block being repeatedly submerged. After such a block had been taken out of the water it was placed on a grid and tray stand. Surface temperatures were subsequently measured at hourly intervals, while mass losses (where they occurred) were recorded simultaneously.

- Two blocks were left to cool in the pots. Thermocouples were inserted into one of these blocks directly after tapping. This experiment was repeated during Campaign 10 and is discussed further in Part 3 of this document. For the purposes of Part 1, this block – of which the open end was exposed to air – is compared to the second pot-cooled block which was covered with a lid for the full duration of cooling.

Within these cooling method groupings, block composition (%FeO) and tap mass were varied. A summary of the different blocks, their most important attributes and cooling methods is given in Table 1.

Subsequent to complete cooling, the block yield was calculated for each block by dividing the final remaining block mass by its original tapped mass. Higher block yields indicate less material losses due to decrepitation, and hence a more successful cooling method.

Table 1 Summary of the cooling methods used during the pilot plant trials of Campaign 9.

Cooling method		%FeO	%TiO_2	Block mass (kg)	Block yield (%)	Tap number
Air cooling		7.83	90.18	1,021	37.5	38
		10.39	87.49	1,281	33.6	51
		11.46	85.99	1,420	42.3	64
		9.38	88.03	1,097	10.8	59[†]
Water cooling		9.74	88.29	622	91.3	49
		9.83	88.03	1,091	96.2	50
		9.60	88.52	1,535	95.9	48
		9.78	87.57	1,557	97.9	60
Intermittent water cooling		9.46	88.82	929	92.4	36
		11.99	85.66	1,017	96.2	42[‡]
		9.49	88.17	1,099	91.0	37
		10.56	87.01	1,471	90.3	61
Submerged cooling	1 hr	10.22	87.66	986	45.2	46
	2 hrs	10.13	87.78	1,029	50.1	52
	3 hrs	11.06	86.53	1,069	74.5	47
	5 hrs	10.99	86.85	1,133	91.7	45
	8 hrs	10.42	87.43	1,062	92.9	43
	16 hrs	10.17	87.09	1,131	96.2	58
	Repeat	10.71	87.27	1,498	95.2	65
Pot cooled	Uncovered block	10.72	87.06	1,275	nd	62
	Covered block	11.47	86.29	855	nd	44

2.2.2 Results

The surface temperatures of the air cooled blocks over time are shown in Figure 7. The average block yield of the air cooled blocks which were placed on grid and tray stands was 38% (Table 1). Since the particle size distribution of decrepitated material is 80% - 90% below 100 μm (refer to Part 2), 50% to 56% of the original mass of these blocks is therefore immediately classed as the lower valued fine slag, even before any further crushing or milling has been applied.

[†] Block was placed on solid concrete flooring; decrepitated material hence accumulated around and on the block surface.

[‡] The surface temperatures of this block were recorded with both a handheld pyrometer and thermographic camera.

Figure 5 Grid and tray stand on which slag blocks were placed to cool

Figure 6 Slag block under water cooling during Campaign 9

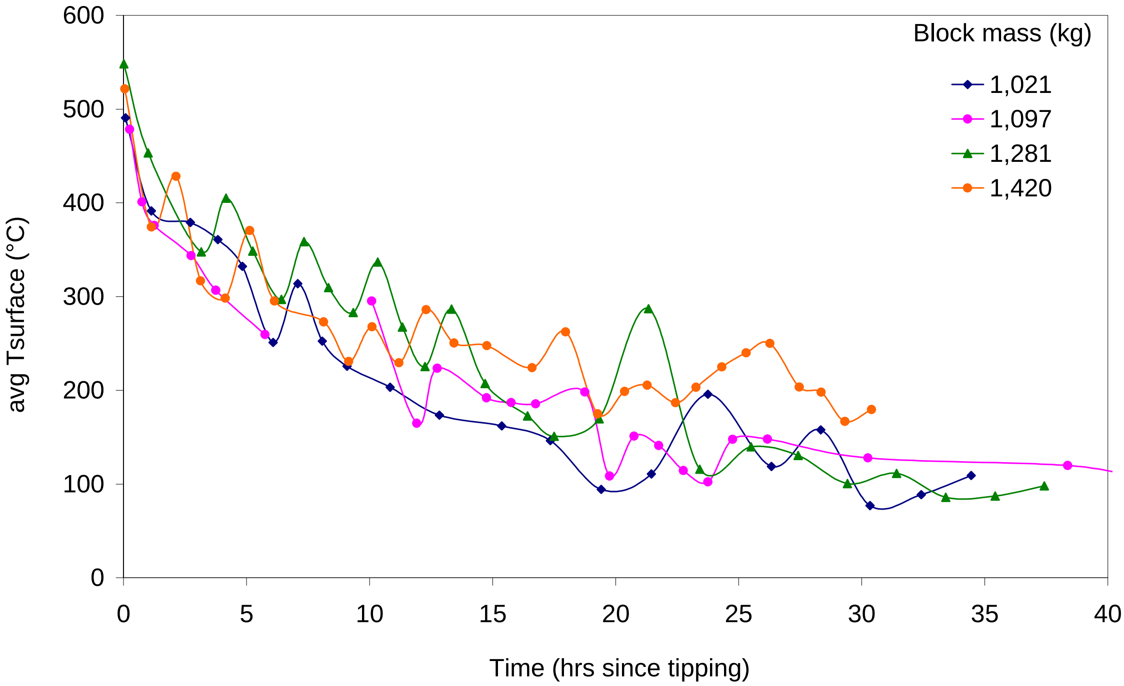

Figure 7 Average surface temperature of slag blocks cooled in air.

In contrast with the other three air cooled blocks, tap 59 was tipped onto a solid concrete floor to cool. Decrepitated material did not fall off and away from the surface of this block through the grid, but accumulated on and around the block surface. Between hours 15 and 50 (counting from the time of tipping), the outer layer (5 – 20 mm) of the decrepitated material was periodically removed at a small localised area and the temperature of the newly exposed surface was measured. These subsurface temperatures, shown as the broken line in Figure 8, were up to 120 ºC higher than the original surface temperatures. An example of the decrepitated flakes which formed on this block is shown in Figure 9. These flakes were flimsy and broke up into a powder on further handing. The yield of block 59 was 10.8%, and although intact when compared to the decrepitated surface layer, the core was too weak to withstand further handling required for crushing and/or milling.

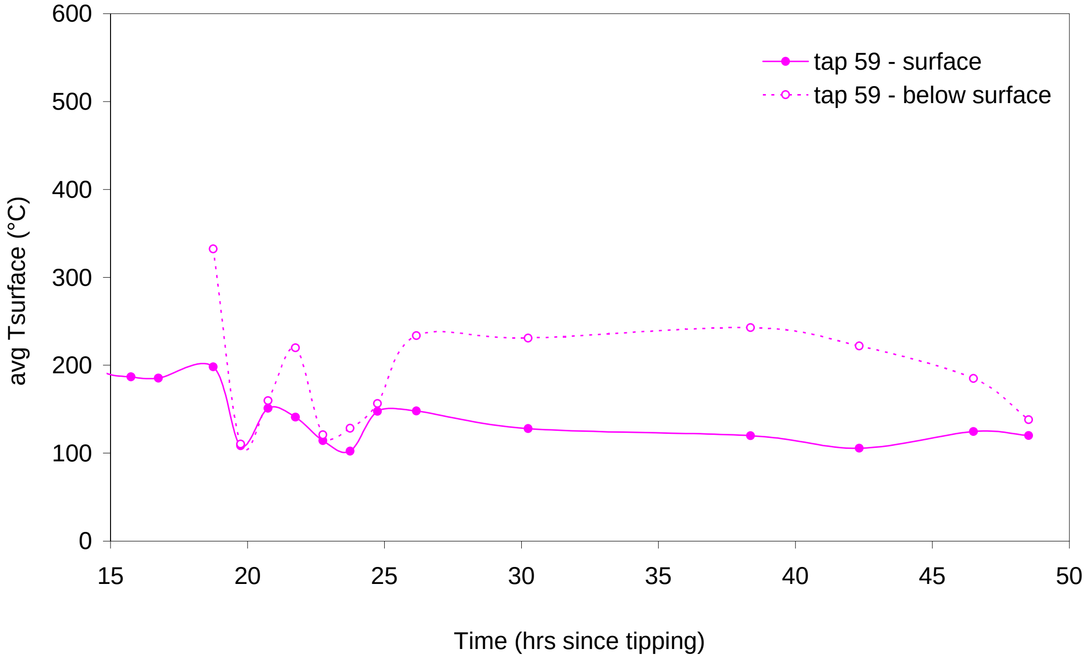

Figure 8 Average surface and subsurface temperatures of tap 59 (isolating block).

Figure 9 Example of decrepitated material showing the flake-like structure which captures air to form an isolating layer round the block when left to accumulate.

The surface temperatures of the water cooled blocks over time are shown in Figure 10. The average yield for these blocks was 93% (Table 1). The surface temperatures of the intermittently water cooled blocks are shown in Figure 11. The average block yield for these was 95% (Table 1). Clearly the block yields of the water cooled blocks, were markedly higher than those of the air cooled blocks, for both continuous and intermittent water cooling.

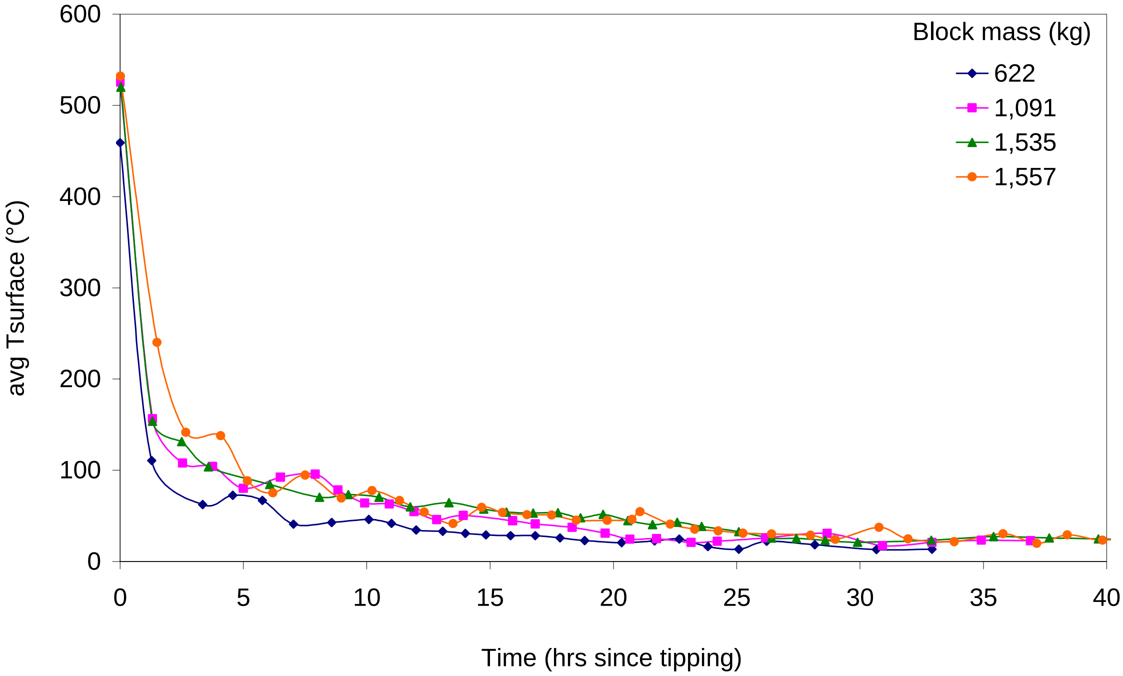

Figure 10 Average surface temperature of blocks cooled continuously with water.

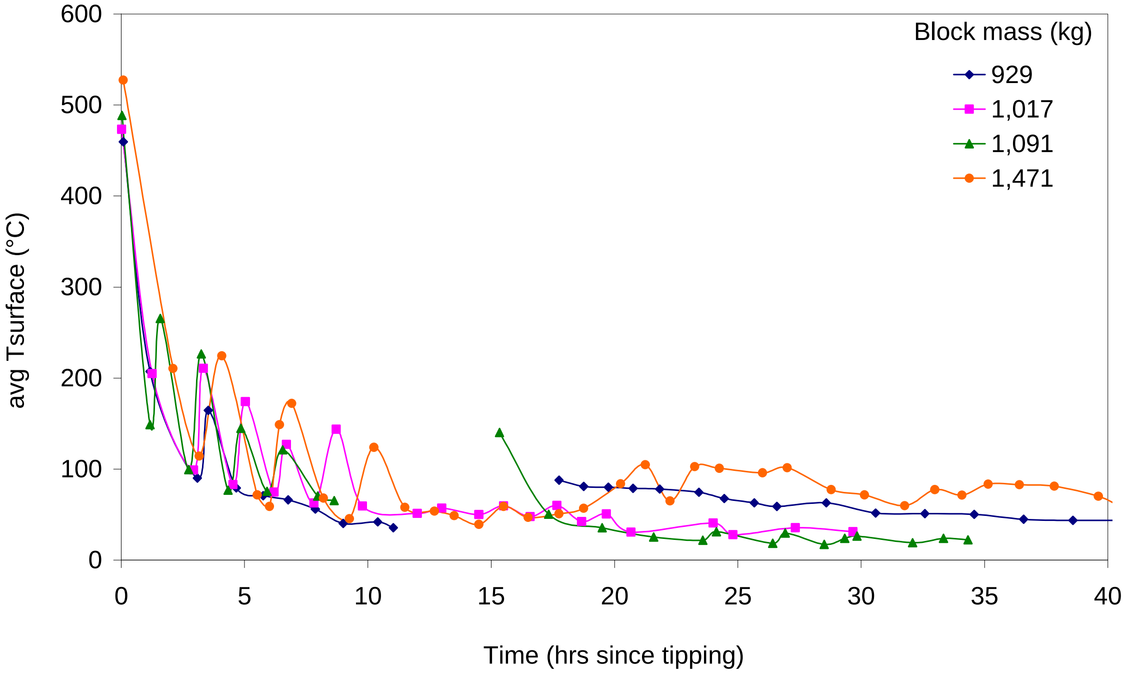

Figure 11 Average surface temperature of blocks cooled intermittently with water.

The measured surface temperatures of the blocks submerged in water are shown in Figure 12. The surface temperatures of these blocks were taken directly after being tipped out of the pots, and thereafter only when each block was removed from the water tank. One of these blocks was repeatedly submerged until no increase in the surface temperature was detected. This point was reached after 9 submersions, 32.3 hours after closing the taphole. The block yields of the submerged blocks are shown in Table 1. Yields improved significantly with increasing submersion time, with the most significant improvement when the block was cooled for longer than 5 hours before removing it from the water.

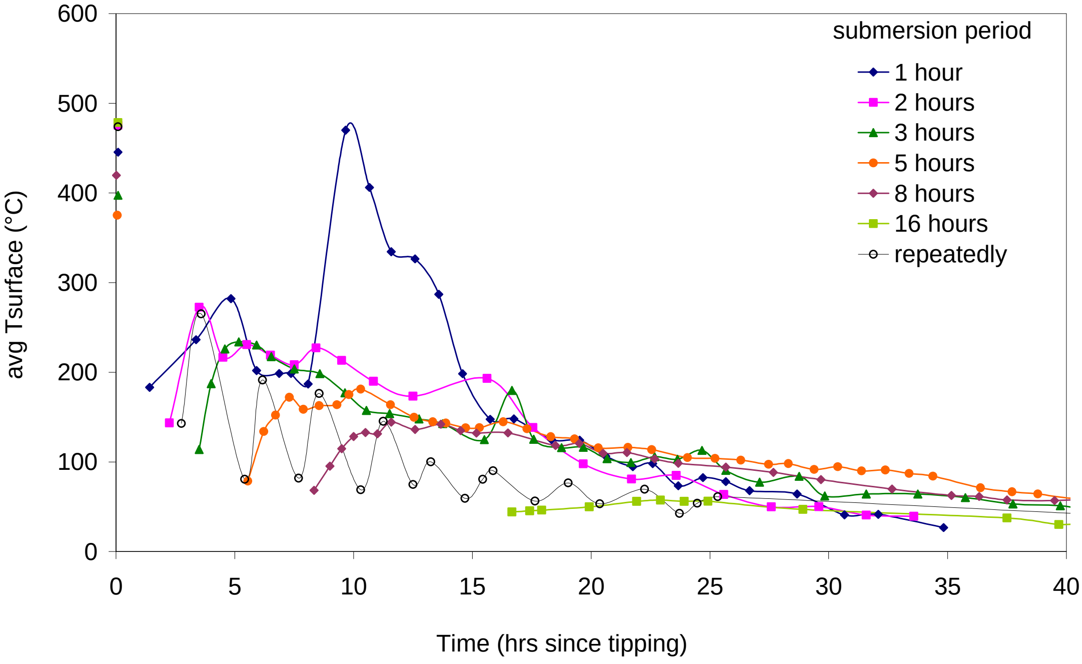

Figure 12 Average surface temperature of blocks after submersion in water.

2.2.3 Conclusions

In terms of block yield, the cooling methods can be classed into four groups:

- Exceptionally poor: natural air cooling combined with accumulation of decrepitated material on and around the block surface.
- Poor: natural air cooling and submerged water cooling for up to 1 hour. These cooling methods resulted in block yields from 33% to 45%.
- Medium: water submersion for 2 to 3 hours. This method resulted in block yields ranging between 50% and 75%.
- Good: continuous and intermittent water cooling to limit the time during which the surface temperature of the block is above 200 ˚C. Water submersion for 5 hours and longer also falls within this group. The block yields from these cooling methods were all above 90%.

The exceptionally poor results recorded where the decrepitated material accumulates is likely due to progressive air ingress between the decrepitation flakes. The combination of slag flakes and air forms an effective thermal insulation layer on the surface of the block. From Figure 8 the temperature within this isolating layer remains in the temperature range where decrepitation is reported to occur[5]. The process therefore becomes self supportive: exposure to air at these temperatures promotes further decrepitation (by the oxidation reaction) which allows progressively deeper air ingress, which in turn results in decrepitation deeper below the surface. The weakness of the block core is indicative that this process – although not fully complete - progressed into the centre of the block. In the case of the three blocks which were placed on grids, the decrepitated material was removed from the block surface by falling under gravity through the grid. This prevented build-up of a substantial isolating layer, hence allowing a steeper subsurface temperature gradient with less air ingress, effectively limiting decrepitation.

The effect of surface temperature is illustrated by the series of submerged cooled blocks: the yields of blocks which were initially water-cooled by submersion for 3 hours and for 5 hours were 74.5% and 91.7% respectively. The maximum surface temperatures of these blocks were 234 ˚C (3 hours submersion) and 181 ˚C (5 hours submersion). It therefore appears that decrepitation is notably reduced at surface temperatures below around 200 ˚C. Decrepitation furthermore seems to be largely suppressed at surface temperatures lower than 100 ˚C to 80 ˚C: the maximum surface temperature of the block submerged for 8 hours was 144 ˚C, in comparison with 58 ˚C of the block submerged for 16 hours. The corresponding block yields were 92.9% (8 hours submerged) vs. 96.2% (16 hours submerged). This is supported by the surface temperatures of the intermittently water cooled blocks as shown in Figure 11: the highest block yield was from tap 42 with surface temperatures which were consistently below 60 ˚C from 10 hours after tipping and onwards.

The good block yields of the intermittently water cooled blocks despite surface temperatures in the temperature range where decrepitation typically occurs during the initial 10 hours of cooling, is interpreted as an indication of the kinetic component of the decrepitation mechanism; that is, the time spent within the temperature range for decrepitation is also important.

The inclined surfaces of the blocks cooled in the pots showed no indication of any decrepitation: the mould coating§ was still clearly visible on the whole of these surfaces. Varying extents of decrepitation did occur on the horizontal (upper) surfaces of these blocks, however. The block yields of these blocks could unfortunately not be determined accurately since, after standing for a prolonged period in the pot, these blocks were stuck in the pots and broke into several pieces when they were eventually were removed from the pots.

Decrepitation can thus be eliminated or at least be reduced through:

1. removing air from the surface when the surface is at elevated temperatures
2. reducing the surface temperature to below 200 ˚C, but preferably even lower temperatures.
3. limiting the period when the surface is exposed to air when at elevated temperatures.

Block losses of continuously water cooled blocks occurred predominantly as 2 - 10 mm thick crusts peeling from the surface. The appearance of these crusts does not fit in with the

---

[§] A water based slurry containing alumina powder is sprayed on the inside of the pots before every tap to reduce the occurance of blocks sticking to the pot surface.

definition or mechanism of decrepitation. The fact that the block yield for the smallest block (622 kg vs. 1,091 – 1,557 kg) was lowest within the continuously water cooled group (91.3% vs. an average of 96.7%) indicates that the origin of this “peeling” effect is likely to also be surface driven.

No significant correlation between slag composition and block yield was obvious. However, since the chemistry range within the various cooling method groups was narrow (Table 1), this does not rule out the possibility that differences in chemistry might affect block yield. However, for the range tested, if chemistry does play a role, it is overshadowed by the effect of the cooling method.

2.3 Crushing and Milling

2.3.1 Experimental procedure

Out of the blocks discussed in section 2.2 eleven blocks were selected when proceeding with the crushing and milling trials. Details of these blocks are shown in Table 2. A hydraulic press was used to break each individual block down to -200 mm lumps. Each block was individually further crushed down to initially -50 mm particles and then -20 mm particles utilising the Exxaro R&D pilot scale primary and secondary jaw crusher facilities. A 50 kg sample was riffled from the -20 mm product and passed through a roll crusher producing a -2 mm product. The roll diameter of this crusher was 300 mm and had a length of 200 mm. The crusher was driven by a 2.2 kW motor which resulted in a rotating speed of 638 rpm. The roll crusher product was passed over a series of screens following the Canadian Standard Sieve Series[25] between 1400 µm and 75 µm. The +850 µm fraction was circulated back through the roll mill three more times, each time conducting a screen analysis on the product and separating out the +850 µm fraction. This procedure gave four sieve analyses in total for each block.

The breaking and crushing procedure described above (and shown in Figure 13) was accepted at the time as not representative of the material flow or the comminution equipment of the industrial scale slag processing plant (which was still being designed and engineered at the time). Hence, the absolute values of the particle size distributions obtained from these trials were not treated as representative of those experienced on the industrial scale plant. However, since all eleven blocks were broken and crushed according to the same procedure, the value of the test work lies in the comparative conclusions which can be drawn.

Table 2 Blocks produced during campaign 9 which were used for the crushing trials.

Cooling method		Tap number	Block yield (%)
Air cooling		64	42.3
Water & air cooling		36	92.4
		37	91.0
		42	96.2
Water cooling		49	91.3
		60	97.9
Submersion cooling	3 hours	47	74.5
	8 hours	43	92.9
	repeatedly	65	95.2
Pot cooling - covered		44	-
Pot cooling - open		62	-

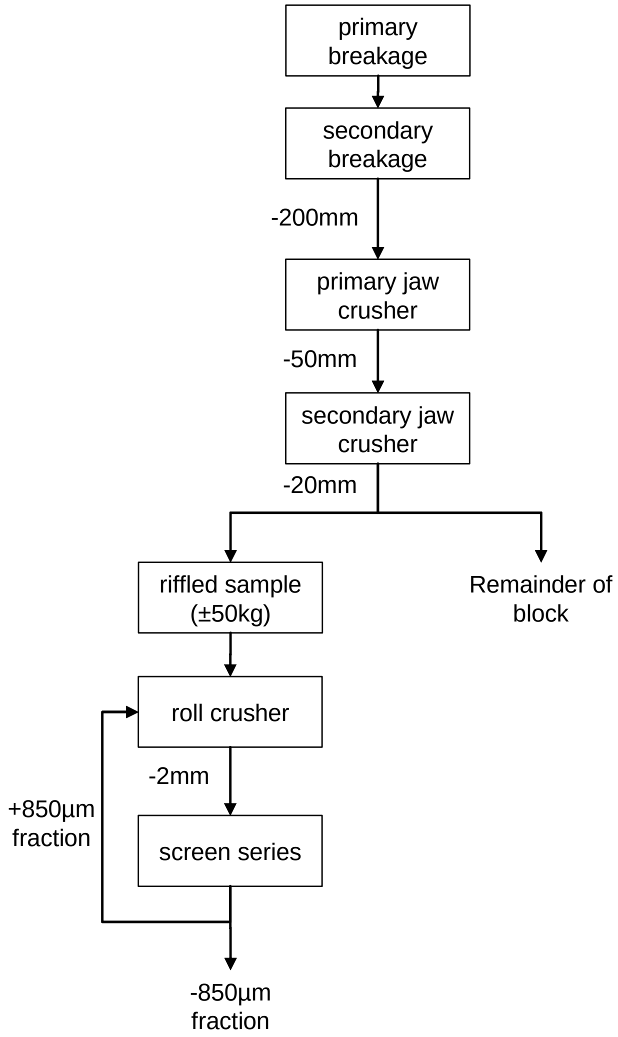

Figure 13 Block diagram showing the breaking and crushing procedure of the Campaign 9 blocks.

Statistical analysis was used to identify parameters which played a significant role in determining the final particle size distribution of the slag (as opposed to accurately predicting the absolute extent of fines generation and/or the residual coarse fraction). However, due to the limited number of blocks available, traditional statistical analysis could not be used. Statistical linear regression analyses were consequently applied to predict the *relative rating* of the blocks with regard to fines generation and residual coarse material[**]. From these ratings, parameters significant to particle size were identified, with their relative importance.

In order to test the validity of the relative importance of the statistically identified parameters, the actual relative rating of a block (in terms of fines generation and residual coarse mass) was compared with its rating as predicted by the regression coefficients. The difference between these two sets of ratings was quantified with a root-mean-square error (rms error) - a low rms error hence indicating a close correspondence between the actual and predicted ratings of the

---

[**] The residual coarse fraction is indicative of a higher or lower mill circulating mass, which in turn implies a higher or lower probability of generating more fines. This is termed “indirect” fines generation, in this study.

specific parameters and their relative importance. The coefficient of determination (r^2) of the regression analysis was considered to be of secondary importance (relative to the rms error).

Potential parameters which could influence fines generation and the residual coarse mass were identified based on two proposed hypotheses: (i) the final particle size distribution is a function of the block solidification structures, and (ii) the particle size distribution is a result of oxidation effects.

Should solidification structures play a role in slag breakage, evidence of intergranular breakage is expected. This could result in liberation of the silicate phases typically found between M_3O_5 grains. The parameter (SiO_2+$Al_2O_{3\ \mathrm{glass}}$+CaO)[††] was therefore included in the analysis.

Should oxidation effects play a role, the block cooling method, specific area of the block, and block chemistry (composition) should be considered:

- Whereas in the previous section block yield was used to quantify the fines generated *during cooling* (i.e. the extent of decrepitation), block yield was used in this context to quantify the effect of the cooling method on the fines generation during *crushing and milling*.

- The specific surface area of the block was calculated by approximating the block surface as the sum of a spherical cap and a truncated cone, and dividing this surface area by the block volume. Due to the mass loss of the blocks during cooling, the specific surface areas of the blocks both before (as tapped) and after cooling were considered.

- Since FeO, TiO_2 and Ti_2O_3 are interrelated, the equivalent %Ti_2O_3 (calculated as per equation (2)[26], which is for analyses in mass percentages), was selected to represent the composition of the block. The Ti_2O_3 (Ti^{3+}) content of the slag is determined through a wet chemistry technique (Appendix 5.1). The correlation between FeO and Ti_2O_3 as determined from XRF and wet chemistry analyses during Campaign 9 is shown in Figure 14. Since only XRF analyses were done on the 11 blocks used in this investigation, the correlation as shown in Figure 14 was used to calculate the corresponding %Ti_2O_3 of the specific blocks.

$$\begin{aligned}(\%Ti_2O_3)_{eq} &= \%Ti_2O_3 + \%V_2O_5\left(\frac{M_{Ti_2O_3}}{M_{V_2O_5}}\right)\\ &\quad +\%Cr_2O_3\left(\frac{M_{Ti_2O_3}}{M_{Cr_2O_3}}\right)+\left(\%Al_2O_3-\frac{\%SiO_2}{3}\right)\left(\frac{M_{Ti_2O_3}}{M_{Al_2O_3}}\right)\end{aligned} \tag{2}$$

[††] The (SiO_2+$Al_2O_{3(\mathrm{glass})}$+CaO) content of the slag combines to form the glassy and crystalline silicate phases in the solidified slag. Some of the Al_2O_3 reports to the M_3O_5 solid solution where it replaces the Ti^{3+} atoms, while the remainder reports to the silicate phases. An amount of Al_2O_3 equal to a third of the SiO_2 content is assumed to report to the glass phase.

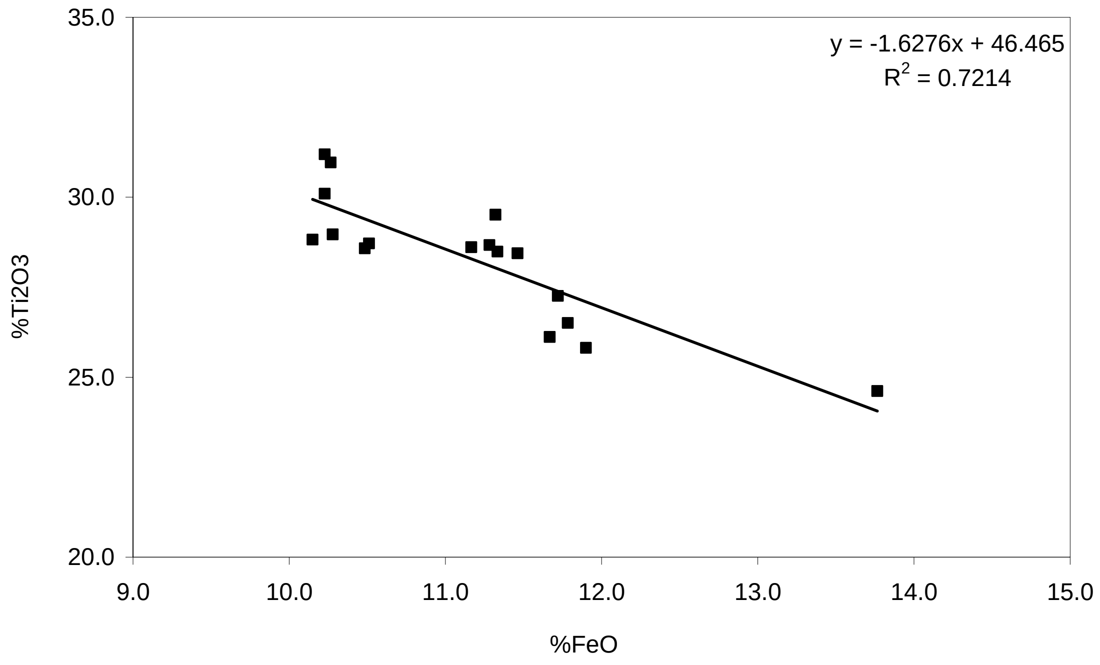

Figure 14 Correlation between FeO and Ti_2O_3 as analysed during the Campaign 9 trials.

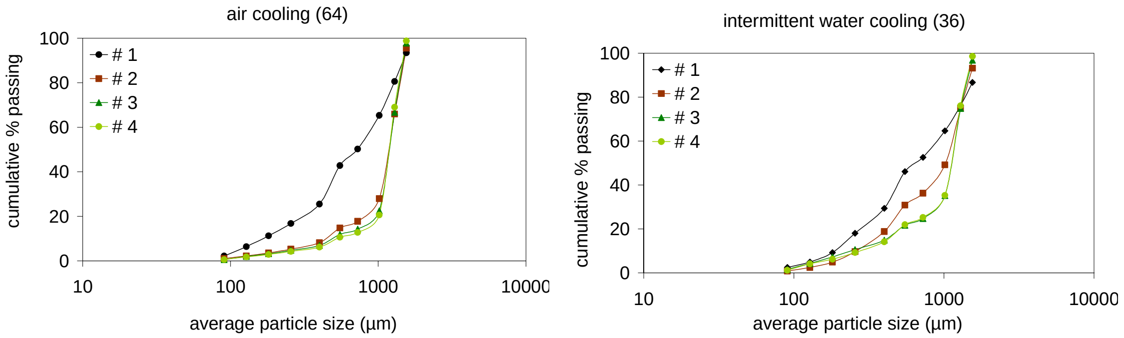

(a)

(b)

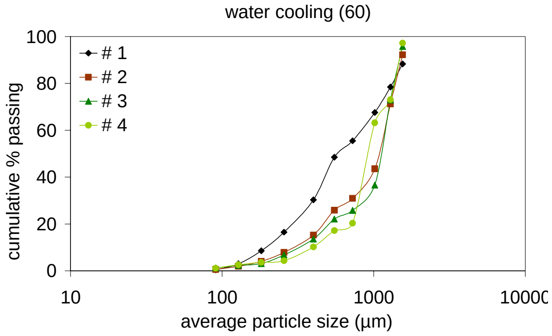

(c)

Figure 15 Particle size distributions of material in the crushing & milling trials: (a) air cooled block; (b) intermittently water-cooled block, and (c) continuously water-cooled block. Tap numbers are indicated in brackets in graph headings. Numbers 1 to 4 indicate the change in size distribution following initial crushing (nr 1), and three subsequent steps of recirculating oversize (nr 2 to 4).

2.3.2 Results

The particle size distributions of the product during the four milling steps of the air cooled block are shown in Figure 15. The -106 µm vs. +850 µm mass fractions have a linear log-log correlation (Figure 16). The majority of the fines are generated in the first step of milling. The absolute number of fines generated and residual coarse fraction shift slightly towards lower values from the second to the fourth milling steps.

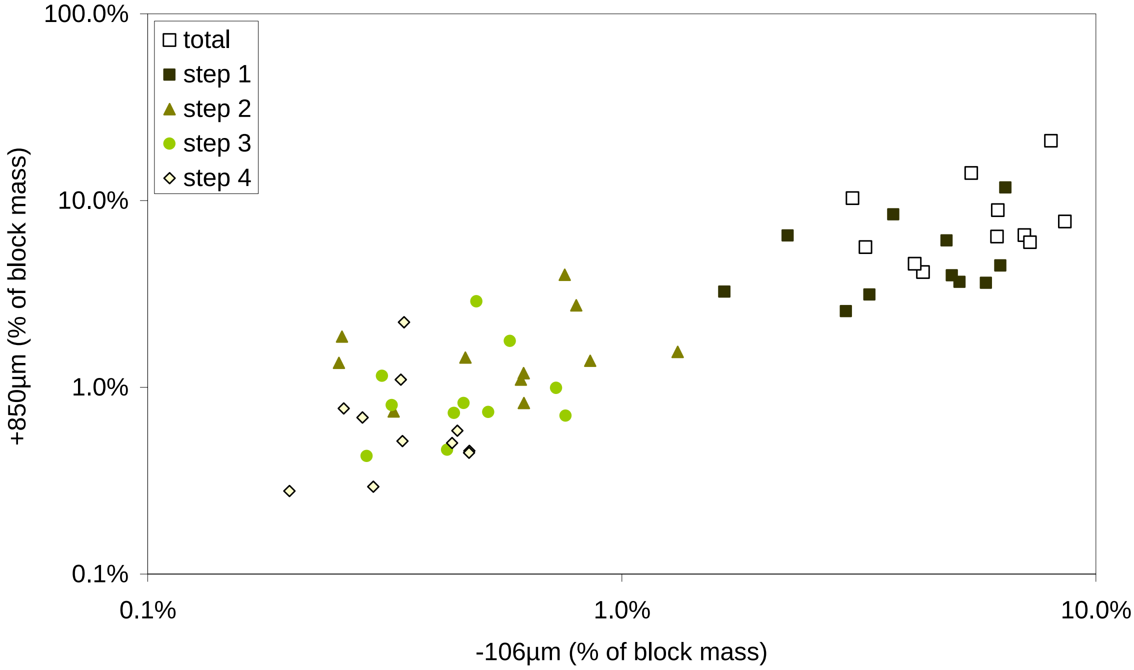

Figure 16 -106µm vs. +850µm mass percentages of the Campaign 9 crushed blocks.

2.3.2.1 **Fines generation (-106 µm size fraction)**

The cumulative fines generated for each block, arranged from worst to best (least), are shown in Figure 17. The intermittently water-cooled and air-cooled blocks cover the worst end of the graph, while the pot-cooled blocks and repeatedly submerged block yielded the smallest amount of fines.

Statistical linear regression analysis on the total amount of -106 µm material generated during milling and several parameters generated the correlation coefficients as shown in Table 3. (A complete list of all parameters which were tested for correlation is given in Appendix 5.2. These statistical results should be interpreted bearing in mind that only 11 blocks were used in the analysis.) Significant improvements of the correlation coefficients were observed in some instances when omitting one or two blocks from the regression analysis. This effect was interpreted as indicative of the presence of a dominant factor with regard to fines generation in the omitted block.

The correlation coefficient between the fines generated and the (SiO_2+$Al_2O_{3(glass)}$+CaO) content of the slag is 0.717. This number increases to 0.774 and 0.787 when excluding water-cooled block 49 and intermittent water-cooled block 36. Excluding both these blocks increased the value of the correlation coefficient to 0.836. The positive sign of the correlation coefficient indicates a direct linear correlation between the (SiO_2+$Al_2O_{3(glass)}$+CaO) content and fines generated. The fines generated per block is shown in Figure 18 in order of increasing (SiO_2+$Al_2O_{3(glass)}$+CaO). The average fines generated appears to be lower for blocks with (SiO_2+$Al_2O_{3(glass)}$+CaO) contents below 1.93% (the four blocks on the left in Figure 18) when compared with the average fines generated from the remainder of the blocks.

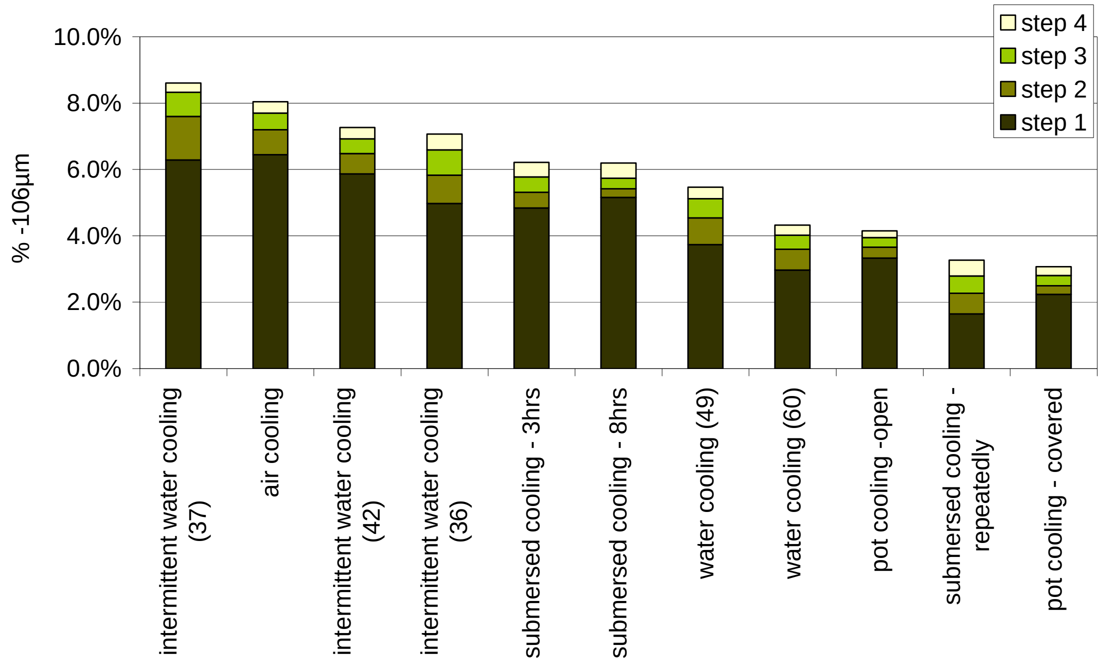

Figure 17 Mass percentage fines generated (-106 µm fraction) per milling step 1 to 4, shown per cooling method (tap numbers are shown in brackets), arranged from worst to least fines generation.

Table 3 Correlation coefficients of parameters affecting the fines generation during crushing & milling.

Variable	Correlation coefficient (including all 11 blocks)	Best correlation coefficient	Exclusions
$\%SiO_2+Al_2O_{3(glass)}+CaO$	0.717	0.774	Water cooled (49)
		0.787	Intermittent water cooled (36)
		0.836	water cooled (49) & intermittent water cooled (36)
Tapping rate[‡‡]	-0.353	-0.733	Covered pot cooled (44)
		-0.728	Intermittent water cooled (37)
Block yield	-0.280	-0.492	Intermittent water cooled (37)
Equivalent $\%Ti_2O_3$	0.109	0.367	Air cooled block (64)
Specific surface area – cooled block	0.278	0.624	Intermittent water cooled (37)
		0.481	Covered pot cooled (44)
Specific surface area – as tapped block	0.051	0.256	Intermittent water cooled (37)

[‡‡] The tapping rate was calculated by dividing the as tapped block mass (in kg) by the total tapping time (in minutes). The total tapping time was calculated as the time difference between opening (observing the first slag flow) and closing of the taphole).

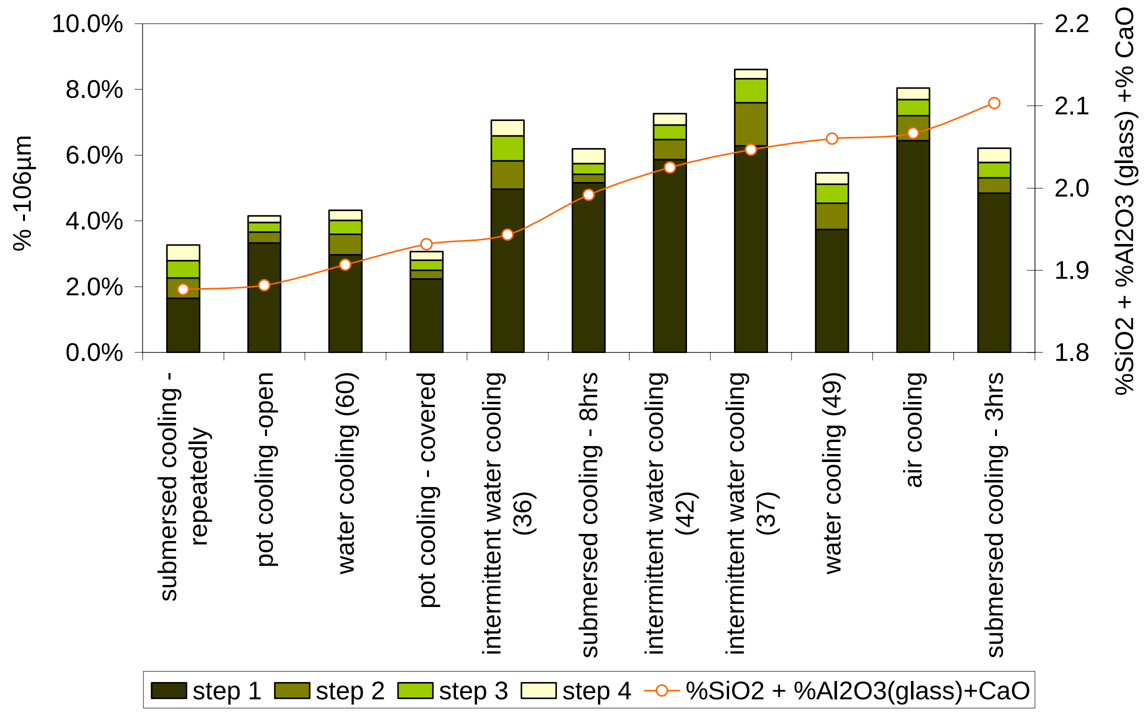

Figure 18 Mass percentage fines generated (-106 µm) ordered with increasing ($\%SiO_2+Al_2O_{3(glass)}+CaO$).

Exclusion of the covered pot 44 and intermittently water-cooled pot 37 increases the correlation coefficient between the fines generated and the tapping rate from -0.353 to -0.733 and -0.728 respectively. The negative sign of the coefficient indicates an indirect correlation – higher tapping rates correlate with reduced fines generation. The fines generation ordered with increasing tapping rate is shown in Figure 19.

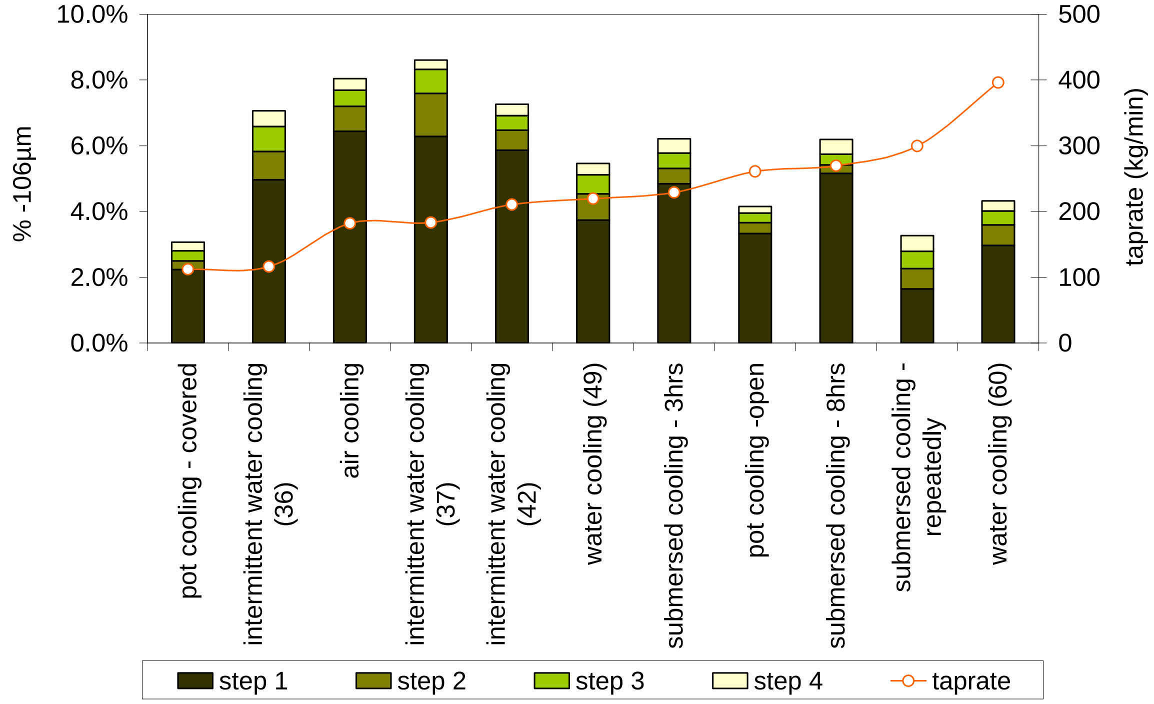

Figure 19 Mass percentage -106µm generated shown against increasing tapping rate.

Correlation coefficients between the fines generated and the block yield and %Ti_2O_3 respectively were low (Table 3). Of potential value, however, is the sign of these correlation coefficients: an indirect correlation between the fines generated and the block yield indicates that good cooling method practices have a positive influence on reducing fines generation. The maximum coefficient (obtained when excluding air cooled block 64) between %Ti_2O_3 and fines generation is positive. However, its sign changes to negative when either intermittently water-cooled block 37 or the covered pot block is excluded from the analysis, so the effect is not clear.

The correlation coefficients between the fines generated and the two different specific block surface areas are also low – in particular that for the as-tapped block (Table 3). However, the coefficient increases significantly – from 0.278 to 0.624 - for the cooled block when omitting the intermittently water-cooled block 37. Of possible significance when considering the difference in correlation coefficients of the two specific surface areas is the time lapse of approximately four months between the blocks being tapped and their actual breaking, crushing and subsequent particle size determination.

Regression analysis including the glass phase content (SiO_2+$Al_2O_{3(glass)}$+CaO) and tapping rate only resulted in an rms error between the actual and predicted relative ratings of the blocks of 2.5 and a coefficient of determination (r^2) of 0.53. Including the %Ti_2O_3, block yield and specific surface area after cooling into the regression analysis reduced the rms error to 1.4, with a coefficient of determination (r^2) at 77.2% indicating that the fines generation of between 8 and 9 of the 11 blocks could be explained by the five block attributes (SiO_2+$Al_2O_{3(glass)}$+CaO), tapping rate, block yield, equivalent %Ti_2O_3 and specific surface area after cooling – in this order of importance. A comparison of the worst to best relative position of the actual and regression results is shown in Table 4.

Table 4 Comparison of the experimental worst to best ranking and that predicted by the regression model when including the (SiO_2+$Al_2O_{3(glass)}$+CaO), tapping rate, block yield, specific surface area after cooling and equivalent %Ti_2O_3.

Cooling method and block number		Experimental rating	Regression model rating	Deviation in relative rating
air cooling	64	10	9	-1
water & air cooling	36	8	8	0
water & air cooling	37	11	11	0
water & air cooling	42	9	7	-2
water cooling	49	5	5	0
water cooling	60	4	4	0
submersion cooling - 3hrs	47	7	10	3
submersion cooling - 8hrs	43	6	6	0
submersion cooling – repeatedly	65	2	2	0
pot cooling – open	62	3	1	-2
pot cooling - covered	44	1	3	2
Root-mean-square (rms) error				1.4

2.3.2.2 **Residual coarse material (+850 µm size fraction)**

The residual coarse mass (after four milling passes) is shown in Figure 20, arranged in order from worst (highest) to lowest. A larger amount of residual coarse material is viewed as undesirable, since such material would circulate to be recrushed, in the industrial plant. Such circulation is expected to increase the proportion of fine material; this is termed "indirect fines generation" in this work, in contrast with "direct fines generation", which refers to the fine material which forms during initial crushing. The order of blocks in Figure 20 differs substantially from that in Figure 17 (which is the corresponding graph for the fines generated). It therefore appears that the parameters influencing fines generation differ from those influencing the residual coarse mass, and/or the relative importance of the parameters differs for the two size fractions.

The correlation coefficients between the residual coarse mass and six potential parameters are shown in Table 5 (a complete list of all parameters considered is shown in Appendix 5.2).

The specific surface area of the cooled block has a significant correlation coefficient of 0.846 which increases to 0.915 when air-cooled block 64 is omitted. The positive sign of the coefficient indicates a tendency for more residual coarse mass with increasing specific surface area. The residual coarse fractions arranged in order of increasing specific surface area of the cooled blocks are shown in Figure 21. The increase in the correlation coefficient between the specific surface area of the *tapped* block and the residual coarse mass with the exclusion of the air-cooled block 64, is more likely due to the interdependency between the two different surface areas.

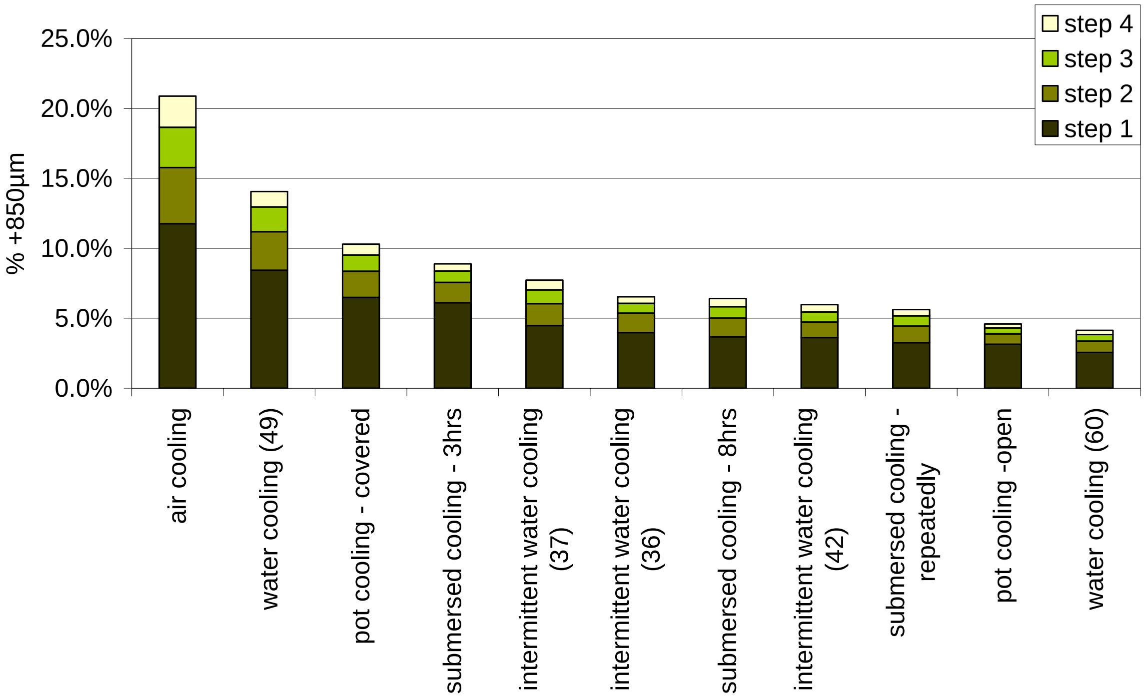

Figure 20 Mass percentage residual coarse fraction (+850µm) ordered from worst to best.

Table 5 Correlation coefficients of independent variables affecting the residual coarse fractions during crushing. The best correlation coefficients were obtained by excluding the blocks named in the right hand column.

Variable	Correlation coefficient (all 11 blocks analysed)	Best correlation coefficient	Exclusions
Specific surface area – cooled block	0.846	0.915	Air cooled (64)
Specific surface area – as tapped block	0.242	0.901	Air cooled (64)
Block yield	-0.807	-0.924	Water cooled (49)
		-0.866	Open pot cooled (62)
%SiO_2+$Al_2O_{3(glass)}$+CaO	0.591	0.666	Water & air cooled (37)
		0.634	Covered pot cooled (44)
Tapping rate	-0.415	-0.539	Water & air cooled (36)
Equivalent %Ti_2O_3	-0.263	-0.488	Water cooled (49)

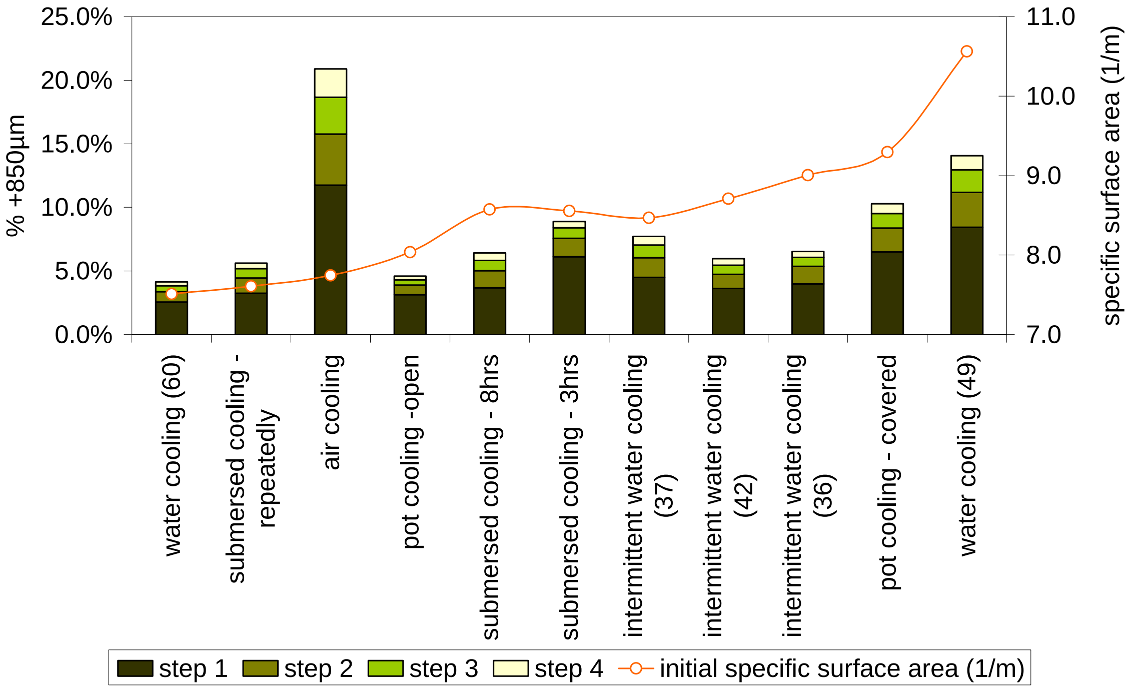

Figure 21 Residual coarse fractions arranged in order of increasing specific surface area of the blocks – after cooling.

The cooling method as quantified by the block yield has a correlation coefficient of -0.807 with the residual coarse fraction. Omitting water-cooled block 49 and the open-pot-cooled block 62, the coefficient increases to -0.924 and -0.866 respectively. The negative sign of the coefficient indicates and indirect correlation - less residual coarse mass is associated with higher block yields. The residual coarse fraction from each block arranged in order of increasing block yield is shown in Figure 22.

The correlation coefficients between the residual coarse mass and the three parameters: glass phase, tapping rate and %Ti_2O_3, showed lower and insignificant values – even when omitting seemingly outlying blocks. The residual coarse fractions arranged in order of increasing parameter are shown in Figure 23, Figure 24 & Figure 25.

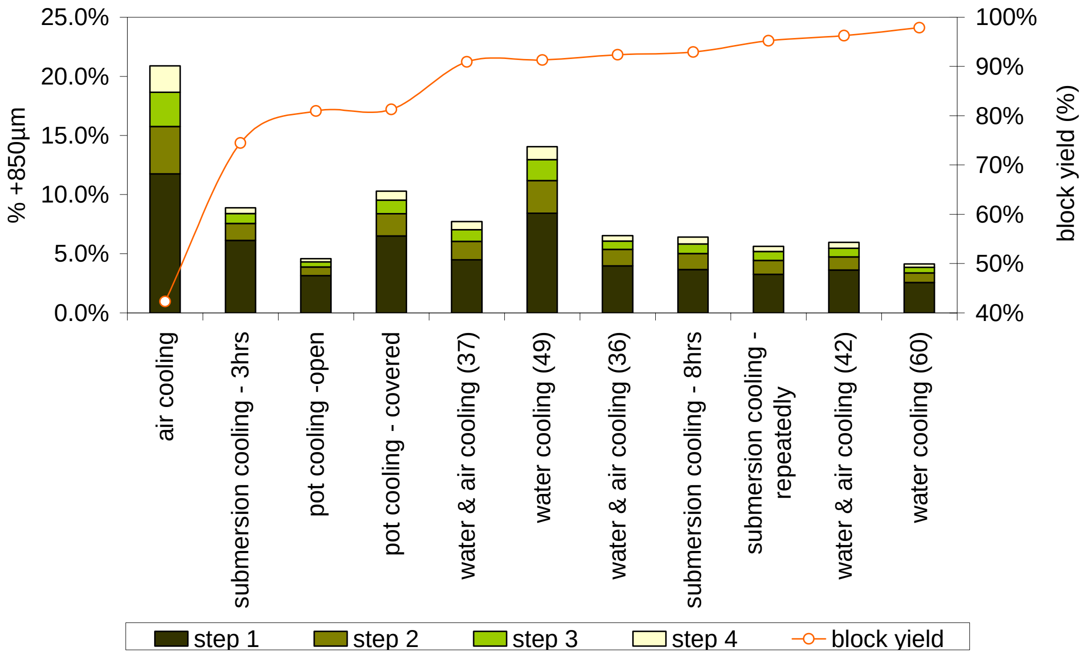

Figure 22 Residual +850 µm with increasing block mass yield.

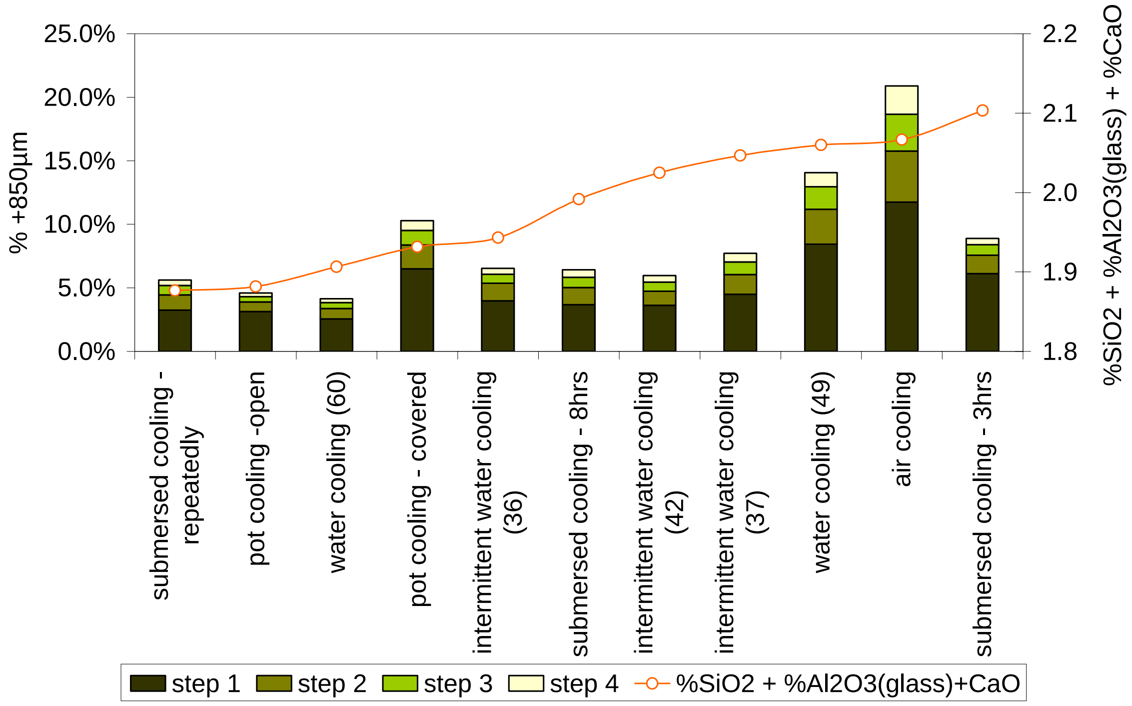

Figure 23 Residual coarse fraction arranged in order of increasing (SiO_2+$Al_2O_{3(glass)}$+CaO).

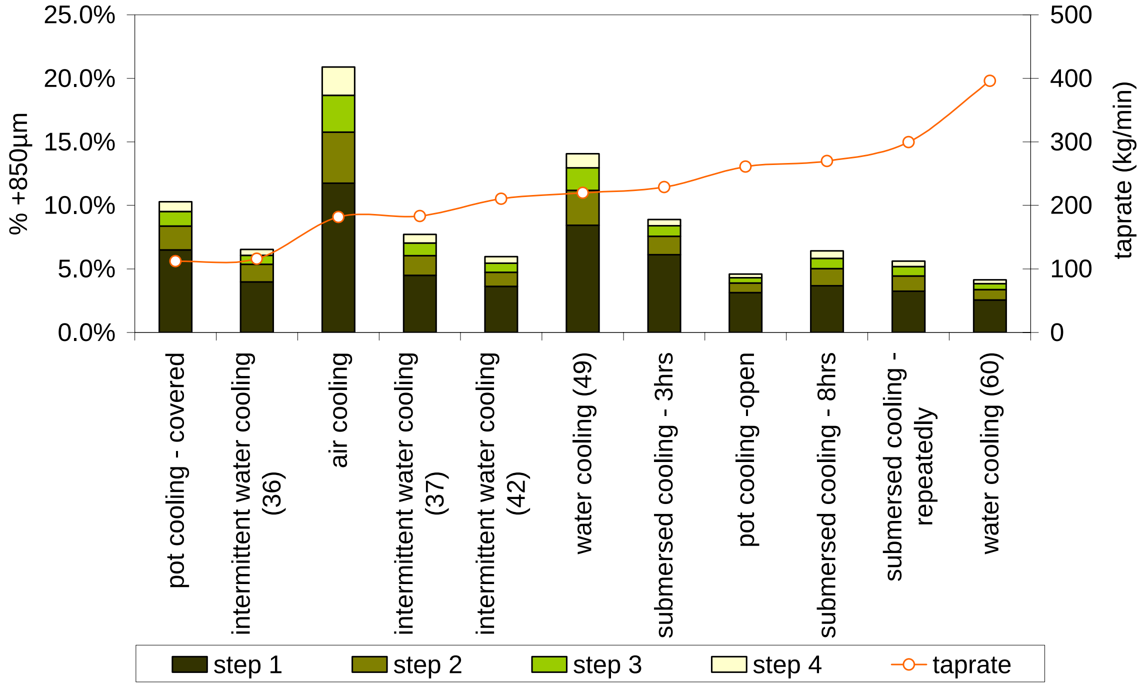

Figure 24 Residual coarse fraction arranged in order of increasing tapping rate.

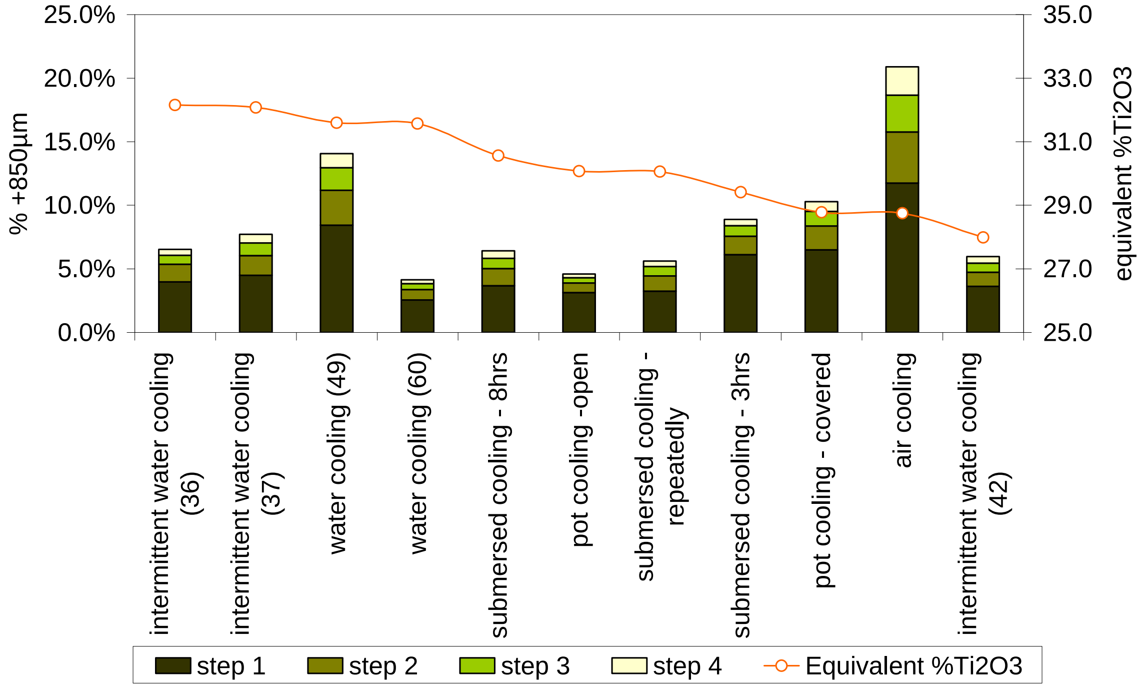

Figure 25 Residual coarse fraction arranged in order of increasing equivalent Ti_2O_3.

Similar to the parameter testing with fines generation, the actual relative order of the blocks with regard to residual coarse mass was compared with that predicted by the regression analysis. Including only the specific surface area after cooling and the block yield in the regression analysis resulted in an rms error of 1.7. (The coefficient of determination of the regression analysis r^2, was 0.860; hence explaining the residual coarse mass for 86% of the blocks – between 9 to 10 of the 11 blocks.) Although the best improvement in the coefficient of determination (reaching 0.885) results from including all five parameters block yield, specific surface area after cooling, tapping rate, (SiO_2+$Al_2O_{3(glass)}$+CaO) and equivalent %Ti_2O_3, the rms error for this combination is 2.0. The lowest rms error results from the combination block yield, specific surface area after cooling and (SiO_2+$Al_2O_{3(glass)}$+CaO) – 1.5 with a coefficient of determination of 0.863. The comparison between the actual worst to best order and the predicted worst to best order from the regression analysis which included the latter three parameters is shown in Table 6.

Table 6 Comparison between the actual worst to best order and the predicted order (including the block yield, specific surface area after cooling and glass phase variables).

Cooling method and block number		Experimental ranking	Regression model ranking	Deviance in relative rating
air cooling	64	11	11	0
water & air cooling	36	6	7	1
water & air cooling	37	7	5	-2
water & air cooling	42	4	3	-1
water cooling	49	10	10	0
water cooling	60	1	1	0
submersion cooling - 3hrs	47	8	9	1
submersion cooling - 8hrs	43	5	4	-1
submersion cooling – repeatedly	65	3	2	-1
pot cooling - open	62	2	6	4
pot cooling - covered	44	9	8	-1
Root-mean-square (rms) error				1.5

2.3.3 Conclusions

Dominant parameters influencing the *fines generation* (-106 µm) in order of importance, starting with the most important, are therefore concluded to be:

- The amount of glass phase (SiO_2+$Al_2O_{3(glass)}$+CaO);
- Tapping rate;
- Cooling method as quantified by the block yield;
- Specific surface area of the block after cooling, and
- Block composition as represented by the %Ti_2O_3.

The amount of glass phase present and tapping rate explain the fines generation of approximately half of the blocks. Including the other three parameters - specific surface area after cooling, block yield and equivalent %Ti_2O_3 increases the accuracy of the linear regression analysis to 79% (accurately predicting the relative rating of between 8 to 9 of the 11 blocks). The root-mean-square (rms) error between the actual rating of worst to best performance compared to similar predicted order is 1.5.

The dominant parameters influencing the *residual coarse mass* (+850 µm after four milling passes) in order of importance; starting with the most important, are concluded to be:

- Specific surface area of the block after cooling;
- Cooling method as quantified by the block yield;
- The amount of glass phase (SiO_2+$Al_2O_{3(glass)}$+CaO);

- Tapping rate, and
- Block composition as represented by the %Ti_2O_3.

The specific surface area after cooling, and block yield, explain the residual coarse fractions of 86% (between 9 to 10 out of 11) of the blocks. The inclusion of (SiO_2+$Al_2O_{3(glass)}$+CaO), tapping rate and equivalent %Ti_2O_3 improves the root-mean-square error of the actual vs. predicted orders and/or the coefficient of determination (r^2) slightly - e.g. improving the rms error from 1.7 to 1.5 when including the glass phase, or increasing the r^2 from 0.86 to 0.89 when including all five parameters.

2.3.3.1 **Slag composition and mineralogy**

Excluding the air-cooled block 64 from the analysis results in a negative correlation coefficient between the %Ti_2O_3 and residual coarse mass. However, inclusion of air-cooled block 64 in the analysis yields a positive coefficient. Similar dual behaviour of the %Ti_2O_3 is seen with fines generation. The dual behaviour of slag composition – as represented by the equivalent %Ti_2O_3 – suggests that the composition is of secondary importance with regard to direct and indirect fines generation.

As in the case of fines generation, the sign of the coefficient between the glass phase and the residual coarse mass is positive. A higher glass phase therefore results in more fines generation, both directly and indirectly (the latter via a higher circulating load). The importance of the glass phase indicates that the generation of fines (directly and indirectly) occurs through a mechanism which is associated with the solidification structure.

2.3.3.2 **Tapping rate**

The sign of the correlation coefficients between fines generation and tapping rate indicates a tendency for decreased fines generation due to higher tapping rates; while the coefficient between residual coarse mass and tapping rate indicates potential for an increase in fines generation due to a higher circulating load. The effect of tapping rate is presumed to operate through one or both of the following mechanisms:

- Lower tapping rates are characterised by increased oxygen lancing by the tapping personnel (in an attempt to improve the flow). This action in itself creates an oxidising atmosphere.

- Lower tapping rates result in spraying tap streams – creating an increased specific slag surface area which is exposed to air while the slag flows from the launder into the pot. Due to the high slag temperatures at this stage (1600 °C – 1720 °C), oxidation is highly likely.

Should either or both of the two mechanisms occur – which is regarded as highly likely due to the high temperatures and excess oxygen present– the link between tapping rate, and fines generation and residual coarse fraction, is based on an oxidation mechanism. Oxidised slag will contain more rutile in the solidified microstructure (as discussed in section 1); it appears that this favours fines formation.

2.3.3.3 **Block surface area**

The oxidation hypothesis is supported by the inclusion of the specific surface area after cooling, and the cooling method, amongst the important parameters for both fines generation and residual coarse fractions: further oxidation is expected to occur during the cooling period while the surface is still at relatively high temperatures. The significant difference between the correlation coefficients of the specific surfaces of the as "tapped surface" and the "after cooling surface", combined with the four-month time lapse between the tapping and breaking activities suggests the possibility that oxidation at low temperatures (< 200 °C) may also affect fines generation. This was studied further, and the results are reported in section 3.7.

The influence of the three parameters, slag mineralogy, tapping rate and block surface area, is discussed further in Part 2 of this document.

3 Part 2: Plant Trials

3.1 Background

From Part 1 parameters affecting the generation of fines (-106µm fraction) appear to be the amount of silicates (SiO_2+$Al_2O_{3(glass)}$+CaO) in the slag, tapping rate, the cooling method (block yield), specific surface area after cooling and the equivalent %Ti_2O_3. Similarly the residual coarse material (+850µm fraction) appears to depend primarily on specific surface area after cooling, and on block yield. The objective of the plant (industrial) trials was therefore to test these observations from the pilot-plant trials with regard to the effects of the tapping rate, cooling method and slag composition. A further objective of the plant trials was to gain further insight into the mechanism(s) driving final slag product particle size distributions.

The flexibility of parameters needs to be understood in context of the plant constraints: the (SiO_2+$Al_2O_{3(glass)}$+CaO) is a function of the orebody and to a limited extent of the upstream beneficiation processes. The specific surface area of the block is a function of the block shape and mass. These two parameters are determined by the slag pot shape and capacity – therefore this is not a controllable variable within the logistics of the existing plant either, at least not without extensive capital re-investment. The slag Ti_2O_3 content is a function of the required %TiO_2 set by market specifications and the ilmenite quality fed (and the ilmenite quality in turn is a function of upstream beneficiation and the orebody). Of the above variables tapping rate, and to an extent the cooling method and ilmenite quality, are thus the only controllable (or partially controllable) parameters within the capabilities of the existing plant design.

3.2 Block selection

Four blocks were selected for the plant trials – two blocks from the same tap having individual tapping rates of 3.63 t/min and 3.70 t/min respectively, and two more blocks from another tap, having relatively low tapping rates of 0.96 t/min and 1.29 t/min respectively. (Typical tapping rates on the industrial plant vary from 0.5 t/min to 4 t/min). Selecting the four blocks from two taps enabled a narrower spread in the compositional differences between the four blocks. The compositions and tapping rates of the four blocks are shown in Table 7. The %Ti_2O_3 was calculated from the correlation shown in Figure 26. The linear equation on the left hand side of Figure 26 is derived from the plant data, while the right hand side equation represents the pilot plant data.

Following tapping, the four blocks were initially left to cool in the pots, with natural air cooling only. After this primary cooling period of 17 to 19 hours, the blocks were tipped out of the pots, transported to the block yard and water cooled with spray water. After 3 days the water sprays of lane 1 (L1 blocks) were closed and the block surface temperatures were recorded using a manual optical pyrometer (see results in Figure 27). In lane 2 (L2 blocks) the water sprays were left on for the full 10 days. Unfortunately, due to windy conditions, water was occasionally sprayed from lane 2 over into lane 1, causing the lane 1 blocks to receive limited cooling water, while the side of the lane 2 blocks (facing the oncoming wind) lost its water cooling.

Table 7 Details of the four blocks selected for the plant trials.

Block number	Tapping rate (ton/min)	%FeO (equivalent %FeO)	Equivalent %TiO$_2$	%Ti$_2$O$_3$ (calculated) (equivalent %Ti$_2$O$_3$, calculated)	%(SiO$_2$+ Al$_2$O$_{3(glass)}$+ CaO)	Cooling method (wc: water cooling; ac: air cooling)
L1R9	3.64	9.90 (13.43)	86.42	30.68 (32.16)	1.638	3 days wc 7 days ac
L2R9	3.70	10.04 (13.58)	86.17	30.45 (31.92)	1.643	10 days wc
L1R11	0.96	10.35 (13.92)	86.43	29.95 (31.44)	1.678	3 days wc 7 days ac
L2R11	1.29	10.45 (14.01)	86.31	29.78 (31.28)	1.671	10 days wc

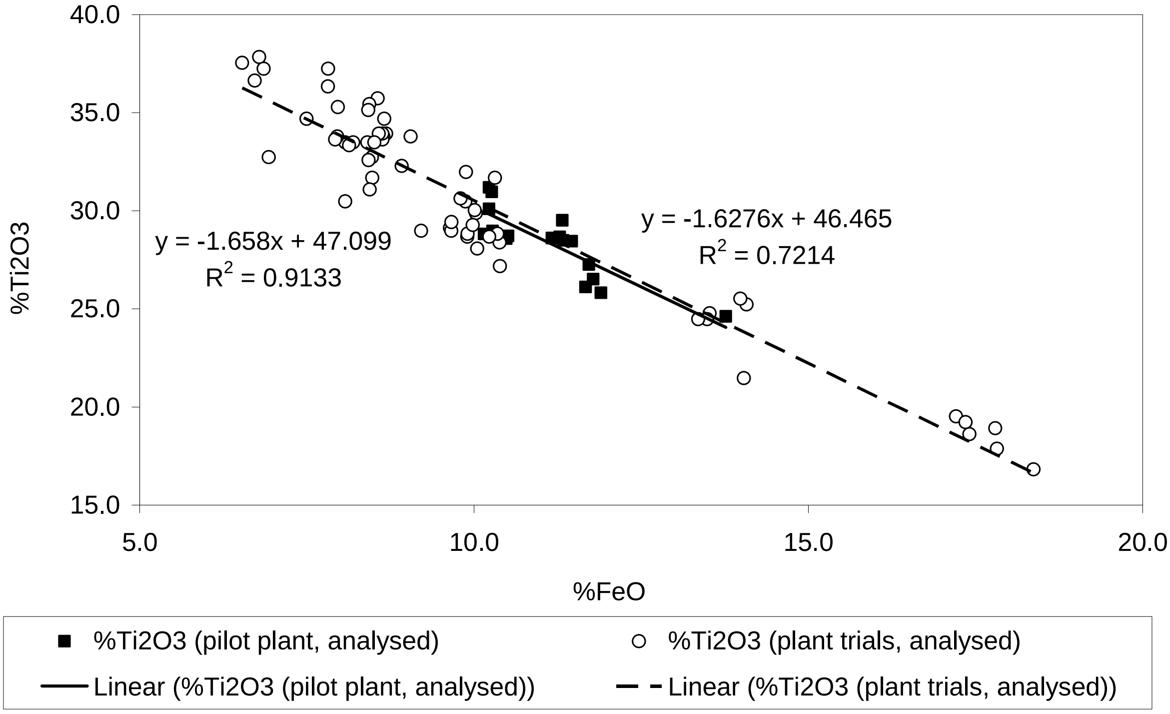

Figure 26 Correlation between %FeO and %Ti$_2$O$_3$ for pilot plant slags (solid squares and line; equation on right hand side) and plant slags (open circles and dotted line; equation on left hand side).

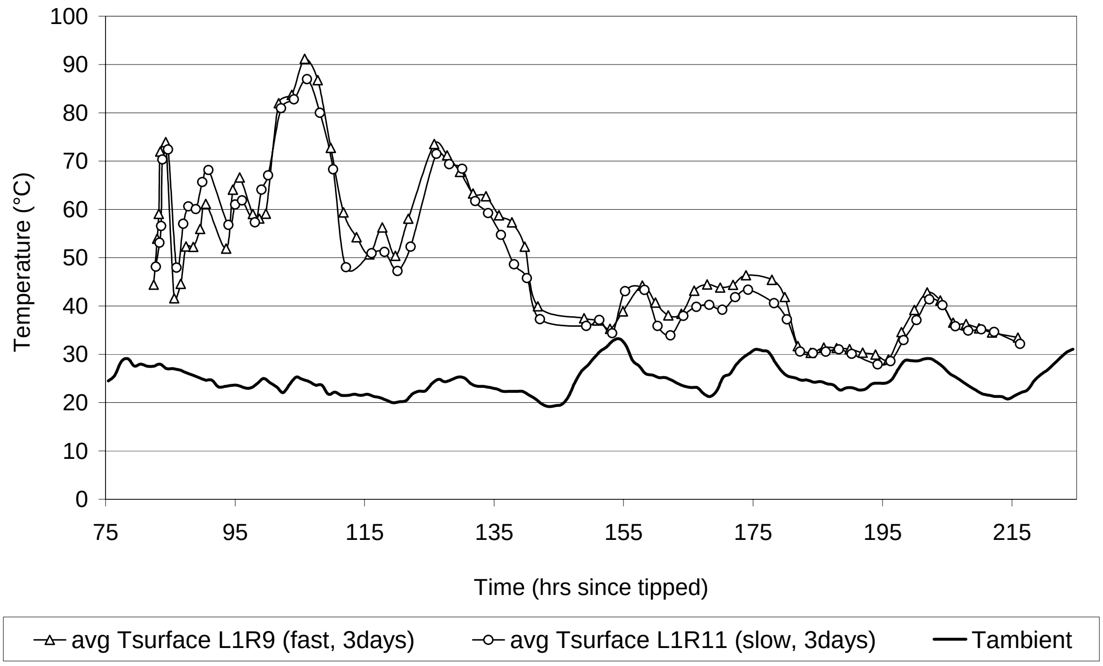

Figure 27 Average surface temperature of blocks L1R9 and L1R11 after closure of the cooling water.

Figure 28 Photograph of an industrial-size block showing fine decrepitated material and large chunks breaking off from the block corners. As an indication of scale, the bottom diameter of the block is approximately 1.8 to 2 m.

During the 10 days of cooling, limited decrepitation occurred with all four blocks. In addition, relatively large chunks – from 10 mm up to 400 mm – broke off from the block corners. Both these two types of block yard remains are visible in Figure 28. After 10 days of cooling, the intact part of all four blocks was broken individually with the hydraulic hammer. The -400 mm fraction passed through the static grizzly to the jaw crusher with a closed side setting of

-45 mm. The jaw crusher product was passed over a 50 mm screen with the oversize fraction being circulated back to the jaw crusher. The undersize (and day bin feed) was sampled with a hammer sampler and sent to the Exxaro Research and Development laboratories for further testwork. Care was taken to run the equipment clean between processing the four blocks. (Refer to Figure 1 for a block diagram of the Slag Plant process flow). The particle size distributions of the block yard remains and jaw crusher product for the four blocks are shown in Figure 29 and Figure 31 respectively.

Since no mass measurement facility exists between the block yard and the first point of entry into the Slag Plant (static grizzly), no mass measurement of the blocks was done at this point.

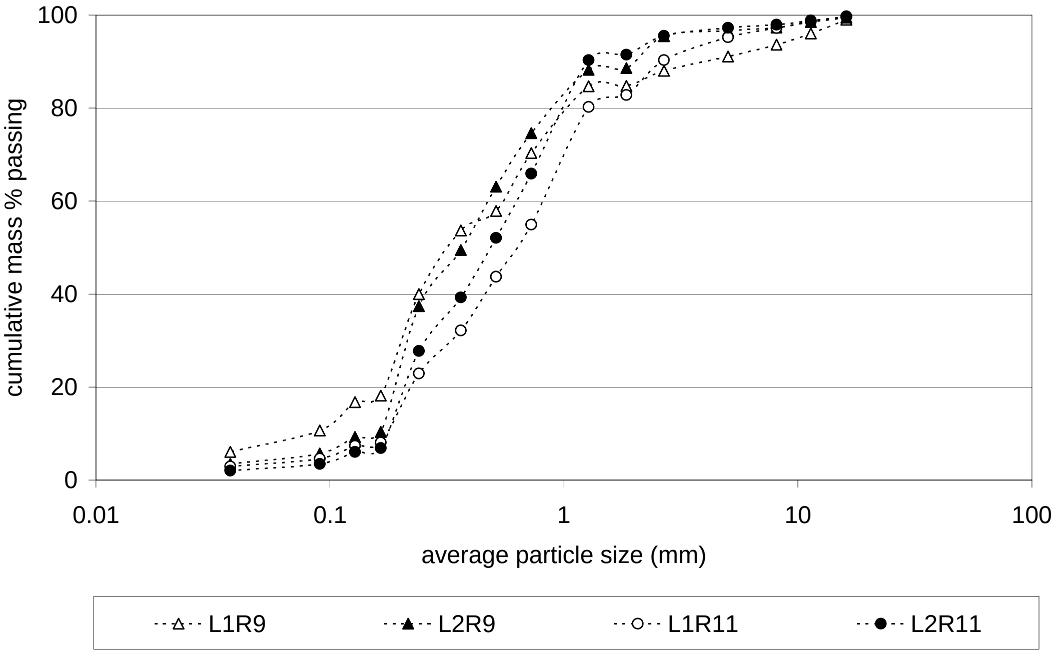

Figure 29 Particle size distribution of the block yard remains – decepitated material and coarser broken-off sections.

3.3 Tumbling tests

Tumbling tests were used to determine the tendency of the slag to break down due to abrasion between slag particles. This form of breakdown typically occurs during materials handling – mainly at transfer points and mass movement within bins of the plant.

Particle breakdown during materials handling within the plant is not problematic in itself; however, when this breakdown increases the fines fraction (-106 µm) of the slag, it reduces the ratio of higher vs. lower value product produced from the plant. On the other hand, any coarse material (+850 µm) resisting breakdown (either during handling, crushing or milling according to the process (Figure 1), increases the need for higher circulating loads which in turn increases the opportunity for indirect fines generation.

A sample with good tumbling characteristics will therefore show some breakdown, but the size distribution would tend to stabilise after a certain degree of tumbling, with little further breakdown. The fines generated at this point must ideally be as low as possible. Good tumbling characteristics will furthermore be seen where the coarse material breaks down to below 850 µm within the very first material handling steps.

3.3.1 Method

In the first series of tests, five 15 kg sub-samples were riffled from the samples taken as described in section 3.2 and autogenously tumbled for 100, 200, 500, 1000 and 2000 revolutions each. The tumbling mill had an internal diameter of 1,000 mm and an internal length of 500 mm. Two steel angle lifters were positioned 180° apart longitudinally on the inside of the drum. The rotation speed of the drum was 25±1 rpm. The particle size distribution for each sample was determined before and after each test utilising the Canadian Standard Sieve Series[25] between 45 mm and 75 µm. Figure 30 shows the feed and product size distributions for block L1R11 (slow tapping rate, 3 days water cooling); significant variance is apparent in the particle size distributions of the samples taken from each of the four blocks.

The average particle size distribution for each block together with a 90% confidence interval for each size fraction is shown in Figure 31. The particle size distributions of blocks L1R9 (higher tapping rate, 3 days water cooling) and L1R11 (low tapping rate, 3 days water cooling) differ significantly, with those of blocks L2R9 (higher tapping rate, 10 days water cooling) and L2R11 (low tapping rate, 10 days water cooling) being very much the same.

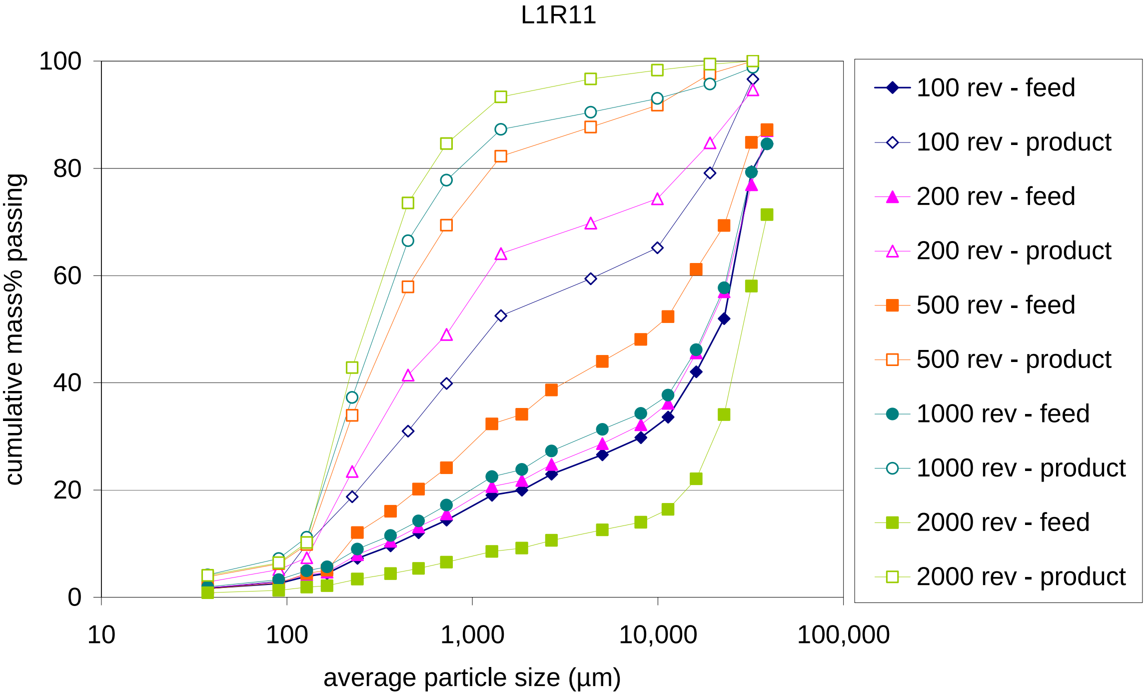

Figure 30 Particle size distribution of the feed to and product material from the tumbling testwork done on block L1R11 (slow, 10 days).

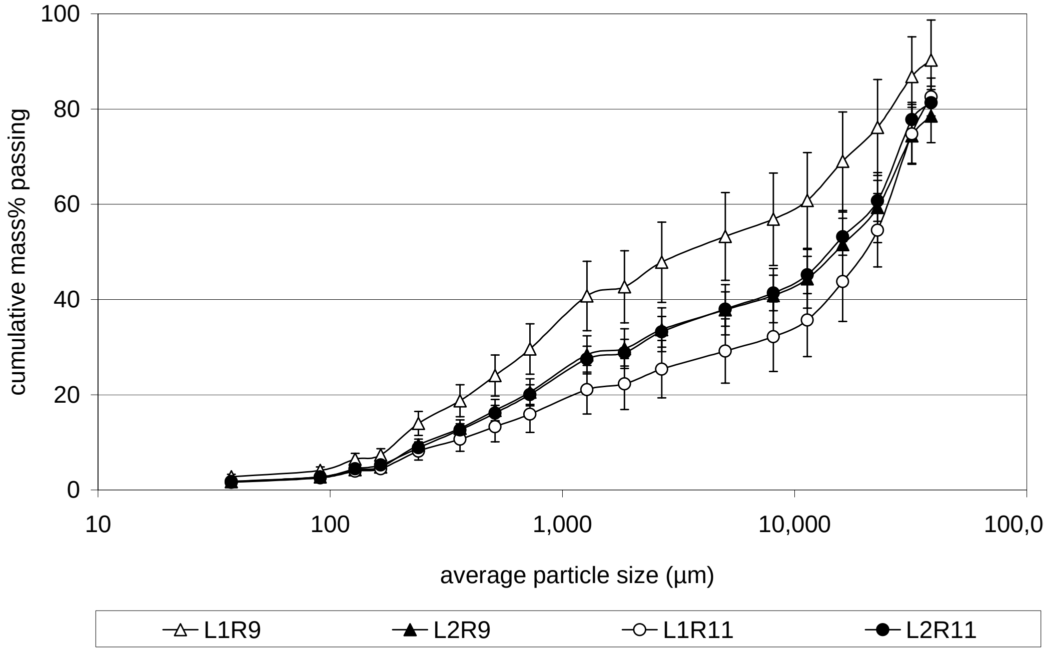

Figure 31 Average particle size distribution of the four blocks (90% confidence intervals shown). Triangles represent higher tapping rates, while circles represent lower tapping rates. Open symbols of 3 days water cooling; solid symbols for 10 days water cooling.

3.3.2 Results

The particle size distributions of the feed and tumble test products, shown as mass percentages retained, are given in Figure 32. A general shift in the peaks of the particle size distribution occurs for all four blocks: after 100 revolutions the +40 mm fraction is reduced considerably, with a substantial increase in the mass percentages for the -850 µm range. After 200 revolutions the peaks at the +850 µm and 300 µm size fractions increased at the expense of the +25 mm peak. From 1000 revolutions onwards, the +25 mm peak continued to decrease. However, the +850 µm peak now started to decrease, yielding an increase in the +600 to +106 µm range. With regard to specifically fines generation (-106 µm) a notable increase occurred after 100 revolutions, and again after 2000 revolutions.

Due to the variation in the feed particle size analyses, the fines (-106µm) generated with each test is shown in Figure 33 together with that present in the initial feed sample. For blocks L1R9 and L1R11 (both 3 days water cooling) the absolute -106µm fraction appears to stabilize at 1000 revolutions. The fines generated with block L2R9 (higher tapping rate, 10 days water cooling) appears to be a strong function of the amount of fines present in the feed sample. The fines generated from block L2R11 (low tapping rate, 10 days water cooled) does not appear to stabilize, even after 2000 revolutions and is greater than that of any of the other blocks.

In order to compensate for the variation in the particle size distributions of the feed material, the product-to-feed ratios of the fines are shown in Figure 34. In this graph, a product-to-feed ratio of 1 would indicate no generation of additional fines during the test, while a product-to-feed ratio larger than 1 indicates that fines were generated in the tumble test.

Already from 200 revolutions and onwards, the more slowly tapped blocks L1R11 and L2R11 show more fines generation than the faster-tapped blocks L1R9 and L2R9. At 2000 revolutions the fines generated from block L1R11 (lower tapping rate, 3 days water cooled) is the most, with the least generated from block L2R9 (higher tapping rate, 10 days water cooled). The second best performer in terms of fines generation is block L1R9 (fast tapping, 3 days water cooled), with block L2R11 (low tapping rate, 10 days water cooled) rated as third best performer.

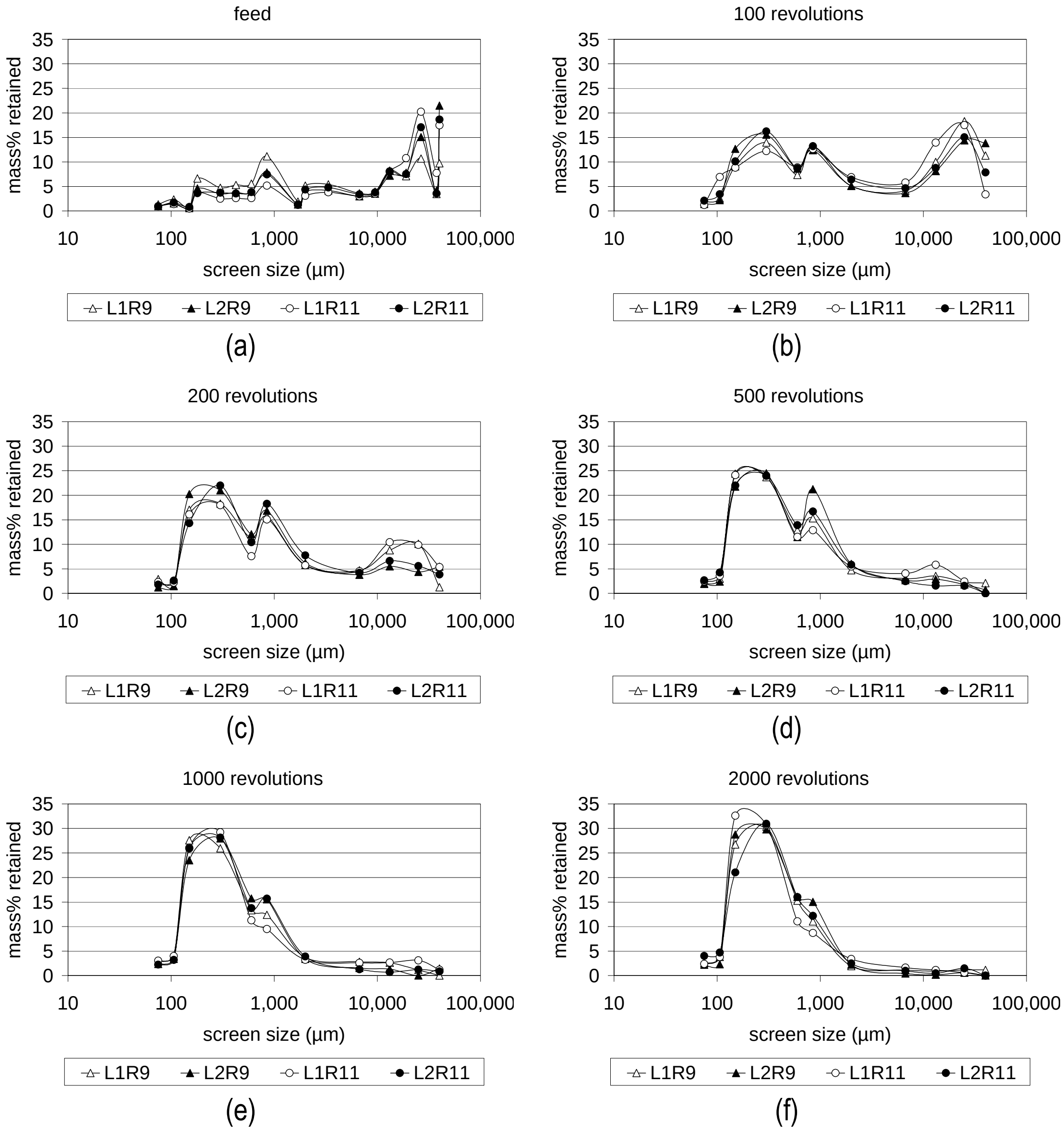

(a) (b)

(c) (d)

(e) (f)

Figure 32 Particle size distributions of the tumble test feed and products.

For a given tapping rate, it is furthermore clear (Figure 34) that the blocks which were cooled for 10 days generated less fines during tumbling than those cooled under water for 3 days only.

The residual coarse fraction present in the product, together with that present in the feed of each tumble test, is shown in Figure 35. Similar to evaluation of fines generation, the variation in particle size distribution of the feed was compensated for by expressing the residual coarse in the feed relative to that in the product (Figure 36). In this graph a ratio of 1 would indicate that the coarse material (+850 µm fraction) in the product is equal to that in the feed; hence no breakdown. A feed-to-product ratio larger than 1 indicates that the coarse material in the feed is more than that in the product - hence breakdown of the coarse fraction (+850 µm) did occur.

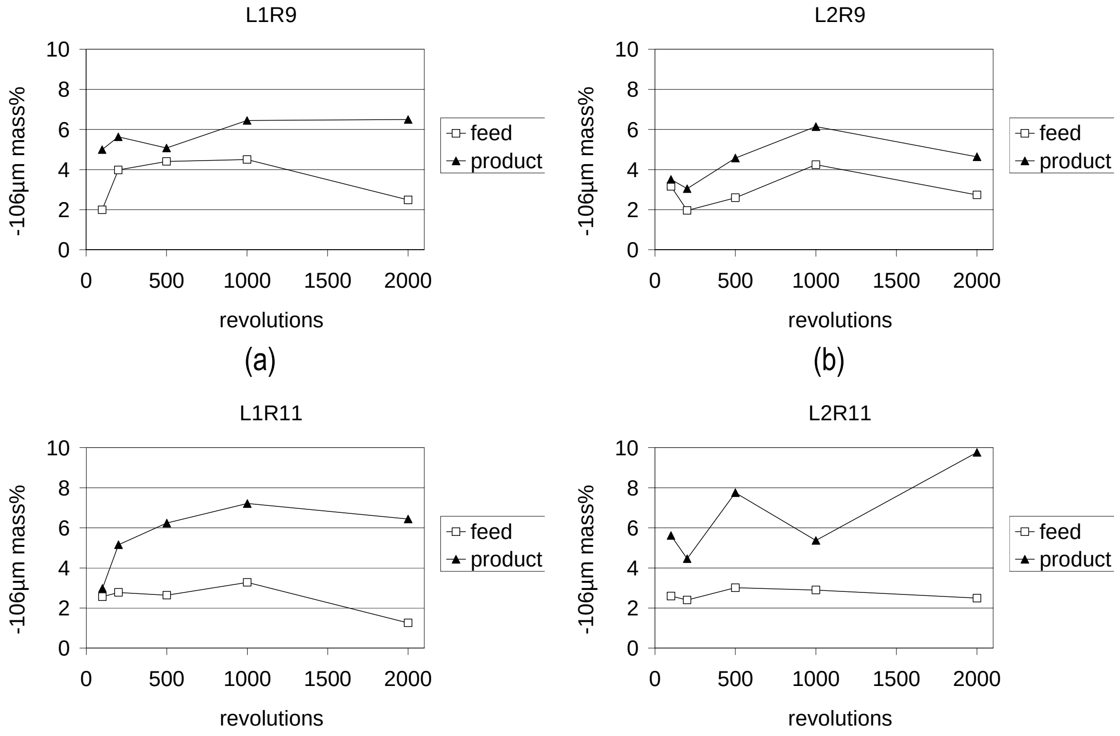

(a) (b)

(c) (d)

Figure 33 -106µm fraction (fines) generated with each tumbling test (solid markers). The fines present in the feed are shown by the open markers.

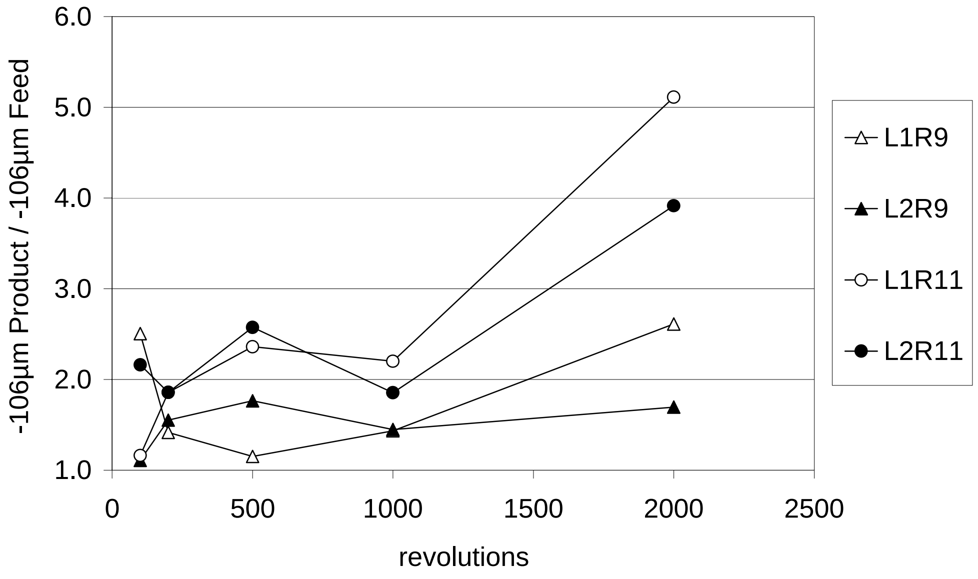

Figure 34 Ratio of -106 µm in the product to that in the feed of the tumbling tests. Circles denote low tapping rates and triangles high tapping rates. Solid symbols denote 10 days of water cooling while open symbols represent 3 days of water cooling.

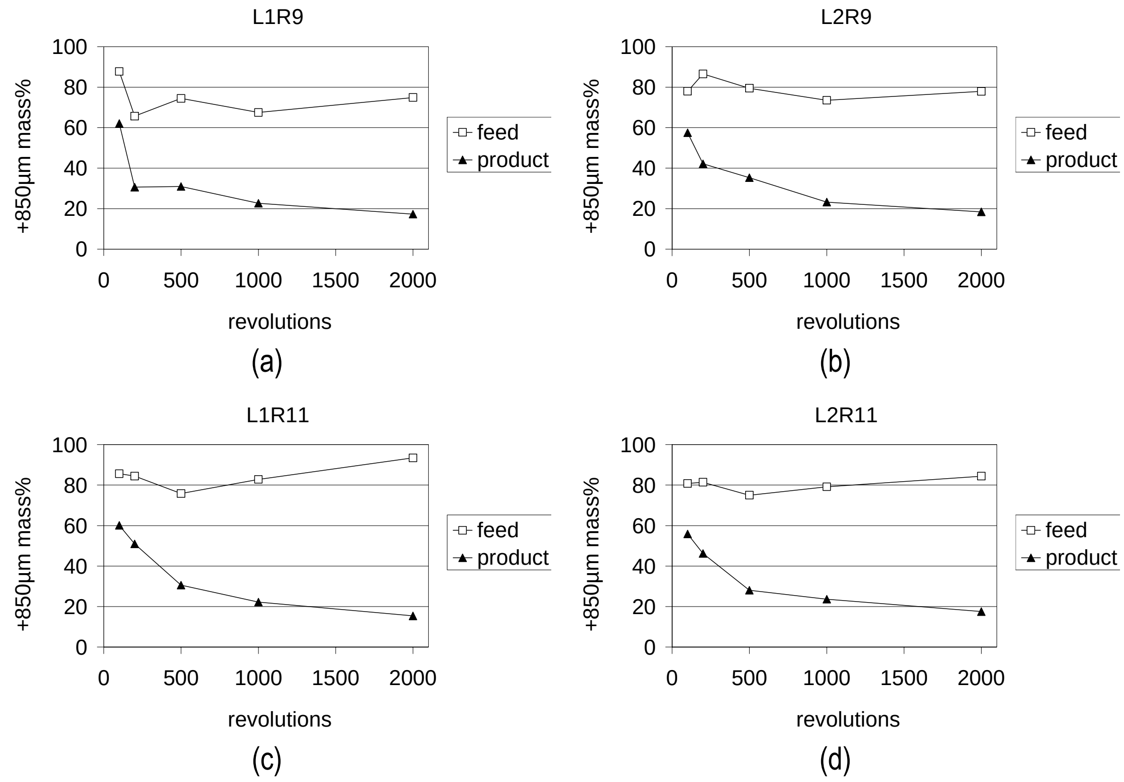

(a) (b)

(c) (d)

Figure 35 The +850 µm fraction (residual coarse) remaining after each tumbling test (solid symbols). The coarse material present in the feed is shown by the open symbols.

Breakdown of the coarse material occurred with all four blocks from 100 revolutions and continued to 2000 revolutions (Figure 36). The initial breakdown (at 200 revolutions) is more for the faster-tapped blocks (L1R9 and L2R9) than for the more slowly tapped blocks. With further tumbling the breakdown slows down for the faster-tapped blocks compared to that of the more slowly tapped blocks.

The absolute values of the coarse material for all four blocks appears however to have stabilised from 1000 revolutions onwards between the four blocks (Table 8). The higher level of breakdown as implied by Figure 36 is attributed to the difference in feed particle size distribution – especially that of the coarser block L1R11 (Figure 31).

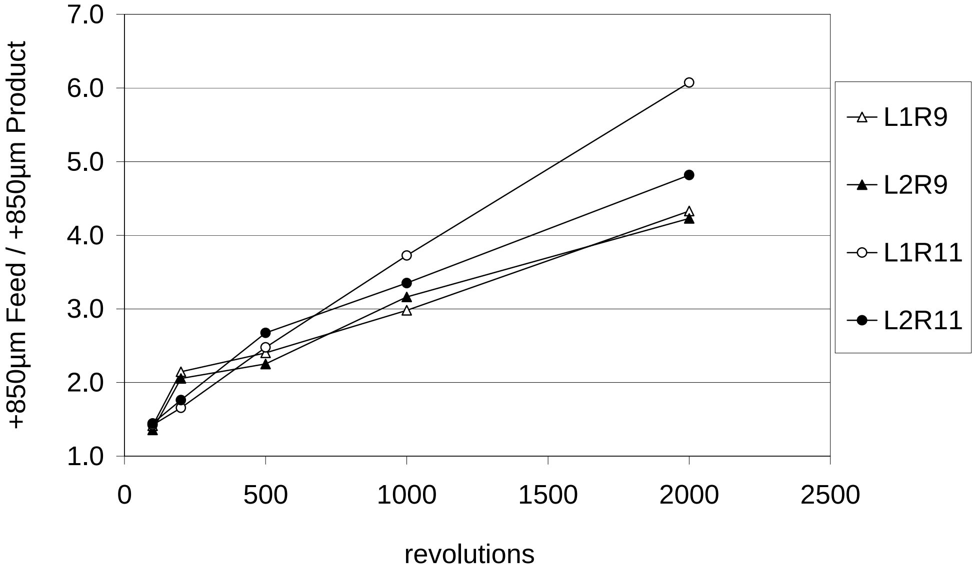

Figure 36 Ratio of the +850 µm in the product to that in the feed of the tumbling tests. Circles denote low tapping rates and triangles high tapping rates. Solid symbols denote 10 days of water cooling while open symbols represent 3 days of water cooling.

Table 8 Absolute values of the residual coarse fraction (+850 µm) of the tumbling products.

Revolutions	100	200	500	1000	2000
L1R9	62.04	30.59	30.96	22.64	17.30
L2R9	57.47	42.12	35.29	23.24	18.43
L1R11	60.13	50.97	30.61	22.24	15.39
L2R11	55.92	46.21	28.05	23.64	17.52
average	58.89	42.47	31.23	22.94	17.16
std. deviation	2.726	8.708	3.002	0.623	1.280

Based on these results, and assuming that the tumbling test is a simulation of material abrasion during handling the following is concluded:

- The effects of tapping rate and cooling history on the abrasion resistance of the slag are noticeable in the fines generation, and less so in the residual coarse fraction of the four blocks.

- The two blocks which were water cooled for 10 days generated less fines during extended handling (2000 revolutions, Figure 34) than their counterparts which were water cooled for 3 days only.

- The faster-tapped blocks outperformed their more slowly tapped counterparts in terms of limited fines generation (Figure 31).

Hence a faster-tapped block, cooled for 10 days yields the best abrasion resistance properties, while a more slowly tapped, insufficiently cooled block yields the poorest abrasion resistant properties. Increased water cooling of a more slowly tapped block mitigates the abrasion of a slowly tapped block to some extent.

3.4 Compression tests

3.4.1 Method

The objective with the compression tests was to simulate the milling action of the Loesche mill (Figure 37). Similar to the Loesche mill, the experimental set-up used for the compression tests utilised in-bed compression breakage principles where[27]

(i) The bed of particles shield a particle from secondary breakage (i.e. the further breakdown of particles which formed from the mother particle during primary breakage);

(ii) The limited force applied limits secondary breakage, and

(iii) The porosity of the bed allows particles and fragments to "hide" from the applied force.

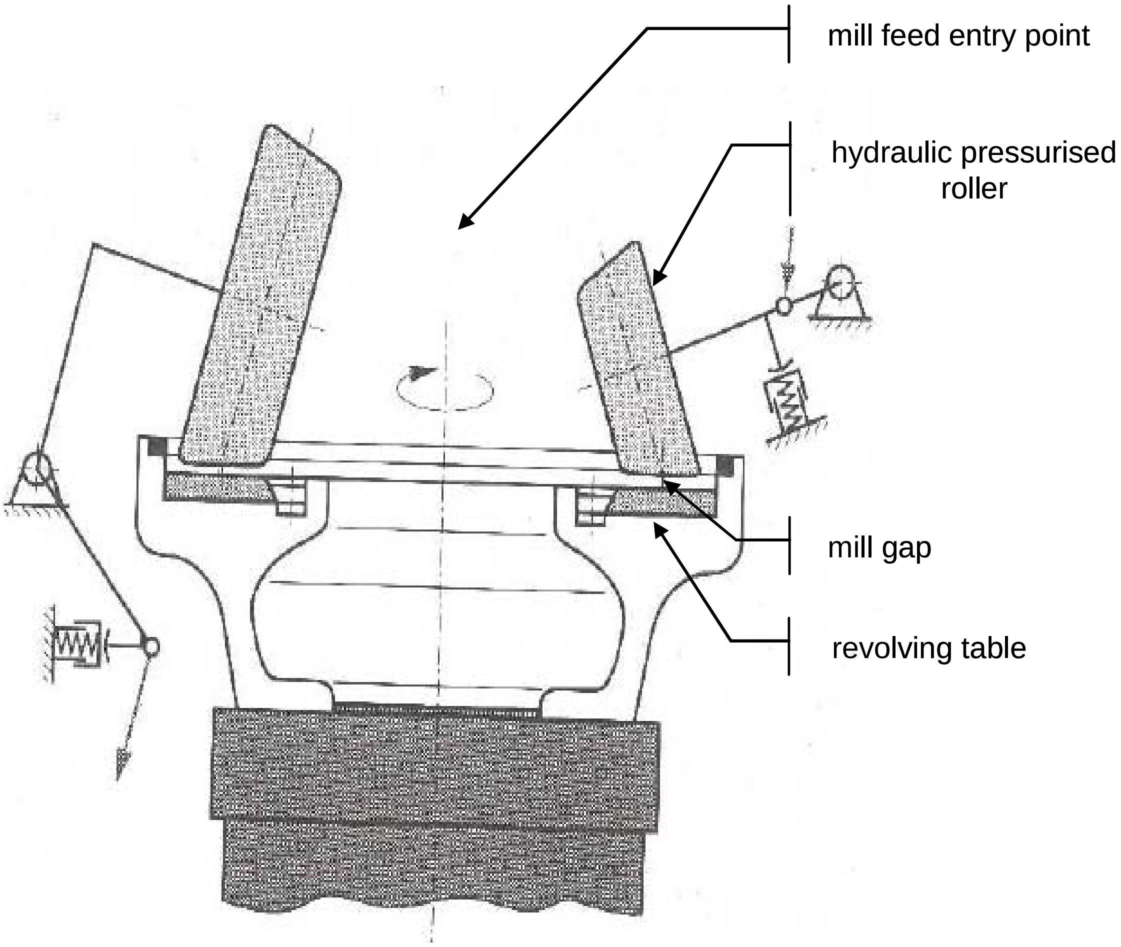

Figure 37 Sketch of a typical Loesche mill[28].

The experimental compression equipment (Figure 38) consisted of a steel sample container with inner diameter of 140 mm. Compression was applied in a vertical direction with an anvil pressing down into the sample container. On compression the anvil travelled 20 mm from its starting position, recording distance and applied force (recorded in tons) against time (Figure 39(a)). The compression force was calculated from the product of the "ton force" and the gravity constant – assumed to be 9.81 N/kg. The total compression energy was calculated by integrating the area below the distance-force curve. To determine the compression energy exerted onto the slag (Figure 39(b)), the compression energy stored in the machine was determined and deducted from the total compression energy. (That is, elastic deformation of the testing machine absorbs some energy which is not transferred to the sample.)

The energy stored in the machine itself is calculated from equation (3), where k is a constant quantifying the machine stiffness. The machine stiffness was hence determined from a series of sample-free compression tests. By inserting the force and energy parameters into equation (3) the machine stiffness was calculated as 314.4 ±21.5 kN/m (at a 95% confidence level).

$$E_{machine} = \frac{1}{2}\frac{F^2}{k} \qquad (3)$$

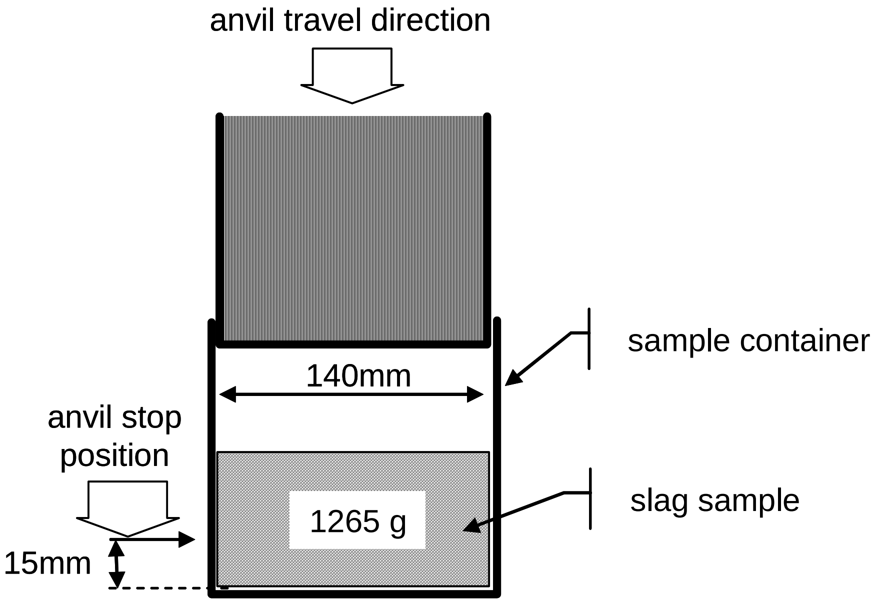

Figure 38 Schematic depiction of the experimental set-up for the compression testwork.

The sample container was filled with a 1265 g sample, corresponding to a sample height of approximately 35 mm - varying slightly according to sample heap density (due to varying particle size distributions). The anvil travelled a maximum of 20 mm downwards, aiming to compress the sample to 15 mm, which is similar to the gap setting between the Loesche mill table and roller. Since the maximum force was kept constant for each test – averaging 198.6 kN within a range of 194.5 and 203.3 kN (Figure 40(b)) – the travel distances ranged from 7.7 to 15 mm with an average of 9.8 mm (Figure 40(a)). On completion of a test, the -850 µm size fraction was removed from the sample (by screening) and replaced with an equal mass of fresh material and the test repeated. Removing the -850µm product fraction from the sample simulates the process flow of the plant (Figure 1) where the finer fraction is removed by screening in a closed loop with the Loesche mill. Six compression runs were conducted with each sample.

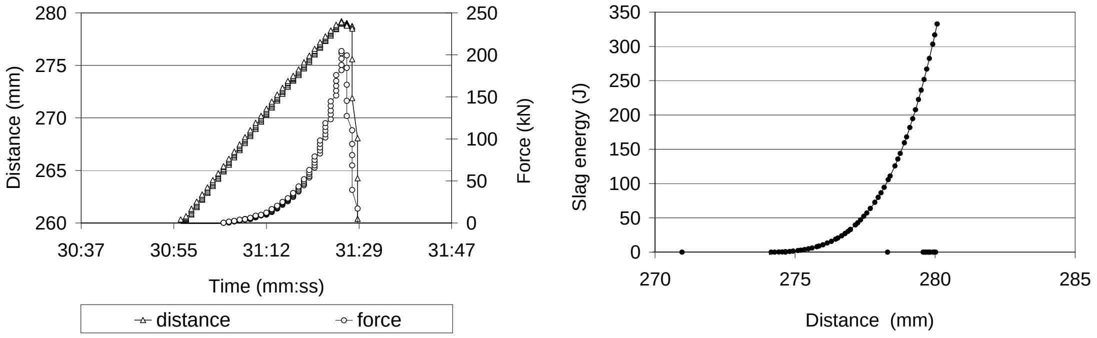

(a) (b)

Figure 39 Example of (a) recorded distance and force and (b) compression energy as calculated during the compression tests.

The compression distance for sample L1R9 was significantly larger than that for the other three samples. This could be attributed to the smaller particle sizes of sample L1R9 (Figure 31), leading to a more compressible bed compared with that of the other three samples.

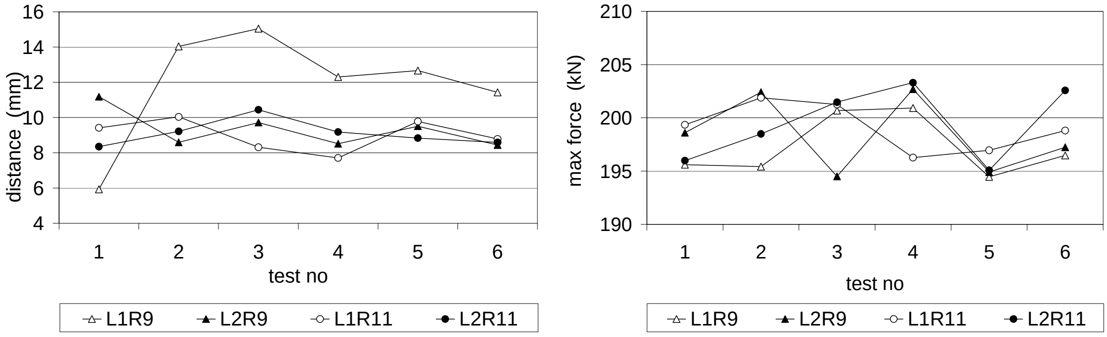

(a) (b)

Figure 40. Distance (a) and maximum force (b) per test as recorded during the compression tests.

The specific energy input for each run (measured in kJ per total kg sample mass) is shown in Figure 41. Due to the further distance recorded for sample L1R9, the specific energy for the latter is higher than that of the others.

The typical energy consumption in the industrial scale Loesche mill is 0.4 to 0.8 kWh/t slag in comparison with 0.11 kWh/t slag (0.4 kJ/kg sample) of the experimental work.

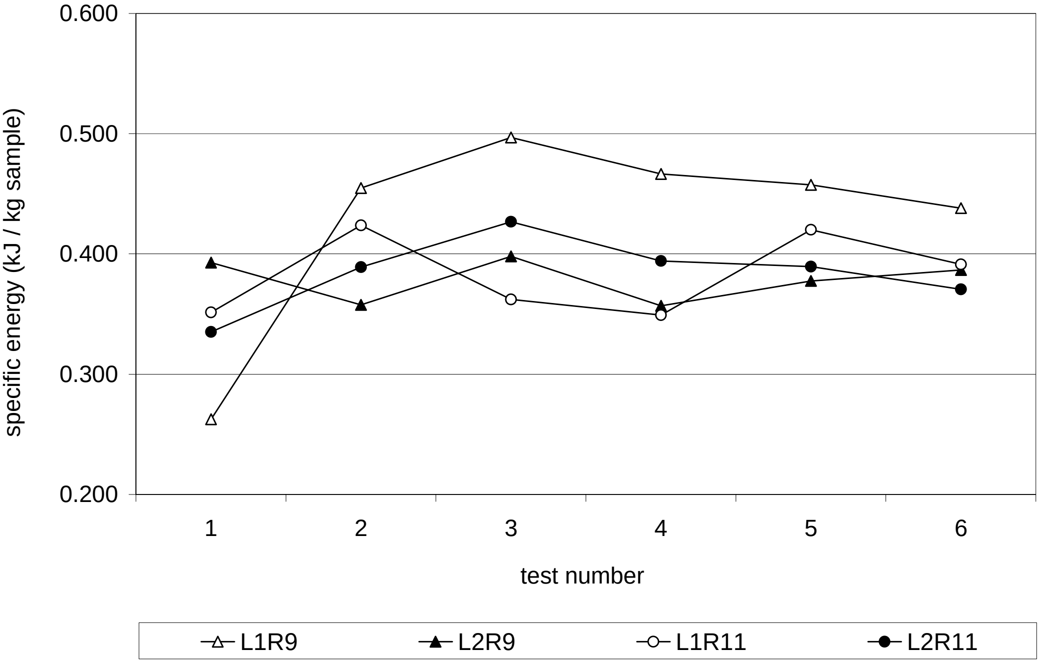

Figure 41. Specific energy exerted on the samples during the compression tests.

3.4.2 Results

The absolute mass percentage fines generated with each compression run is relatively constant from the second to the sixth run for all four blocks, Figure 42(a). The specific energy (measured in kJ per mass%-106µm) also appears to be relatively constant over the second to sixth runs for all four blocks, Figure 42(b).

The absolute mass% residual +850 µm is consequently lower for the two slower tapped blocks L1R11 and L2R11 from run 3 onwards (Figure 43).

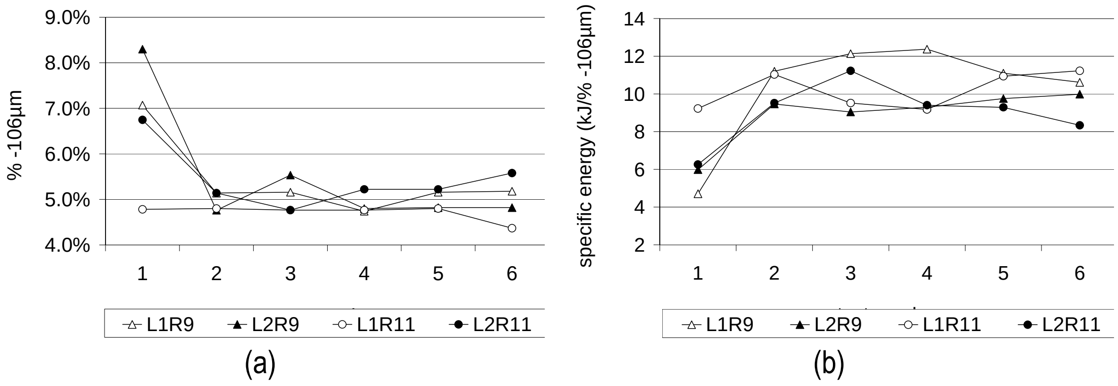

Figure 42 (a) Amount of fines generated with the 1st to 6th run of the compression test series for the four blocks. (b) Specific energy (kJ per mass% -106 µm) per compression run for the four blocks.

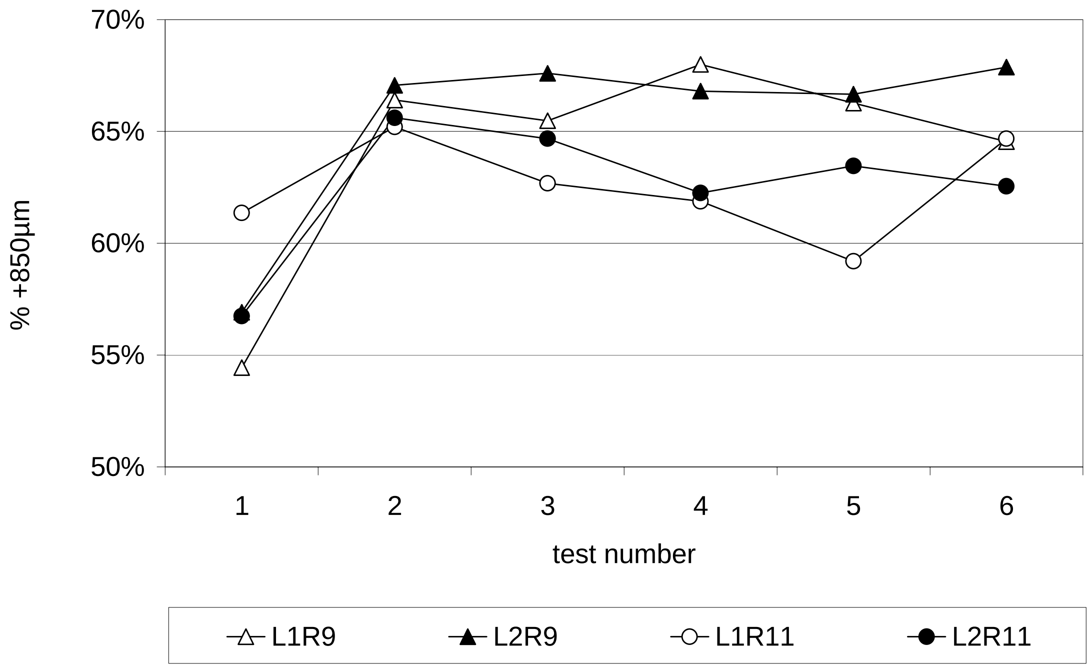

Figure 43 (a) Residual +850 µm mass% from the 1st to 6th test of the compression test series for the four blocks; (b) Specific energy (kJ per mass% +850 µm) per compression run for the four blocks.

Averages over the last 3 runs of each test, for both the fine and coarse fractions, are given in Table 9 and are graphically represented in Figure 44 and Figure 45 (variations are calculated for a 95% confidence interval).

The absolute value for fines generated for the four blocks overlap to a large extent; as does the specific energy requirement (Figure 44). The variation in the specific energy requirement for fines generation is relatively large for the L1 blocks which were water cooled for 3 days only.

The residual coarse mass% of the R9 blocks which were tapped faster is higher than that of the more slowly tapped blocks. This is in agreement with the results from Part 1. Block L1R11 (more slowly tapped and water cooled for 3 days only) showed a large variation in its residual coarse fraction (Figure 45). The specific energy required per mass unit +850 µm overlaps largely, while block L1R11 continues with the tendency to have the largest variation in its particle size distribution.

Table 9 Average numbers for the last 3 compression tests ran for each block, including 95% confidence intervals.

	% -106 µm	Specific energy (kJ / %-106 µm)	% +850 µm
L1R9	5.03 ±0.28	11.36 ±1.027	66.3 ±1.95
L2R9	4.81 ±0.01	9.68 ±0.400	67.1 ±0.75
L1R11	4.64 ±0.27	10.45 ±1.255	61.9 ±3.10
L2R11	5.34 ±0.23	9.01 ±0.660	62.8 ±0.71

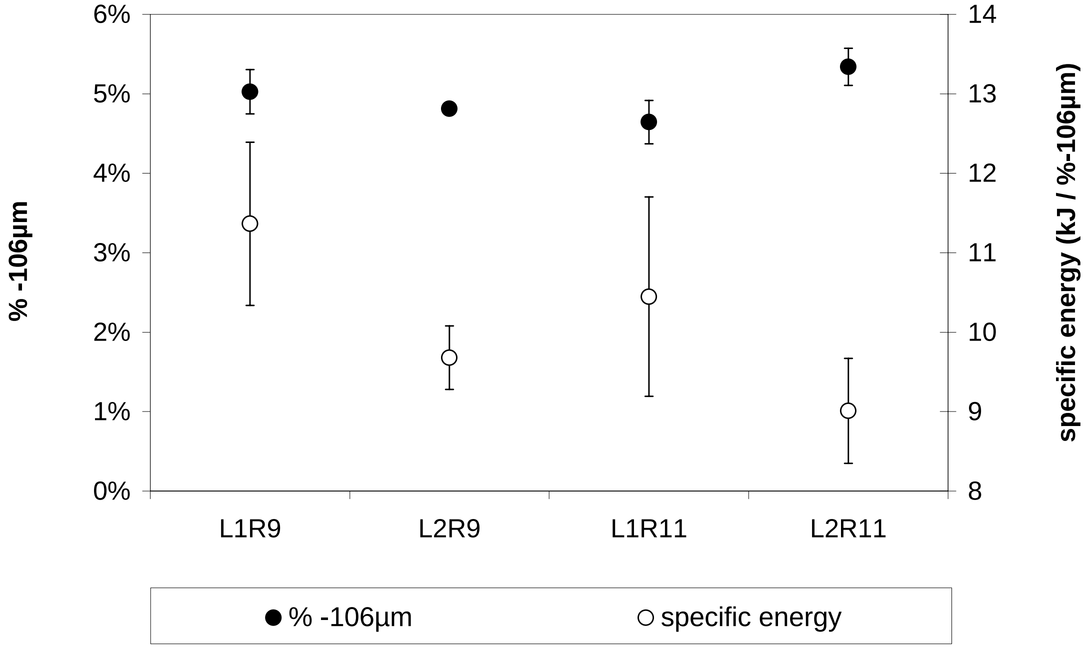

Figure 44 Average % -106 µm and specific energy in kJ/% -106 µm per compression test for each of the four blocks. (Error bars showing a 95% confidence interval).

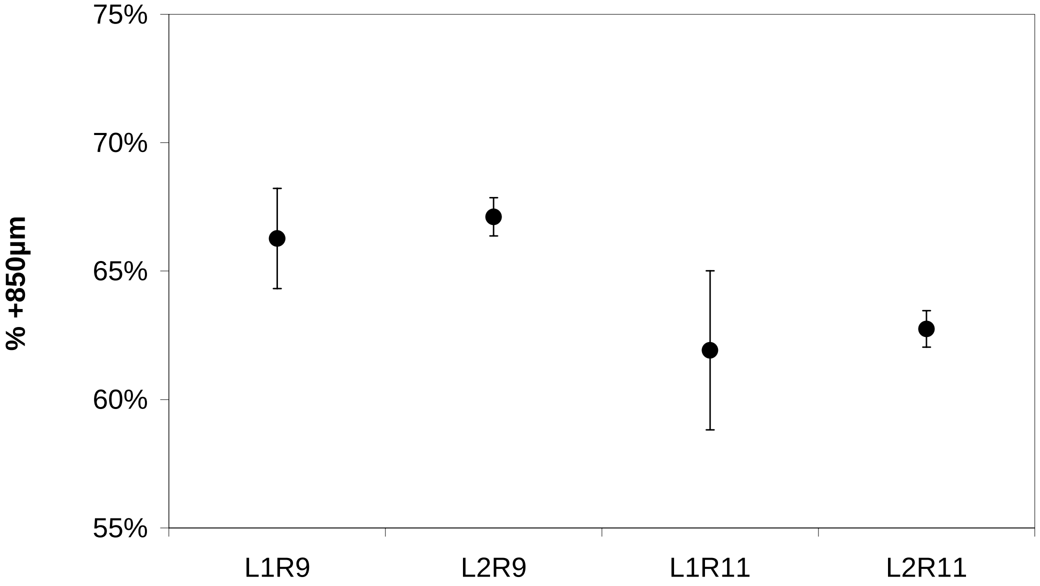

Figure 45 Average % +850 µm per compression test for each of the four blocks. (Error bars showing a 95% confidence interval).

Despite the larger travel distance imposed on the sample from block L1R9 (and hence the larger applied specific energy) the particle size distribution of its compression product does not differ significantly from those of the other three blocks. This is likely attributable to the “hiding” opportunity the slag has under the inter particle (or in-bed) compression conditions characteristic of this compression method. This implies that the particle size distribution of the mill product is primarily a function of the feed size distribution, which in turn appears to be a function of the tapping rate and cooling history (Figure 31) – and not the energy applied within the mill.

Block L1R11 which tapped more slowly and was water-cooled for 3 days showed a larger variation in particle size distribution relatively to the other three blocks. On the other hand, block L2R9 (tapped faster and cooled for 10 days under water) consistently showed small variations in its particle size distribution. The small variations in especially the coarser fractions of the R11 blocks (10 days water cooled) combined with the similar particle size distributions of these fully water cooled blocks (as per Figure 31) – despite their differing tapping rates - supports a line of reasoning that sufficient water cooling "homogenises" the particle size distribution of the block during subsequent comminution.

3.5 Slag composition and mineralogy

A drill core which was prepared from one of the pilot-campaign slag blocks, and samples from a slag block from the industrial plant, were examined by scanning electron microscopy. The objective was to test possible relationships between the slag block microstructure and its crushing behaviour. At least three microstructural links are possible: (i) the role of silicates, (ii) the karrooite (M_3O_5) grain size, and (iii) cracking by incipient low-temperature oxidation.

As discussed in section 1, silica and calcia are not soluble in the karrooite matrix phase, and form silicates which solidify at a lower temperature than the karrooite. During solidification of the karrooite, the silica and calcium oxide (and also some alumina, titanium oxide, iron oxide and manganese oxide) hence form a separate, low-melting phase which is expected to collect within the solidified matrix. Depending on the nature of the solidification front, the silicate may collect in the middle of the solidifying block, or it may be present between the karrooite dendrites. If the latter, the presence of the silicates can be expected to affect the size reduction behaviour, by means of fracture through the silicates or between the silicates and the karrooite (in line with the effect of silica content on fines generation, as observed from the pilot-campaign slags).

Given that cleavage of the karrooite grains is the fracture mechanism, grain size and grain shape are important. Visual observation of polished sections of slag indicates that individual grains are needlelike in shape, up to several millimetres long, and less than a millimetre in width. This is comparable with the required grain size for the chloride slag product, which is between 106 µm and 850 µm.

Finally, as mentioned earlier, low-temperature oxidation can cause fine slag fragments to form (triggered by the volume change associated with the appearance of the M_6O_{11} phase[7]).

3.5.1 Method

Block 60 produced during the Campaign 9 pilot plant trials were horizontally core drilled as shown in Figure 46. The outer end of the core shows the typical denser structure, while porosity is apparent in the centre portion of the core. Block 60 had a tapping rate of 396 kg/min (the third highest tapping rate of the taps discussed in Part 1); had a mass of 1,557 kg and was continuously water cooled. The tap analysis of this block is shown in Table 10.

Figure 46 Cross section of block 60 showing the horizontal groove where the drill core was removed. The block surface is apparent from the rusty coloured area in the upper left hand corner of the photo.

Table 10 Tap composition of block 60 (mass percentages; XRF)

FeO	TiO_2	Al_2O_3	CaO	Cr_2O_3	MgO	MnO	SiO_2	V_2O_5
9.78	87.57	0.81	0.20	0.11	1.49	1.21	1.28	0.48

Polished sections were prepared from three positions along the drill core. These were at the surface of the block (where it had been in contact with the mould), halfway between the surface and the centre, and at the centre of the block. The sections were sputter-coated with gold, and examined by scanning electron microscopy, using back-scattered electron imaging to yield atomic-number contrast. Micro-analyses were performed by energy-dispersive spectroscopy (EDS), in the scanning electron microscope. At least four regions were analysed per phase or area, and 95% confidence intervals on the mean composition calculated. Similar samples were obtained from the industrial plant; plant personnel collected samples from a single block, for regions at the surface of the slag block, within the block interior (but away from the centre), and at the centre (at the position of final solidification, as indicated by noticeably greater porosity).

Crushed plant slag samples were also examined. These were examined without mounting, by simply pouring some of the slag over conductive carbon tape, and then sputter-coating the adhering particles with gold.

To limit the size of the interaction volume an acceleration voltage of 12 kV was used.

3.5.2 Results

3.5.2.1 **Slag block microstructure**

The observed microstructure for the drill core was similar for all three samples (which spanned the distance from the slag block surface to its centre) with the exception of the outer surface, which showed a chill zone – which also displayed substantial oxidation – next to the mould surface. Figure 47 shows a chill zone, at low and higher magnifications. The presence of a substantial amount of rutile indicates that oxidation of the slag had taken place, during or after solidification: if some of the Ti_2O_3 in the slag is oxidised, the slag composition departs from M_3O_5 stoichiometry; specifically, the slag contains more TiO_2 than M_3O_5 stoichiometry would require, with the result that rutile would form as primary phase during solidification. Such a structure could also arise by oxidation of the slag after solidification. Approximately 3 mm away from the chilled surface, no free rutile was observed in the microstructure, which then consisted of the dominant karrooite phase, with some silicates. Fine cracking of the karrooite was visible, probably as a result of some low-temperature oxidation. The lower-magnification micrograph (left hand side of Figure 48) shows the karrooite grains to be delineated by the silicate phases. Two types of silicate phase were observed; one (S_1) appeared darker in the back-scattered electron image (indicative of a lower average atomic number). Both S_1 and S_2 contained an internal structure of secondary phases. These phases could not be identified, since they were too small to analyse by EDS.

The same general features were observed in the other two samples: rutile was present, apparently as a solidification product, in both the "halfway" and "centre" samples. The karrooite grain size is not readily apparent, but – based on delineation of the karrooite grains by the silicate phases – there is not a major difference in the grain size or shape for the different positions within the block. In all cases, the grains appeared elongated in the polished sections, up to 0.5 mm long, and typically 100 µm or less across.

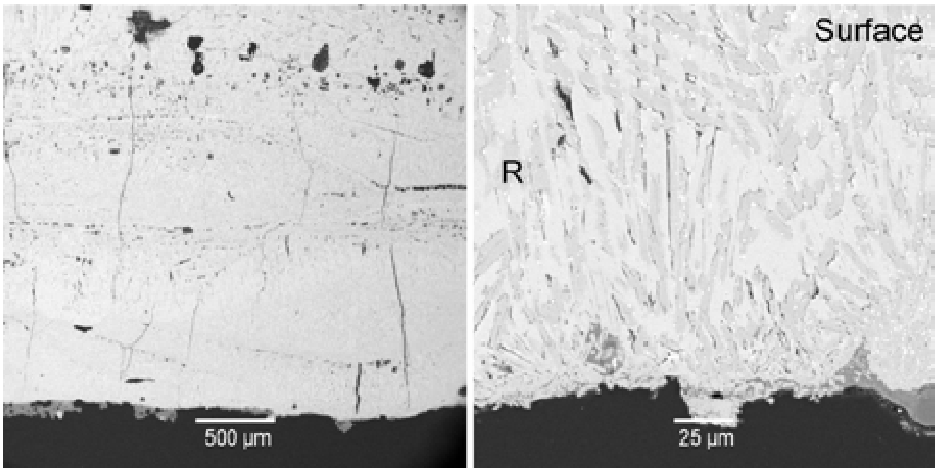

Figure 47 Microstructure of the chill zone in the pilot-plant slag block, next to the mould. The outer surface is at the bottom of both images. The higher-magnification image at right shows that this region largely consists of two phases; the darker phase (marked "R") was found to be TiO_2 (rutile or anatase).

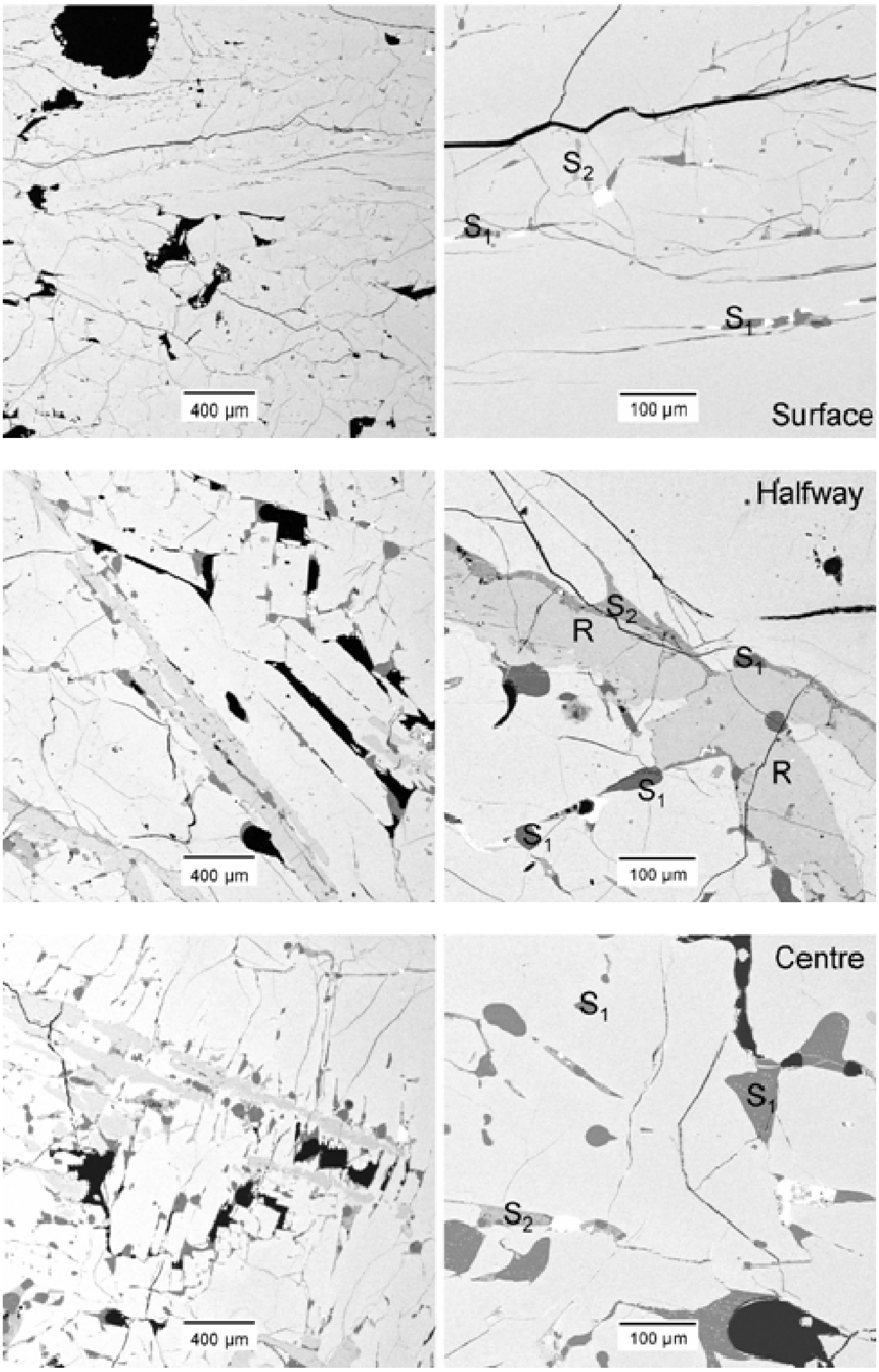

Figure 48 Typical microstructures found within the pilot-plant slag block, near the surface of the slag block, but outside the oxidised zone (top two images), halfway between the surface and the centre (middle two images), and at the centre (bottom two images). The light-gray matrix phase is karrooite (M_3O_5), the black lines are cracks, larger black areas are pores, dark grey areas are silicate phases (S_1 and S_2), and the phase with intermediate brightness is TiO_2 (likely rutile; indicated with R).

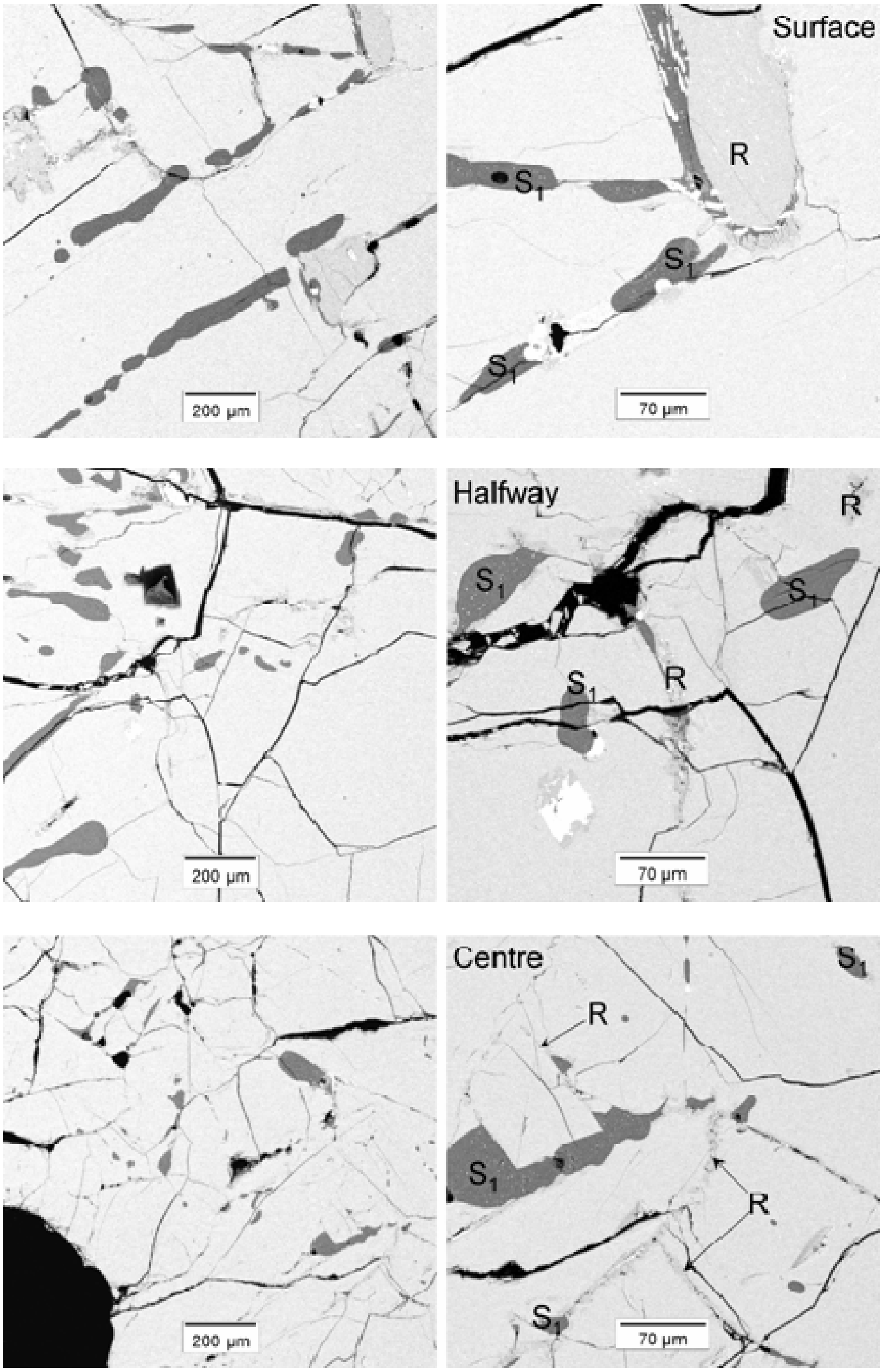

Figure 49 Typical microstructures found within the industrial-plant slag block, near the surface of the slag block, (top two images), within the body of the slag block (middle two images), and at the centre (bottom two images). Phase identification is as for the images of the pilot-plant slag block.

Table 11 Average compositions (with 95% confidence intervals on average values), as found by EDS. Compositions are in mass percentages. For the karrooite phase, the Ti_2O_3 content was calculated by assuming that M_3O_5 stoichiometry holds. For the area analyses and silicate analyses, all titanium is expressed as TiO_2.

Karrooite (pilot-plant slag):

Position	TiO_2	Ti_2O_3	FeO	MnO	MgO	Al_2O_3
Surface	49.6±2.0	37.7±3.9	8.9±1.9	0.9±0.4	1.9±0.3	0.9±0.2
Halfway	55.0±1.4	27.3±2.7	13.0±0.7	2.1±0.4	1.7±0.4	0.9±0.2
Centre	55.3±1.8	26.6±3.4	13.5±1.5	2.0±0.6	1.7±0.2	0.9±0.1

Darker silicate (labelled "S1" in micrographs):

Position	SiO_2	TiO_2	CaO	K_2O	Al_2O_3	FeO	MnO	MgO
Pilot plant slag								
Surface	76.2±5.2	9.8±3.3	3.7±1.2	2.1±0.1	3.4±0.2	2.8±1.3	1.8±0.7	0.1±0.1
Halfway	81.9±1.3	7.1±0.8	2.6±0.4	2.5±0.1	3.7±0.2	1.5±0.3	0.8±0.4	0.0±0.1
Centre	78.6±5.7	9.1±3.6	3.1±1.7	2.3±0.5	3.7±0.3	2.1±0.8	1.0±0.4	0.1±0.1
Industrial slag								
Surface	82.5±1.1	7.6±0.9	2.3±0.5	2.7±0.2	3.7±0.2	0.8±0.6	0.3±0.3	0.1±0.1
Halfway	82.1±0.8	8.4±0.5	2.0±0.9	2.8±0.5	3.4±0.2	1.0±0.5	0.2±0.2	0.1±0.1
Centre	79.0±1.7	10.4±1.1	2.1±0.4	2.9±0.4	3.4±0.4	1.4±0.8	0.7±0.4	0.1±0.1

Brighter silicate ("S2" in micrographs): Only found in pilot-plant slag

Position	SiO_2	TiO_2	CaO	K_2O	Al_2O_3	FeO	MnO	MgO
Surface	38.1±5.6	33.1±6.9	20.3±3.2	0.6±0.3	1.6±0.8	1.7±3.0	4.4±2.9	0.2±0.1
Halfway	48.2±9.4	19.4±11.7	18.2±2.8	0.9±0.3	5.3±2.1	2.1±1.0	4.9±3.0	0.9±1.0
Centre	45.4±8.4	20.1±13.7	17.2±4.3	0.8±0.5	4.8±1.7	3.5±1.4	7.1±6.1	1.0±2.0

Average of phases (area analyses):

Position	SiO_2	TiO_2	CaO	K_2O	Al_2O_3	FeO	MnO	MgO
Pilot plant slag								
Surface	1.3±0.2	87.4±0.8	0.1±0.2	0.1±0.1	0.8±0.1	7.9±1.1	1.1±0.6	1.2±0.1
Halfway	3.2±1.4	81.1±2.5	0.4±0.4	0.0±0.1	1.0±0.3	10.7±1.3	2.4±0.7	1.3±0.1
Centre	3.3±1.4	80.1±4.2	0.4±0.3	0.0±0.1	0.9±0.2	11.3±2.3	2.8±1.2	1.2±0.3
Industrial slag								
Surface	2.7±1.6	83.8±3.1	0.1±0.2	0.0±0.1	1.0±0.2	9.1±1.9	2.3±0.7	0.8±0.1
Halfway	2.5±2.8	85.4±4.8	0.1±0.3	0.1±0.2	1.2±0.2	7.1±2.2	2.7±0.7	0.9±0.4
Centre	1.9±0.3	86.1±3.4	0.0±0.1	0.1±0.2	1.2±0.3	7.3±2.2	2.5±1.2	0.9±0.2

The two silicate phase regions were observed throughout. Both contained a substructure of finer phases (which could not be analysed, because of their small size). The two types of silicates were distinguished on the basis of their appearance in the back-scattered electron images.

The observed internal cracking has the morphology of the cracking caused by low-temperature oxidation (M_6O_{11} formation).

The microstructures of the slag samples from the industrial plant were remarkably similar to those from the pilot plant. The only difference was that the silicate phase S_2 was not present.

A noticeable feature of the microstructures is that the internal cracks are often associated with the silicate phases and with the rutile grains (the silicates and rutile are present in the same region of the microstructure, namely where final solidification occurred between the karrooite grains). As noted below, this association was confirmed by the presence of silicate phases on the surface of crushed slag. This also supports the plant observation (discussed in Part 1) that both the silica content and the degree of oxidation during tapping (or tapping rate) affect fines formation. (The significance of oxidation is that rutile is present as a result of oxidation during tapping.)

3.5.2.2 **Micro-analyses**

The analyses found by EDS are summarised in Table 11. In the case of the pilot-plant slag, the composition is different for the sample from the block surface, but the average compositions and those of the individual phases are the same (or at least not significantly different) for the other two positions. This indicates that little macro segregation takes place during solidification, and also that the silicate phases are trapped between the karrooite grains as solidification progresses: there is no significant rejection of the silicates to the centre of the slag block. (The obvious exception to these observations is the near-surface chill region, where the titanium content of the karrooite is higher, and the silicate content is lower.) The same observations were made for the samples from the industrial plant.

3.5.2.3 **Crushed slag**

The main microstructural features observed from the drill-core (pilot-plant) and industrial samples are elongated karrooite grains (of similar size throughout), silicates present between the karrooite grains, and microcracking. Microscopic examination of the crushed chloride-grade slag (between 106 µm and 850 µm in size) indicates that the silicates do affect the crushing behaviour significantly for this size fraction. This conclusion is based on the observation that silicates are present on the surfaces of the crushed slag. Examples are shown in Figure 50. Each of these figures shows a pair of back-scattered electron images (BEI) and secondary electron images (SEI) of the same slag particles. The secondary electron images show particle shape, whereas contrast in the back-scattered electron images arises from both shape (orientation) and composition. Where dark patches are present in the back-scattered electron images, these indicate the presence of silicates. Micro-analysis shows these patches to have the same composition as silicate phase S_1, as revealed by Table 12 (note specifically the similar levels of calcium, potassium and aluminium). This means that these silica-containing regions on the surface are most unlikely to be contaminants which were transferred to the particles during crushing, but rather are a feature of the slag itself.

The high concentration of silicates on the particle surfaces does indicate a significant effect of the silicates on crushing behaviour, when the slag is crushed to the chloride-grade size. (Note that, while only two examples are shown below, the association of silicates with the surfaces of crushed chloride-grade particles was found commonly; more examples are given in Appendix 5.3).

Table 12 Micro-analyses of dark regions (silicates) identified in crushed slag (mass percentages)

	SiO_2	TiO_2	CaO	K_2O	Al_2O_3	FeO	MnO	MgO
CP slag	73.0±7.3	12.2±3.4	2.2±0.9	2.2±0.5	3.6±0.8	5.1±3.8	1.6±1.2	0.1±0.1
Fine slag	73.5±8.3	13.8±5.9	1.7±0.5	2.0±0.7	3.6±0.4	4.7±2.4	0.7±0.4	0.1±0.1

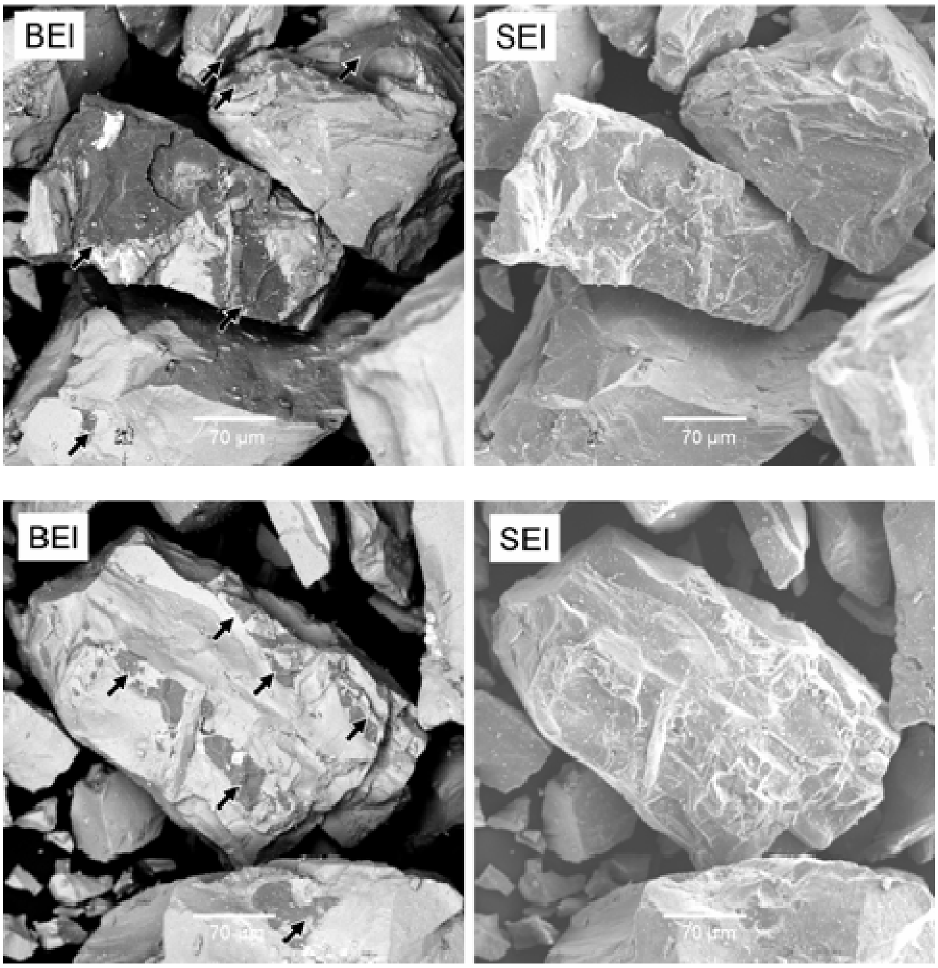

Figure 50 Pairs of images of the same particles of chloride-grade crushed slag. Arrowed black patches in the back-scattered electron images (BEI) at left indicate silicates. The secondary electron images (SEI) at right show the particle morphologies.

In contrast, the smaller, fine-grade slag particles do not show such an obvious association between silicates and particle surfaces (fracture surfaces). The smaller size and irregular shape (often apparently flakelike) of the sulphate-grade slag particles made it more difficult to identify silicate phases (by scanning electron microscopy). In all cases, identification of silicates was based on both brightness in the back-scattered electron image, and microanalysis by EDS. Examples of such silicate-containing particles are shown in Figure 51. As these examples illustrate, the silicate particles were generally found as liberated particles; the table of EDS analyses demonstrates that their compositions also agree with that of silicate S_1 in the microstructure. Note also that many of the crushed slag particles are much smaller than the silicate particles. It hence appears unlikely that the formation of these fine particles were affected by the presence of the silicates.

The visual observations in Figure 51 are confirmed by fractional chemical analyses done on composite industrial samples (shown in Figure 52). The oxides present in the glass phase increase markedly for particle sizes below 250 µm, whereas the same does not happen for Cr_2O_3, V_2O_5, and MgO, Figure 52(b). Note that chromium, vanadium and magnesium report to the karrooite (M_3O_5) phase, and not to the silicates. MnO does show a slight increase towards smaller particles sizes – likely due to a small portion of MnO reporting to the glass phase as mentioned earlier.

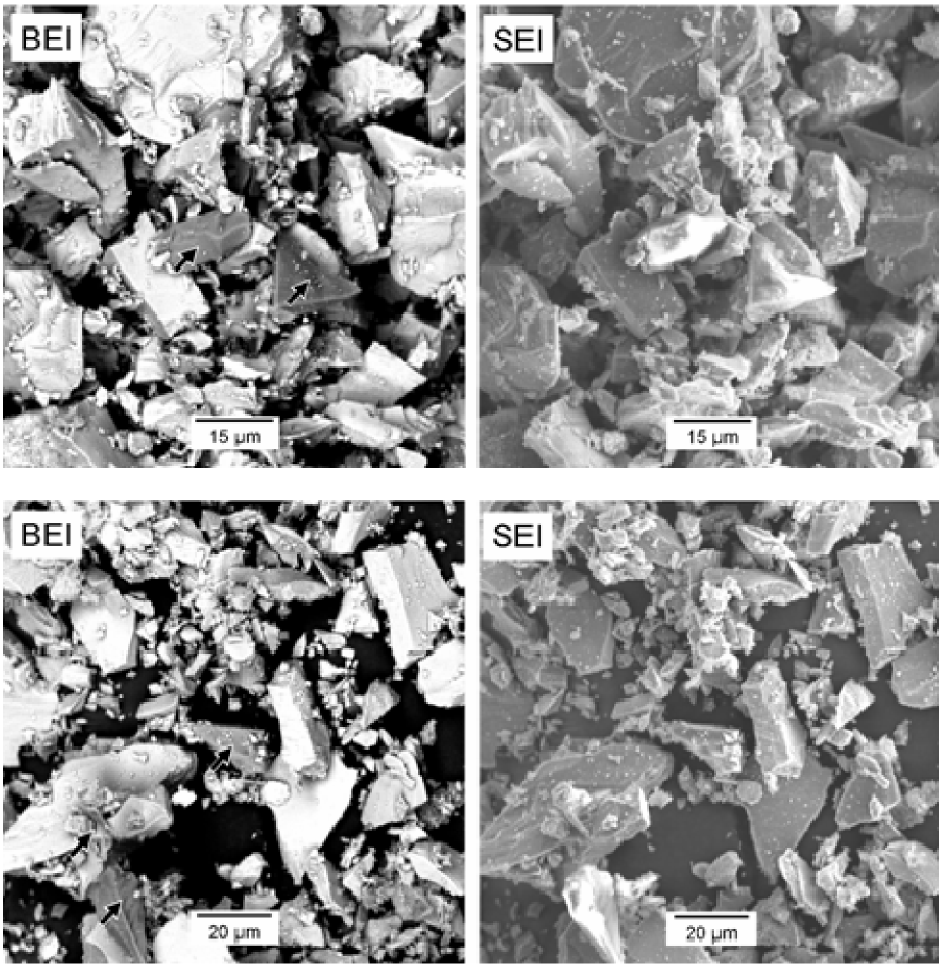

Figure 51 Pairs of images of the same particles of fine-grade crushed slag. Arrowed darker particles in the back-scattered electron images (BEI) at left indicate silicates. The secondary electron images (SEI) at right show the particle morphologies.

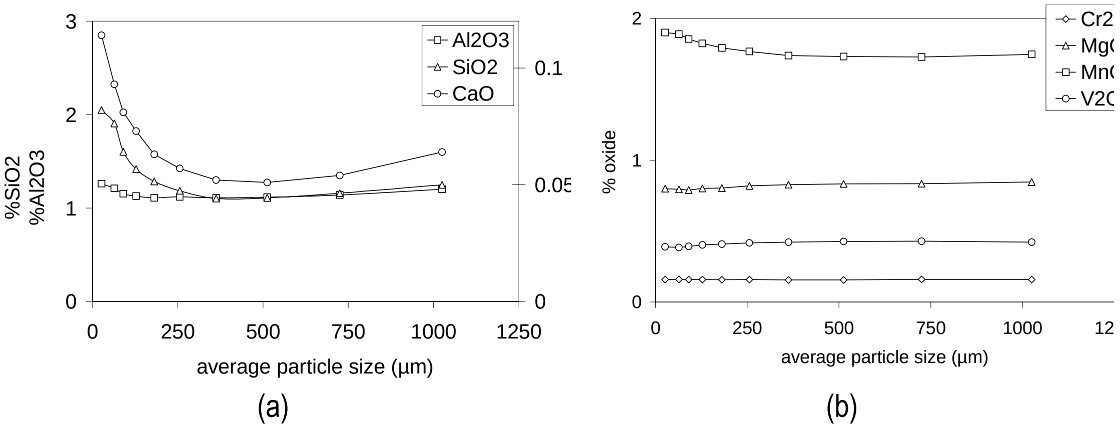

(a) (b)

Figure 52 %Oxide per average particle size fraction (a) SiO_2, Al_2O_3 and CaO, and (b) Cr_2O_3, MgO, MnO and V_2O_3.

3.6 Tapping rate

In order to reduce the generation of fines (-106 µm fraction) during the handling of slag, high slag tapping rates were shown to be beneficial. Tapping rate, in turn, depends on factors which can be grouped into three categories (i) those external to the smelting process, e.g. taphole diameter and taphole opening and closing practices (ii) physical conditions within the furnace, e.g. bank formation and slag level, and (iii) physico-chemical and energy (temperature) properties of the slag at the time of tap. The following follows from an investigation into the chemical and energy properties of the slag which could impact on the slag at the time of a tap.

The characteristic FeO-TiO_2-Ti_2O_3 relationship of the titanium dioxide slags is well documented and investigated[26]. A comparison between the normalised components %TiO_2, equivalent %Ti_2O_3 and equivalent %FeO as produced during Campaign 9 and at the plant is given in Figure 53. Slags from both sources follow the same relationships between these three components. Hence any correlation between the tapping rate and one of these three major slag composition components should extend to the other two components as well. Since the slag is in the liquid phase during tapping the solid phase mineralogical components ilmenite, rutile, etc. were not considered.

With the components MnO, MgO being included with the equivalent %FeO, and Cr_2O_3, V_2O_5 and Al_2O_3 being included in the equivalent %Ti_2O_3, the only other significant chemical components are SiO_2, CaO and the remainder of the Al_2O_3 which does not report to the equivalent %Ti_2O_3. These components are grouped together into the glass phase. For the purposes of this investigation, the %SiO_2 was selected as representative component of the silicate phases.

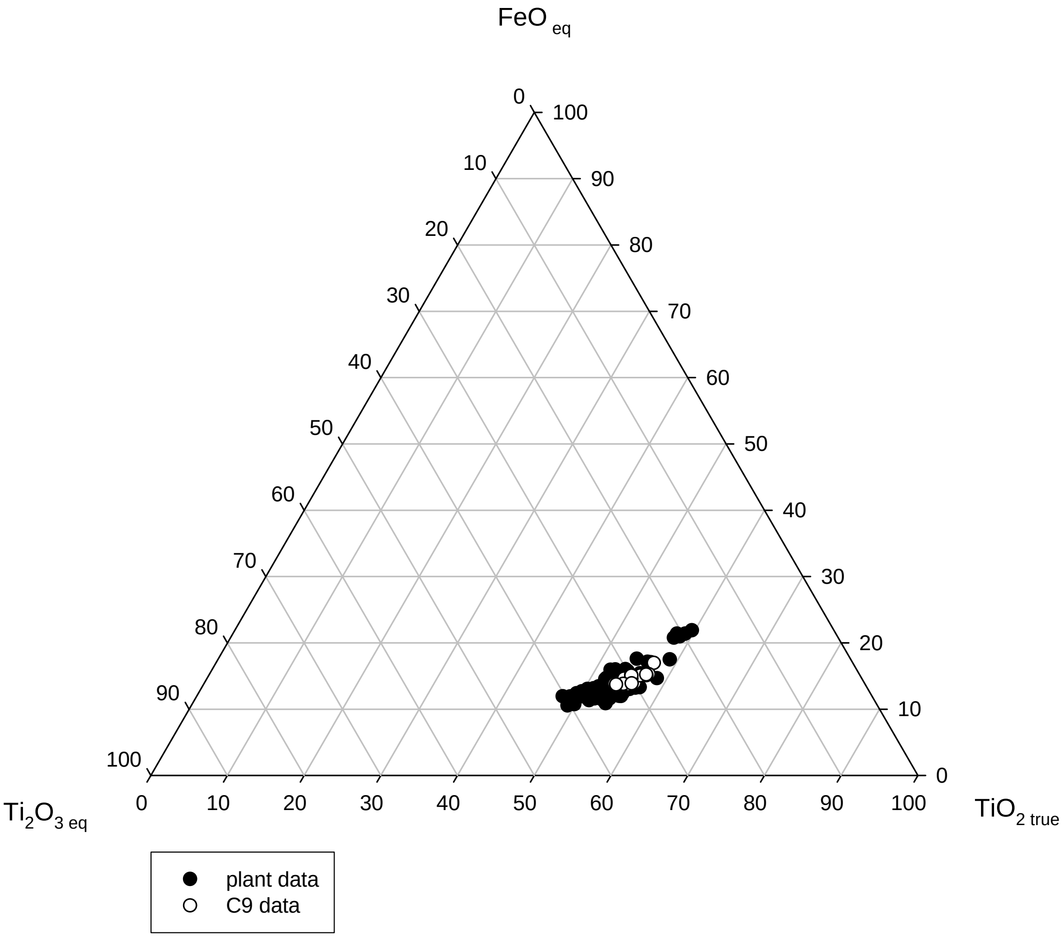

Figure 53 Relationship between equivalent %FeO, equivalent $\%Ti_2O_3$ and $\%TiO_2$ of slags produced at the pilot facility during campaign 9 and at the industrial scale plant.

3.6.1 Method

During a sampling trial the tapping rate of each pot from 43 taps made from the industrial scale furnaces was measured and recorded (one tap consisting of anything from 1 to 3 pots). For each pot a slag sample was taken at the lower end of the launder (Figure 54). As part of the hypothesis that oxidation plays a determining role in the final particle size distribution of the slag, the extent to which the sample is exposed to air is relevant. Samples taken at the end of the launder were therefore exposed to the oxidation conditions prevailing up to, and including flow over the launder. This includes exposure to oxygen lancing – which is used more extensively during slow taps in an attempt to encourage flows.

However, the oxidation level of these samples does not include further oxidation as the slag flows from the launder tip into the pot. Examples of the appearance of the tapping stream during fast and slow tapping are shown in Figure 55. During fast tapping the outer layers of the slag stream shield the core of the stream against oxidation; while the whole of the tapping stream of a slow tap – often individual droplets as in Figure 55(b) - is exposed to air. The probability of oxidation during a slow tap is therefore considerably higher than for a fast tap. However, the extent of oxidation in the falling slag stream was not quantified due to difficulties in obtaining safe access, preventing re-sampling from the pot.

The tap samples were analysed with XRF and wet chemistry – the latter to determine the Ti^{3+} content.

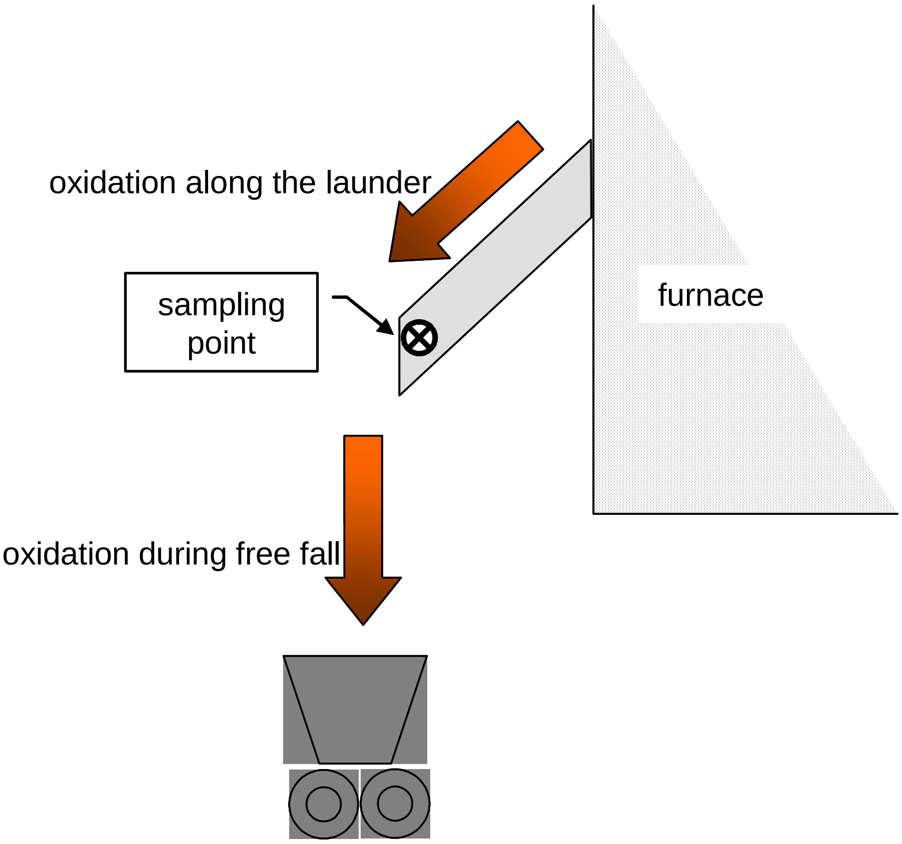

Figure 54 Sketch of the tapping system layout.

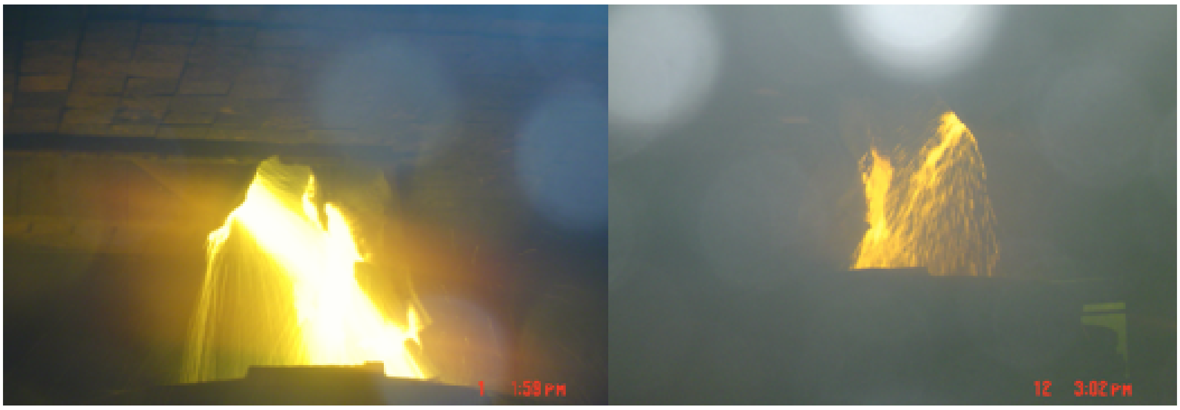

(a) (b)

Figure 55 Photographs of the tapping stream of (a) a fast and (b) a slow tap.

3.6.2 Results

The tapping rate as a function of %Ti_2O_3 is given in Figure 56. A weak tendency for the tapping rate to decrease with increasing %Ti_2O_3 is apparent. Although there does appear to be a stronger correlation between the %Ti_2O_3 and superheat[§§] (Figure 58), this correlation does not extend to tapping rate vs. superheat (Figure 57).

From Figure 59 a slight decrease in the equivalent %Ti_2O_3 for a given %FeO is apparent with slower tapping rates. Partial oxidation (of Ti^{3+} to Ti^{4+}) occurring up to the lower end of the launder is therefore implied. The occurrence of further oxidation is evident further downstream in the process: the trendline in Figure 59 for the cooled blocks shifts to even lower equivalent %Ti_2O_3 levels for a given equivalent %FeO level.

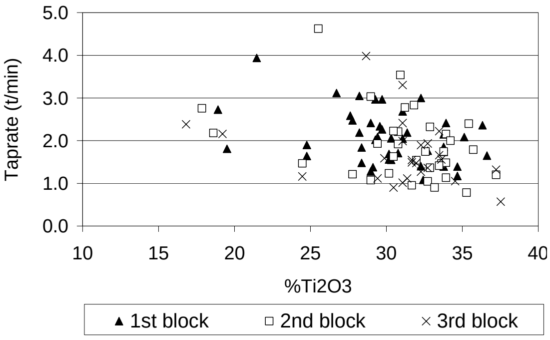

Figure 56 Tapping rate vs. %Ti_2O_3.

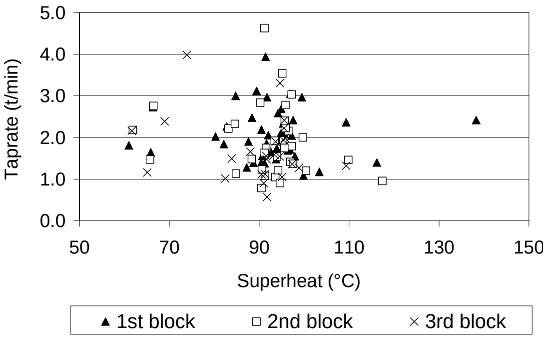

Figure 57 Tapping rate vs. superheat.

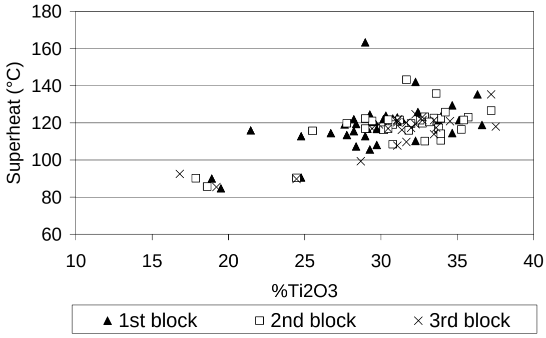

Figure 58 Superheat vs. %Ti_2O_3.

[§§] Superheat is defined as the temperature difference between the tap temperature and the calculated liquidus temperature for the given slag analysis. Details on the calculation of the liquidus temperatures are given in Part 3.

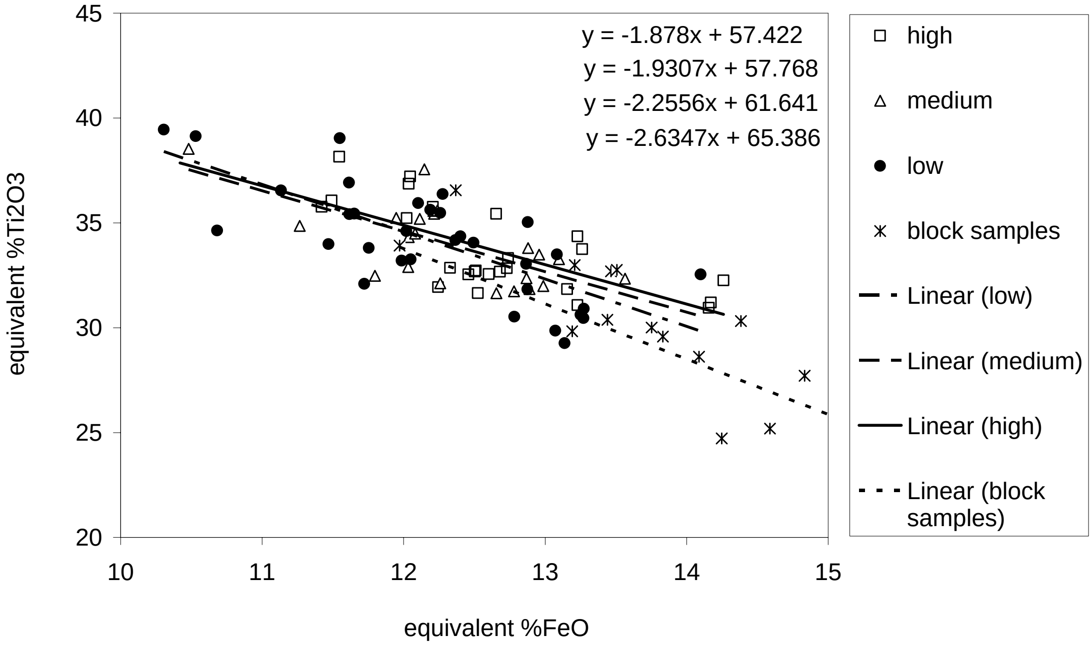

Figure 59 Equivalent %FeO vs. equivalent %Ti_2O_3 grouped for high, medium and low tapping rates. Also shown is the ratio for samples taken from the blocks following cooling in the block yard. The order of the correlations in the upper right corner corresponds with the order of the legend.

The shift in composition during oxidation is explained by the work of Pistorius et al.[4,22] with rutile being a reaction product of oxidation at temperatures in the solidification range of titania slags (Figure 3 and repeated here for ease of reference as Figure 60) and solid state temperatures (Figure 61). (Note that compositions are plotted as mole fractions in these figures). A typical slag composition lies at approximately 0.58 mole fraction $TiO_2/(TiO_2+FeO+Ti_2O_3)$ on the x-axis in Figure 60. On oxidation of the slag in the solidification temperature range, the slag composition moves toward the right of Figure 60 (with Ti_2O_3 decreasing and TiO_2 increasing proportionally) resulting in the formation of rutile.

Similarly, during oxidation in the solid state the initial slag composition moves along the oxidation path to the right of Figure 61 (with fully oxidised TiO_2 and Fe_2O_3 as the final reaction products). In the case of titania slag blocks the oxidation reaction does not progress into the FeO-$FeO_{1.5}$-TiO_2 system, but it does lead to an increased proportion of rutile, as expected from the shift in intersection point between the oxidation path and the M_3O_5-rutile tie line.

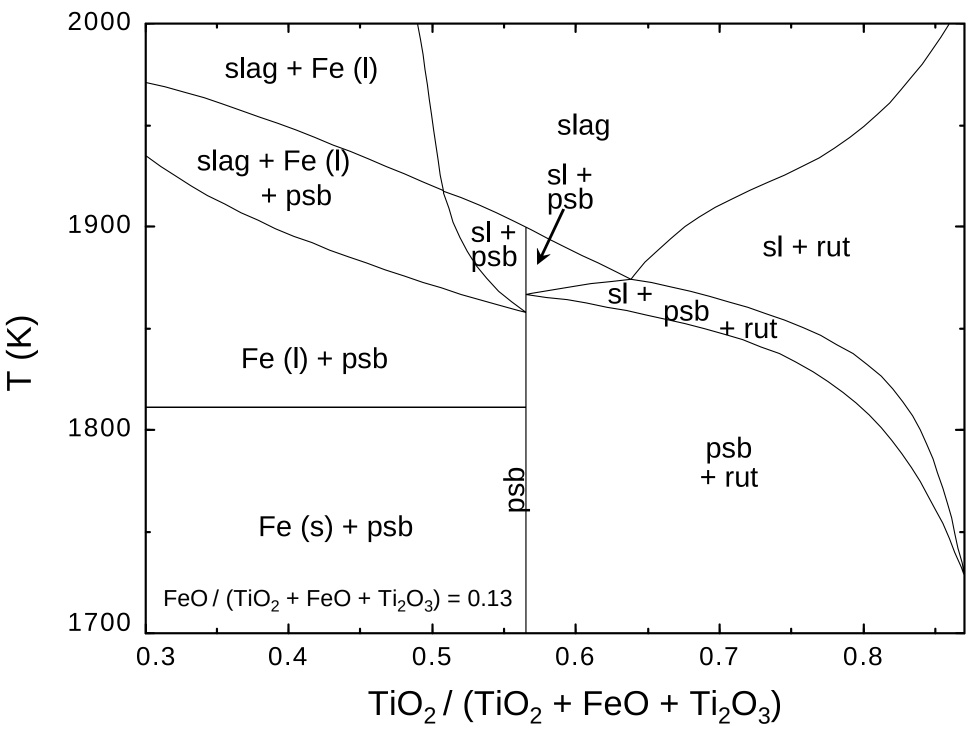

Figure 60 Calculated section through the TiO_2-Ti_2O_3-FeO phase diagram, at a constant FeO mole fraction of 0.13 (assuming that Magnéli phases are absent). Phases are identified as follows: "sl" is the molten oxide (slag), "psb" is the M_3O_5 phase, "rut" is the rutile-based solid solution (TiO_2 with some Ti_2O_3 in solution), and "Fe" is metallic iron[4].

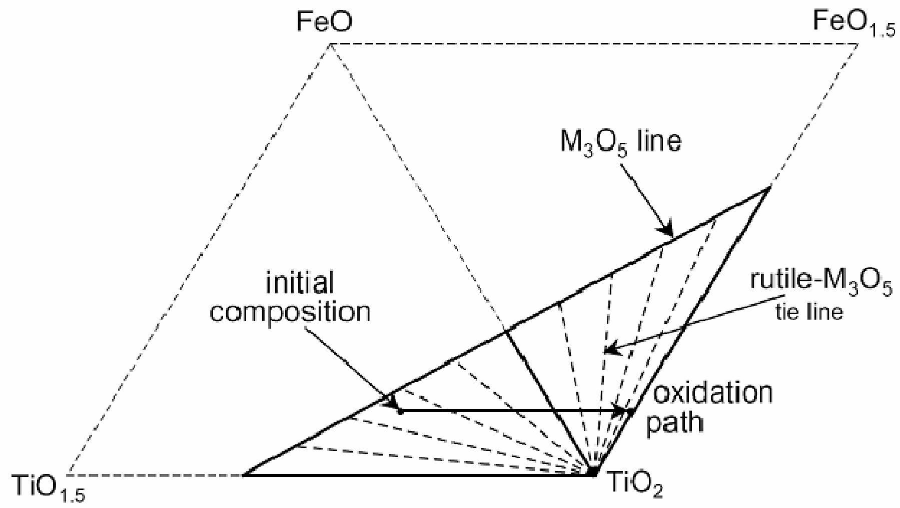

Figure 61 Change in phase relationships in high-titanium slag during solid-state oxidation above 550°C[4].

From Figure 62 the tapping rate does not appear to be a strong function of the $\%SiO_2$. It is interesting to note the strong correlation between %FeO and $\%SiO_2$ (Figure 63). The correlation coefficient between $\%SiO_2$ and %FeO is very strong at -0.906. (The correlation coefficients between the $\%SiO_2$ and $\%TiO_2$ or $\%Ti_2O_3$ are 0.866 and 0.780 respectively.) At FeO contents above 10% this correlation seems to be less pronounced. This correlation cannot be explained by a dilution effect: removing 1 mass% of FeO from the slag and increasing the equivalent %TiO_2 as per the correlation in Figure 53, while keeping the other oxide units constant, would increase the SiO_2 from 1.165% to 1.166% - an insignificant effect. The linear correlation in Figure 63 predicts an increase in excess of 0.05% SiO_2 for every 1% increase in FeO.

A possible explanation for the strong correlation between SiO_2 and FeO is the relationship between the reductant added to the process and the level of reduction in the slag: in the ilmenite smelting process the slag composition is mainly controlled with the amount of reductant added (in the form of anthracite) to the slag bath. Typically 30% to 45% of the total SiO_2 input into the process originates from the anthracite, of which close to 45% ends up in the titania slag (the remainder of the SiO_2 reports to the process dust and liquid metal). The strong correlation between the %SiO_2 and %FeO does not appear in the Campaign 9 data (Figure 64).

Hence, although the effect of SiO_2 on fines formation can be an indirect result of differences in the tapping rate (which in turn is presumed to depend on the major chemical components of the slag, notably the FeO level), it is not clear that this is the mechanistic link. The microstructural effects – of cracks associated with silicates (SiO_2 level) and rutile (present because of oxidation during tapping) – are much more evident.

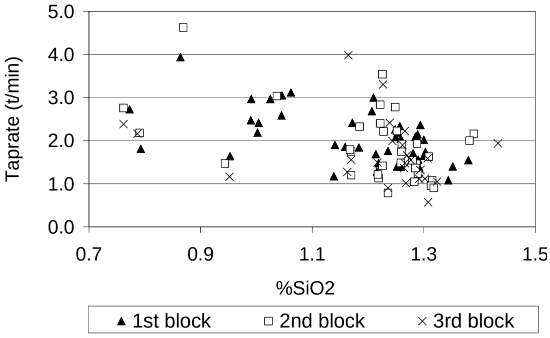

Figure 62 Tapping rate vs. %SiO_2.

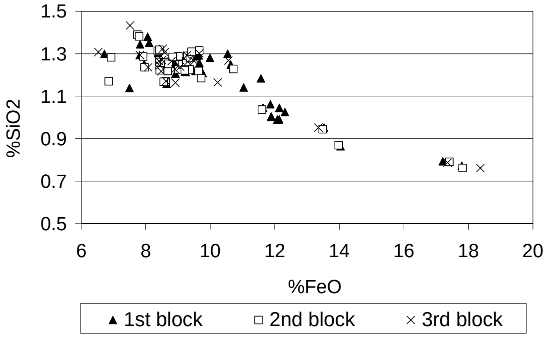

Figure 63 %FeO vs. %SiO_2.

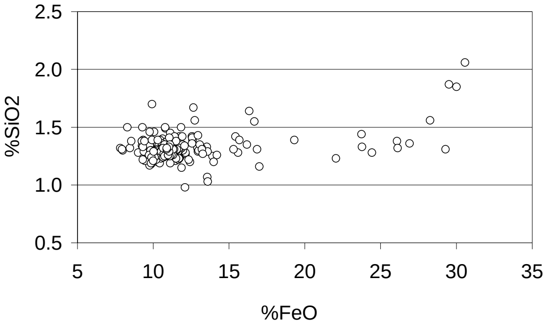

Figure 64 %FeO vs. %SiO_2 from campaign 9 data.

3.7 Surface temperatures

The average surface temperatures of the two blocks cooled under water for 3 days only are given in Figure 27. Although the two blocks were tapped 5 hours 9 minutes apart, they were tipped out of the pots 20 minutes apart. The surface temperatures of the two blocks ran remarkably close together – both reheated to approximately 90 ˚C some 105 - 106 hours after tipping, and again to 72 ˚C after approximately 125 hours after tipping. From 140 hours after tipping onwards, the surface temperatures remained below 50 ˚C and followed the variation in the ambient temperatures.

Since the spray water circuit was open to atmosphere, the temperature of the spray water is assumed to be equal to ambient temperature; and hence the surface temperatures of the blocks cooled under water for the full 10 days were also assumed to be close to ambient temperature.

The surfaces of all four blocks experienced little or no exposure to typical temperatures where decrepitation occurs[5,6] - limited decrepitation was therefore expected. However, as in the case of the pilot plant blocks discussed in Part 1, the blocks with an inferior cooling history resulted in higher fines generation during handling (Figure 34) and a larger variation in particle size distributions (Figure 44 and Figure 45). Should an oxidation mechanism be the cause of this – as suggested by the difference in %Ti_2O_3 between the tap samples and corresponding block samples (Figure 59) – it appears that oxidation occurs at temperatures as low as 100 ºC. This was tested by performing X-ray diffraction while the sample was exposed to air at 100 ºC, as reported in this section.

3.7.1 Method[***]

Finely ground samples of the four blocks were subsequently exposed to air at 100 ºC for prolonged periods and analysed for possible oxidation products. Initial experimental work on four samples from each block oxidised for periods of 2, 4, 7 and 15 days showed phase percentages within the range of sample heterogeneity. The heterogeneity of the samples was confirmed by a series of tests which served to evaluate the error in the machine (tested by re-analysing the same sample), error in sample preparation (tested by re-mounting the same sample) and error in sub samples (tested by analysing different sub-samples). The variation in sample composition was removed by exposing one sample from block L2R9 (fast tapped, 10 days water cooling) and L1R11 (slow tapped, 3 days water cooled) each, for in-situ XRD analysis at 100 ºC in an Anton Paar heating chamber using a platinum heating strip. Initially 8 measurements were done every 15 minutes, then 4 measurements every 30 minutes, and finally 8 measurements every 8 hours.

3.7.2 Results

The phase percentages over time are given in Figure 65. The M_3O_5 content of block L2R9 remains fairly constant over the duration of the oxidation period. A slight decrease in M_3O_5 is possible after approximately 40 hours which appears to be mirrored in the increase in the amount of amorphous phase. At 3.5 hours at 100 ºC the M_3O_5 in the sample from block L1R11 decreases significantly, with an accompanied increase in the amorphous phase. A slight decrease in rutile and anatase also appears at this time. No similar behaviour is apparent in the sample from block L2R9. After cooling for 10 days in water the mineralogy of block L2R9 appeared to have stabilised, while that of block L1R11 still shows the potential to oxidise further, transforming M_3O_5 to a weakly crystalline phase – possibly a forerunner of the M_6O_{11} phase. It is inconclusive on whether the faster-tapped and 10 day water-cooled block L2R9

[***] This work was conducted by Professor J. de Villiers of the Department of Materials Science and Metallurgical Engineering of the University of Pretoria.

has a more stable phase composition due to its tapping rate or to the more intense water cooling – or both.

It is however conclusive that oxidation can occur in a block at temperatures as low as 100 ºC. It furthermore appears that the tendency for this to occur is a function of the block history.

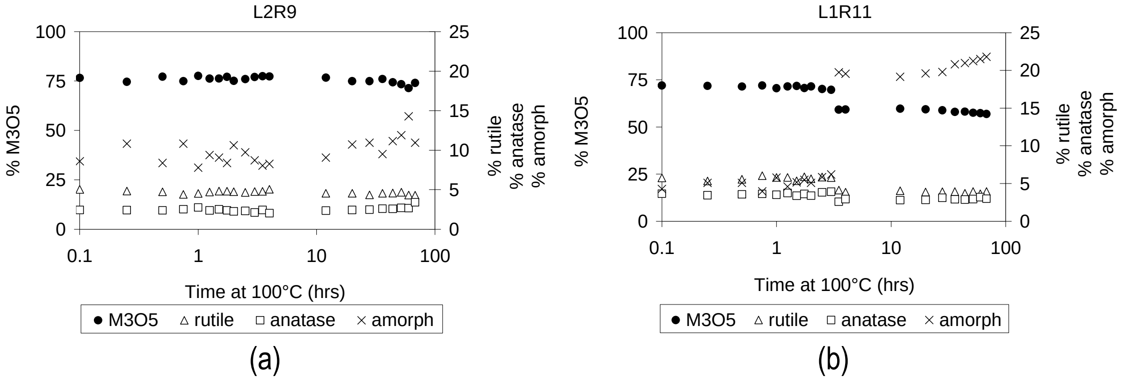

(a) (b)

Figure 65 Mineralogy of blocks (a) L2R9 and (b) L1R11 when exposed to air at 100 ºC.

3.8 Conclusions

The findings of Part 2 confirm the importance of the glass phase, tapping rate and cooling history on the final particle size distribution of a slag block.

A higher tapping rate reduces the extent of fines generated during materials handling. The mechanism behind this phenomenon appears to be driven by oxidation of the slag during the various processing steps. Extensive solid-state oxidation of the M_3O_5 phase to M_6O_{11} is known to cause formation of very fine particles. However, from the preceding results it is clear that more subtle forms, or less advanced stages of oxidation, influence the particle size distribution of a slag block. Such solid-state oxidation can occur at high temperatures, e.g. during tapping, during intermediate temperatures, e.g. initial cooling of the block, or at relatively low temperatures – of the order of 100 ˚C or lower. Although a link between oxidation and particle size distribution is obvious, the mechanism is still unclear.

Such oxidation can be suppressed with intensive water cooling. Apart from decreasing the block surface temperature to levels where the reaction kinetics is retarded, intensive water cooling seems to enhance phase stability. This is in contrast with insufficiently cooled slag which showed further oxidation at 100 ˚C.

Practical implementation of the above knowledge requires quantification of “intensive” and “insufficient”. This is addressed in Part 3.

The variation in particle size distribution of an intensely water cooled block is furthermore much less. Insufficiently water cooled blocks hence require broader operating ranges and equipment settings – preventing the attainment of optimum processing conditions which are required to maximise the ratio of the higher valued chloride to fine grade slag.

Of all chemistry parameters, the effect of the silicate phases is predominant in determining the particle size distribution. From the preceding results it is clear that the silicate phases are trapped during solidification between the karrooite (M_3O_5) granules. On subsequent breakage, intergranular breakage liberates some of these silicate phases while some remain attached to the surface of the coarser grains. The narrow range of silicate content within the samples used in this study does not provide an answer to the question as to how higher silicate levels would affect the grain size of the crushed and milled karrooite.

4 Part 3: Cooling Model

4.1 Background

Knowledge of the inner and outer temperatures of a block during cooling as functions of time should provide additional information which would be helpful in answering some of the questions posed in Part 2. To this end fully integrated partial differential equation solver software, FlexPDE[†††] was utilised to construct a numerical model predicting the surface and internal temperatures of a cooling slag block. The finite element model was constructed by Dr Johan Zietsman from Ex-Mente[‡‡‡] (a process modelling company) utilising FlexPDE version 5.0.13. The full model specification and all the inputs (such as slag properties, calculation procedure for heat transfer coefficients and pot dimensions) were provided by the author; the role of Dr Zietsman was to perform the actual coding of the model within FlexPDE. The accuracy of the numerically calculated solution via FlexPDE (version 5.0.13) was tested against the results of an analytical solution for a simple geometry. The numerical solution yield results similar to that of the analytical method. Details of this comparison are provided below. The model output was calibrated against actual internal slag block temperature measurements by adjusting the thermal conductivity of the slag (the only adjustable parameter, apart from boundary conditions such as cooling regimes, pouring temperature and block size). Subsequent verification of the model was done against actual surface temperature measurements and the thickness of the solidified shell after primary cooling.

4.2 Comparison of analytical and numerical solutions

Analytical solutions are not available for the situation considered here, with a fairly complex geometry, temperature-dependent materials properties, and time-dependent boundary conditions. For this reason, a numerical method had to be used to calculate the temperature changes during cooling of the blocks. However, to test the accuracy of the numerical solution calculated by FlexPDE, the "Neumann problem" (for which an analytical solution is available[29]) was used for comparison.

The Neumann problem considers a one-dimensional semi-infinite volume of material with a congruent melting point (T_f), which is originally at a uniform temperature (T_0) above the melting point. The face of the semi-infinite body is suddenly cooled (at time zero) to a temperature (T_s) which is below the melting point. The thickness of the solidified shell is then given by

$$X = 2\gamma\sqrt{\alpha_1 t}$$

where γ is a constant which is determined as mentioned below, and α_1 is the thermal diffusivity of the solid.

The temperature profiles in the solid ($x < X$) and liquid ($x > X$) are given by

---

[†††] See www.pdesolutions.com

[‡‡‡] See www.ex-mente.co.za

Solid: $$T_1 = T_s + \frac{T_f - T_s}{\mathrm{erf}(\gamma)} \mathrm{erf}\left(\frac{x}{2\sqrt{\alpha_1 t}} \right)$$

Liquid: $$T_2 = T_o - \frac{T_0 - T_f}{\mathrm{erfc}(\gamma\sqrt{\alpha_1/\alpha_2})} \mathrm{erfc}\left(\frac{x}{2\sqrt{\alpha_2 t}} \right)$$

where α_2 is the thermal diffusivity of the liquid, x is the distance from the cooled face, and *t* is time.

The value of γ is found by solving the following equation:

$$\frac{\exp(-\gamma^2)}{\mathrm{erf}(\gamma)} - \frac{k_2}{k_1}\sqrt{\frac{\alpha_1}{\alpha_2}} \frac{(T_o - T_f)\exp(-\alpha_1\gamma^2/\alpha_2)}{(T_f - T_s)\,\mathrm{erfc}(\gamma\sqrt{\alpha_1/\alpha_2})} = \frac{L\sqrt{\pi}}{c_1(T_f - T_s)}\gamma$$

In this expression, the subscript 1 refers to solid and 2 to liquid, k is the thermal conductivity, c is the heat capacity, and L is the heat of solidification.

For comparison of the analytical and numerical solutions, material properties which are similar to those of the real slag were assumed. These properties were as listed below:

C_1 (J/kgK)	C_2 (J/kgK)	L (J/kg)	ρ (kg/m^3)	k_1 (W/mK)	k_2 (W/mK)	α_1 (m^2/s)	α_2 (m^2/s)
900	1000	650000	4000	2	4	5.56×10^{-7}	1.0×10^{-6}

The initial temperature was taken as T_0 = 1550°C, the melting point as T_f =1520°C (for the numerical solution, the liquidus and solidus were set at 1530 ˚C and 1510 ˚C respectively), and the surface temperature as T_s = 100°C.

As in the numerical solution for the block, the apparent heat capacity was increased – by an amount of $L/(T_{liquidus} - T_{solidus})$ – between the solidus and liquidus temperatures, to include the heat of solidification. To avoid the discontinuities caused by the step changes in both the heat capacity and conductivity values, the SWAGE function of FlexPDE was used. This function generates a smooth transition from one value to another over a specified transition width (this width was taken to be one-tenth of the liquidus-solidus gap for the heat capacity, in this case). The SWAGE function also has smooth derivatives. The FlexPDE code of this example is given in section 5.4. As the code indicates, the surface temperature was not changed instantaneously in the numerical solution, but was ramped from the initial value to the required surface temperature over a period of 500 s; this (rather than an instantaneous change in temperature) was used to avoid numerical instability.

The temperature profile along this one dimensional domain for time increments starting at 1 hour, and for times double thus up to 128 hours are given in Figure 66. In this figure solid lines represent the results of the analytical solution while broken lines represent that of the FlexPDE solution. Figure 67 shows the shell thickness as calculated by both methods as a function of cooling time. Initially the numerical solution predicts a thicker shell that what the analytical solution does. This is a remnant of the initial difference in boundary conditions. After approximately 16 hours of cooling the two methods give comparable results.

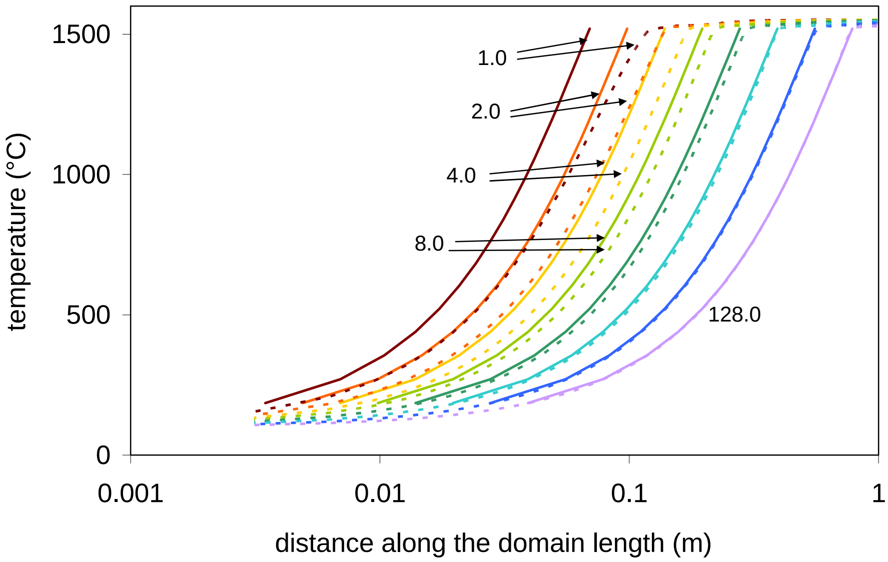

Figure 66 Temperature of the one dimensional semi-infinite body as a function of its distance during solidification (Neumann problem). Solid lines represent the results of the analytical solution, while broken lines represent the numerical results. The unit of the numbers is in hours.

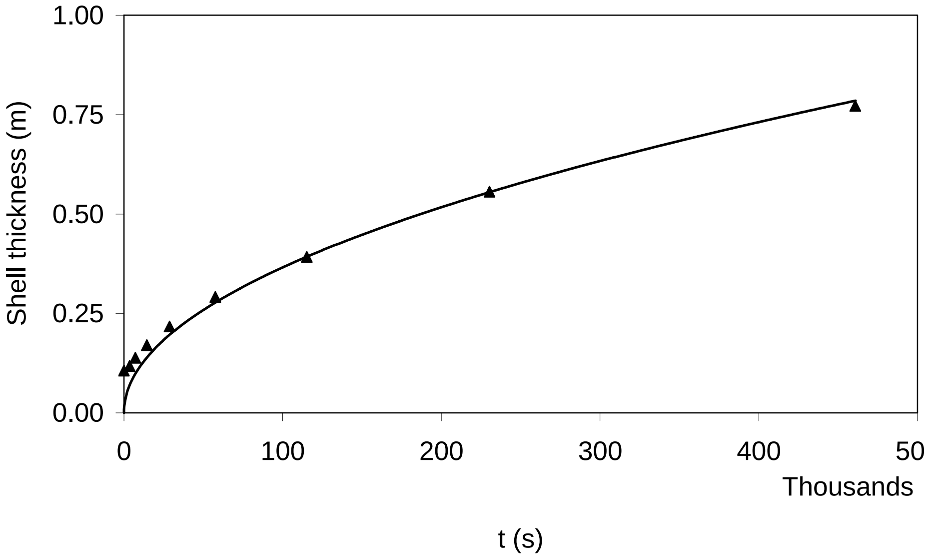

Figure 67 The shell thickness of a one dimensional semi-infinite shape solidifying from 1550 ˚C. The solid line represent the solution from the analytical method described above, while the triangles represent that of the numerical model as calculated by FlexPDE.

4.3 Model formulation

The following is a description of the model inputs, outputs, assumptions and material properties:

4.3.1 Requirements

In order to verify the model calculations on small scale 1 to 1.5 ton blocks, and to simulate large scale 17 to 20 ton blocks, the model provides for the following input:

Pot dimensions for the 1.5 ton pilot plant and 20 ton industrial plant pots

- Capacity (1.5 or 20 tons);
- Radius of the open end (0.523 or 1.175 m);
- Slope of the upper sidewall (15˚);
- Pot shell thickness (0.04 or 0.11 mm) and
- Pot temperature before tapping commences (25ºC).

Tap data

- Tap mass (ton);
- Tap temperature (ºC) and
- Slag FeO content (%).

Cooling conditions

- Time when the block is tipped out of the pot (with reference to the time at which the taphole was closed being time zero);
- Provision for several cycles of air and water cooling at adjustable durations;
- Water volumetric flow (m^3/hr);
- Drop diameter (mm) and
- Drop speed (m/s).

Other

- Ambient temperature and
- The time duration for which the model must perform the heat transfer calculations

The modelling software was able to provide calculated results in the following formats:

- Contour plots of isotherms within the block at a given time(s);
- Parameter (e.g. temperature) vs. time graphs for a named feature (e.g. horizontal surface) of the block;
- Parameter vs. position on a feature for a given time series.

4.3.2 Simplifications

- The pot shell is level with the upper surface of the block.

This is a valid assumption when the pot is filled up to capacity. Smaller taps do however result in the pot shell extending above the block. Such an extension of the pot will likely act as a fin for heat transfer: resulting in additional cooling at the corner between the horizontal and inclined surfaces of the block. However, given that conduction through the solidified solid slag shell is rate-determining (as the results show), the effect of this extra area for convection is small.

- The pot consists of a shell only, i.e. no provision was made for trunnions and feet.

  The additional mass and feet of the pot theoretically add to the heat extraction capacity of the pot. However, with the thermal resistance of the solidified slag as the rate limiting parameter (Section 4.10), the cooling of the block should not be different with or without this detail.

- The slag density is constant at 3.8 t/m^3.

  From visual inspections the slag is less dense closer to the (upper) horizontal surface in comparison with the bulk of the block: the internal structure closer to the horizontal surface typically contains gas holes which will result in a less dense material. This, combined with decrepitation occurring on the upper horizontal surface of the block during primary cooling, impacts notably on the accuracy of the heat transfer predictions (Section 4.8). However, in the absence of a detailed model of liquid flow and solidification shrinkage within the block during solidification, this effect could not be taken into account.

4.4 Energy balance

The primary partial differential equation to solve is:

$$\rho_{slag} Cp_{slag} \frac{dT}{dt} - k_{slag}\left(\frac{\partial^2 T}{\partial r^2} + \frac{\partial^2 T}{\partial z^2}\right) = 0 \tag{4}$$

Where ρ_{slag} is the density of the slag

Cp_{slag} is the heat capacity of the slag

$\frac{dT}{dt}$ is the rate of change of temperature at a given position

k_{slag} is the thermal conductivity of the slag

$\frac{\partial^2 T}{\partial r^2}$ and $\frac{\partial^2 T}{\partial z^2}$ are the second-order partial differentials of temperature in the r and z directions respectively. In a matrix format (as applied in the software calculations) the term $k_{slag}\left(\frac{\partial^2 T}{\partial r^2} + \frac{\partial^2 T}{\partial z^2}\right)$ translates to $\nabla \bullet \left(k_{slag} \nabla T\right)$ or in software recognizable nomenclature: $div\left(k_{slag} \times grad\left(T\right)\right)$.

The allowable error of the model is set at 0.1%. Should it be required the software refines the mesh in order to comply with this error limit.

In the instance of the two dimensional block, the numerical model was capable of utilising the heat capacity values (discussed in section 4.6.1) without the need of the SWAGE function as described in section 4.2. The heat conduction values were furthermore coded in as a linear function of temperature – hence also eliminating a potential discontinuity. As with the one-dimensional example, the heat of solidification was included by increasing the apparent heat capacity between the liquidus and solidus temperatures.

An energy balance check was run for a pilot scale size slag block. The results of this exercise are shown in Figure 68. The figure shows the total energy content of the cooling slag block, together with the total heat lost from the sides of the pot and the top surface of the ingot (up to a given time). The total of the energy content of the slag block and pot, and the integrated heat lost, is constant - demonstrating that the energy balance is maintained during the solidification simulation.

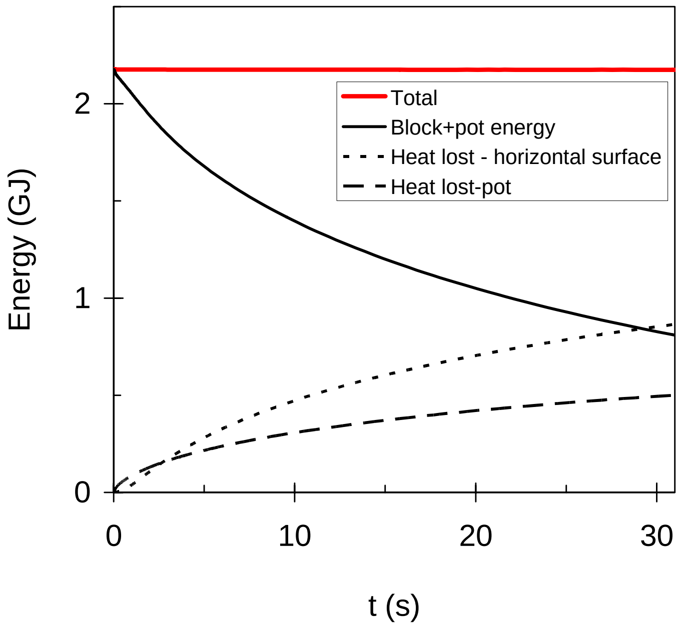

Figure 68 Results of an energy balance check conducted over a pilot scale size slag block.

4.5 Shape notations, dimensions and calculations

A sketch of a slice out of the block is shown in Figure 69. The important shape notations and their meaning are listed in Table 13.

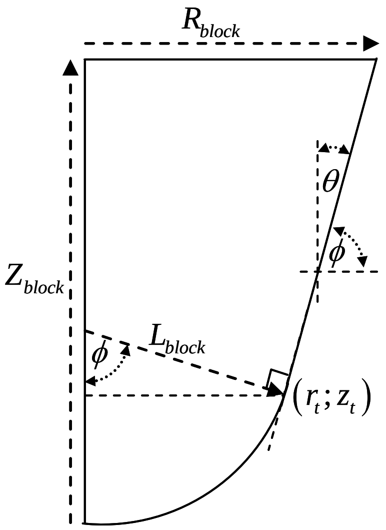

Figure 69 A sketch of the block illustrating the important shape notations.

Table 13 List of shape notations and their meaning used in describing the block shape.

Symbol	**Description**
R_{block}, Z_{block}	Maximum radius and full height of the slag block
L_{block}	Radius of the spherical section of the block
θ	Angle of upper pot shell with the vertical
ϕ	Angle of upper pot shell with the horizontal
r_t, z_t	Radius and height of the block where the conical and spherical sections meet

The following primary relationships were used to derive all shape dimensions:

- $V_{pot} = \dfrac{pot\ capacity}{slag\ density}$
- $V_{block} = \dfrac{tap\ mass}{slag\ density}$
- $r_t = L_{block} \cos\theta$
- $z_t = L_{block}(1-\sin\theta)$
- Volume of a cone, $V_{cone} = \dfrac{\pi}{3} radius^2 \times height$
- Volume of a spherical cap, $V_{sphere} = \dfrac{\pi}{3} radius^3 \left(2+\cos\phi\right)\left(1-\cos\phi\right)^2$
- Area of a conical section, $A_{cone} = \pi\left(r_t + R_{block}\right)\sqrt{\left(Z_{block} - z_t\right) + \left(R_{block} - r_t\right)}$
- Area of a spherical cap, $A_{sphere} = 2\pi radius^2 \times \left(1-\cos\phi\right)$

Hence, with the volume and radius of the pot, V_{pot} R_{pot} respectively as input parameters, the radius of the spherical section of the block is calculated from:

$$L_{block} = \left(\frac{V_{pot} - \dfrac{\pi R_{pot}{}^{3}}{3\tan\theta}}{\dfrac{-\pi\cos\theta^{3}}{3\tan\theta} + \dfrac{\pi}{3}\left(2+\cos\phi\right)\left(1-\cos\phi\right)^{2}} \right)^{\frac{1}{3}} \tag{5}$$

The block radius and height is calculated from:

$$R_{block} = \left(\frac{3\tan\theta}{\pi}\left(V_{block} - V_{sphere}\right) + r_t^{3} \right)^{\frac{1}{3}} \tag{6}$$

$$Z_{block} = \frac{\left(R_{block} - r_r\right)}{\tan\theta} + z_t + L_{block} \tag{7}$$

With the shape specified according to the above equations FlexPDE5 constructs a mesh with triangular nodes. The mesh is adapted with consistency checks over the solutions of the partial differential equations. When required the node size and/or time step is reduced. This typically occurs close to the solidification front, because of the sharp change in enthalpy with temperature. An example of a mesh configuration showing original and reduced size nodes are shown in Figure 70.

To accommodate the change in the boundary conditions of the system (cooling of a combined slag block and pot vs. cooling of a slag block alone, after tipping of the slag block from the pot), two FlexPDE codes were constructed. The first provided for a volume consisting of two materials (the block and pot) each with its own material properties. In this instance heat transfer from the pot and horizontal block surface to the surroundings was by natural air cooling. The second file provided for the block on its own. Heat transfer to the surroundings could be selected as either natural air cooling or water cooling. Data transfer from the first to the second file was established through the TRANSFER statement of FlexPDE. This statement enables full data sharing between different FlexPDE runs. The boundary conditions for both these systems are discussed in section 4.7. The full code of both FlexPDE files is given in section 5.5.

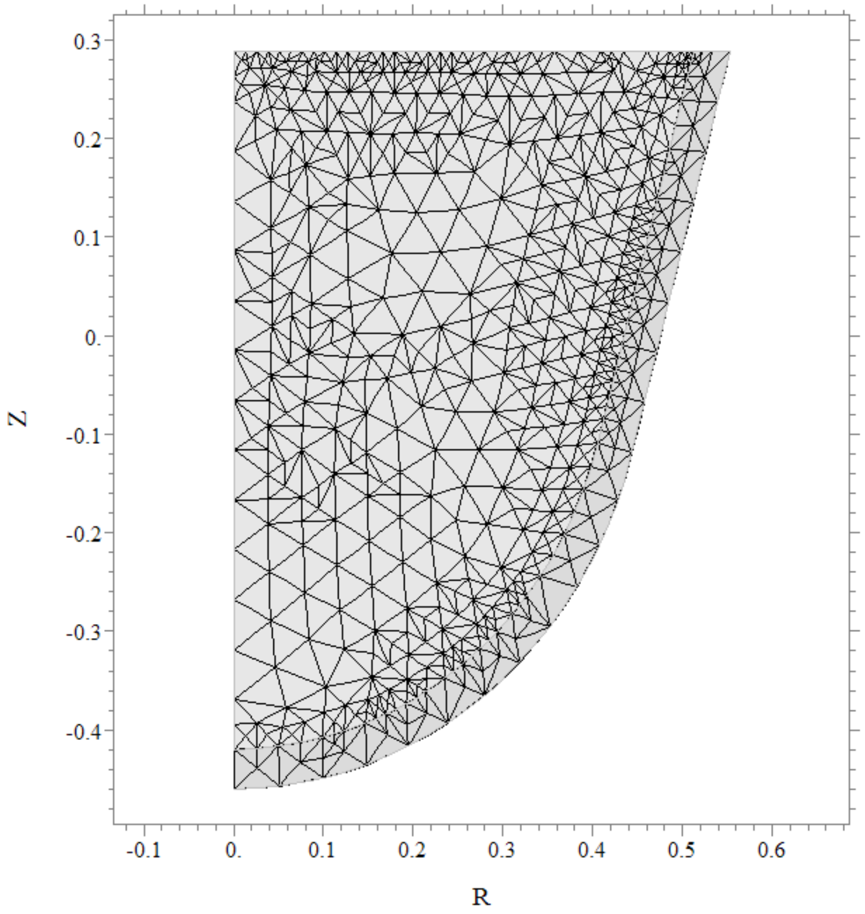

Figure 70 Example of the mesh configuration for the slag block (Z and R are in metre). Areas of denser node configurations are shown where FlexPDE reduced the node size to remain within the accuracy tolerance of 0.1%.

4.6 Material definitions

4.6.1 Slag thermodynamic properties

The liquidus and solidus temperatures of the slag, and the change in enthalpy of the slag with temperature, are important inputs into the heat transfer model. These properties were estimated by means of FactSage[17], and approximated with simple mathematical relationships (based on the FeO content of the slag as the independent variable). The procedure followed is outlined below.

4.6.1.1 **Choice of slag compositions**

A database of 112 full plant slag analyses was obtained (elemental composition determined by X-ray fluorescence, and Ti^{3+} by titration). These analyses are shown in Figure 71. The mass percentages of the other components varied approximately linearly with FeO content, for FeO levels ranging from just above 6% to more than 18%. These analyses were grouped together by FeO content, and an average analysis per FeO range was obtained (a valid approach, given the approximately linear variation of slag analysis with FeO content). These average analyses are listed in Table 14. Note that these analyses are normalised to 100%; small amounts of other impurities (K_2O, V_2O_3, Nb_2O_3 and ZrO_2) - making up less than 1% of the slag - are hence neglected.

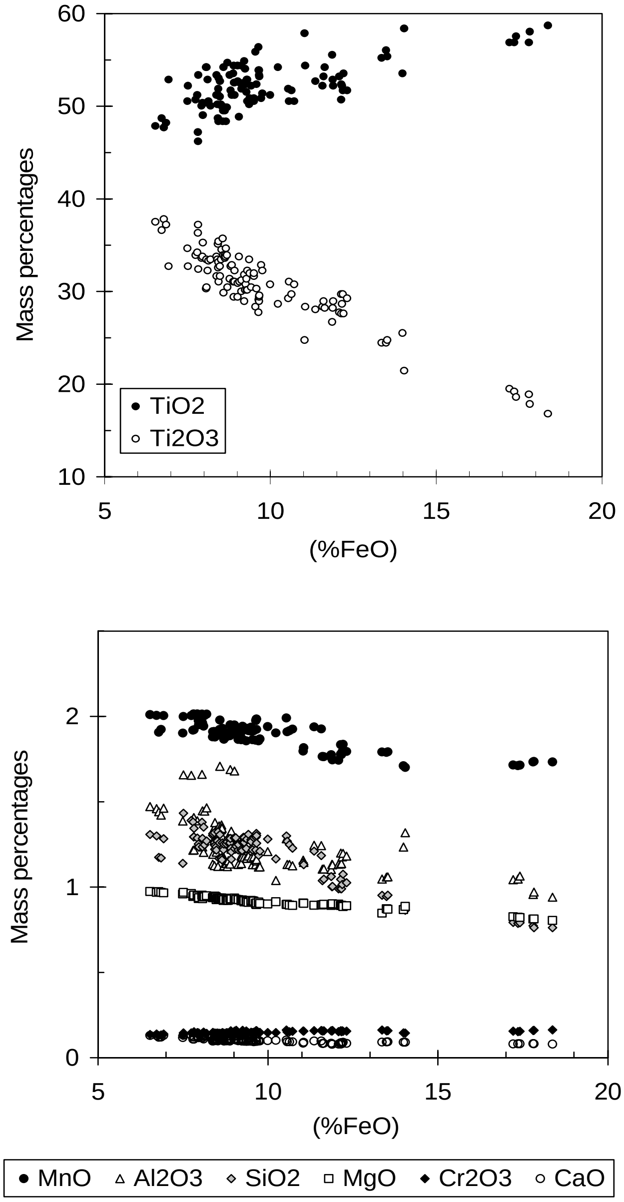

Figure 71 Analyses (mass%) of industrial plant slags.

4.6.1.2 **Thermodynamic properties**

FactSage was used to predict the changes in phase composition and enthalpy with temperature, for each of the eight slag compositions. The following phases (from the "FT oxid" database of FactSage were considered):

- Solutions: SlagA, pseudobrookite (karrooite), $Ca_3Ti_2O_7$-$Ca_3Ti_2O_6$ and perovskite
- Stoichiometric solid phases: all relevant oxides, except the Ti_nO_{2n-1} Magnéli phases.

In addition to suppression of the Magnéli phases, ilmenite and spinel solid solutions were also not considered. This was to ensure stability of pseudobrookite down to room temperature (in line with the observed persistence of pseudobrookite in the actual solidified slag).

Typical changes in the liquid fraction and enthalpy for one of the slags (no. 4 in Table 14) are given in Figure 72. The continuous curves give the temperature dependence as predicted by FactSage. This shows a sharp decrease in liquid fraction just below the liquidus, with a tail extending to lower temperatures. For the purpose of the model, this relationship was approximated by a linear one, matching the calculated profile at the liquidus temperature and at 80% solidification (indicated by T_{20} in the figure). The effective solidus temperature ("$T_{solidus}$" in Figure 72) was found by extending the linear relationship to zero liquid.

Table 14 Average compositions of eight groups of slags from the full plant dataset; each group spans a specific range of FeO contents.

No.	FeO	Ti_2O_3	TiO_2	MnO	Al_2O_3	SiO_2	MgO	Cr_2O_3	CaO
1	6.86	38.05	49.09	2.00	1.48	1.26	0.99	0.14	0.13
2	8.05	34.21	51.75	2.01	1.42	1.33	0.97	0.15	0.12
3	8.85	33.09	52.34	1.94	1.31	1.27	0.95	0.15	0.11
4	9.71	31.28	53.38	1.96	1.21	1.29	0.93	0.15	0.10
5	10.85	30.28	53.33	1.95	1.17	1.25	0.92	0.16	0.10
5	12.14	28.93	53.69	1.83	1.18	1.07	0.91	0.16	0.09
7	13.89	24.51	56.59	1.78	1.16	0.93	0.88	0.16	0.09
8	17.98	18.83	58.55	1.76	1.02	0.79	0.83	0.16	0.08

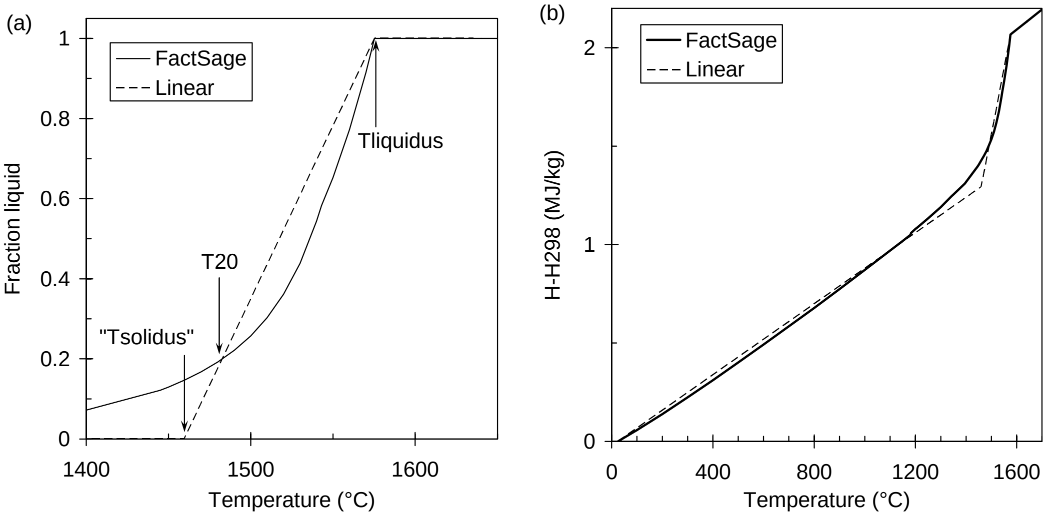

Figure 72 Predicted effect of temperature on (a) the fraction liquid and (b) the enthalpy (relative to that of solid slag at 298 K) of slag no. 4. The broken line gives the linear approximation which was used as model input.

A linear enthalpy relationship was similarly used as model input. This matched the calculated enthalpy at the liquidus temperatures, and in the fully liquid region (where FactSage reports a constant heat capacity). In the solid region, the linear relationship matched the calculated trend at 298 K and at 1373 K (1373 K is just below the generally observed true solidus); all enthalpies were expressed relative to that of the solid at 298 K. The estimated solid enthalpy at the extrapolated solidus temperature, "$T_{solidus}$", was found by extrapolating this 298 K – 1373 K linear relationship for the solidified slag; the enthalpy was also assumed to change linearly (between that of the solid slag and that of the liquid slag) over the temperature range $"T_{solidus}"-T_{liquidus}$. Hence the effective heat capacity between $"T_{solidus}"$ and $T_{liquidus}$ is given by equation (8) (with temperatures in ˚C). These linear approximations are given in Table 15. The fitted relationships are given in equations (9) to (14).

$$Cp^{solid-liquid} = \left(\frac{H_{298}^{liquid} + Cp^{liquid}\left(T_{liquid} - 25\right) - Cp^{solid}\left("T_{solid}" - 25\right)}{T_{liquid} - "T_{solidus}"} \right) \tag{8}$$

Table 15 Parameters of linear approximations to thermodynamic properties, and fitted relationships.

No.	$T_{liquidus}$	$"T_{solidus}"$	Cp^{solid}	Cp^{liquid}	H_{298}^{liquid}
	(°C)	(°C)	(J/kgK)	(J/kgK)	(MJ/kg)
1	1601.17	1470.34	903.60	1024.32	0.5014
2	1586.19	1451.36	903.73	1020.45	0.4989
3	1581.56	1463.56	902.75	1018.46	0.4957
4	1575.25	1459.53	901.88	1016.48	0.4916
5	1570.31	1453.99	900.64	1015.02	0.4867
6	1564.82	1450.26	898.56	1012.52	0.4819
7	1553.52	1440.63	896.46	1007.64	0.4745
8	1537.42	1427.74	891.26	1001.96	0.4510

$$T_{liquidus} = 0.2351(\%FeO)^2 - 11.24(\%FeO) + 1664.1 \qquad °C \tag{9}$$

$$"T_{solidus}" = 0.0364(\%FeO)^2 - 4.845(\%FeO) + 1502.7 \qquad °C \tag{10}$$

$$Cp^{solid} = -0.0314(\%FeO)^2 - 0.4042(\%FeO) + 908.51 \qquad J/kgK \tag{11}$$

$$Cp^{liquid} = 0.0561(\%FeO)^2 - 3.3668(\%FeO) + 1044.3 \qquad J/kgK \tag{12}$$

$$H_{298}^{liquid} = -139.51(\%FeO)^2 - 1086.1(\%FeO) + 515805 \qquad J/kg \tag{13}$$

$$f_{liquid} = \min\left(\max\left(\frac{T - "T_{solidus}"}{T_{liquidus} - "T_{solidus}"}, 0 \right), 1 \right) \tag{14}$$

The conductivity of titania slag is incorporated in the model as a linear function of temperature (equation (15)). The values of the constants a and b were determined by fitting the model results to the actual measurements from thermocouples inserted into the slag blocks directly after tapping. This work was conducted during Campaign 10 on the pilot plant. This calibration procedure is discussed in detail in section 4.8.

$$k = aT + b \tag{15}$$

4.6.2 Pot thermodynamic properties

The heat capacity of the cast steel pot was assumed to be constant at 465 W/kg˚C[30], while the thermal conductivity of the pot was expressed as a function of temperature (equation (16)). Both these values are representative of a 0.5%C steel. To test this approach, the heat losses from the outer surface of the pot are shown by the black line in Figure 73. The black line in Figure 73 represents the heat losses from the outer surface with a constant heat capacity; while the brown line represents model results with the heat capacity of the pot equal to that of pure iron - and varying with temperature (Figure 74). The heat losses from the block surface to the pot differed at most by 20,000 J for the full and simplified expressions for pot heat capacity. This difference furthermore occurs only over the first hour of cooling. Hence, seen relative to the magnitude of energies present in the block during the first hour of cooling (1 kg of slag at 1600˚C has an energy content in the order of 2 MJ - Figure 72), this difference was treated as negligible and the heat capacity of the steel pot was set at a constant value.

$$k_{pot} = -0.03488\left(T_{slag}^{surface}\right) + 59.1 \tag{16}$$

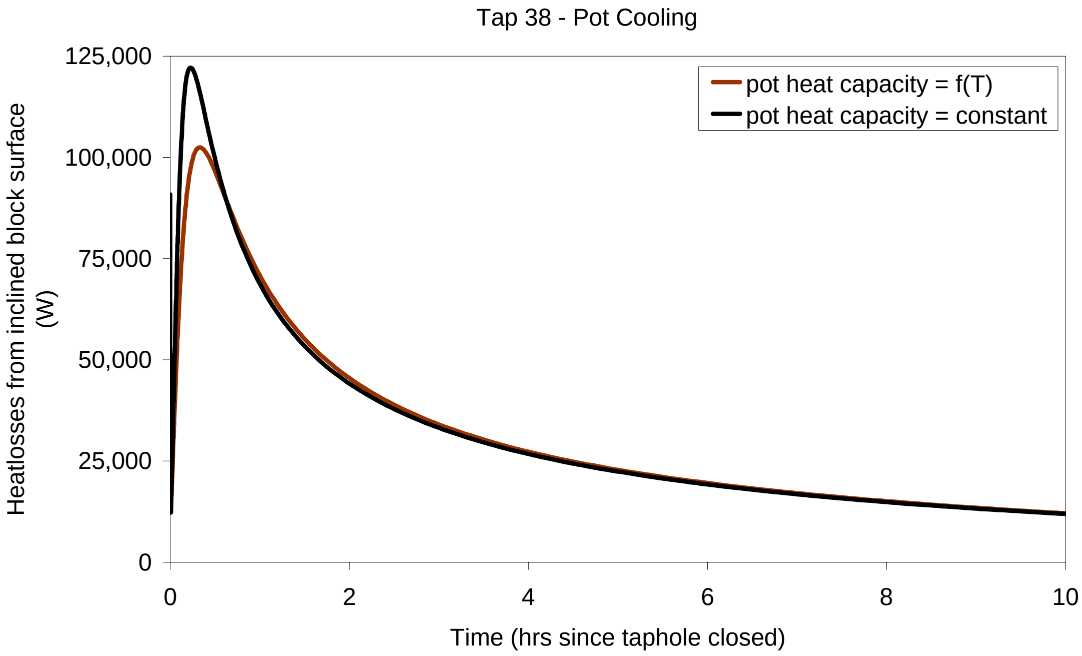

Figure 73 Heat losses from the outer pot surface during solidification of a 1,365 kg block. The black line represents model results with constant heat capacity of the pot, while the brown line represents model results where the pot heat capacity is that of pure iron.

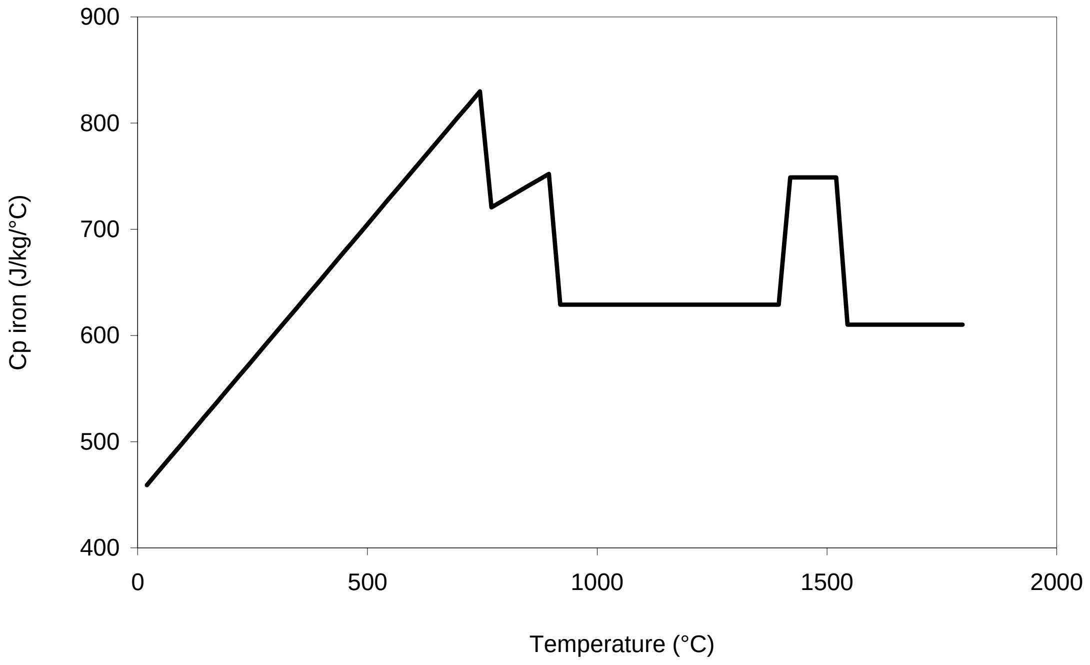

Figure 74 Heat capacity of pure iron.

4.7 Boundary conditions

4.7.1 Contact coefficient between the block and pot surfaces

A thermal contact resistance arises between the slag block and the pot, and this may affect the solidification process by lowering the rate of heat transfer from the block to the pot. It is hence important to evaluate whether this contact resistance is as significant here as it is in the solidification of other materials in metal moulds, for example aluminium alloy castings[31] and partially crystalline polymers.[32]

The thermal contact resistance arises because the solid surfaces (of the pot and the slag block) are not in perfect contact, but rather contact one another at asperities.[33] Conductive heat transfer between the solids is limited to the small area of the asperities; the conduction area hence depends on the roughness of the two surfaces, and the pressure on the surfaces. In parallel, conduction occurs through the layer of gas (air in this case) between the surfaces.

The temperature drop across the contact resistance is then given by:

$$\Delta T = AR_c \frac{q}{A}$$

where ΔT is the temperature drop, A the apparent interfacial area (that is, not just the contact area at the asperities), and $\frac{q}{A}$ is the heat flux across the interface.

The contact resistance represents the parallel contribution of conduction through the asperities, and conduction through the air gap:

$$\frac{1}{R_c} = \frac{1}{R_{asperities}} + \frac{1}{R_{gap}}$$

The resistance of the air gap is given simply by

$$AR_{gap} = \frac{L}{k_{air}}$$

where L is the average width of the air gap, and k_{air} the average thermal conductivity of the air in the gap.

For conforming solid surfaces (that is, solid surfaces in good macroscopic contact, as is the case here for the block in the conical pot, one expression for the contact resistance of the asperities is:[33,34]

$$AR_{asperities} = \frac{\sigma / m}{\left[1.25 k_s \left(\frac{P}{H_c}\right)^{0.95}\right]}$$

where σ is the average roughness of the surface (in m), m is the average slope of the asperities, k_s is the harmonic mean of the thermal conductivities of the contact surfaces (defined below), P is the pressure (in Pa) on the interface, and H_c is the Vickers hardness (in Pa) of the surface.

The value of m can be estimated from the surface roughness (for σ in μm) as follows:[33]

$$m = 0.076\sigma^{-0.52}$$

The harmonic mean thermal conductivity is given by

$$\frac{1}{k_s} = \frac{1}{2}\left(\frac{1}{k_{pot}} + \frac{1}{k_{block}}\right)$$

These expressions were used to estimate the size of the contact resistance.

In this application, the effect of the contact resistance is expected to be small, for two reasons. First, the conical shape of the pot ensures good contact with the solid surface of the block: if temperature changes cause the block to shrink (or the pot to expand), the block simply descends in the pot. Second, the low thermal conductivity and large size of the block imply a low heat flux through the block-pot contact area, and large solidification times. Solidification times are several hours (pilot-scale blocks) to tens of hours (plant-scale blocks); in comparison, the solidification times of the aluminium alloy and polymer castings quoted above are of the order of minutes. The low heat flux through the block-pot contact implies a small temperature drop across the thermal contact resistance.

The approach to evaluation of the effect of the contact resistance was twofold. First, the expressions as given above were used to estimate the thermal contact resistance. Second, temperature measurements were conducted on the pot during solidification of a pilot-scale block.

To estimate the contact resistance, a simplified conical block was considered, as illustrated in the figure below. An upper-bound estimate of the force normal to the conical interface between the pot and the block (F_N) is obtained if it assumed that the pot-block surface is frictionless. The vertical force (F_V) must equal the weight of the block, hence F_N is given by:

$$F_N = \frac{\rho V g}{\sin\theta}$$

where ρ is the density of the slag, V the volume the block, g acceleration due to gravity, and θ the half-angle of the apex of the cone.

The volume of the cone is given by

$$V = \frac{\pi r^2 h}{3}$$

The pressure across the interface is then given by

$$P = \frac{F_N}{A_{cone}} = \frac{g\rho h}{3}$$

In deriving this relationship, the expressions for the area of the cone $A = \pi r\left(r^2 + h^2\right)^{0.5}$ and $\sin\theta = \frac{r}{\left(r^2 + h^2\right)^{0.5}}$ were used.

Since the contact resistance decreases if the contact pressure (P) increases, the largest contact resistance is expected for the pilot-scale block, with the smallest height.

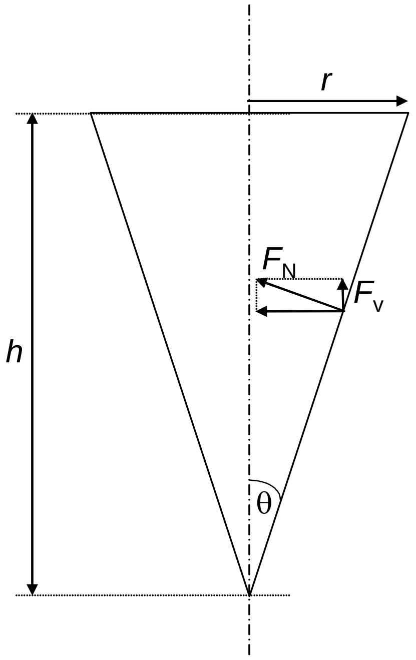

Figure 75 Simplified conical pot and block, which was used to estimate the thermal contact resistance.

Estimated values of the contact resistance, based on these expressions, are given in Table 16. In these expressions, the surface roughness (σ) is taken to be 100μm; microscopic inspection of solidified slag surfaces indicates that this is an upper bound on the actual roughness. The thermal conductivity of air is taken to be 0.04 W/mK, which is a reasonable average for the gap temperatures during solidification. The average width of the air gap was taken to be equal to the surface roughness. The results in the table indicate that conduction across the interface is expected to be dominated by conduction through the air, with a total thermal resistance of 0.0025 m^{2}K/W, for a 100 μm gap.

This estimated thermal resistance is small compared with the thermal resistance of the solidifying shell of the slag block; a thermal resistance of 0.0025 m^{2}K/W (equal to the estimated contact resistance) is given by a slag layer which is 2.5 mm thick (assuming a thermal conductivity of 1 W/mK). The conclusion that the contact resistance is small compared with the thermal resistance of the solidified slag holds even for a much larger pot-block air gap. For example, an air gap of 1 mm is equivalent (in thermal resistance) to a solidified slag layer with a thickness of 25 mm, which is also small compared with the size of the block.

Table 16 Input data used to estimate contact resistance for pilot-scale block, with estimated resistances.

ρ_{slag} (kg/m^3)	k_{slag} (W/mK)	k_{steel} (W/mK)	k_s (W/mK)	k_{air} (W/mK)	σ (μm)	m	h (m)	P (Pa)	H (kg/mm^2)	H (GPa)
4000	1	50	1.96	0.04	100	0.83	0.6	7848	150	1.47

Thermal resistance of asperities: (m^{2}K/W)	Thermal resistance of air gap: (m^{2}K/W)
5.0	0.0025

Based on these considerations, the thermal contact resistance is expected to play an insignificant role in solidification of the block. Note that radiative heat transfer was not considered in this analysis, since radiation effects can be neglected for temperatures below 900 K[35] (which is typical for the pot for most of the cooling period). Any role of radiation would decrease the contact resistance, in any case.

The above conclusion was tested by comparing pilot-plant measurements of the pot temperatures with model predictions. For these model predictions, the effect of the contact resistance was neglected. If the contact resistance were significant, the pot temperature would hence be significantly lower than the predicted values. The results of this comparison (conducted during campaign 10) are shown in Figure 76, with the model predictions shown as lines, and measured temperatures as data points. The locations of the thermocouples are shown in Figure 85; the three thermocouples were located between the open end of the pot (black line in Figure 76) and the transition point between the spherical and conical sections of the pot (brown line in Figure 76). The temperature measurements from thermocouples 2 and 3 fit neatly between these two lines. The deviation between the readings from thermocouple 1 and the model predictions of the pot open end edge could be explained by the model assumption that the pot height is equal to that of the block. This differs from the actual situation where the pot edge extends above the slag block. As mentioned earlier, this edge could act as a cooling fin leading to lower temperatures in the upper ring of the pot which is exposed to natural air cooling.

The accuracy of the model predictions hence confirms that omitting a contact resistance between the block and pot does not impact on the accuracy of the model results.

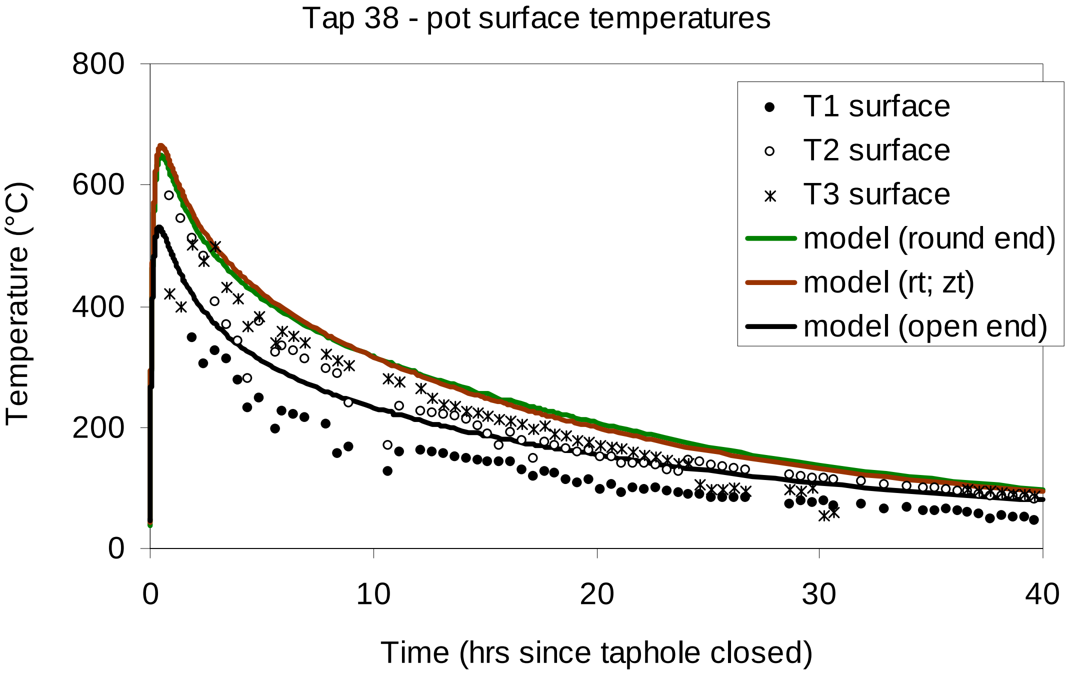

Figure 76 Pot surface temperatures as predicted by the cooling model (lines). Symbols indicate surface measurements derived from actual temperature measurements within the pot shell.

4.7.2 Contact coefficient between the block and ground surface

During secondary cooling the horizontal surface of the block faces the ground. With the hot downward-facing surface effectively suppressing natural air convection, this boundary condition was modelled via a contact resistance as per equation (17). This resistance depended on the thermal conductivity of air, k_{air}; average height of the air gap between the block and ground surfaces, $\overline{d}$, and the radiation coefficient, h_{rad} which is calculated as per equation (21). While the width of the air gap between the block and ground surfaces does vary, an average gap height of 10 mm was assumed. Comparisons of the heat losses from the horizontal surface of the block after tipping where the average air gap varied between 5 and 50 mm showed block cooling to be fairly insensitive to the size of the air gap (Figure 77). Subsequent model runs were conducted assuming an average gap height of 10 mm.

$$h_{contact} = \frac{k_{air}}{\overline{d}} + h_{rad} \tag{17}$$

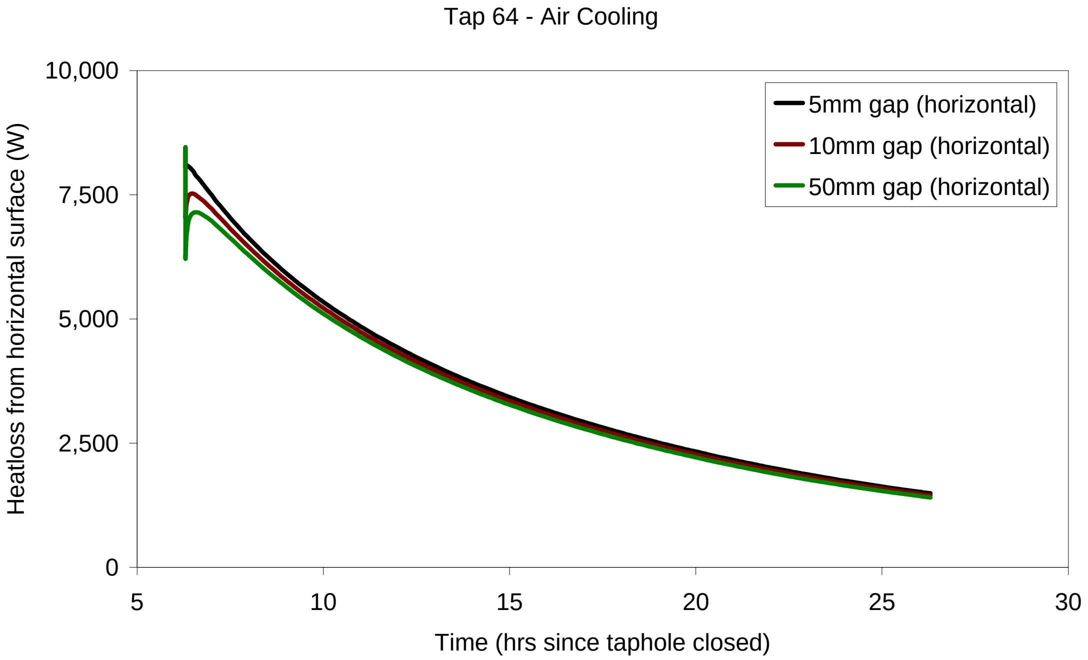

Figure 77 Heat losses from the horizontal downward-facing surface of the block during secondary cooling. The different lines show the insensitivity of heat losses to the assumed height of the air gap between the block surface and ground.

4.7.3 Natural convection in air

During primary cooling in the pot, the pot outer surface and horizontal block surface are exposed to natural convection in air. During this time the pot surface acts as an inclined heated surface facing downwards. After being tipped out of the pot, the conical and spherical surface of the block acts as an inclined heated surface, facing upwards. The convection heat transfer coefficient for the above conditions was calculated from correlations and constants provided by Holman[36] and summarised below.

The average heat transfer coefficient, $\overline{h_{conv}}$ is calculated from equation (18).

$$\overline{Nu}_f = C\left(Gr_f \Pr_f\right)^m = \frac{\overline{h_{conv}}L}{k_f}$$

so that (18)

$$\overline{h_{conv}} = \frac{k_f}{L} C\left(Gr_f \Pr_f\right)^m$$

Where k_f and $\Pr_f$ are the thermal conductivity and Prandtl number of air at film temperature respectively.

L is the characteristic dimension of the shape. For the horizontal surface of the block $L = \dfrac{surface\ area}{surface\ perimeter} = \dfrac{1}{4} diameter$. For the pot surface facing downwards (during primary cooling and the block surface facing upwards (after the block is tipped out of the pot) $L = \dfrac{\cos\theta}{Z_{block}}$.

The Grashof number at film temperature, Gr_f, is calculated from

$$Gr_f = \frac{g\,\beta\left(T_{surface} - T_\infty\right)L^3}{\upsilon^2}$$

with $g = 9.81\ \text{m.s}^{-2}$

$\beta =$ inverse of the average film temperature in K (19)

$T_{surface} =$ surface temperature

$T_\infty =$ temperature of the surroundings

$\upsilon =$ kinematic viscosity of air at film temperature

For the block surface facing downwards, the Grashof number is modified to:

$$Gr_f = Gr_f \cos^2\theta \tag{20}$$

The values for the constants C and m are as per Table 17.

Table 17 Constants used for calculation of the heat transfer coefficient as per equation (18).

	Horizontal		**Vertical**	
Grashof number	$\leq 8\times10^6$	$> 8\times10^6$	$\leq 10^9$	$> 10^9$
C	0.54	0.15	0.59	0.10
m	$\frac{1}{4}$	$\frac{1}{3}$	$\frac{1}{4}$	$\frac{1}{3}$

The total heat transfer coefficient (Figure 78) is calculated from the sum of the convection component as described above and the radiation component as per equation (21).

$$h_{rad} = \sigma\varepsilon\left(T_{surface}{}^{2} + T_{\infty}{}^{2}\right)\left(T_{surface} + T_{\infty}\right) \text{ with } T \text{ in K} \qquad (21)$$

where $\sigma = 5.669\text{x}10^{-8}$ in $\text{W/m}^2\text{K}^4$, and

$\varepsilon = 0.8$

The resulting heat transfer coefficients for the horizontal and inclined surfaces are shown in Figure 78. At higher temperatures the contribution of the radiation coefficient (brown line in Figure 78) becomes increasingly predominant.

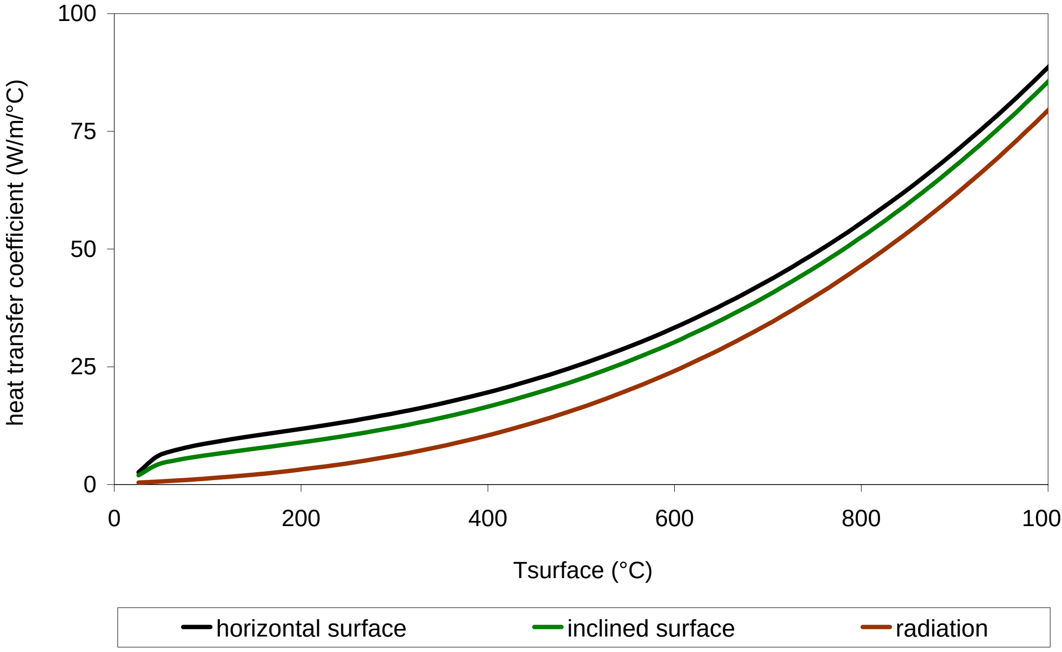

Figure 78 Heat transfer coefficients for natural cooling in air.

4.7.4 Forced spray water cooling

The heat transfer conditions in spray water cooling are considered similar to the known heat transfer conditions of pool boiling[37,38]. The heat transfer regimes of pool boiling are illustrated in Figure 79: at high surface temperatures – above the Leidenfrost point –film boiling prevails. In this regime a vapour blanket prevents direct contact between the surface and liquid and effectively limits heat transfer. On further cooling of the surface to below the Leidenfrost point, the heat transfer gradually increases up to the point of critical heat flux. This increase in heat transfer is driven by breaking up of the vapour film resulting in partial contact between the liquid and surface. Below the critical heat flux, nucleate boiling determines the rate of heat transfer; and at temperatures below the point of incipience of nucleate boiling, natural convection prevails. The shape of the boiling curve for a given heat transfer situation depends (amongst others) on the surface roughness, water temperature and spray hydrodynamics. For the purposes of the block cooling model the heat transfer coefficient for spray water cooling was derived from the work of Klinzing et al[37], utilising the original expressions of Mudawar[38].

Heat transfer coefficients calculated for varying volumetric flows, drop speeds and drop diameters are shown in Figure 80. A list of expressions used to calculate the heat transfer coefficient is given in Appendix 5.4 Within the tested range of parameters, the heat transfer coefficient is sensitive to the volumetric water flow rate, but insensitive to the drop diameter. Increasing drop speed moves the Leidenfrost temperature to higher values. It is interesting to note that the lowest heat transfer coefficients are experienced at surface temperatures in the range where decrepitation typically occurs.

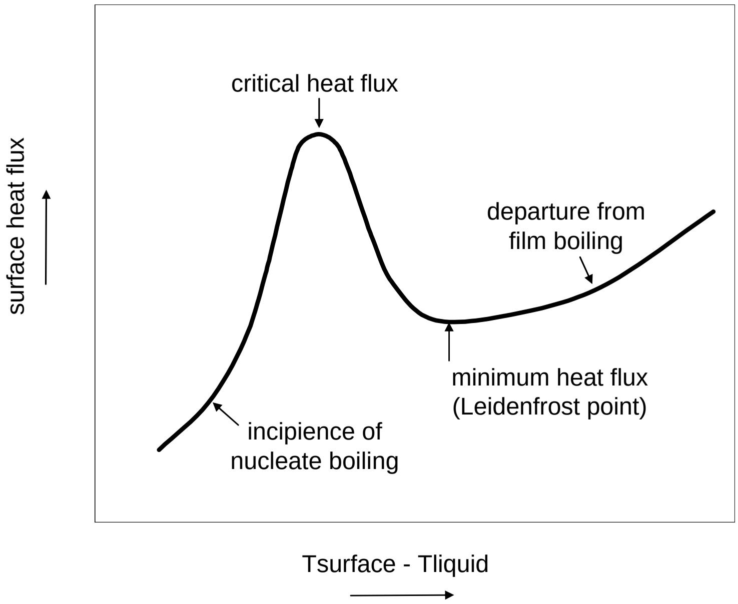

Figure 79 Boiling curve associated with quenching of a hot surface in a stagnant pool.[37,38]

The model-predicted surface temperatures of block 42 (campaign 9) are shown in Figure 81 with varying water volumetric flow and drop speed values. The black line represents the average surface temperature of a narrow (±10mm) vertical area along the inclined surface of the block as measured with a stationary thermal camera. The surface temperatures appear to be insensitive to the spray water parameters. Note that the periodic temperature increases are reheating of the block surface when the spray water was turned off. With the spray water turned on, the water flow was clearly sufficient to quench the surface temperature to close to the water temperature (hence the insensitivity to spray water parameters).

The change in heat transfer coefficient between water and air cooling is shown in Figure 82. (During periods of water cooling on a given surface, the heat transfer coefficient of air is ignored for that surface – during air cooling the water-cooling heat transfer coefficient is not used.) While the heat transfer coefficient in natural air cooling is usually around 10 $W/m^2{}^\circ C$, it increases by two to three magnitudes during spray water cooling (note the logarithmic scale of heat transfer coefficient on the right hand side of the graphs in Figure 82).

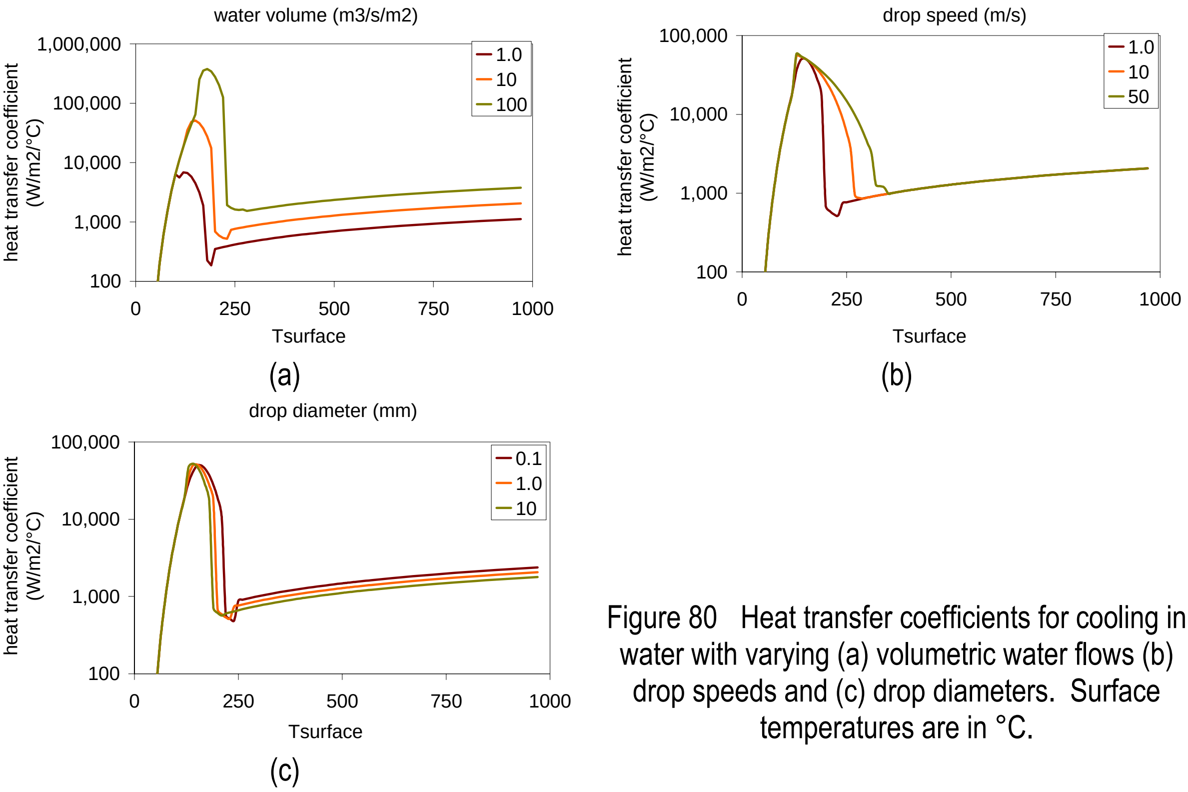

(a) (b)

(c)

Figure 80 Heat transfer coefficients for cooling in water with varying (a) volumetric water flows (b) drop speeds and (c) drop diameters. Surface temperatures are in °C.

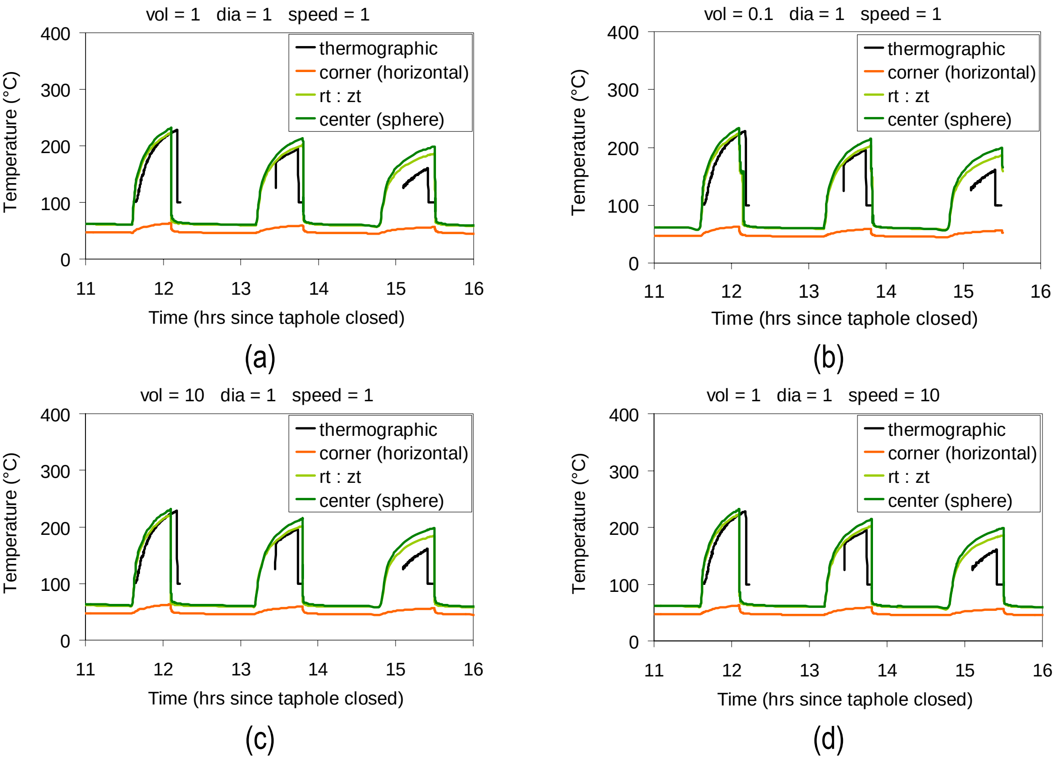

(a) (b)

(c) (d)

Figure 81 Model-predicted results for block surface temperatures for different of water volumetric flow rates and drop speeds.

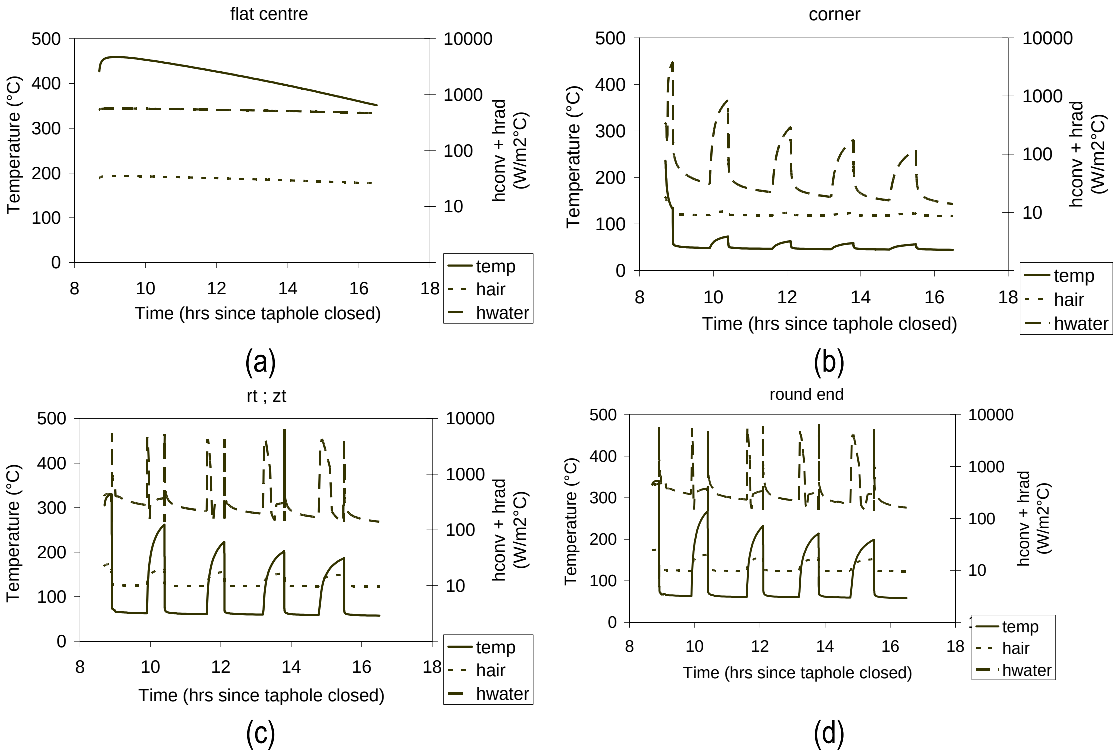

Figure 82 Surface temperature and heat transfer coefficients for intermittent water cooling at four positions on the block. “Flat centre” is the centre of the horizontal surface, “corner” is the corner between the horizontal and inclined surfaces of the block, “r_t : z_t” is the join on the surface of the spherical and conical block volumes, and “round end” is the centre of the round end of the block.

4.8 Model calibration

During the 10th 3 MVA pilot-plant ilmenite-smelting campaign thermocouples were inserted into two blocks directly after tapping. These thermocouples were positioned as shown in Figure 83 and Figure 85. The configuration of the three centre line thermocouples is shown in Figure 84. The Alsint tube (alumina thermocouple sheath) was inserted into the silicon carbide tube and both these tubes were closed at the bottom end. Three 0.25 mm (wire diameter) type S-thermocouple and sheath combinations were positioned within the Alsint tube at different heights as shown in Figure 85. The thermocouples marked A, B and C denote the thermocouples which were inserted down the centre line of the block; while those marked 1, 2 and 3 were double thermocouples inserted into holes drilled into the shell of the pot. The thermocouple inserted off-centre into the block (Figure 83) failed and hence no data was obtained from it.

The tap information and slag composition of the two taps are given in Appendix 5.8.

The thermal conductivity of titania slag is not a well known number – especially not as a function of temperature[39]. The model results were hence calibrated to the actual thermocouple measurements by adjusting the slag thermal conductivity. The accuracy of the fit was determined by calculating the sum of the errors as per equation (22). The RMS error proved to be smallest with the thermal conductivity expressed as a linear function of temperature: $k = aT + b$. The relationships between the choice of constants a and b and the resulting RMS errors are shown in Figure 86 and Figure 87 for taps 37 and 38 respectively. The best-fit values for the respective coefficients for each of the thermocouples are shown in Table 18, while the best fit k-value for each thermocouple is plotted in Figure 90. The uppermost thermocouple inserted into tap 37 (T_A) deviated substantially from the close grouping of the other five thermocouples. From visual observations the upper layer of the slag block typically has a very porous structure. Hence, with thermocouple T_A being located high up in the block (Figure 85) it was likely positioned within this porous upper layer where the thermal conductivity is apparently dominated by the porous slag structure. The best fit k-value for this layer seems to be 0.5 W/m.˚C, much lower than elsewhere in the block. As mentioned earlier, the effects of the porous structure of the upper layer were not included in the model; the thermal conductivity everywhere in the slag block was hence described by equation (23).

$$RMS\ error = \sqrt{\frac{\sum\left(T^t_{actual} - T^t_{\text{mod}\,el}\right)^2}{n}} \tag{22}$$

$$k_{slag} = 0.00175T + 0.3 \text{ where } T \text{ is in } {}^\circ C \tag{23}$$

Figure 83 Photograph of a slag block and pot directly after thermocouples were inserted into the block. For support the refractory tubes were inserted into the slag through slots in a steel channel which was placed horizontally over the pot edge.

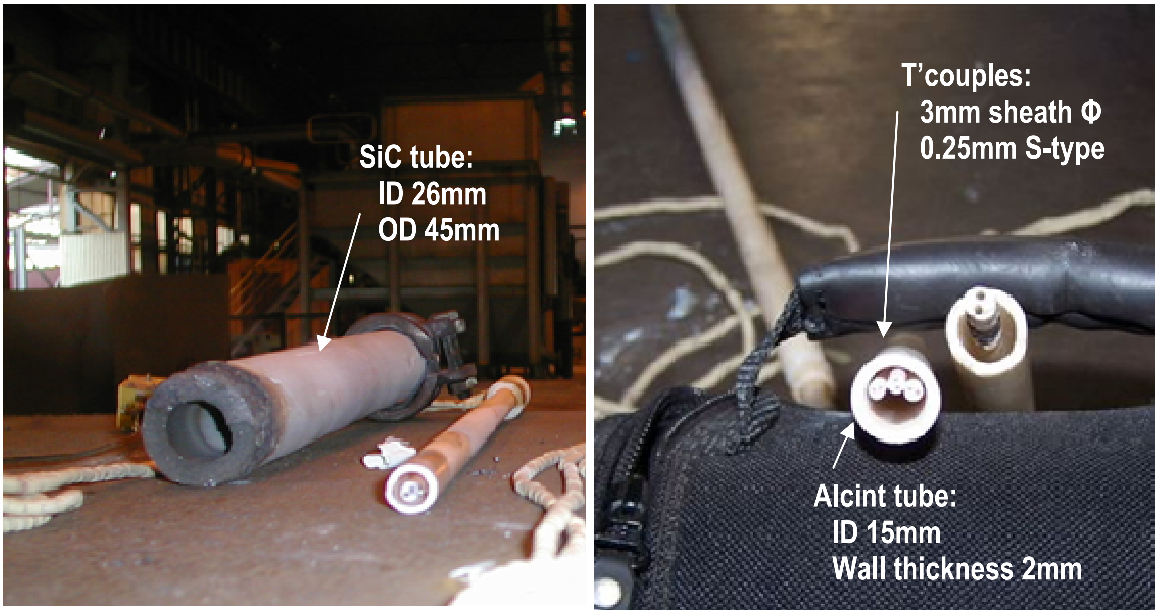

(a) (b)

Figure 84 Photograph showing the configuration of the thermocouples which were inserted into the slag blocks.

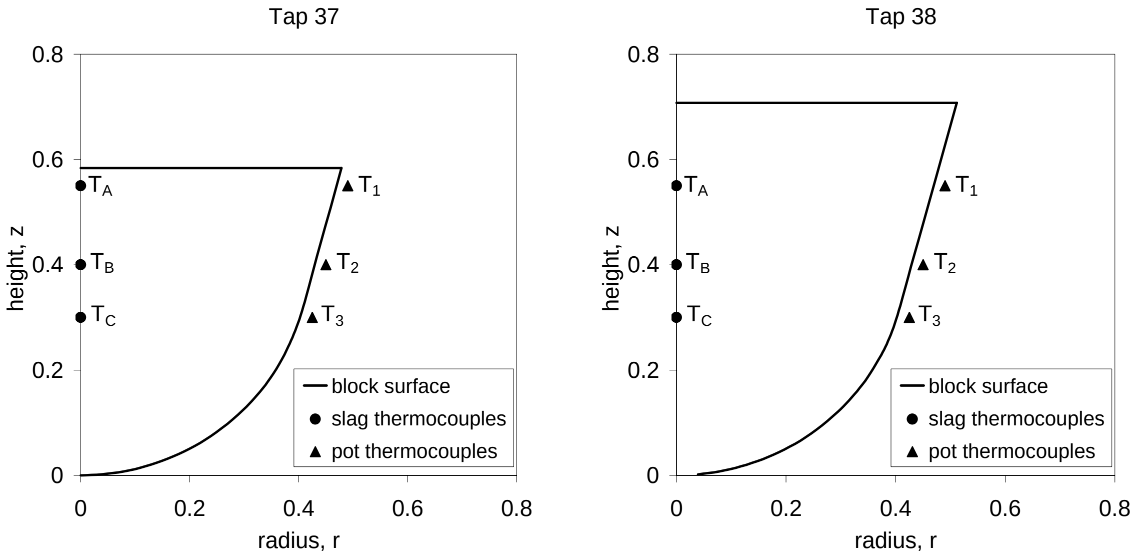

(a) (b)

Figure 85 Thermocouple positions for blocks 37 and 38 tapped during Campaign 10. Alphabetic subscripts denote thermocouple positions inserted into the slag, while numeric subscripts denote positions of thermocouples inserted into the pot shell.

Table 18 Best-fit values for coefficients a and b for each of the thermocouples inserted into the slag blocks (expression: $k_{slag} = aT + b$).

	Thermocouple	a (W/m°C^2)	b (W/m°C)
Tap 37	A	0.0000	0.50
	B	0.0019	0.30
	C	0.0018	0.30
Tap 38	A	0.0017	0.30
	B	0.0018	0.35
	C	0.0016	0.20
Model		0.00175	0.3

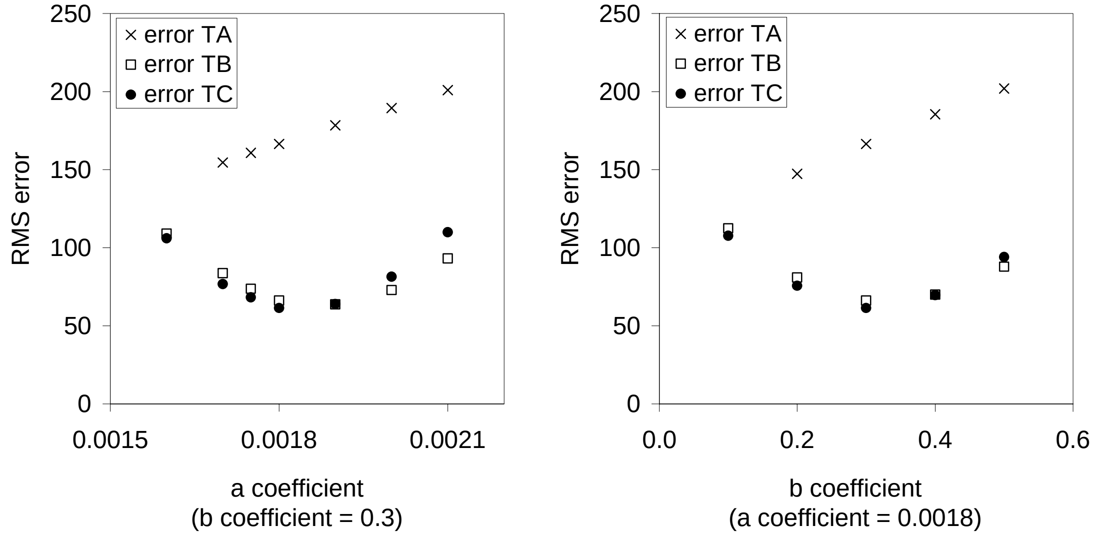

(a)

(b)

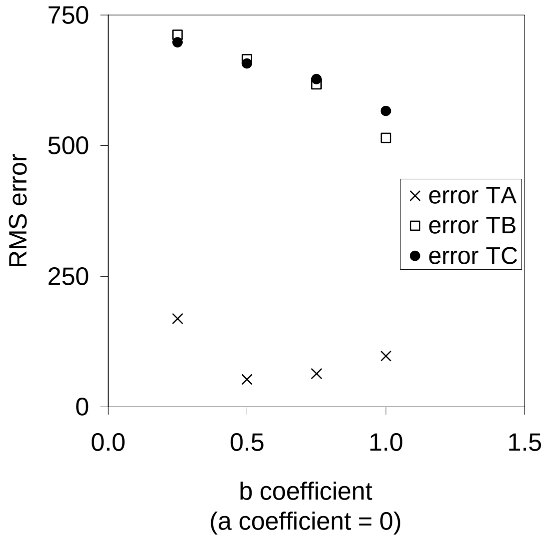

(c)

Figure 86 RMS error (in ˚C) of actual vs. model predictions for slag temperatures within tap 37.

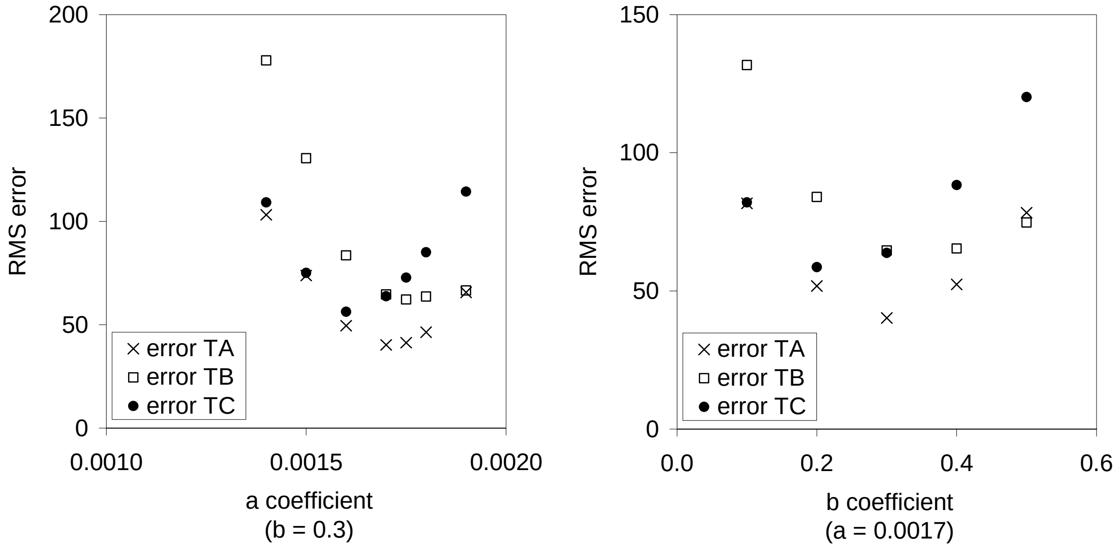

(a) (b)

Figure 87 RMS error (in ˚C) between actual temperature measurements and model predictions for tap 38.

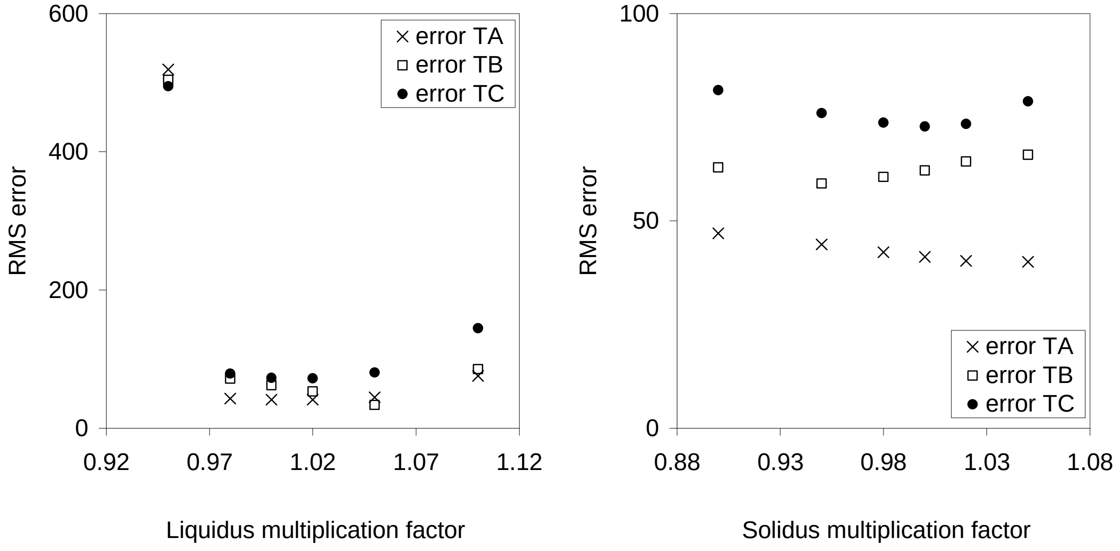

(a) (b)

Figure 88 RMS errors (in ˚C) between the actual and model predicted slag temperatures with $k_{slag} = 0.00175T + 0.3$. (a) Liquidus and (b) solidus temperatures were varied with ± 2% and ± 5%.

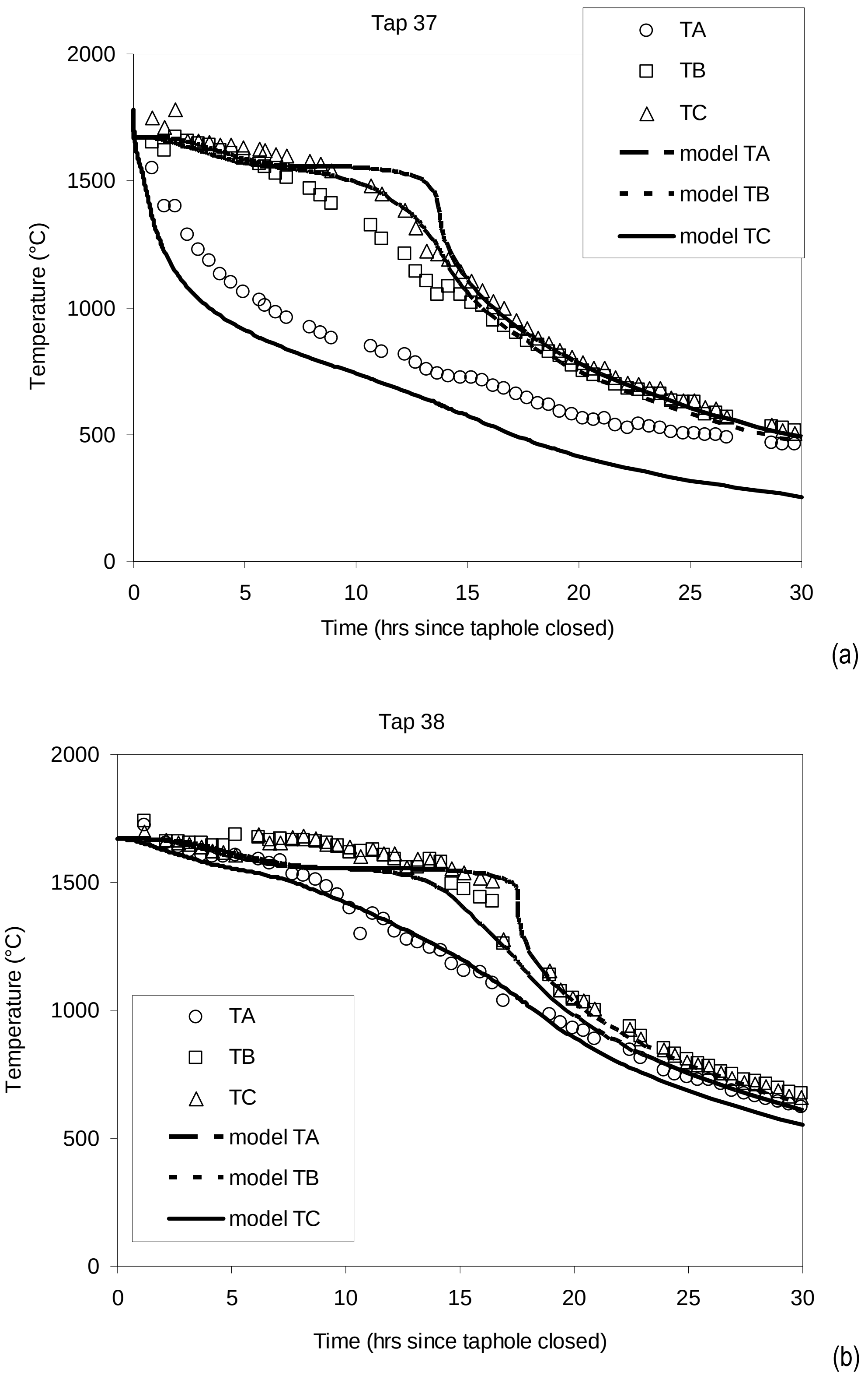

Figure 89 Internal slag temperatures for (a) tap 37 and (b) tap 38. Lines indicate model predictions, while symbols represent actual temperature measurements (k=0.00175T+0.3).

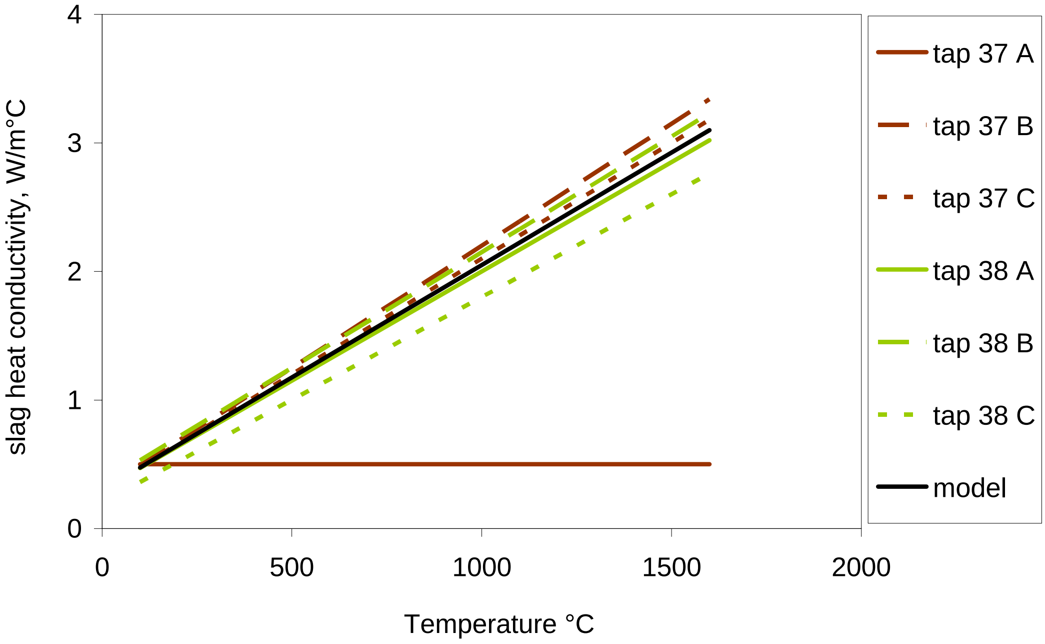

Figure 90 Best fit k-values for taps 37 and 38. For modelling purposes the k-value was expressed as given by the solid black line.

The fitted values of the thermal conductivity of the solidified slag – increasing from approximately 1 to 3 W/mK, for a temperature increase from 200°C to 1500°C – is in line with what is expected for this type of material. This is illustrated by Figure 91, which compares the fitted thermal conductivity with those of natural rocks, and synthetic pseudobrookite. The main mechanism of heat conduction in these materials is phonon conductivity (diffusion of lattice vibrations), for which the expected relationship is an inverse proportionality of the thermal conductivity to absolute temperature.[40] However, the presence of anisotropy and disorder in real structures cause deviation from this relationship.[40] The increase in the fitted slag thermal conductivity with temperature is in agreement with the observation that natural rocks with thermal conductivities below 2 W/mK at room temperature show increases in thermal conductivity with increasing temperature.[40]

The values for the M_3O_5 materials in Figure 91 were recalculated from thermal diffusivity values reported by Siebeneck et al.[44,45], using the average heat capacity over the range of temperatures (using enthalpies from FactSage), the room-temperature values for density[41,42], and the thermal expansion coefficients.[44,45] The strong hysteresis in the thermal conductivity of these materials (that is, the measured values differ upon heating and cooling) was ascribed to microcracking of the material. Microcracking arises because of significant anisotropy of the thermal expansion coefficients: for Fe_2TiO_5 these coefficients are $\alpha_a=0.6\times10^{-6}\,K^{-1}$, $\alpha_b=10.1\times10^{-6}\,K^{-1}$ and $\alpha_c=16.3\times10^{-6}\,K^{-1}$, and for $MgTi_2O_5$ $\alpha_a=2.3\times10^{-6}\,K^{-1}$, $\alpha_b=10.8\times10^{-6}\,K^{-1}$ and $\alpha_c=15.9\times10^{-6}\,K^{-1}$.[44,45] The microstructure of the solidified slag, as studied in this project, also displayed considerable microcracking (and the crystal structure of the solidified slag is also that of pseudobrookite, with considerable anisotropy of thermal expansion[7]). This is one likely reason for the relatively low thermal conductivity of the solidified slag. Other likely reasons include the relatively high molar mass of the cations in the solidified slag, and that the slag is a solid solution.[43] As with metals, solid solutions of oxides are observed to have considerably lower thermal conductivities than the pure end members.[43]

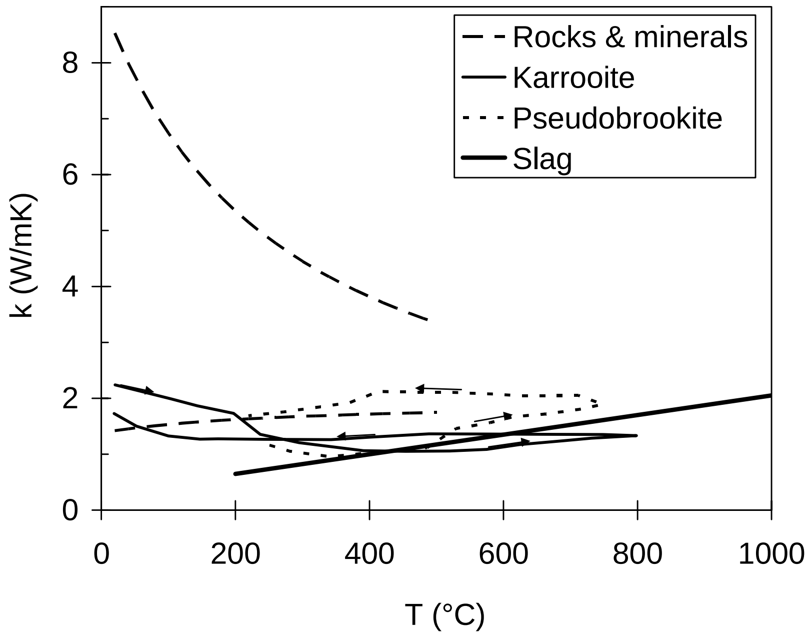

Figure 91 Comparison of the fitted thermal conductivity of the solidified slag (heavy line), with literature data on the range of thermal conductivity of natural rocks[40] (broken line), and synthetic karrooite[44] ($MgTi_2O_5$) and pseudobrookite[45] (Fe_2TiO_5). For the M_3O_5 materials, the arrows indicate the direction of temperature change during the measurements.

4.9 Model verification

The block cooling model was verified against the following information from 18 ton (plant-scale) blocks: (i) the thickness of the crust after primary cooling (18 hours in the pot) and (ii) the surface temperatures of the block after 3 days of cooling under water sprays.

4.9.1 Crust thickness

In Figure 92 the thickness of the block shell after 18 hours of cooling in the pot could be seen clearly because the block fractured directly after being tipped out of the pot. In this instance the thickness of the shell is of the order of 300 mm to 320 mm. The model predicts the liquidus and solidus contours for a similar sized block - cooled for an equal duration in the pot - to be 371 mm and 276 mm from the round end of the block surface respectively (Figure 93). The actual crust thickness is therefore close to halfway between the liquidus and solidus contours.

Evidence was found in both the industrial and pilot trials of the formation of a gap between typical dome and ball structures within the block (Figure 94(c)). This is thought to be a direct result of shell formation during primary cooling, followed by the tipping action and further shrinkage during subsequent cooling. The measured dome thickness of these blocks was around 400 mm. Unfortunately the primary cooling duration of these blocks are unknown. It is not clear why the gap forms in some instances and not in others.

Figure 92 Internal structure of a partially solidified block, as revealed by failure during tipping after primary cooling in the pot.

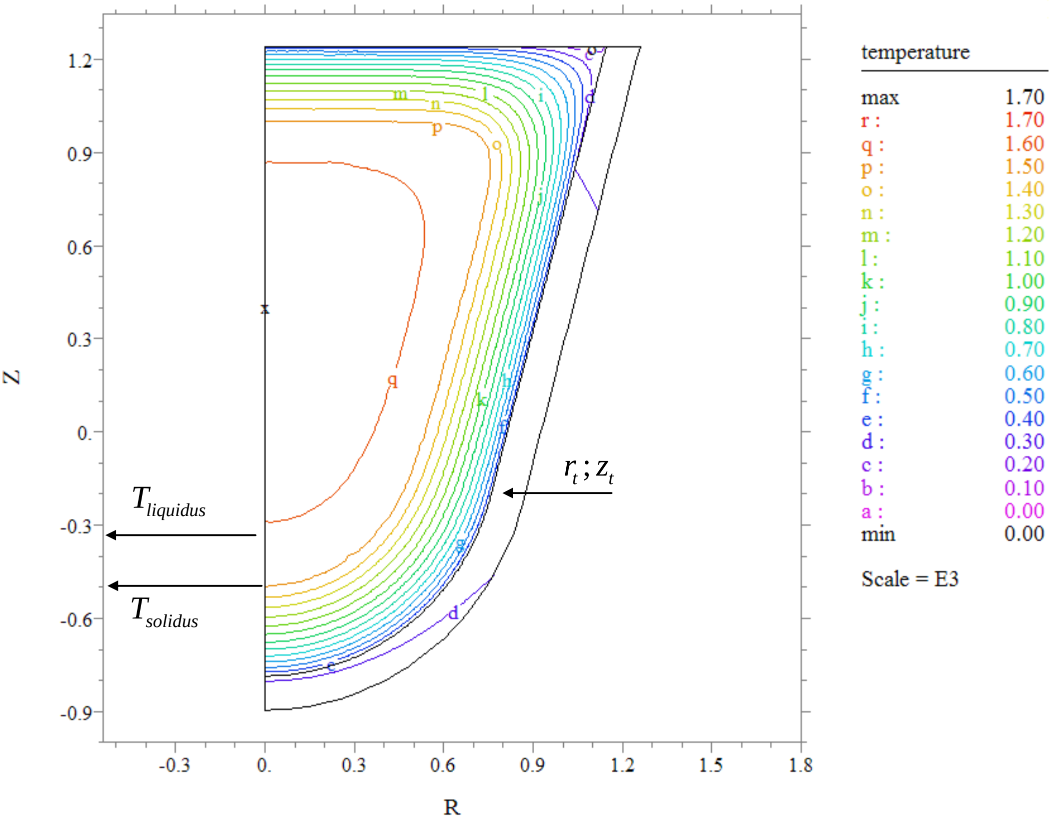

Figure 93 Temperature contours (scale in thousands of ˚C) of an 18 t block after 18 hours primary cooling (in pot).

(a) (b)

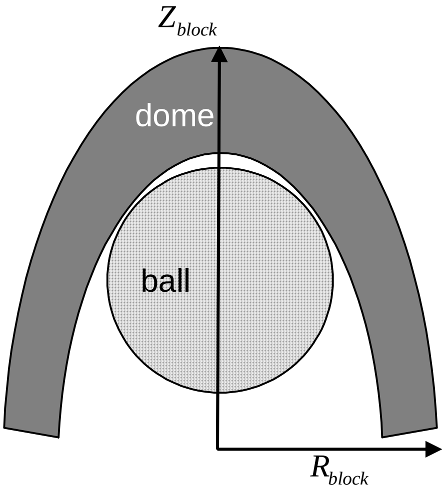

(c)

Figure 94 Internal macro structure of solidified blocks showing the shell formation during primary cooling and the ball formation in the centre of the block: (a) and (b) blocks weighing approximately 18 ton; (c) sketch illustrating the ball and dome macro structures which are displayed in (a) and (b).

4.9.2 Surface temperatures

The surface temperatures of the two blocks L1R9 and L2R11 (discussed in Part 2) were measured with an optical pyrometer when the spray water was stopped after 3 days. These temperatures are shown in Figure 95 together with the model predicted surface temperatures of the block surface. The average surface temperature was calculated from two to four actual measurements taken below the 0.5 m height. This band corresponds with the 0.6 m to 1.2 m marks on the Z-axis of Figure 93 and Figure 96. The model predictions correlate well with the actual temperature measurements.

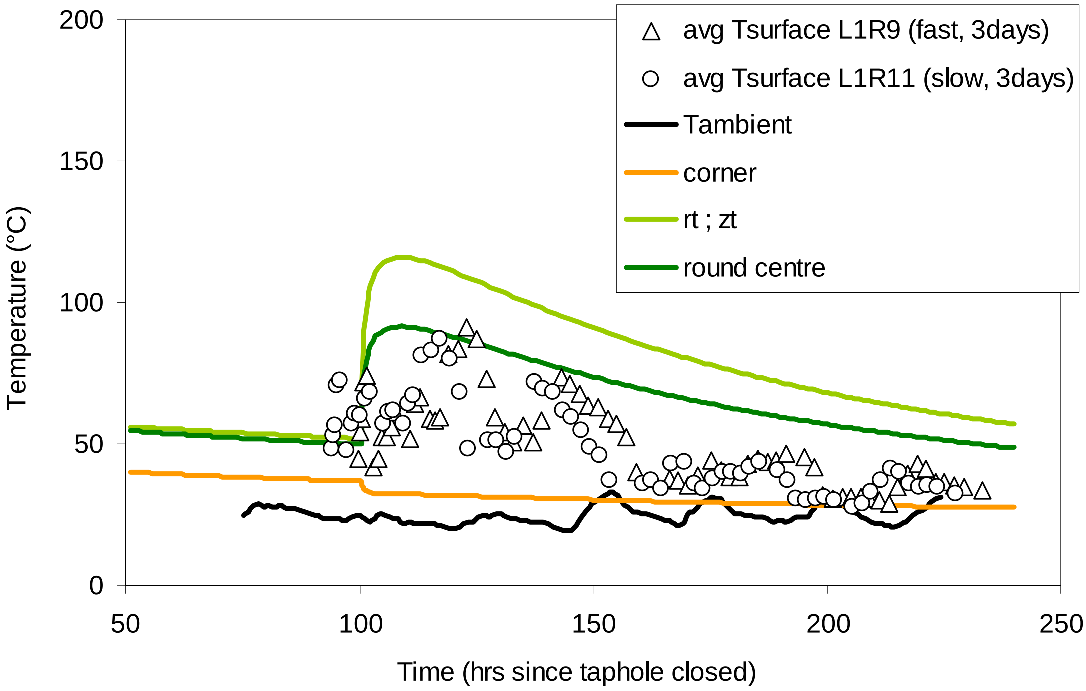

Figure 95 Surface temperatures of two 18 ton blocks. Symbols represent actual measurements while lines represent model predictions.

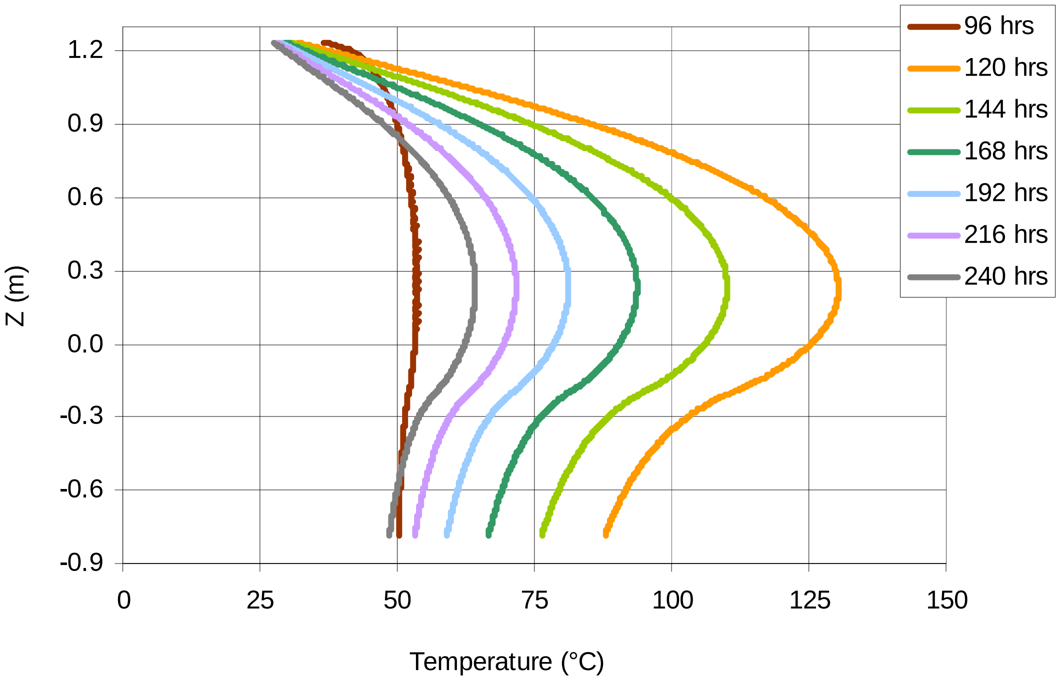

Figure 96 Surface temperatures of an 18 ton block; times are expressed relative to the time of closing the taphole.

4.10 Implication for large scale operations

4.10.1 Solidification

Following primary cooling the block is tilted out of the pot, by means of an overhead crane. The block is then picked up, and driven by a front end loader to be placed in the block yard. As soon as the front end loader is out of the range of the water sprays, the water is turned on. In view of this relatively crude handling method the thickness, strength and toughness of the crust at the end of primary cooling are important. Failure of the crust and subsequent trapping of water underneath liquid slag results in powerful hydrogen or steam explosions – an occurrence which must be avoided to prevent serious injury and/or damage.

It is of interest to test whether this potentially unsafe situation could be eliminated by cooling the block in the pot for longer periods. In Figure 97 the growth of the shell along the vertical centre line of the block (z-axis) for the flat and round ends of the block is shown. The last fully liquid node disappears between 52 and 53 hours of cooling. At this point in time the mushy zones (partially solidified slag, between liquidus and solidus temperatures), which are growing from the top and bottom, meet. The last mushy zones disappear between 92 and 93 hours. The solidification rates of a pot-cooled block are compared with those of water and air cooled blocks in Figure 98: the water-cooled block undergoes final solidification between 90 and 91 hours. Other than this relatively small difference in solidification time, the blocks solidify identically.

The shrinkage of the diameter of the liquid core along the block height (z-axis) can be described by equation (24). Similarly the diameter of the mushy zone can be described by equation (25). In both instances d is in metre and t in hours, counting from the time of closing the taphole.

$$d_{liquid} = -2.413\times10^{-5}t^3 + 1.664\times10^{-3}t^2 - 5.696\times10^{-2}t + 1.951 \qquad (24)$$

$$d_{mushy} = -2.041\times10^{-6}t^3 + 2.101\times10^{-4}t^2 - 2.135\times10^{-2}t + 1.847 \qquad (25)$$

From Figure 99 – which zooms in on the first half hour after tapping - the initial crust growth on the flat surface of the block is rapid, but re-melts after approximately 100 seconds. Similar behaviour is not shown by the round end of the block. The inverse resistances to heat flux at the block's horizontal surface ($h_{convection} + h_{radiation}$) and inclined surface ($\frac{k_{pot}}{pot\,thickness}$) are shown in Figure 100. At the horizontal surface the heat flux conductance (that is, the inverse of the thermal resistivity) is initially high at 406 W/m^2˚C, declining to 64 W/m^2˚C after 1 hour. On the inclined surface the conductance remains in the range 300 – 450 W/m^2˚C for the first hour of cooling. The conductance of the horizontal surface drops below this range after only 15 seconds following closure of the taphole. This can be explained by to the large contribution of radiation to the heat flux on the horizontal surface and the rapid formation of a dark crust on this surface, limiting radiation. This then opens the opportunity for the horizontal crust to be re-melted by the molten mass underneath.

On closer inspection the same phenomenon does occur at the slag-pot interface as shown in Figure 100(a) and (b): the conductance starts off around 300 W/m^2˚C, increases to approximately 440 W/m^2˚C after 100 seconds and then decreases to below 350 W/m^2˚C after 1 hour of closing the taphole. In this instance the reheating manifests in the steel pot shell.

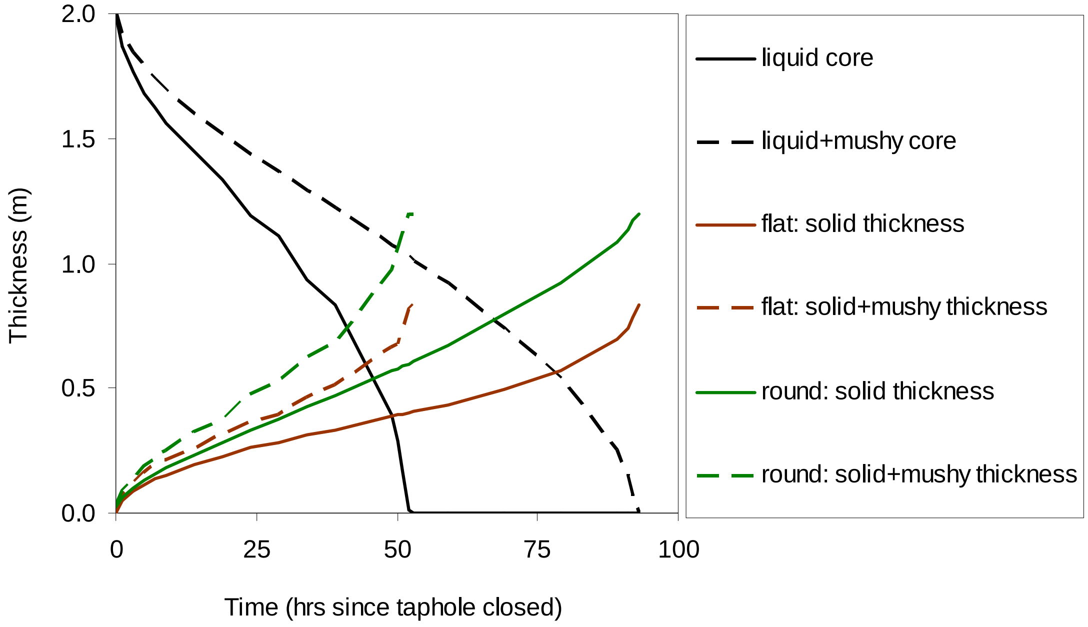

Figure 97 Remaining liquid core and shell thicknesses of a slag block cooling in a pot up to complete solidification.

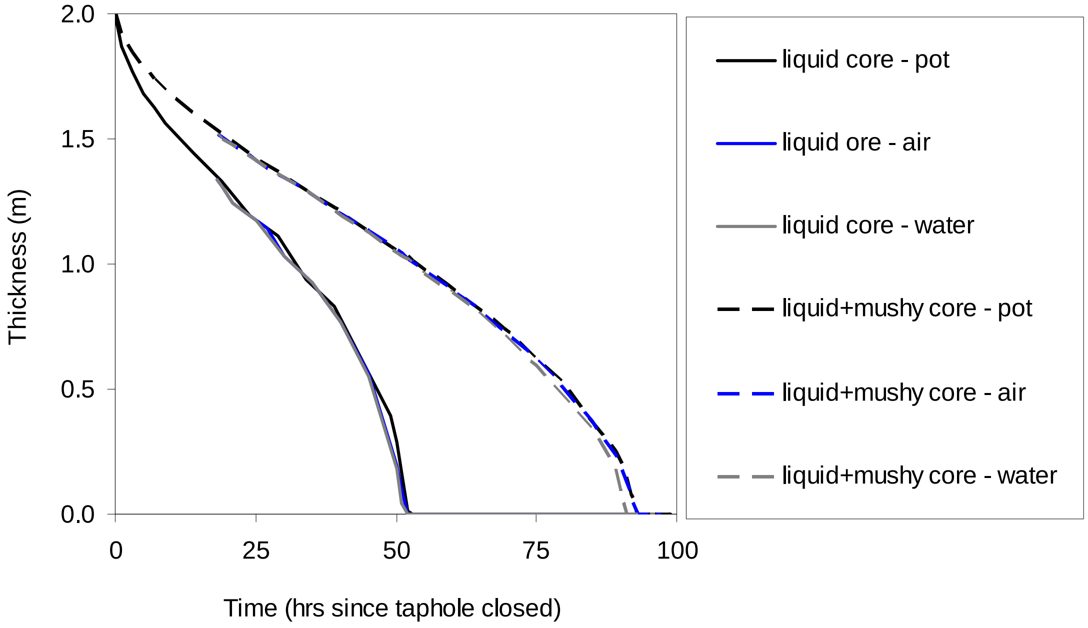

Figure 98 Comparison of the remaining liquid and mushy cores, for slag blocks cooled in the pot, in air and with water cooling.

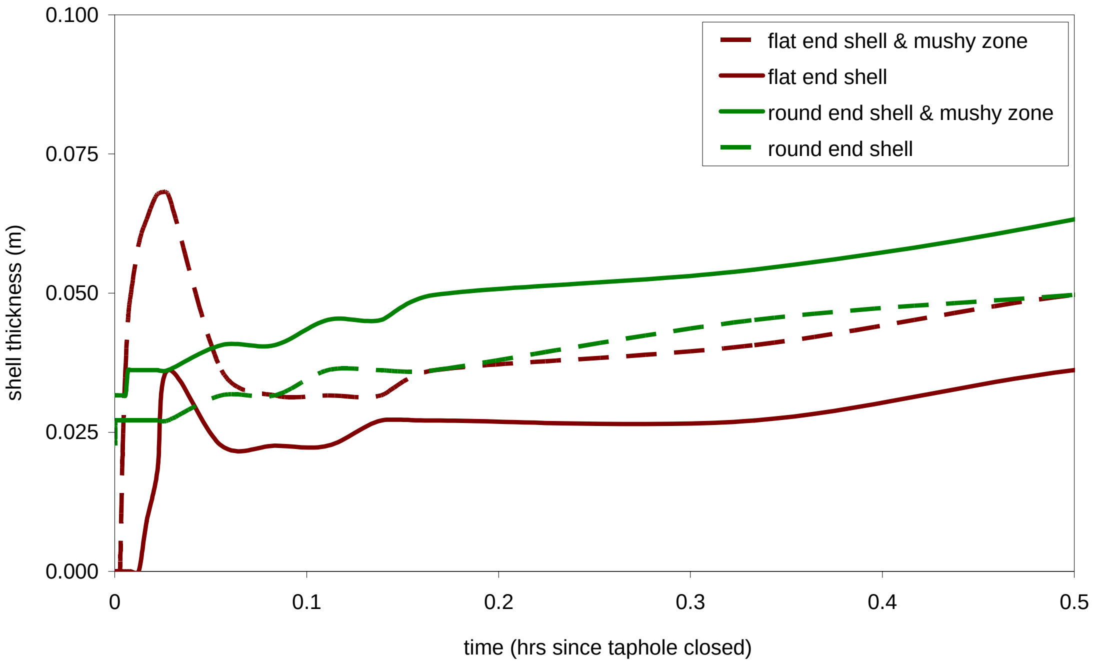

Figure 99 Shell growth of the slag block for the first half hour of cooling in a pot.

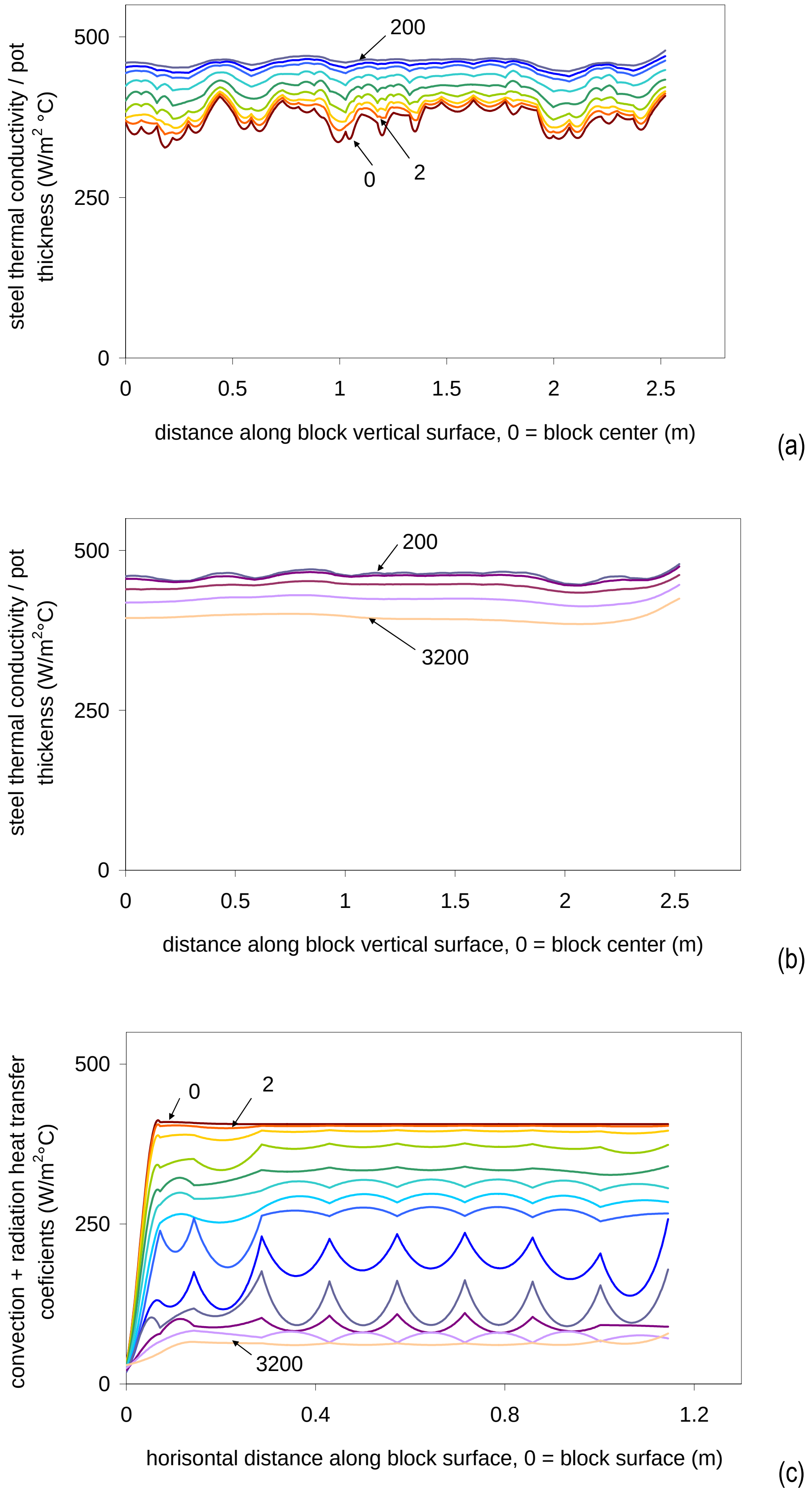

Figure 100 Thermal conductance for horizontal and inclined (vertical) surfaces. The units of the values within the above graphs are in seconds, counting from closing of the taphole. Time increments run according to the series 0, 2, 4, 8, 16, 32, 64, 100, 200, 400, 800, 1600, 3200

4.10.2 Surface temperatures

Although the solidification rates do not differ between the various cooling methods, the block surface temperatures do – as shown in Figure 101. With continuous water cooling the surface temperatures immediately fall below 70˚C and continue to fall below 50˚C after 10 days. The surface of an air-cooled block remains in the temperature range where decrepitation typically occurs for 3 to 4 days. Only after 7 days is the whole surface below 100˚C.

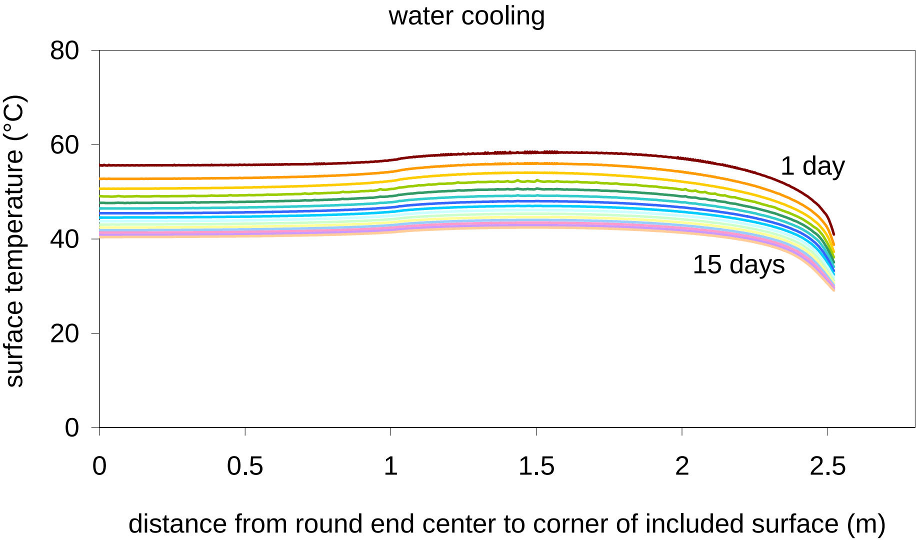

(a)

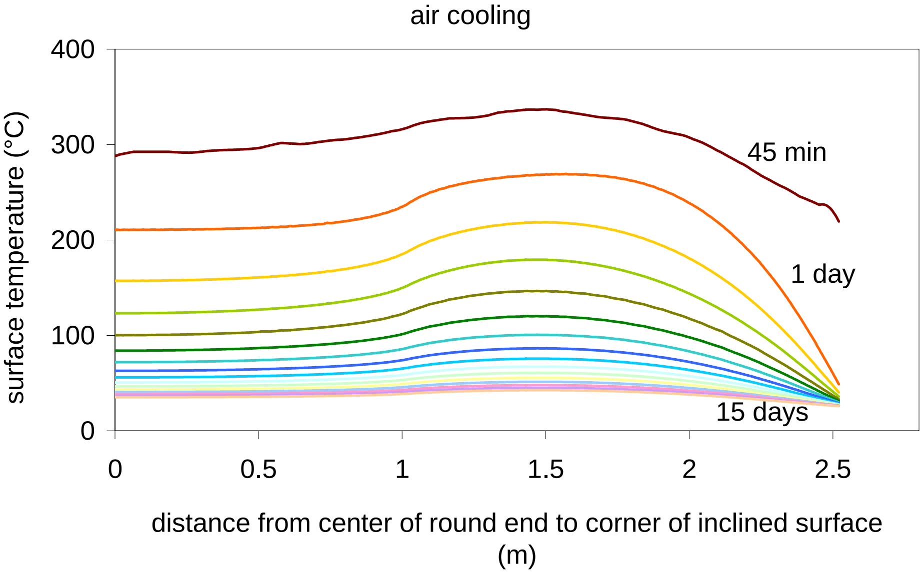

(b)

Figure 101 Surface temperatures along the inclined surface of the block for (a) cooling in water and (b) cooling in air. 0 denotes the block centre at the round end of the block, with the corner between the horizontal and inclined surface the furthest point.

The two dimensional heat transfer effects occurring at the corner between the horizontal and inclined surfaces show clearly in the steep temperature gradients of Figure 101. These temperature gradients are the likely cause of breakage of these corners as is typically seen in the block yard (Figure 102). Although still steep, the gradient for the water cooled block is an order of magnitude smaller than that of the air cooled block. Sufficiently water-cooled blocks should hence be less prone to breaking corners. Materials handling difficulties caused by such breaking behaviour can therefore be reduced by ensuring sufficient cooling water.

From previous work[5], decrepitation typically occurs at temperatures in the low hundreds of degrees Celsius. Evidence was furthermore given in section 2 showing that phase transformations occur at temperatures as low as 100˚C. From Figure 103(a) the time that the inclined surface spends in the decrepitation/transformation temperature range is sufficiently long for these two oxidation mechanisms to occur simultaneously on different areas of the surface of one block. Should such oxidation mechanisms influence the mechanical strength of the slag, it can be expected that the comminution equipment of the slag processing plant would receive, and produce, a wide variation in the particle size distribution. This would lead to particle size distribution behaviour as displayed by the two plant blocks which were cooled under water for 3 days only (Figure 31). The actual differences in structure leading to such differences in breaking behaviour could not be pinpointed in this study. Microstructural and microtoughness studies on a very fine scale would be required to provide answers to this question.

Figure 102 Photograph of a 17-18 ton slag block showing typical breaking off of the corner between the horizontal and inclined surfaces. To the left of the broken-off corner decrepitated material has formed.

The internal temperature gradient within the block along the line from the block centre to the point on the surface where the spherical and conical sections meet (points (0;0 and $r_t; z_t$ respectively on Figure 97), are shown in Figure 104(a) and (b). For a given time the water cooled block (dotted lines) is at lower internal temperatures than the air cooled block (solid lines). Closer to the surface the temperature gradient of the water cooled block is steeper – even more so in the initial cooling stages. The steepest temperature gradients are experienced at the surface of a water cooled block during the first hour of cooling with temperature differences of up to 12.5 ˚C/mm (Figure 104(b)). Such temperature gradients are likely the cause of “peeling” (spalling) on the block surface (visible in Figure 102). The thickness of such spalled material is typically in the range 2-15 mm. The thermal gradient across this distance on the shell of a water cooled block ranges between 9 to 13˚C/mm. Stresses resulting from these temperature gradients are thus likely to exceed the fracture stress of the slag[7], causing crack initiation.

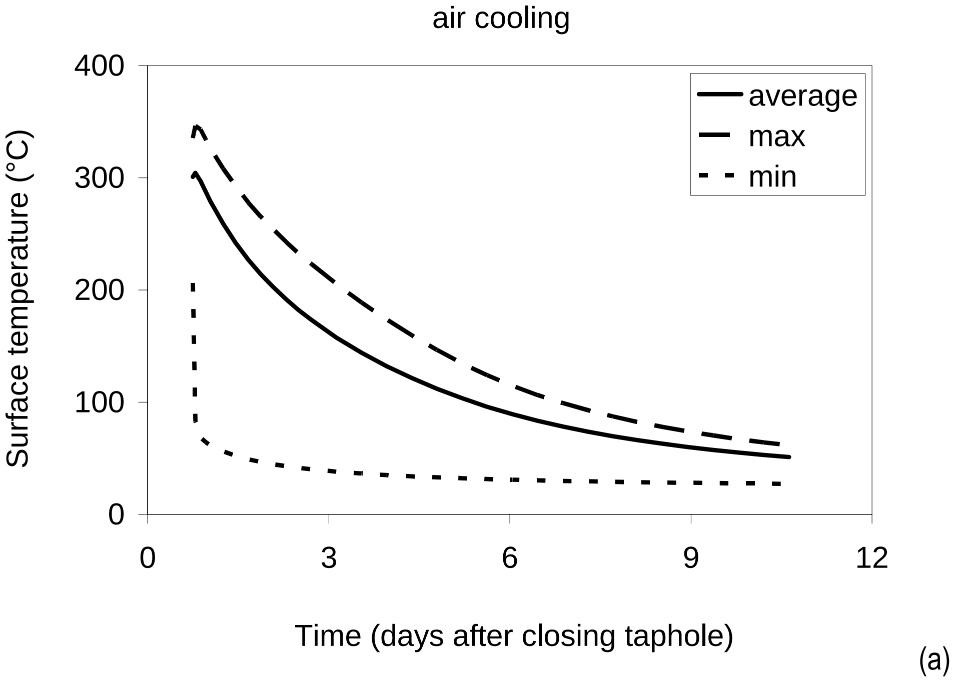

(a)

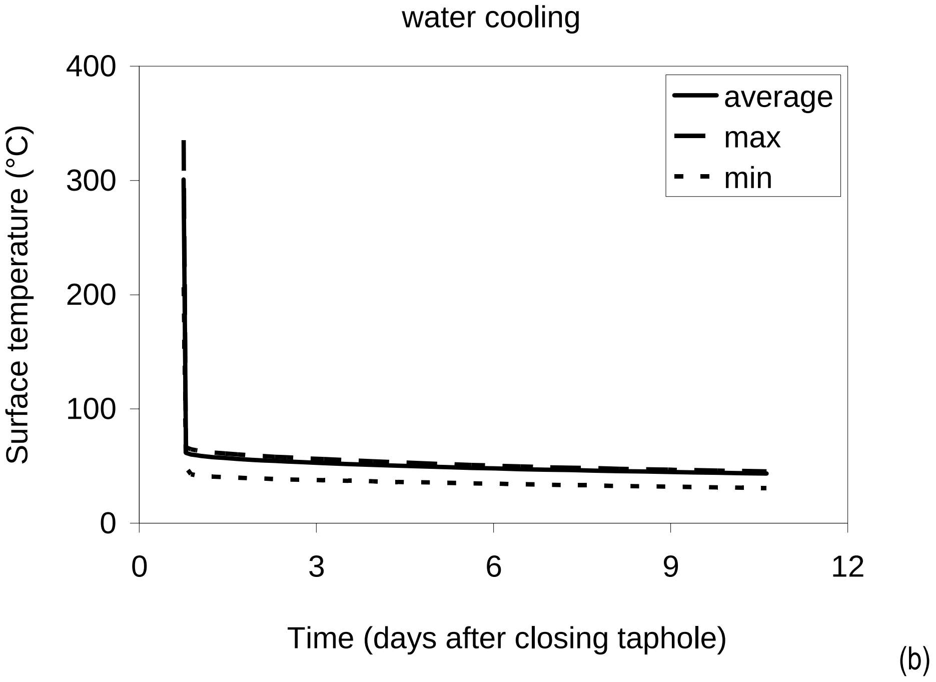

(b)

Figure 103 Average surface temperatures of (a) air and (b) water cooled blocks. Maximum and minimum surface temperatures are shown with dotted lines.

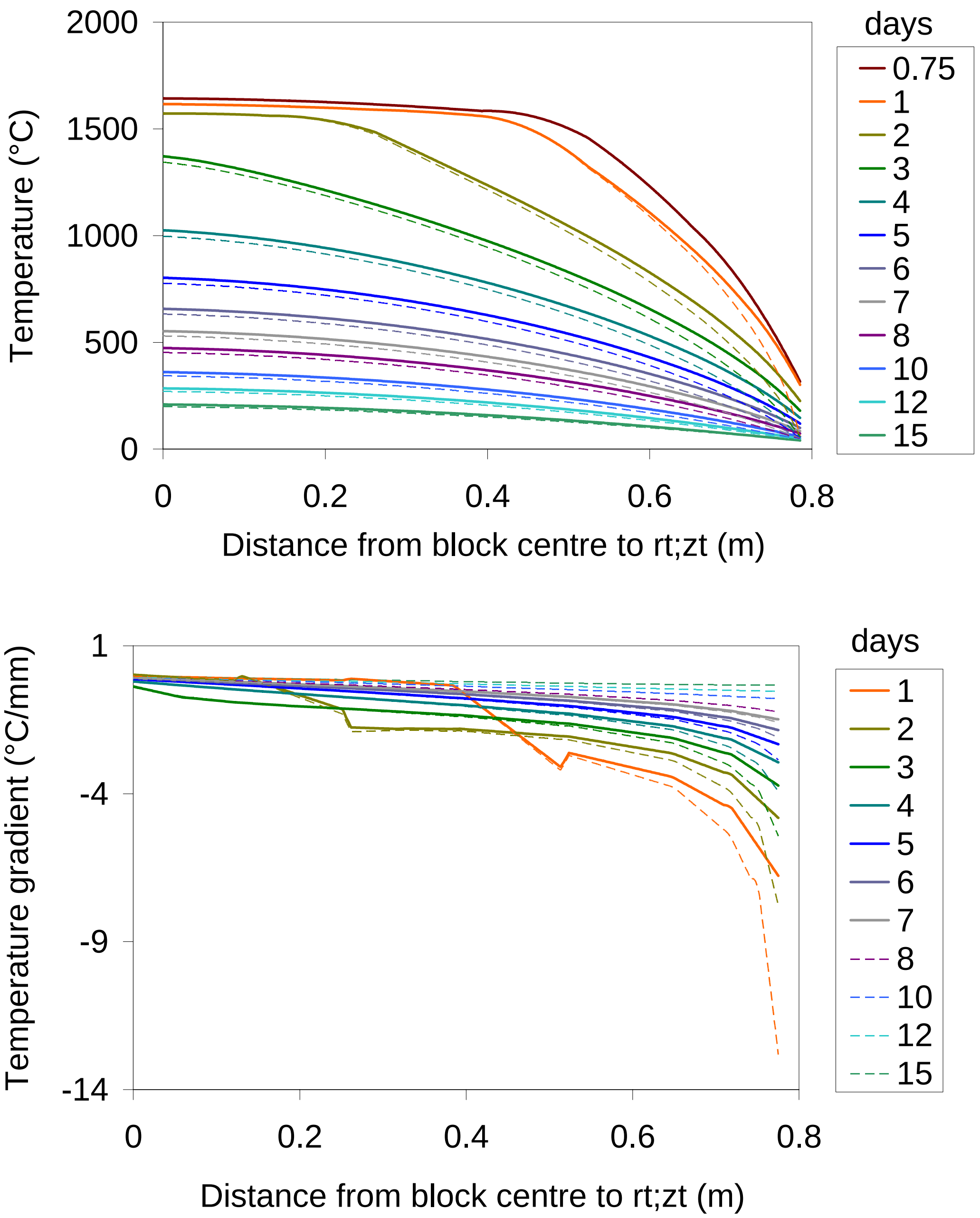

(a)

(b)

Figure 104 Internal temperature gradient of an air and water cooled block along the line from the centre point of the block to the transition point between the spherical and conical section of the block – points (0;0) and $(r_t; z_t)$ respectively on Figure 93. Solid lines indicate air cooling while dotted lines indicate water cooling.

Further with regard to surface temperatures: premature closure of the spray cooling water was observed (during both pilot and plant trials) to be followed by reheating of the block surface. The model-predicted surface temperatures of an industrial size (17-20 ton) slag block one hour after closing the cooling water are shown in Figure 105, where the period of water cooling was varied from 1 to 10 days. The initial surface temperature immediately after closing the cooling water is shown by the black line in Figure 105. After one day of water cooling, the entire block surface reheats to above 200 ˚C within 1 hour of closing the cooling water. After 3 days of water cooling the surface reheats to above 100 ˚C one hour after closing the cooling water.

Surface reheating reduces notably with increasing water cooling time, but does not disappear completely, even after 10 days of water cooling when a temperature increase of 6 ˚C is predicted for the corner of the block (46 ˚C immediately after closing the water, increasing to 52 ˚C after one hour of air cooling).

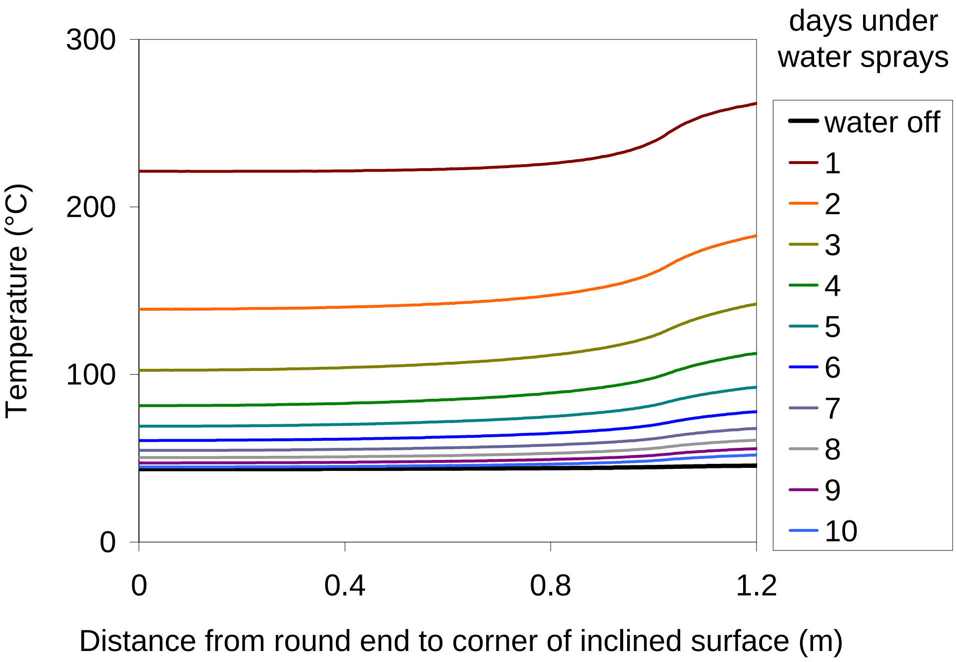

Figure 105 Surface temperatures of a slag block cooled between 1 and 10 days under water and allowed to re-heat for 1 hour.

4.10.3 Internal temperatures

From time to time, it is required (on the industrial plant) to break and crush the slag blocks before the normal cooling period of 10 days has elapsed. In these circumstances it is important - from a safety point of view - to note that the blocks solidify completely after 90 to 93 hours (close to 4 days) after closing the taphole. There is hence no danger of liquid material escaping. However, if hot internal material is exposed by breaking, oxidation is expected. To limit such oxidation effects on the newly exposed inner surfaces of a block after breaking, the inner temperatures of the block as a function of time must hence be known.

A series of contours comparing the isotherms of a water and air cooled block on a daily basis from 1 to 10 days of cooling is given in Appendix 5.9. From these and Figure 104(a) the centre of the block is still at 200˚C even after 15 days of cooling. At this stage the temperature gradient from the block centre to surface ranges from 0 to 0.3 ˚C/mm. From the previous paragraphs it is clear that the solidified slag crust is the rate limiting step in block cooling. Hence, with the temperature gradient over the block centre to surface controlling the rate of cooling, 0.3 ˚C/mm is a small driving force for cooling.

From extrapolation of the cooling rate at 15 days the block centre will reach 100˚C after 25 days of cooling. From Part 1 and 2 low temperature oxidation (≤100 ˚C) does occur and appears to negatively affect the particle size distribution of the slag. It therefore unlikely that exposure of the block centre to air while still at temperatures above 100 ˚C can be prevented for practical cooling programmes. However, it would be beneficial to promote rapid cooling of the fragments which are produced by primary breakage, for example by not packing the fragments directly on top of one another, but rather spreading these out in a single layer. The time which would be required for such (natural) cooling of primary crushing fragments was not estimated in this study, but a similar numerical cooling model (to the one used here for slag solidification) could be used for this purpose.

4.11 Conclusions

From the model calibration work the best-fit thermal conductivity for titanium dioxide slag is shown in Figure 90 and given by equation (23). The values of the constants in the latter equation are relatively insensitive to errors and assumptions in the calculated liquidus and solidus temperatures – except when the liquidus temperature drops by 5%. From plant experience, the probability that the liquidus temperature is higher than the theoretical estimates, rather than lower, is much greater in any case.

Of significance is the fact that final solidification and cooling of the block centre are independent of the cooling method. It is therefore confirmed that the thermal conductivity of the slag (or, more exactly, the thermal resistance of the layer of solidified slag) is the rate determining parameter in the block cooling process.

The surface temperatures of blocks in an industrial set-up will likely be somewhere between the two extremes predicted by the cooling model for water and air cooled surfaces. The efficiency of the water sprays influences the success of large scale water cooling (e.g. block nozzles, wind direction and speed, etc.).

From the Part 1 it was evident that decrepitation is self-sustaining in the sense that where left undisturbed, decrepitated material creates an environment favourable for further decrepitation (refer to tap 59 which ended up with a block yield of 10.8%). An instance of this is found in the industrial plant during primary cooling where the (upper) horizontal surface of the block decrepitates and the fine product accumulates on this surface. The layer of decrepitated material forms a very effective insulation layer which limits heat transfer from this surface. The internal slag temperatures beneath the horizontal surface are therefore expected to be higher than what is predicted by the block cooling model. It is therefore feasible that when the decrepitated layer is removed from this surface when the block is tipped out of the pot, the block has a thinner crust on this surface – and this is the surface which must withstand all handling when moving the block via front-end loader to the block yard. The advantages of preventing or limiting decrepitation during primary cooling are therefore less fines generation and likely a reduction in the probability of block explosions during handling.

In summary, the final particle size distribution of titania slag is predominantly influenced by

(i) The amount of intergranular silicate phases, and

(ii) Oxidation reactions over the full temperature range of cooling

With regard to the silicate glass phases (which originate from both ilmenite and the reductant, and are primarily functions of the orebodies, but which can be influenced to a limited extent by the beneficiation processes upstream of the smelter) the question is whether an increase thereof would limit the growth of the karrooite (M_3O_5) grains. If an increased silicate fraction were to limit the karrooite grain growth, this would most definitely be detrimental to achieving the specified product size distribution (since the smallest dimension of the karrooite grains is already at or below the minimum of the specified product size range). The other extreme possibility would be where the karrooite grains were free to grow, with the intergranular silicate/glass region simply growing in thickness with increased volume fraction of silicates. In this case, fracture of the silicates (during comminution) is expected to increase the proportion of the silicates which report to the fine slag, causing a decrease in the grade of the fine slag (and a likely increase in the proportion of fine slag). Microscopy on samples with a wider range of silicate contents, but similar solidification conditions, would be required to provide answers to these questions.

With regard to oxidation during the cooling stages, it is evident that water cooling limits oxidation. Intense water cooling does unfortunately have advantages and disadvantages. The advantages of intense water cooling are summarized as follows:

- Intense water cooling limits decrepitation - likely due to suppression of the block surface temperatures below 50˚C which slows down the rate of the M_3O_5 to M_6O_{11} oxidation reaction.

- From section 3.7.2 there are indications that intensive water cooling stabilises phases, preventing (or at least limiting) further low temperature (< 100 ˚C) oxidation. Such low temperature oxidation was linked to blocks performing poorly with regards to particle size distribution.

- An additional advantage of a water cooled block is the narrower temperature range over the whole surface which in turn leads to a narrower particle size distribution during processing. This in turn allows narrower equipment settings, which would result in optimum control over particle size distributions.

- Intensive water cooling furthermore reduces the thermal gradient – and resultant stresses – along the inclined surface of the block, which in turn should reduce the occurrence of corner chunks breaking off while cooling in the block yard. Where such breakage does occur, additional and tedious materials handling is required to prevent material losses.

Intense water cooling has the following disadvantages:

- It was found in Part 2 that intense water cooled blocks yielded higher residual coarse fractions. Translated to a production environment this implies higher circulating loads to the mill. Hence the probability for indirect fines generation increases, while total capacity of the mill is also reduced.

- Although the temperature gradient along the inclined surface of the block is less for an intensely water cooled block, a steep temperature gradient exists along the radial axis of the block with intense water cooling. The stresses associated with such temperature gradients promotes “peeling” (2-15 mm thick spalled material) to separate from the block surface. Careful and tedious materials handling is therefore required to prevent material losses.

4.11.1 Proposed further research

Although this study positively links oxidation with the final particle size distribution, the exact mechanism is still unknown. The anisotropic expansion behaviour of the pseudobrookite phase of the slag provides a possible avenue to explain this link. Insight into this mechanism could identify opportunities to further decrease the fraction of the fine slag.

Further insight into these slags can be obtained by studying the composition-oxidation link of these slags by conducting phase analyses on a micro scale, at different positions within the slag block. This study can be further expanded by adding varying cooling environments and rates.

In terms of decrepitation the advantages of water cooling is obvious. The remaining question to answer is whether the benefit from intense water cooling in terms of preventing low temperature oxidation (which was linked to high direct fines generation) and narrower particle size distribution (and hence optimum plant control), is greater than the indirect increase in fines generation due to higher circulating loads to the mill. Since the equipment and process flow used in the experimental work of Part 2 were not representative of the industrial plant, the question can unfortunately not be answered from these results. Practical investigations on the industrial plant would be required to resolve this.

5 Appendices

5.1 Determination of tri-valent titanium (Ti^{3+}) in titania slag

Calculations

The principle behind the determination of the trivalent titanium is the formation of reduced forms of titanium and iron when leached with ferric sulphate. The ferrous sulphate formed during the reduction of ferric ammonium sulphate is determined by titration with 0.1N potassium permanganate using 1.10-phenanthroline as an indicator. Iron will form iron (II) and therefore a correction must be made in the determination of Ti^3+.

Equations

$$Fe^0 + 2Fe^{3+} \rightarrow 3Fe^{2+}$$

$$Ti^{3+} + Fe^{3+} \rightarrow Ti^{4+} + Fe^{2+}$$

$$\%Ti_2O_3 \text{ (expression in terms of } TiO_2) = \left[0.00799(A-B)\frac{100}{W}\right] - \left[1.43(C+2D)\right]$$

Where A = Titrant value of potassium permanganate solution, cm^3

B = Blank titrant value of potassium permanganate solution, cm^3

C = Fe (tot) (from XRF)

D = Metallic iron content (Determined as per Standard Task Procedure for **Determination of metallic iron (Fe^0) in Titanium Slag**)

W = Mass of the sample (mg)

1.43 = Conversion factor for Fe to Fe_2O_3

79.9 = Molar mass of TiO_2

Allowable variance in Ti^{3+}: 0.5%

Steps	Operating/Quality Criteria			✓×	Hazard and Risk Exposure	Control Measures	✓×
Check equipment/ tools/chemicals	Analytical balance (4 decimal place)		Titrasol ampoule (0.1N $KMnO_4$)		Do not have the correct equipment, tools or chemicals	Obtain new or safe replacement before commencing with the task.	
	Water purifier		Stop watch				
	Magnetic stirrer bars		Stainless sink				
	Stirrer rod		Funnel, glass				
	Indicator bottle with a medicine dropper		Measuring cylinders, glass (25ml, 100ml, 500ml, 1000ml)				
	Volumetric flask, (100ml, 1000ml)		Measuring cylinder, plastic (10ml)				
	Hotplate with sand bath		Erlenmeyer flask				
	Magnetic stirrer/hotplate		1.1 Phenanthroline				
	Wash bottle		Sulphuric Acid (95-99%)				
	Beaker, teflon (250ml)		Boric Acid crystals (AR)				
	Beaker, glass (50ml, 250ml, 1000ml)		Calcium Gluconate Solution				
	Hydrofluoric Acid, HF (48%)		Ammonium Ferric Sulphate				
	Burette (50ml)		Ferrous sulphate				

Steps	Operating/Quality Criteria			✓×	Hazard and Risk Exposure	Control Measures	✓×
	CRM (SARM 57)						
1. Check Personal Protective Clothing (PPC)	Overalls/Lab coat		Safety shoes		Do not have the correct PPC	Obtain the appropriate PPC before commencing with the task	
2. Check Personnel Protective Equipment (PPE)	Nitrile gloves		Safety glasses		Do not have the correct PPE	Obtain the appropriate PPE before commencing with the ask	
	Latex gloves		Heat resistant gloves				
4. Ensure following documentation is available	Standard Task Procedure for: Calibration of, and weighing on an Analytical Balance (Powerdocs: IHM_CPC# 26953).				Documentation is not accessible from the computerized system.	Place a breakdown log with AST Help Desk, Dial 5000	
	Wet Chemistry Daily Log sheet (Powerdocs: IHM_CPC#47800).						
	Standard Task Procedure for: Cleaning up of chemical spillages (Powerdocs: IHM_CPC#27097).				Documentation is not accessible from the computerized system.	Place a breakdown log with AST Help Desk, Dial 5000	
	Standard Task Procedure for: Waste Management-Hydrogen Fluoride (HF) (Powerdocs: IHM_CPC#60720)						
	Standard Task Procedure for: Waste Management-Altered, Unaltered and Slag waste (Powerdocs: IHM_CPC#60726)						

Steps	Operating/Quality Criteria	✓✗	Hazard and Risk Exposure	Control Measures	✓✗
	Standard Task Procedure for Waste management – Glassware (Powerdocs: IHM_CPC#60724)				
5 Procedure	Inspect all glassware for chips or cracks before and after use.		Injury to hands	Use nitrile gloves	
			Incorrect disposal	Dispose of broken glassware into the “Broken glassware bin”.	
5.1 Preparation of reagents	Ensure that the balance has been calibrated as per Standard Task Procedure for **Calibration of, and weighing on an analytical Balance.**		Not calibrated	Calibrate and verify the balance before commencing with task.	
	Reagents are prepared using only “A” grade calibrated glassware.				
a) **Potassium permanganate solution** (KMnO$_4$) 0.1N	Prepare a titrasol ampoule of 0.1N KMnO$_4$ in a 1000ml volumetric flask.				
	Carefully break off the neck of the ampoule using the blade supplied., or twist off the neck (depending on which container is supplied).		Injury to hands.	Wear nitrile gloves.	
	Quantitatively transfer the contents of the ampoule into a clean dry 1000ml volumetric flask using a funnel.		Spillage	Discard and reprepare the reagent.	
	Rinse the neck and ampoule into the flask, at least 3 times with distilled water from a wash bottle.		Incorrect normality	Ensure that every drop is washed into the flask.	
				Rinse down the funnel as well.	
	Make up to the mark with distilled water.		Over shot the mark	Discard and remake the solution.	

Steps	**Operating/Quality Criteria**	✓×	**Hazard and Risk Exposure**	**Control Measures**	✓×
	Homogenise and transfer the solution into a dark coloured reagent bottle.				
	Seal, and label the reagent bottle with the name of reagent, date, time and name of analyst.		Incorrect labelling.	Ensure that the correct labelling is done.	
b) **Sulphuric Acid Solution** 50 % (1:1) (Stock Solution)	Quantitatively transfer 450ml distilled water into a clean dry 1000ml glass beaker using a 500ml measuring cylinder.		Water purifier not working	Replace DI cartridges.	
	Place the 1000ml beaker into the stainless sink.				
	Plug the sink using the stopper and fill with cold water to create a water bath.		Beaker begins to float and tips over.	Fill sufficient water in the bath to allow the beaker to be immersed without floating.	
	Quantitatively transfer 500ml of Sulphuric acid (95-99%) into a clean dry 500ml measuring cylinder		Inhalation due to fumes	Work in a fume hood.	
			Injury to hands	Wear nitrile gloves.	
			Spillage	Adhere to the Standard Task Procedure for **Cleaning up of chemical spillages.**	
	Slowly transfer small quantities at a time of the 500ml Sulphuric acid into the 1000ml beaker containing the 450ml of distilled water using a glass funnel.		Solution heats rapidly.	Add the acid slowly. Keep the volumetric flask cool by swirling it in the water bath or stir with a stirrer rod.	
				Let the H_2SO_4 run onto the side of the beaker.	
				Always add acid to water.	

Steps	Operating/Quality Criteria	✓×	Hazard and Risk Exposure	Control Measures	✓×
			Injury to hands	Use nitrile gloves	
	Allow the solution to cool to room temperature in the water bath.				
	Once cooled, transfer to a clean dry 1000ml volumetric flask using a funnel and make up to the mark with distilled water.		Mark is over shot	Discard and reprepare.	
	This is now the 50% sulphuric acid stock solution.				
	Transfer to a reagent bottle, seal, and label the reagent bottle with the name of reagent, date, time and name of the laboratory technician.		Incorrect labelling.	Ensure that the correct labelling is done.	
	Transfer the stock solution to the designated auto dispenser when required.		Contamination of reagent	Ensure that the designated dispenser is used.	
				Rinse the dispenser with the new stock solution before filling up.	
c) **Boric Acid Solution** (H_3BO_3)	Add ~500ml of distilled water into a clean 2000ml volumetric flask.				
	Weigh 48g ± 0.01g of dry Boric acid (H_3BO_3) crystals into a clean dry 50ml beaker.		Incorrect sample weight.	Discard and reweigh.	
	Place a clean dry glass funnel into the 2000ml volumetric flask containing the distilled water.				
	Quantitatively transfer the boric acid crystals into the volumetric flask by rinsing out the beaker with ~1000ml distilled water over the glass funnel.		Substances sticking to sides of the glassware	Ensure the sides of the glassware are washed down with water.	

Steps	Operating/Quality Criteria	✓×	Hazard and Risk Exposure	Control Measures	✓×
	Quantitatively transfer 220ml of Sulphuric acid (95-99%) into a clean dry 500ml measuring cylinder.		Inhalation due to fumes	Work in a fume hood.	
			Injury to hands	Wear nitrile gloves.	
			Spillage	Adhere to the Standard Task Procedure for **Cleaning up of chemical spillages.**	
	Slowly transfer small quantities at a time of the 220ml sulphuric acid into the 2000ml volumetric flask containing the boric acid solution.		Solution heats rapidly.	Add the acid slowly. Continuously swirl the flask under running cold water.	
			Injury to hands	Wear nitrile gloves.	
	Allow the solution to cool.				
	Once cooled, make up to the mark with distilled water.				
	Transfer to a reagent bottle, seal, and label the reagent bottle with the name of reagent, date, time and name of the laboratory technician.		Incorrect labelling.	Ensure that the correct labelling is done.	
	Transfer to the designated auto dispenser when required.		Contamination of reagent	Ensure that the designated dispenser is used.	
				Ensure that the designated dispenser is cleaned and rinsed with the new stock solution.	
d) **Ammonium Ferric Sulphate** (Stock Solution)	Weigh out accurately 25g ± 0.01g of Ammonium Ferric Sulphate into a clean dry 250ml beaker.		Incorrect sample weight.	Discard and reweigh.	

Steps	Operating/Quality Criteria	✓×	Hazard and Risk Exposure	Control Measures	✓×
	Using a measuring cylinder, add 150mls of distilled water into the beaker.		Water purifier not working	Replace DI cartridges.	
	Quantitatively transfer 75ml concentrated Sulphuric Acid (95-99%) into a 100ml measuring cylinder		Injury to hands	Wear nitrile gloves.	
			Inhalation due to fumes	Work in the fume hood.	
	Carefully add the 75ml Sulphuric Acid to the beaker containing the Ammonium Ferric Sulphate.		Solution gets hot	Allow the cool water to flow under the beaker.	
	Mix the solution well using a stirring rod.		Injury to hands	Wear nitrile gloves	
	Allow the solution to cool to room temperature.		Cooling takes too long	Force cool in a water bath.	
	Transfer the solution to the designated dark coloured reagent bottle. This is now the ammonium ferric sulphate stock solution.		Contamination of reagent	Ensure that the designated reagent bottle is used.	
				Ensure that the designated reagent bottle is cleaned and rinsed with the new stock solution.	
			Reagent is sensitive to light.	Store in a dark bottle, inside a cupboard.	
	Seal, and label the reagent bottle with the name of reagent, date, time and name of analyst.		Incorrect identification	Ensure the correct labelling is done.	
e) Phenantholine indicator	Weigh out accurately, 0.7g ± 0.01g Ferrous sulphate into a clean dry weighing boat.		Incorrect sample weight.	Discard and reweigh the sample.	
	Weigh 1.0g ± 0.01g of 1.1 Phenantholine into a separate clean dry weighing boat.		Incorrect sample weight.	Discard and reweigh the sample.	

Steps	Operating/Quality Criteria	✓×	Hazard and Risk Exposure	Control Measures	✓×
	Place a clean dry glass funnel into a 100ml volumetric.				
	Quantitatively transfer the chemicals into the volumetric flask by rinsing out the beaker with distilled water over the glass funnel.		Substances sticking to sides of the weighing boats.	Ensure the sides of the weighing boats are washed down with water.	
	Make up to the mark with distilled water.				
	Homogenize the solution.		Spillages.	Hold the flask firmly.	
				Ensure the cap is on tightly.	
	Transfer to a reagent bottle, seal, and label the reagent bottle with the name of reagent, date, time and name of the laboratory technician.		Incorrect labelling.	Ensure that the correct labelling is done.	
5.2 Quality Control	A Quality control sample is prepared and analysed as per section 5.3, in duplicate with every batch of unknown samples.		Quality sample is out of limits	Do not report the production results	
				Repeat the analysis.	
	Perform the analysis on LIMS by selecting the appropriate sample ID from LIMS **SPC Ti_2O_3 & Fe (Metallic)** and the method T**rivalent (Ti^{3+}) Sarm57**		LIMS not available	Record the sample ID on the Wet chemistry Daily Log sheet.	
	SARM 57 is analysed in duplicate as per section 5.3. The average is reported.				
5.3 Preparation of the blank and sample	Unknown samples are prepared and analysed in duplicate and the average is reported.				

Steps	Operating/Quality Criteria	✓×	Hazard and Risk Exposure	Control Measures	✓×
	A blank should be prepared when new reagents are prepared and analysed with each batch of production samples.				
	Accurately weigh out 0.5000g ± 0.0010g of milled sample into a weighing boat.		Incorrect sample weight.	Discard and reweigh.	
				For the preparations of a blank, no sample is added.	
	Quantitatively transfer the weighed sample into a teflon beaker.				
	Add 15ml of the ammonium ferric sulphate stock solution into a teflon beaker, using a 25ml measuring cylinder.				
	Swirl to cover the entire sample.		Injury to hands.	Wear nitrile gloves.	
			Injury to eyes.	Wear safety glasses.	
	Transfer 20ml of 50% sulphuric acid into the teflon beaker, using the dispenser.		Incorrect volume dispensed	Ensure that the desired volume setting on the dispenser is selected before dispensing the solution.	
	Place the teflon beaker on the sand bath of the hot plate.				
	Bring to boil. Allow boiling for 1 minute while swirling by timing with a stopwatch.		1 minute exceeded	Repeat the preparation from step 5.3	
	Quantitatively transfer 10ml HF into 10ml plastic measuring cylinder, or using the dispenser, dispense 10 ml HF directly in to Teflon beaker.		Injury to hands	Use latex/nitrile gloves.	
			Inhalation due to fumes	Work in the fume hood.	

Steps	Operating/Quality Criteria	✓×	Hazard and Risk Exposure	Control Measures	✓×
			Damage to glassware	Use a plastic measuring because HF attacks the silica in glass.	
			Skin Contact	Avoid contact with skin. Wash with copious amount of water and then apply calcium gluconate solution to the area. Calcium gluconate solution is kept in the fridge in the Wet Chemistry Laboratory.	
				Seek medical help.	
	Add the 10ml HF into the teflon beaker.				
	Place the teflon beaker on the hotplate and boil at a lower heat setting for 10 minutes while swirling.				
	After boiling for 10 minutes remove the teflon beaker from hot plate.		Injury to hands.	Use heat resistant/nitrile gloves.	
	Immediately add 100ml boric acid stock solution to the teflon beaker using the dispenser.		Inhalation due to fumes.	Work in the fumehood.	
	Cool to room temperature.				
	Add 10 drops of the Phenanthroline indicator into the teflon beaker, using the medicine dropper.				
	Place a magnetic stirrer bar into the teflon beaker and stir well on the magnetic stirrer.				

Steps	Operating/Quality Criteria	✓×	Hazard and Risk Exposure	Control Measures	✓×
5.4 Titration of the sample	Rinse a clean dry 50ml burette out with 0.1N KMnO4 solution.		Contamination	Rinse the burette with the solution to ensure it is free from contaminants.	
	Fill the 50ml burette to the mark with 0.1N $KMnO_4$.				
	Add drop wise $KMnO_4$ until the endpoint is reached.		Endpoint is exceeded	Repeat the analysis from step 5.3	
				Endpoint is reached when solution changes to a pale blue colour.	
	Enter the titration value (volume of the 0.1N $KMnO_4$used), on LIMS under the appropriate sample type and method		Incorrect LIMS method selected.	Select the appropriate sample ID and the method T**rivalent (Ti^{3+}) Sarm57** for the control sample and **Trivalent titanium (Ti^{3+})** for production samples.	
			LIMS is not accessible	Record the titrant value (volume of the 0.1N $KMnO_4$ used) on the Wet Chemistry Daily Log sheet	
5 Reporting of results	All calculations are performed by LIMS				
	Quality control samples are analysed in duplicate and the average is reported.				
	Unknown samples are analysed in duplicate and the average is reported.				
7 Waste Management	Discard liquid mercury chloride waste and contaminated waste paper in the designated mercury chloride waste bins in the Wet Chemistry Laboratory.		Incorrect waste disposal.	Adhere to Standard Task Procedure for **Waste Management: Mercury Chloride**.	

Steps	**Operating/Quality Criteria**	✓×	**Hazard and Risk Exposure**	**Control Measures**	✓×
	Discard altered slag waste in the appropriate bins in the mill and pressroom.		Incorrect waste disposal	Adhere to Standard Task Procedure for **Waste Management: Altered, Unaltered and Slag Waste**	
	Discard chipped or broken glassware into the appropriate bin in the Wet Chemistry Laboratory.		Incorrect waste disposal	Adhere to Standard Task Procedure for **Waste Management: Glassware**	
8 Housekeeping	Wash all glassware and store away.		Damage to glassware.	Ensure that all damage to equipment/glassware is reported before the end of the shift.	
	Clean the workbench on completion of analysis.				
	Return all reagents to their respective storage cupboards				
	Clean up all spillages		Spillage	Adhere to the standard task procedure for **Cleaning up of chemical spillages.**	

5.2 List of parameters evaluated in the search for parameters correlating with the -106 µm fraction.

initial block mass

block yield

yield mass

%FeO

%TiO_2

%Al_2O_3

%CaO

%Cr_2O_3

%MgO

%MnO

%SiO_2

%V_2O_5

primary cooling time (hrs)

Tapping rate (kg/min)

Tapping rate$^{-0.5957}$ (kg/min)

Equivalent %FeO

(Equivalent %FeO)^2

%Ti_2O_3

%$TiO_{2\ true}$

(%$TiO_{2\ true}$)^2

Equivalent %Ti_2O_3

(Equivalent %Ti_2O_3)^2

SiO_2+Al_2O_3(glass)+CaO

Specific surface area - initial

Ln(spec surface area - initial)

Specific surface area - after

Ln(spec surface area - after)

(Specific surface area - after)$^{3.6321}$

$T_{liquidus}$ (calculated)

$T_{solidus}$ (calculated)

T_{tap}

superheat

5.3 SEM examples of SiO_2 on particle surfaces

Coarse fraction (+850 µm -106 µm)

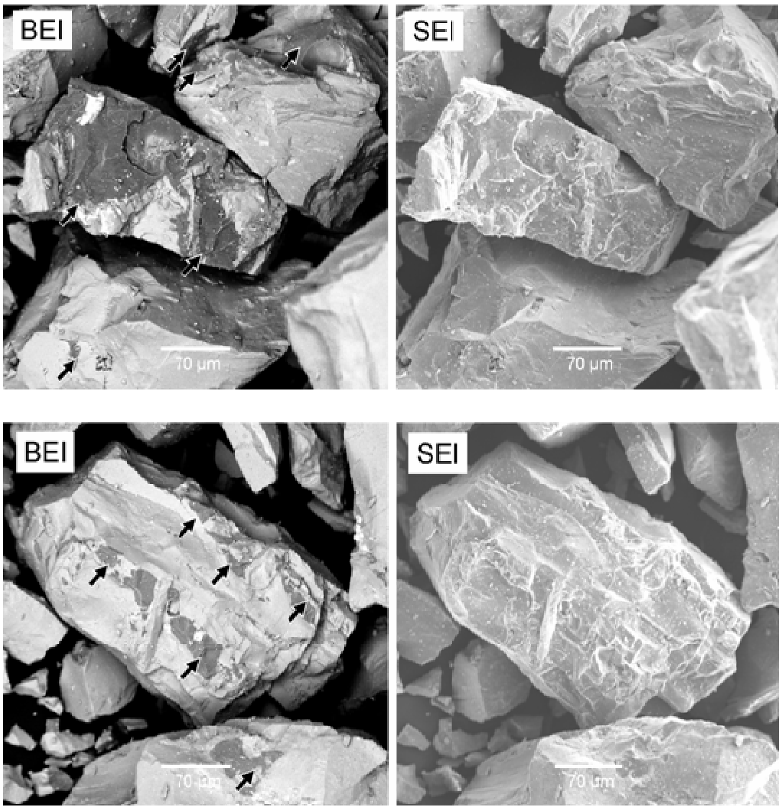

Fine fraction (-106 µm)

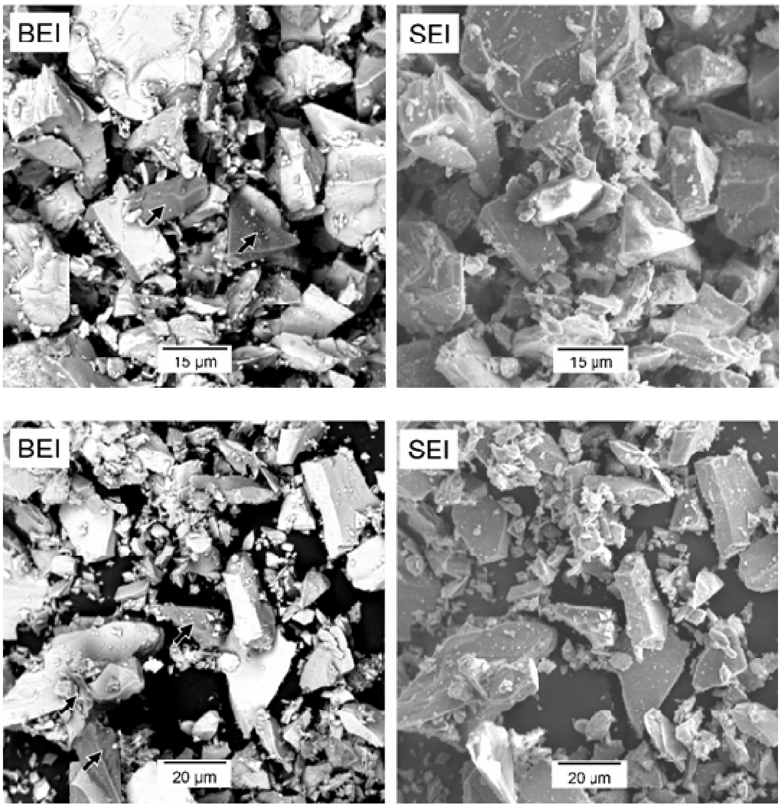

Coarse fraction

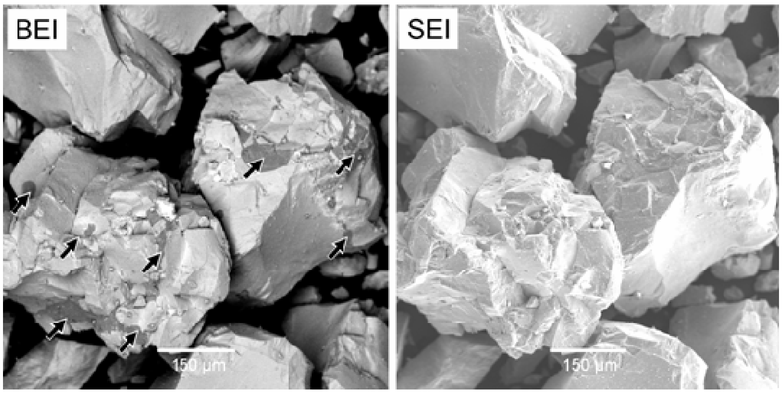

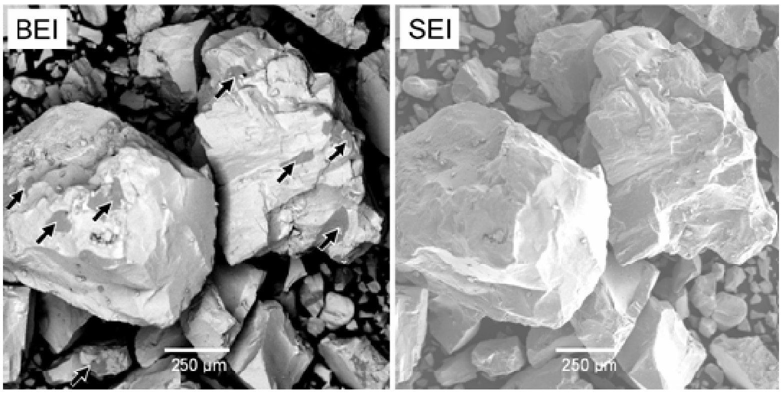

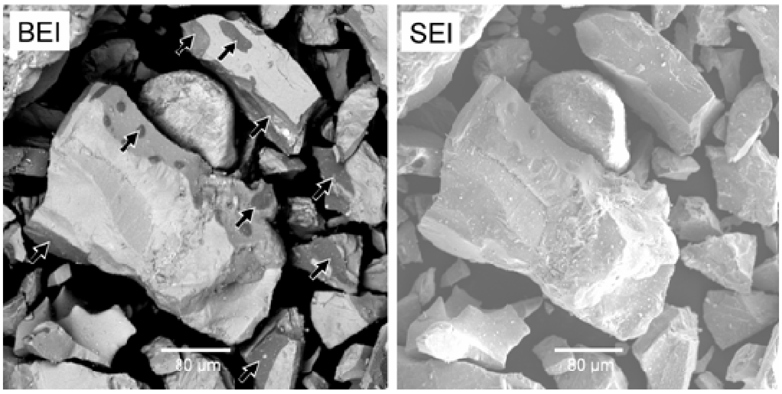

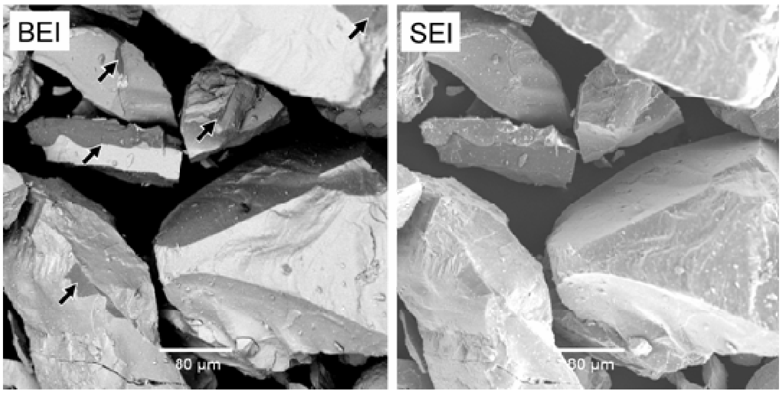

Coarse fraction

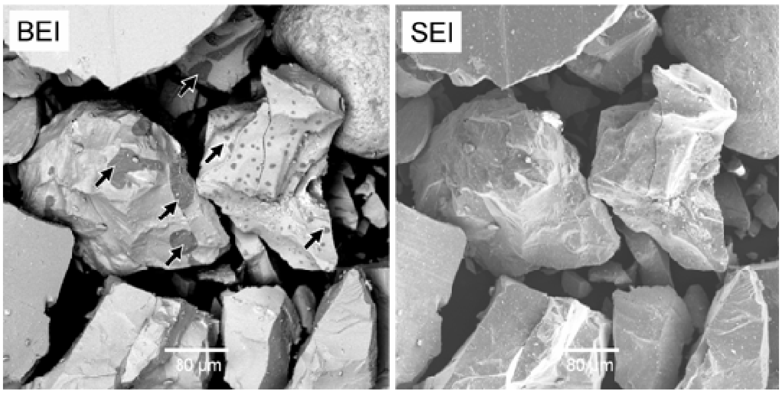

Fine fraction

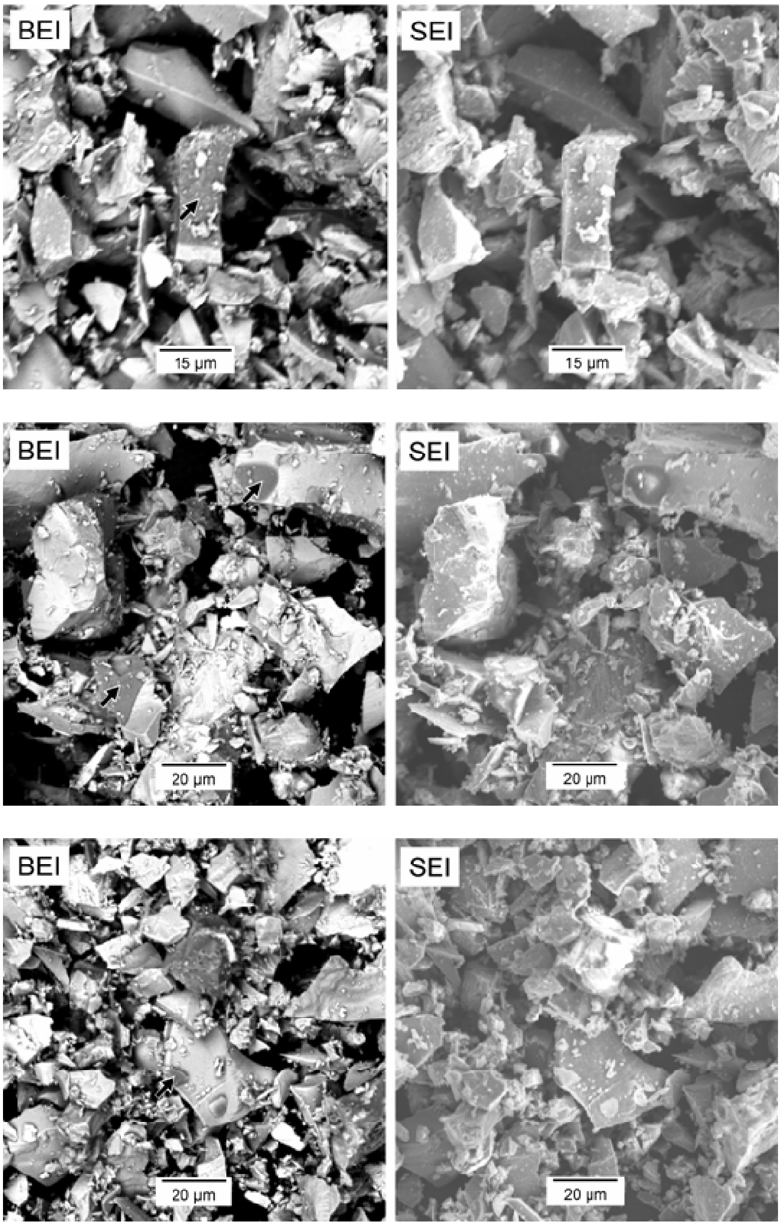

Fine fraction

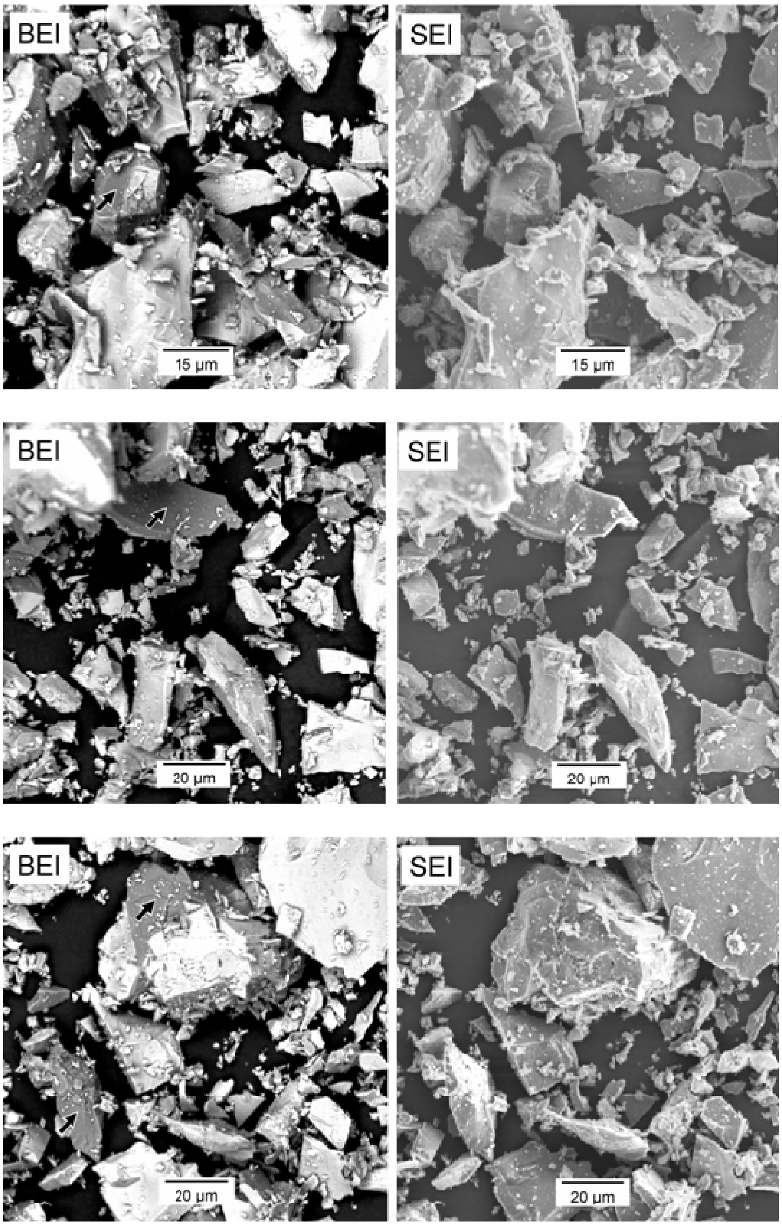

5.4 FlexPDE code for the one dimensional example

```
! #######################################################################################
!  Neumann problem.pde
!
!       Date:            2007-10-28
!       Developer:       Hanlie Kotze
!       Model Purpose:   Part of PhD studies.  Objective is to have a numerical and analytical solutions of
a  semi-infinite  volume  which  starts  off  at  a  temperature  above  it's  liquidus  and  cools  down  to
solidiifcation.
!       The shell thickness as a function of time, and temperature profile at a given time, are compared
for the two solutions.  The analytical solution was done by Prof Chris Pistorius - "Neumann problem.xls".
Equations are from Carslaw & Jaeger, 1959.  The following is the numerical solution.
!       Units:           Temperature              [°C]
!                        Distance         [m]
!                        Time                     [s]
!                        Density          [kg/m3]
!                        Mass                     [kg]
!                        Heat Capacity            [J/(kg.°C)]
!                        Thermal Conductivity     [W/(m.°C)]
!       References:
!       1       Carslaw & Jaeger, 1959
!       Assumptions:
!       1       Material properties are constant (not a function of temperature)
!       2
!
! #######################################################################################

TITLE
        'Neumann problem'

COORDINATES
        CARTESIAN1

SELECT
        SMOOTHINIT
        ERRLIM = 1E-8
        NGRID = 10
        NODELIMIT = 100

VARIABLES
        temperature

 DEFINITIONS
        ! ####################################################################################
        ! Physical Properties
        ! ######################################################################################
        Cpsolid = 900                             ! heat capacity of the solid [J/kgK]
        Cpliquid = 1000                   ! heat capacity of the liquid [J/kgK]
        Hf = 650000                               ! heat of fusion [J/kg]
        ksolid = 2                                ! thermal conductivity of the solid [W/mK]
        kliquid = 4                               ! thermal conductivity of the liquid [W/mK]
        density = 4000                    ! material density [kg/m3]

        ! #######################################################################################
        ! Boundary Conditions
        ! #######################################################################################
        Tsolidus = 1510
        Tliquidus = 1530
        Tinitial = 1550
        Tsurface = 100
        Maxtime = 10*24*3600
        Domainlength = 2.0
        Fliquid = max( min((temperature - Tsolidus) / (Tliquidus - Tsolidus),1.0), 0)
        Fsolid = max( min((Tliquidus - temperature) / (Tliquidus - Tsolidus), 1), 0)

        Cp =     Cpsolid + SWAGE(temperature-Tsolidus,0,(Cpliquid-Cpsolid)/2+Hf/(Tliquidus-
Tsolidus),(Tliquidus - Tsolidus)/10) - SWAGE(temperature-Tliquidus,0,Hf/(Tliquidus-Tsolidus)+(Cpsolid-
Cpliquid)/2,(Tliquidus - Tsolidus)/10)

        k =      SWAGE(temperature-Tsolidus, ksolid, kliquid, (Tliquidus-Tsolidus))

INITIAL VALUES
        temperature = Tinitial

EQUATIONS
        temperature:     (density*Cp)*dt(temperature) - div(k*grad(temperature)) = 0.0

BOUNDARIES
        REGION 1
                START(0) POINT VALUE(temperature) = Tinitial
                LINE TO (Domainlength) POINT VALUE(temperature) = RAMP(t-50, Tinitial, Tsurface, 500)
        FEATURE 'Line'
                START(0) LINE TO (Domainlength)

TIME
        FROM 0 TO Maxtime
```

```
MONITORS
        FOR t = 0,1,2,4,8,16,32,50 BY 100 TO ENDTIME
        ELEVATION(temperature) ON 'Line'
        ELEVATION(Fliquid, Fsolid) ON 'Line'

PLOTS
        FOR t = 0, 3600, 7200, 14400, 28800, 57600, 115200, 230400, 460800, 921600
        ELEVATION(temperature) ON 'Line' EXPORT FORMAT "#d, #1"
        ELEVATION(Fliquid, Fsolid) ON 'Line'EXPORT FORMAT "#d, #1, #2"

HISTORIES
        HISTORY(temperature) AT (0) AT (Domainlength*.2) AT (Domainlength*.4) AT (Domainlength*.6) AT
(Domainlength*.8) AT (Domainlength*.9) AT (Domainlength-0.1) AT (Domainlength-0.05) AT (Domainlength-0.02)
AT (Domainlength) EXPORT FORMAT "#t #r, #i"

        HISTORY(Fliquid) AT (0) AT (Domainlength*.2) AT (Domainlength*.4) AT (Domainlength*.6) AT
(Domainlength*.8) AT (Domainlength*.9) AT (Domainlength-0.1) AT (Domainlength-0.05) AT (Domainlength-0.02)
AT (Domainlength) EXPORT FORMAT "#t #r, #i"

        HISTORY(Cp) AT (0) AT (Domainlength*.2) AT (Domainlength*.4) AT (Domainlength*.6) AT
(Domainlength*.8) AT (Domainlength*.9) AT (Domainlength-0.1) AT (Domainlength-0.05) AT (Domainlength-0.02)
AT (Domainlength) EXPORT FORMAT "#t #r, #i"

        HISTORY(k) AT (0) AT (Domainlength*.2) AT (Domainlength*.4) AT (Domainlength*.6) AT
(Domainlength*.8) AT (Domainlength*.9) AT (Domainlength-0.1) AT (Domainlength-0.05) AT (Domainlength-0.02)
AT (Domainlength) EXPORT FORMAT "#t #r, #i"

 END
```

5.5 Flex PDE code for the slag block model

File 1: slag block and pot system

```
! ##############################################################################################
!  UP Slag Block Cooling 3a.pde
!
!        Client:          Department of Material Science and Metallurgical Engineering
!                         University of Pretoria
!        Date:            2007-02-13
!
!        Developer:       Johan Zietsman
!
!        Model Type:      Transient
!        Model Purpose:   The model is part of Hanlie Kotze's Ph.D. study. Chris Pistorius requested Ex
Mente to assist with the development of a
!                         model based on Hanlie's formulation. Hanlie would then use this model to
!                         generate results required for the completion of her Ph.D.
!                         The purpose of the model is to describe the cooling and solidification
!                         of a high-TiO2 slag block as it moves through the various cooling stages
!                         and cooling conditions on the plant.
!                         The model must take into account the following factors:
!                         - tap temperature,
!                         - tap composition,
!                         - cooling conditions.
!                         The model must also be able to describe a small pilot-plant configuration
!                         and the full-scale industrial configuration.
!
!        Units:           Temperature                 [°C]
!                         Distance            [m]
!                         Time                        [s]
!                         Fraction            []
!                         Chemical Composition        [%]
!                         Density                     [kg/m3]
!                         Mass                        [kg]
!                         Heat Capacity               [J/(kg.°C)]
!                         Thermal Conductivity        [W/(m.°C)]
!
! #################################################################################################

TITLE
        'UP Slag Block Cooling 6a'

COORDINATES
        YCYLINDER

SELECT
        ERRLIM = 1E-4
        SMOOTHINIT
        GRAY
        NODELIMIT = 1000

VARIABLES
        temperature (1700)

DEFINITIONS
        ! ##########################################################################################
        ! Constants
        ! ##########################################################################################

        g = 9.81          ! Gravitational acceleration      [m/s2]
        sigma = 5.669E-8 ! Stefan-Boltzmann constant        [W/(m2.K4)]
        slagDensity = 3800.0      ! Slag density                    [kg/m3
        steelDensity = 7600       ! Steel density                   [kg/m3]

        ! ##########################################################################################
        ! Model Inputs
        ! ##########################################################################################

!%%%% TAP37
{       slagFeOContent_Analysed = 13.25
        slagTemperature_AtTap = 1669.0
        tapMass = 1002.0}

!%%%%TAP38
{       slagFeOContent_Analysed =13.92
        slagTemperature_AtTap = 1668.0
        tapMass = 1365.0}

!%%%% TAP42 C9 WATERcooling
{       slagFeOContent_Analysed = 11.99
        slagTemperature_AtTap = 1709.0
        tapMass = 1017.0}
```

```
!       %%% Tap 64 C9 AIRcooling
{       slagFeOContent_Analysed = 11.46
        slagTemperature_AtTap = 1683.0
        tapMass = 1420.0}

!       Big tap
        slagFeOContent_Analysed = 10.10
        slagTemperature_AtTap = 1678.0
        tapMass = 18200

        potTemperature_BeforeTap = 25.0
        slagFeOContent = slagFeOContent_Analysed
        slagLiquidusTemperature = (0.2351*slagFeOContent^2 - 11.24*slagFeOContent    + 1664.1)
        slagSolidusTemperature_0 = (0.0364*slagFeOContent^2 - 4.845*slagFeOContent + 1502.7)

        ! Domain Dimension Inputs (1.5 t)
{       potMassCapacity = 1500.0
        potR = 0.523
        potTheta_Degrees = 15.0
        potTheta_Radians = (potTheta_Degrees / 360.0) * 2.0 * PI
        potWallThickness = 0.04}

        ! Domain Dimension Inputs (20 t, dwg 615-BZ00 0002G)
        potMassCapacity = 20000.0
        potR = 1.175
        potTheta_Degrees = 15.0
        potTheta_Radians = (potTheta_Degrees / 360.0) * 2.0 * PI
        potWallThickness = 0.11
        ! ##########################################################################################
        ! Domain Dimensions
        ! ##########################################################################################

        ! Domain Dimension Calculations
        potVolume = potMassCapacity / slagDensity
        blockVolume = tapMass / slagDensity
        potPhi_Degrees = 90.0 - potTheta_Degrees
        potPhi_Radians = (potPhi_Degrees / 360.0) * 2.0 * PI
        blockL = ((potVolume - PI * potR ^ 3.0 / 3.0 / tan(potTheta_Radians)) / (-PI * 
(cos(potTheta_Radians)) ^ 3.0 / 3.0 / tan(potTheta_Radians) + PI / 3.0 * (2.0 + cos(potPhi_Radians)) * (1.0 
- cos(potPhi_Radians)) ^ 2.0)) ^ (1.0 / 3.0)
        blockrt = blockL*cos(potTheta_Radians)
        blockzt = blockL*(1.0 - sin(potTheta_Radians)) - blockL
        blockVolume_SpericalCap = (PI/3.0) * blockL^3.0 * (2.0 + cos(potPhi_Radians)) * (1.0 - 
cos(potPhi_Radians))^2.0
        blockVolume_ConicalSection = (PI/3.0) / tan(potTheta_Radians) * (potR^3.0 - blockrt^3.0)
        blockR = ((3.0*tan(potTheta_Radians)/PI)*(blockVolume - blockVolume_SpericalCap) + 
blockrt^3.0)^(1.0/3.0)
        blockZ = (blockR - blockrt)/tan(potTheta_Radians) + blockzt + blockL
        ! ##########################################################################################
        ! Conditions
        ! ##########################################################################################

        ambientTemperature = 25.0

        ! ##########################################################################################
        ! Physical Properties
        ! ##########################################################################################

        k = 0.0          ! Thermal conductivity
        Cp = 0.0 ! Heat capacity

        slagk = (max(0.00175*temperature+0.3,0.3))*1

        slagCp_Solid = - 0.0314*slagFeOContent^2 - 0.4042*slagFeOContent^2 + 908.51
        slagCp_Liquid = 0.0561*SlagFeOContent^2 - 3.3668*slagFeOContent + 1044.3
        slagEnthalpy_At25 = - 139.51*slagFeOContent^2 - 1086.1*slagFeOContent + 515805
        CpSolidify = (slagEnthalpy_At25 + slagCp_Liquid*(slagLiquidusTemperature - 25) - 
slagCp_Solid*(slagSolidusTemperature_0 - 25)) / (slagLiquidusTemperature-slagSolidusTemperature_0)

        slagCp=  IF (temperature <= slagSolidusTemperature_0) THEN slagCp_Solid
                         ELSE     IF (temperature >= slagLiquidusTemperature) THEN slagCp_Liquid
                         ELSE (slagEnthalpy_At25 + slagCp_Liquid*(slagLiquidusTemperature - 25) - 
slagCp_Solid*(slagSolidusTemperature_0 - 25)) / (slagLiquidusTemperature-slagSolidusTemperature_0)
        slagEnthalpy = IF (temperature <= slagSolidusTemperature_0) THEN slagCp_Solid*(temperature-25)
                         ELSE     IF (temperature >= slagLiquidusTemperature) THEN 
slagEnthalpy_At25+slagCp_Liquid*(temperature-25)
                         ELSE     slagCp_Solid*(slagSolidusTemperature_0-25)+CpSolidify*(temperature-
slagSolidusTemperature_0)
        ! Steel
        steelCp = 465.0/slagDensity*steelDensity   ! Carbon Steel 0.5% (Holman)

        steelk = -0.03488*(temperature) + 59.1     ! cast steel, Holman
        ! ##########################################################################################
        ! Initial Conditions
        ! ##########################################################################################

        initialTemperature = 25.0
```

```
        initialLiquidFraction = min(max((temperature - slagSolidusTemperature_0)/( slagLiquidusTemperature
- slagSolidusTemperature_0),0),1)

        !TRANSFER("transfer_1.dat", initialTemperature, initialLiquidFraction)
        ! ##########################################################################################
        ! Boundary Conditions
        ! ##########################################################################################

        ! Water cooling.
        waterVapourDensity = 0.5863                ! At 107°C (Holman)
        waterLatentHeat = 2256000.0                ! Latent heat of water to gas reaction, J/kg (internet
data)
        waterSurfaceTension = 0.0588               ! [N/m] (internet data)
        waterDensity = 994.9                       ! At 32°C (Holman)
        waterCp = 4174.0                  ! (Holman)
        waterSaturationTemperature = 100.0
        waterPr = 0.9                              ! Prandtl number of water
        waterk = 0.68                              ! Thermal conductivity of water
        waterViscosity = 0.003                     ! Kinematic viscosity of water in m2/s

        coolingwaterVolumetricFlowRate = 1.0 / 3600.0       ! m3/hr to m3/s
        coolingwaterDropSpeed = 1.0                         ! m/s
        coolingwaterDropDiameter = 1.0 / 1000.0    ! mm to m
        coolingwaterWaterTemperature = ambientTemperature
        coolingwaterBlockArea = 2 * Pi * blockL ^ 2 * (1 - COS(potPhi_Radians)) + Pi * (blockrt + blockR) *
SQRT((blockZ - blockzt) ^ 2 + (blockR - blockrt) ^ 2)
        coolingwaterVolumetricFlux = coolingwaterVolumetricFlowRate / coolingwaterBlockArea

        coolingwaterRe = coolingwaterVolumetricFlux * coolingwaterDropDiameter / waterViscosity
        coolingwaterNu = 2.512 * coolingwaterRe ^ 0.76 * waterPr ^ 0.56
        coolingwaterTIncip = 13.43 * coolingwaterRe ^ 0.167 * waterPr ^ 0.123 * (waterk /
coolingwaterDropDiameter) ^ 0.22 + coolingwaterWaterTemperature
        coolingwaterTcrit = 18 * ((waterVapourDensity * waterLatentHeat * coolingwaterVolumetricFlux) *
(waterSurfaceTension / (waterDensity * coolingwaterVolumetricFlux^ 2 * coolingwaterDropDiameter)) ^ 0.198)
^ (1 / 5.55) + coolingwaterWaterTemperature
        coolingwaterTmin = 204.895 * coolingwaterVolumetricFlux ^ 0.066 * coolingwaterDropSpeed ^ 0.138 *
coolingwaterDropDiameter ^ (-0.035) + coolingwaterWaterTemperature
        coolingwaterTdfb = 280.762 * coolingwaterVolumetricFlux ^ 0.087 * coolingwaterDropSpeed ^ 0.11 *
coolingwaterDropDiameter ^ (-0.035) + coolingwaterWaterTemperature
        coolingwaterHFdfb = 6100300.0 * coolingwaterVolumetricFlux ^ 0.588 * coolingwaterDropSpeed ^ 0.244
        coolingwaterHFmin = 3324400.0 * coolingwaterVolumetricFlux ^ 0.544 * coolingwaterDropSpeed ^ 0.324
        coolingwaterHFcrit = waterVapourDensity * waterLatentHeat * coolingwaterVolumetricFlux * 122.4 * (1
+ 0.0118 * (waterDensity / waterVapourDensity) ^ 0.25 * (waterDensity * waterCp *
(waterSaturationTemperature - coolingwaterWaterTemperature) / (waterVapourDensity * waterLatentHeat ))) *
(waterSurfaceTension / (waterDensity * coolingwaterVolumetricFlux ^ 2 * coolingwaterDropDiameter )) ^
0.0198

        coolingwaterN2 = (coolingwaterHFdfb - coolingwaterHFmin) / (coolingwaterTdfb - coolingwaterTmin) ^
2
        coolingwaterEN1 = -2 * coolingwaterN2 * coolingwaterTmin
        coolingwaterN0 = coolingwaterHFmin - coolingwaterEN1 * coolingwaterTmin - coolingwaterN2 *
coolingwaterTmin ^ 2

        coolingwaterh =  IF       temperature > coolingwaterTdfb THEN
                                           (63.25 * (temperature - coolingwaterWaterTemperature) ^ 1.691 *
coolingwaterVolumetricFlux ^ 0.264 / coolingwaterDropDiameter ^ 0.062) / (temperature -
coolingwaterWaterTemperature)
                                  ELSE IF  temperature = coolingwaterTdfb THEN
                                           coolingwaterHFdfb / (temperature - coolingwaterWaterTemperature)
                                  ELSE IF (temperature < coolingwaterTdfb) AND (temperature >
coolingwaterTmin) THEN
                                           ((coolingwaterN0 + coolingwaterEN1 * (temperature -
coolingwaterWaterTemperature) + coolingwaterN2 * (temperature - coolingwaterWaterTemperature) ^ 2)) /
(temperature - coolingwaterWaterTemperature)
                                  ELSE IF temperature = coolingwaterTmin THEN
                                           coolingwaterHFmin / (temperature - coolingwaterWaterTemperature)
                                  ELSE IF (temperature < coolingwaterTmin) AND (temperature >
coolingwaterTcrit) THEN
                                           (coolingwaterHFcrit - (coolingwaterHFcrit - coolingwaterHFmin) /
(coolingwaterTcrit - coolingwaterTmin) ^ 3 * (coolingwaterTcrit ^ 3 - 3 * coolingwaterTcrit ^ 2 *
coolingwaterTmin + 6 * coolingwaterTcrit * coolingwaterTmin * (temperature - coolingwaterWaterTemperature)
- 3 * (coolingwaterTcrit + coolingwaterTmin) * (temperature - coolingwaterWaterTemperature) ^ 2 + 2 *
(temperature - coolingwaterWaterTemperature) ^ 3)) / (temperature - coolingwaterWaterTemperature)
                                  ELSE IF temperature = coolingwaterTcrit THEN
                                           coolingwaterHFcrit / (temperature - coolingwaterWaterTemperature)
                                  ELSE IF (temperature < coolingwaterTcrit) AND (temperature >
coolingwaterTIncip) THEN
                                           (0.0000187 * (temperature - coolingwaterWaterTemperature) ^ 5.55)
/ (temperature - coolingwaterWaterTemperature)
                                  ELSE     coolingwaterNu * waterk / coolingwaterDropDiameter

        ! Air cooling.
        solidsurfaceEmissivity = 0.8
        coolingairTf = 0.5 * (temperature + ambientTemperature)
        coolingairkf = 0.00005581 * coolingairTf + 0.02694
        coolingairb = 2 / (ambientTemperature + 273.15 + temperature + 273.15)
        coolingairv = 0.00000000006054 * coolingairTf ^ 2 + 0.000000102 * coolingairTf + 0.0000121
```

```
        coolingairPr = -9.11E-17 * coolingairTf ^ 5 + 5.007E-13 * coolingairTf ^ 4 - 0.000000001021 *
coolingairTf ^ 3 + 0.000000916 * coolingairTf ^ 2 - 0.0003139 * coolingairTf + 0.7153
        coolingairhRadiation = solidsurfaceEmissivity * 5.669 * (((temperature + 273.15) / 100) ^ 4 -
((ambientTemperature + 273) / 100) ^ 4) / (temperature - ambientTemperature) !equation 8-126, p471, Holman

        coolingairHorizontal_L = 0.25 * blockR * 2
        coolingairHorizontal_Gr = g * coolingairb * (temperature - ambientTemperature) *
coolingairHorizontal_L ^ 3 / coolingairv ^ 2
        coolingairHorizontal_C = IF coolingairHorizontal_Gr <= 8.0E6 THEN 0.54 ELSE 0.15
        coolingairHorizontal_m = IF coolingairHorizontal_Gr <= 8.0E6 THEN 1.0/4.0 ELSE 1.0/3.0
        coolingairHorizontal_hConvection = (coolingairkf / coolingairHorizontal_L) * coolingairHorizontal_C
*( (MAX(coolingairHorizontal_Gr, 0.0) * coolingairPr) ^ coolingairHorizontal_m)
        coolingairHorizontal_h = coolingairhRadiation + coolingairHorizontal_hConvection

        coolingairVertical_L = Cos(potTheta_Radians) / blockZ
        coolingairVertical_Gr = (g * coolingairb * (temperature - ambientTemperature) *
coolingairVertical_L ^ 3 / coolingairv ^ 2) * (Cos(potTheta_Radians)) ^ 2
        coolingairVertical_C = IF coolingairVertical_Gr <= 1.0E9 THEN 0.59 ELSE 0.1
        coolingairVertical_m = IF coolingairVertical_Gr <= 1.0E9 THEN 1.0/4.0 ELSE 1.0/3.0
        coolingairVertical_hConvection = coolingairkf / coolingairVertical_L * coolingairVertical_C *
(coolingairVertical_Gr * coolingairPr) ^ coolingairVertical_m
        coolingairVertical_h = coolingairhRadiation + coolingairVertical_hConvection

        ! Boundary Condition Schedule
        endTimeCoolingStep00 = 3600*18                                                  ! Block in pot.

        endTimeCoolingStep01 =  endTimeCoolingStep00 + 3600
        endTimeCoolingStep02 =  endTimeCoolingStep01 + 3600
        endTimeCoolingStep03 =  endTimeCoolingStep02 + 3600
        endTimeCoolingStep04 =  endTimeCoolingStep03 + 3600
        endTimeCoolingStep05 =  endTimeCoolingStep04 + 3600
        endTimeCoolingStep06 =  endTimeCoolingStep05 + 3600
        endTimeCoolingStep07 =  endTimeCoolingStep06 + 3600
        endTimeCoolingStep08 =  endTimeCoolingStep07 + 3600
        endTimeCoolingStep09 =  endTimeCoolingStep08 + 3600
        endTimeCoolingStep10 =  endTimeCoolingStep09 + 3600

        ! Boundary Conditions
        horizontalAirCooling = URAMP(t - 0.0, t - 5.0) * coolingairHorizontal_h * (temperature -
ambientTemperature)
        verticalAirCooling = coolingairVertical_h * (temperature - ambientTemperature)
        verticalWaterCooling = coolingwaterh * (temperature - coolingwaterWaterTemperature )

        blockVerticalCooling =    IF       t <=endTimeCoolingStep00 THEN
                                                   0.0
{                                          ELSE IF t <=endTimeCoolingStep01 THEN
                                                   verticalAirCooling
                                           ELSE IF t <=endTimeCoolingStep02 THEN
                                                   verticalWaterCooling
                                           ELSE IF t <=endTimeCoolingStep03 THEN
                                                   verticalAirCooling
                                           ELSE IF t <=endTimeCoolingStep04 THEN
                                                   verticalWaterCooling
                                           ELSE IF t <=endTimeCoolingStep05 THEN
                                                   verticalAirCooling
                                           ELSE IF t <=endTimeCoolingStep06 THEN
                                                   verticalWaterCooling
                                           ELSE IF t <=endTimeCoolingStep07 THEN
                                                   verticalAirCooling
                                           ELSE IF t <=endTimeCoolingStep08 THEN
                                                   verticalWaterCooling
                                           ELSE IF t <=endTimeCoolingStep09 THEN
                                                   verticalAirCooling
                                           ELSE IF t <=endTimeCoolingStep10 THEN
                                                   verticalWaterCooling}
                                           ELSE 0.0

        blockHorizontalCooling =  IF       t <=endTimeCoolingStep00 THEN
                                                   horizontalAirCooling
{                                          ELSE IF t <=endTimeCoolingStep01 THEN
                                                   horizontalContactCooling
                                           ELSE IF t <=endTimeCoolingStep02 THEN
                                                   horizontalContactCooling
                                           ELSE IF t <=endTimeCoolingStep03 THEN
                                                   horizontalContactCooling
                                           ELSE IF t <=endTimeCoolingStep04 THEN
                                                   horizontalContactCooling
                                           ELSE IF t <=endTimeCoolingStep05 THEN
                                                   horizontalContactCooling
                                           ELSE IF t <=endTimeCoolingStep06 THEN
                                                   horizontalContactCooling
                                           ELSE IF t <=endTimeCoolingStep07 THEN
                                                   horizontalContactCooling
                                           ELSE IF t <=endTimeCoolingStep08 THEN
                                                   horizontalContactCooling
                                           ELSE IF t <=endTimeCoolingStep09 THEN
                                                   horizontalContactCooling
                                           ELSE IF t <=endTimeCoolingStep10 THEN
```

```
                                                   horizontalContactCooling}
                                           ELSE    0.0

        potVerticalCooling =               IF      t <=endTimeCoolingStep00 THEN
                                                   verticalAirCooling
                                           ELSE    verticalAirCooling

        ! Other Calculations
        liquidFraction = min(max((temperature -slagSolidusTemperature_0)/( slagLiquidusTemperature -
slagSolidusTemperature_0),0),1)

INITIAL VALUES
        temperature = initialTemperature
        !liquidFraction = initialLiquidFraction

EQUATIONS
        temperature:     slagDensity*Cp*dt(temperature) - div(k*grad(temperature))  = 0.0

BOUNDARIES

        REGION 1 'Block'
                initialTemperature = slagTemperature_AtTap
                k = slagk
                Cp = slagCp
                                                            START           (0.0, -blockL)
                NOBC(temperature)                   ARC(CENTER=0.0, 0.0) TO (blockrt, blockzt)
                NOBC(temperature)                   LINE    TO      (blockR, blockZ - blockL)
                NATURAL(temperature)=blockHorizontalCooling         LINE    TO      (0.0, blockZ - blockL)
                NOBC(temperature)                   LINE    TO      CLOSE

        {REGION 1 'Block'
                k = slagk
                Cp = slagCp
                                                            START           (0.0, -blockL)
                NATURAL(temperature)=blockVerticalCooling  ARC(CENTER=0.0, 0.0) TO (blockrt, blockzt)
                NATURAL(temperature)=blockVerticalCooling  LINE    TO      (blockR, blockZ - blockL)
                NATURAL(temperature)=blockHorizontalCooling         LINE    TO      (0.0, blockZ - blockL)
                NOBC(temperature)                   LINE    TO      CLOSE}

        REGION 2 'Pot'
                initialTemperature = potTemperature_BeforeTap
                k = steelk
                Cp = steelCp
                                                            START           (0.0, -blockL)
                NOBC(temperature)                   ARC(CENTER=0.0, 0.0) TO (blockrt, blockzt)
                NOBC(temperature)                   LINE    TO      (blockR, blockZ - blockL)
                NATURAL(temperature)=horizontalAirCooling  LINE    TO      (blockR + potWallThickness /
cos(potTheta_Radians), blockZ - blockL)
                NATURAL(temperature)=verticalAirCooling             LINE    TO      (blockrt +
potWallThickness * sin(potPhi_Radians), blockzt - potWallThickness * cos(potPhi_Radians))
                NATURAL(temperature)=verticalAirCooling             ARC(CENTER=0.0, 0.0) TO (0.0, -blockL -
potWallThickness)
                NOBC(temperature)                   LINE    TO      CLOSE

        FEATURE 'Block Vertical Outer Surface'
                START           (0.0, -blockL)
                ARC(CENTER=0.0, 0.0) TO (blockrt, blockzt)
                LINE    TO      (blockR, blockZ - blockL)

        FEATURE 'Pot Vertical Outer Surface'
                START           (0.0, -blockL - potWallThickness)
                ARC(CENTER=0.0, 0.0) TO (blockrt + potWallThickness * sin(potPhi_Radians), blockzt -
potWallThickness * cos(potPhi_Radians))
                LINE    TO      (blockR + potWallThickness / cos(potTheta_Radians), blockZ - blockL)

        FEATURE 'Pot Horizontal edge'
                START           (blockR + potWallThickness / cos(potTheta_Radians), blockZ - blockL)
                LINE    TO      (blockR, blockZ - blockL)

        FEATURE 'Block Horizontal Outer Surface'
                START           (blockR, blockZ - blockL)
                LINE    TO      (0.0, blockZ - blockL)

        FEATURE 'Block Centre Line'
                START           (0.0, -blockL)
                LINE TO  (0.0, -blockL + blockZ)

TIME
        0.0 BY 1E-1 TO endTimeCoolingStep00
        {endTimeCoolingStep00 BY 1E-1 TO endTimeCoolingStep10}

MONITORS
        FOR t= 0, 0.1, 0.5, 1, 2, 3, 4, 5, 6, 7, 8, 9, 10, 15, 20, 25, 30, 45, 60, 300, 600 BY 600 TO 3600
BY 3600 TO ENDTIME
        CONTOUR(temperature) RANGE=(0, 1700)
!       CONTOUR(temperature) PAINTED RANGE=(0, 1700)
!       CONTOUR(liquidFraction2) PAINTED RANGE=(0.0, 1.0)
!       CONTOUR(liquidFraction) PAINTED fixed RANGE=(0.0, 1.0)
```

```
!        ELEVATION(temperature) ON 'Block Vertical Outer Surface'
!        ELEVATION(verticalAirCooling) ON 'Block Vertical Outer Surface'
!        ELEVATION(temperature) ON 'Block Horizontal Outer Surface'
!        ELEVATION(horizontalAirCooling) ON 'Block Horizontal Outer Surface'
!        ELEVATION(slagk) ON 'block horizontal outer surface'
!        ELEVATION(steelCp, steelk, temperature) ON 'Block Vertical Outer Surface'

PLOTS
!        FOR t= 0 BY 24*3600 TO ENDTIME

!        CONTOUR(temperature) RANGE=(0, 1700)
!        CONTOUR(temperature) PAINTED RANGE=(0, 1700)
!        CONTOUR(max(min(liquidFraction, 1.0), 0.0)) PAINTED RANGE=(0.0, 1.0)
!        ELEVATION(temperature) ON 'Block Vertical Outer Surface' EXPORT FORMAT "#d,#1"
!        ELEVATION(verticalAirCooling) ON 'Block Vertical Outer Surface'
!        ELEVATION(temperature) ON 'Block Horizontal Outer Surface'
!        ELEVATION(horizontalAirCooling) ON 'Block Horizontal Outer Surface'
!        TABLE(temperature) EXPORT FORMAT "#t,#x,#y,#1"

!        PLANT BLOCK
         FOR t = 0, 0.25, 0.5, 1, 2, 4, 8, 16, 32, 64, 100, 200, 400, 800, 1600, 3200
!        ELEVATION(liquidFraction) ON 'Block Centre Line' EXPORT FORMAT "#y, #1"
!        ELEVATION(verticalAirCooling) ON 'Block Vertical Outer Surface'      EXPORT FORMAT "#d, #1"
!        ELEVATION(horizontalAirCooling) ON 'Block Horizontal Outer Surface' EXPORT FORMAT "#d, #1"
         ELEVATION(coolingairHorizontal_h) ON 'Block Horizontal Outer Surface' EXPORT FORMAT "#d, #1"
         ELEVATION(steelk) ON 'Block Vertical Outer Surface' EXPORT FORMAT "#d, #1"

         SUMMARY
                  REPORT potMassCapacity
                  REPORT tapMass
                  REPORT potR
                  REPORT potTheta_Degrees
                  REPORT potTheta_Radians
                  REPORT potWallThickness

                  REPORT potVolume
                  REPORT blockVolume
                  REPORT potPhi_Degrees
                  REPORT potPhi_Radians
                  REPORT blockL
                  REPORT blockrt
                  REPORT blockzt
                  REPORT blockVolume_SpericalCap
                  REPORT blockVolume_ConicalSection
                  REPORT blockR
                  REPORT blockZ
                  REPORT slagSolidusTemperature_0
                  REPORT slagLiquidusTemperature

         FOR t = ENDTIME
!        TRANSFER(temperature, liquidFraction) FILE="transfer.dat"
         TRANSFER(temperature) FILE="transfer.dat"

HISTORIES
!        HISTORY(SURF_INTEGRAL(blockVerticalCooling, 'Block Vertical Outer Surface') +
SURF_INTEGRAL(potVerticalCooling, 'Pot Vertical Outer Surface') ) AS 'HeatLossV' EXPORT FORMAT "#t#r,#i"
!        HISTORY(SURF_INTEGRAL(blockHorizontalCooling, 'Block Horizontal Outer Surface')  +
SURF_INTEGRAL(horizontalAirCooling,'Pot Horizontal edge')) AS 'HeatLossH' EXPORT FORMAT "#t#r,#i"
!        HISTORY(VOL_INTEGRAL(slagEnthalpy*slagDensity, 1)+VOL_INTEGRAL(steelCp*slagDensity*(temperature-
25), 2))  AS 'TotalEnergy' EXPORT FORMAT "#t#r,#i"
         {Tap 37 & 38 C10 thermocouple positions}
!        HISTORY(temperature) AT (0,0.13)  AT(0,-0.020) AT(0,-0.120)  AS 'ThermocouplePositions' EXPORT
FORMAT "#t#r,#i"

!        TAP 42 &/ 38
!        HISTORY(SURF_INTEGRAL(verticalAirCooling, 'Block vertical outer surface')) AS 'Heatlosses from Pot
surface' EXPORT FORMAT "#t,#1"
!        HISTORY(temperature) AT (0.0, -blockL - potWallThickness) AT(blockrt + potWallThickness *
sin(potPhi_Radians), blockzt - potWallThickness * cos(potPhi_Radians)) AT(blockR + potWallThickness /
cos(potTheta_Radians), blockZ - blockL) AS 'Pot surface temperatures' EXPORT FORMAT "#t#r,#i"

 !       PLANT TAPS
!        HISTORY(temperature)  AT (0.0, blockZ - blockL) AT (blockR, blockZ - blockL) AT (blockrt, blockzt)
AT (0.0, -blockL)  AS  'Block surface temperatures' EXPORT FORMAT "#t #r, #i"

END
```

File 2: slag block

```
! ##################################################################################################
!  UP Slag Block Cooling 3b.pde
!
!        Client:           Department of Material Science and Metallurgical Engineering
!                          University of Pretoria
!        Date:             2007-02-13
!        Drawing: ???
!
!        Developer:        Johan Zietsman
!
!        Model Type:       Transient
!        Model Purpose:    The model is part of Hanlie Kotze's Ph.D. study.  Chris Pistorius requested Ex
Mente to assist with the development of a
!                          model based on Hanlie's formulation. Hanlie would then use this model to
!                          generate results required for the completion of her Ph.D.
!                          The purpose of the model is to describe the cooling and solidification
!                          of a high-TiO2 slag block as it moves through the various cooling stages
!                          and cooling conditions on the plant.
!                          The model must take into account the following factors:
!                          - tap temperature,
!                          - tap composition,
!                          - cooling conditions.
!                          The model must also be able to describe a small pilot-plant configuration
!                          and the full-scale industrial configuration.
!
!        Units:            Temperature              [°C]
!                          Distance         [m]
!                          Time                     [s]
!                          Fraction         []
!                          Chemical Composition     [%]
!                          Density                  [kg/m3]
!                          Mass                     [kg]
!                          Heat Capacity            [J/(kg.°C)]
!                          Thermal Conductivity     [W/(m.°C)]
!
! ##################################################################################################

TITLE
        'UP Slag Block Cooling 5b'

COORDINATES
        YCYLINDER

SELECT
        ERRLIM = 1E-4
        SMOOTHINIT
        GRAY

VARIABLES
        temperature (1700)

DEFINITIONS
        ! #########################################################################################
        ! Constants
        ! #########################################################################################

        g = 9.81          ! Gravitational acceleration       [m/s2]
        sigma = 5.669E-8  ! Stefan-Boltzmann constant        [W/(m2.K4)]
        slagDensity = 3800.0      ! Slag density                     [kg/m3]

        ! #########################################################################################
        ! Model Inputs
        ! #########################################################################################

!       %%% Tap 37
{       slagFeOContent_Analysed = 13.25
        slagTemperature_AtTap = 1669.0
        tapmass = 1002.00}

!       %%% Tap 38
{       slagFeOContent_Analysed = 13.92
        slagTemperature_AtTap = 1668.0
        tapmass = 1365.00}

!       %%%% TAP42 C9 WATERcooling
{       slagFeOContent_Analysed = 11.99
        slagTemperature_AtTap = 1709.0
        tapMass = 1017.0}

!       %%% Tap 64 C9 AIRcooling
{       slagFeOContent_Analysed = 11.46
        slagTemperature_AtTap = 1683.0
        tapMass = 1420.0}
```

```
!       Big tap
        slagFeOContent_Analysed = 10.10
        slagTemperature_AtTap = 1678.0
        tapMass = 18200.0

        potTemperature_BeforeTap = 25.0
        slagFeOContent = slagFeOContent_Analysed
        slagLiquidusTemperature = (0.2351*slagFeOContent^2 - 11.24*slagFeOContent + 1664.1)
        slagSolidusTemperature_0 = (0.0364*slagFeOContent^2 - 4.845*slagFeOContent + 1502.7)

        ! Domain Dimension Inputs (1.5 t)
{       potMassCapacity = 1500.0
        potR = 0.523
        potTheta_Degrees = 15.0
        potTheta_Radians = (potTheta_Degrees / 360.0) * 2.0 * PI
        potWallThickness = 0.04}

        ! Domain Dimension Inputs (20 t)
        potMassCapacity = 20000.0
        potR = 1.175
        potTheta_Degrees = 15.0
        potTheta_Radians = (potTheta_Degrees / 360.0) * 2.0 * PI
        potWallThickness = 0.11

        ! ########################################################################################
        ! Domain Dimensions
        ! ########################################################################################

        ! Domain Dimension Calculations
        potVolume = potMassCapacity / slagDensity
        blockVolume = tapMass / slagDensity
        potPhi_Degrees = 90.0 - potTheta_Degrees
        potPhi_Radians = (potPhi_Degrees / 360.0) * 2.0 * PI
        blockL   =   ((potVolume   -   PI   *   potR   ^   3.0   /   3.0   /   tan(potTheta_Radians))   /   (-PI   *
(cos(potTheta_Radians)) ^ 3.0 / 3.0 / tan(potTheta_Radians) + PI / 3.0 * (2.0 + cos(potPhi_Radians)) * (1.0
- cos(potPhi_Radians)) ^ 2.0)) ^ (1.0 / 3.0)
        blockrt = blockL*cos(potTheta_Radians)
        blockzt = blockL*(1.0 - sin(potTheta_Radians)) - blockL
        blockVolume_SpericalCap   =   (PI/3.0)   *   blockL^3.0   *   (2.0   +   cos(potPhi_Radians))   *   (1.0   -
cos(potPhi_Radians))^2.0
        blockVolume_ConicalSection = (PI/3.0) / tan(potTheta_Radians) * (potR^3.0 - blockrt^3.0)
        blockR     =     ((3.0*tan(potTheta_Radians)/PI)*(blockVolume     -     blockVolume_SpericalCap)     +
blockrt^3.0)^(1.0/3.0)
        blockZ = (blockR - blockrt)/tan(potTheta_Radians) + blockzt + blockL

        ! ########################################################################################
        ! Conditions
        ! ########################################################################################

        ambientTemperature = 25.0

        ! ########################################################################################
        ! Physical Properties
        ! ########################################################################################

        k = 0.0           ! Thermal conductivity
        Cp = 0.0 ! Heat capacity

        ! Slag
        slagk = (max((0.00175*temperature+0.3),0.3))*1

        slagCp_Solid = - 0.0314*slagFeOContent^2 - 0.4042*slagFeOContent^2 + 908.51
        slagCp_Liquid = 0.0561*SlagFeOContent^2 - 3.3668*slagFeOContent + 1044.3
        slagEnthalpy_At25 = - 139.51*slagFeOContent^2 - 1086.1*slagFeOContent + 515805

        slagCp=  if (temperature <= slagSolidusTemperature_0) THEN slagCp_Solid
                        ELSE     IF (temperature >= slagLiquidusTemperature) THEN slagCp_Liquid
                        ELSE   (slagEnthalpy_At25   +   slagCp_Liquid*(slagLiquidusTemperature   -   25)   -
slagCp_Solid*(slagSolidusTemperature_0 - 25)) / (slagLiquidusTemperature-slagSolidusTemperature_0)

        ! Steel
!       steelk = 54.0             ! Carbon Steel 0.5% (Holman)
!       steelCp = 465.0   ! Carbon Steel 0.5% (Holman)

        ! ########################################################################################
        ! Initial Conditions
        ! ########################################################################################

        !initialTemperature = 25.0
        TRANSFER("transfer_1.dat", initialTemperature)

        ! ########################################################################################
        ! Boundary Conditions
        ! ########################################################################################

        ! Water cooling.
        waterVapourDensity = 0.5863               ! At 107°C (Holman)
```

```
        waterLatentHeat = 2256000.0               ! Latent heat of water to gas reaction, J/kg (internet
data)
        waterSurfaceTension = 0.0588              ! [N/m] (internet data)
        waterDensity = 994.9                      ! At 32°C (Holman)
        waterCp = 4174.0                  ! (Holman)
        waterSaturationTemperature = 100.0
        waterPr = 0.9                             ! Prandtl number of water
        waterk = 0.68                             ! Thermal conductivity of water
        waterViscosity = 0.003                    ! Kinematic viscosity of water in m2/s

!       &&& TUNING PARAMETERS
        coolingwaterVolumetricFlowRate = 1 / 3600.0        ! m3/hr to m3/s
        coolingwaterDropSpeed = 1                 ! m/s
        coolingwaterDropDiameter = 1 / 1000.0              ! mm to m
!       &&&&&&&&&&&&&&&&

        coolingwaterWaterTemperature = ambientTemperature
        coolingwaterBlockArea = 2 * Pi * blockL ^ 2 * (1 - COS(potPhi_Radians)) + Pi * (blockrt + blockR) *
SQRT((blockZ - blockzt) ^ 2 + (blockR - blockrt) ^ 2)
        coolingwaterVolumetricFlux = coolingwaterVolumetricFlowRate / coolingwaterBlockArea

        coolingwaterRe = coolingwaterVolumetricFlux * coolingwaterDropDiameter / waterViscosity
        coolingwaterNu = 2.512 * coolingwaterRe ^ 0.76 * waterPr ^ 0.56
        coolingwaterTIncip = 13.43 * coolingwaterRe ^ 0.167 * waterPr ^ 0.123 * (waterk /
coolingwaterDropDiameter) ^ 0.22 + coolingwaterWaterTemperature
        coolingwaterTcrit = 18 * ((waterVapourDensity * waterLatentHeat * coolingwaterVolumetricFlux) *
(waterSurfaceTension / (waterDensity * coolingwaterVolumetricFlux^ 2 * coolingwaterDropDiameter)) ^ 0.198)
^ (1 / 5.55) + coolingwaterWaterTemperature
        coolingwaterTmin = 204.895 * coolingwaterVolumetricFlux ^ 0.066 * coolingwaterDropSpeed ^ 0.138 *
coolingwaterDropDiameter ^ (-0.035) + coolingwaterWaterTemperature
        coolingwaterTdfb = 280.762 * coolingwaterVolumetricFlux ^ 0.087 * coolingwaterDropSpeed ^ 0.11 *
coolingwaterDropDiameter ^ (-0.035) + coolingwaterWaterTemperature
        coolingwaterHFdfb = 6100300.0 * coolingwaterVolumetricFlux ^ 0.588 * coolingwaterDropSpeed ^ 0.244
        coolingwaterHFmin = 3324400.0 * coolingwaterVolumetricFlux ^ 0.544 * coolingwaterDropSpeed ^ 0.324
        coolingwaterHFcrit = waterVapourDensity * waterLatentHeat * coolingwaterVolumetricFlux * 122.4 * (1
+ 0.0118 * (waterDensity / waterVapourDensity) ^ 0.25 * (waterDensity * waterCp *
(waterSaturationTemperature - coolingwaterWaterTemperature) / (waterVapourDensity * waterLatentHeat ))) *
(waterSurfaceTension / (waterDensity * coolingwaterVolumetricFlux ^ 2 * coolingwaterDropDiameter )) ^
0.0198

        coolingwaterN2 = (coolingwaterHFdfb - coolingwaterHFmin) / (coolingwaterTdfb - coolingwaterTmin) ^
2
        coolingwaterEN1 = -2 * coolingwaterN2 * coolingwaterTmin
        coolingwaterN0 = coolingwaterHFmin - coolingwaterEN1 * coolingwaterTmin - coolingwaterN2 *
coolingwaterTmin ^ 2

        coolingwaterh =         IF      temperature > coolingwaterTdfb THEN
                                        (63.25 * (temperature - coolingwaterWaterTemperature) ^ 1.691 *
coolingwaterVolumetricFlux ^ 0.264 / coolingwaterDropDiameter ^ 0.062) / (temperature -
coolingwaterWaterTemperature)
                                ELSE IF temperature = coolingwaterTdfb THEN
                                        coolingwaterHFdfb / (temperature - coolingwaterWaterTemperature)
                                ELSE IF (temperature < coolingwaterTdfb) AND (temperature >
coolingwaterTmin) THEN
                                        ((coolingwaterN0 + coolingwaterEN1 * (temperature -
coolingwaterWaterTemperature) + coolingwaterN2 * (temperature - coolingwaterWaterTemperature) ^ 2)) /
(temperature - coolingwaterWaterTemperature)
                                ELSE IF temperature = coolingwaterTmin THEN
                                        coolingwaterHFmin / (temperature - coolingwaterWaterTemperature)
                                ELSE IF (temperature < coolingwaterTmin) AND (temperature >
coolingwaterTcrit) THEN
                                        (coolingwaterHFcrit - (coolingwaterHFcrit - coolingwaterHFmin) /
(coolingwaterTcrit - coolingwaterTmin) ^ 3 * (coolingwaterTcrit ^ 3 - 3 * coolingwaterTcrit ^ 2 *
coolingwaterTmin + 6 * coolingwaterTcrit * coolingwaterTmin * (temperature - coolingwaterWaterTemperature)
- 3 * (coolingwaterTcrit + coolingwaterTmin) * (temperature - coolingwaterWaterTemperature) ^ 2 + 2 *
(temperature - coolingwaterWaterTemperature) ^ 3)) / (temperature - coolingwaterWaterTemperature)
                                ELSE IF temperature = coolingwaterTcrit THEN
                                        coolingwaterHFcrit / (temperature - coolingwaterWaterTemperature)
                                ELSE IF (temperature < coolingwaterTcrit) AND (temperature >
coolingwaterTIncip) THEN
                                        (0.0000187 * (temperature - coolingwaterWaterTemperature) ^ 5.55)
/ (temperature - coolingwaterWaterTemperature)
                                ELSE    coolingwaterNu * waterk / coolingwaterDropDiameter

        ! Air cooling.
        solidsurfaceEmissivity = 0.8
        coolingairTf = 0.5 * (temperature + ambientTemperature)
        coolingairkf = 0.00005581 * coolingairTf + 0.02694
        coolingairb = 2 / (ambientTemperature + 273.15 + temperature + 273.15)
        coolingairv = 0.00000000006054 * coolingairTf ^ 2 + 0.000000102 * coolingairTf + 0.0000121
        coolingairPr = -9.11E-17 * coolingairTf ^ 5 + 5.007E-13 * coolingairTf ^ 4 - 0.000000001021 *
coolingairTf ^ 3 + 0.000000916 * coolingairTf ^ 2 - 0.0003139 * coolingairTf + 0.7153
        coolingairhRadiation = solidsurfaceEmissivity * 5.669 * (((temperature + 273) / 100) ^ 4 -
((ambientTemperature + 273) / 100) ^ 4) / (temperature - ambientTemperature) !equation 8-126, p471, Holman

        coolingairHorizontal_L = 0.25 * blockR * 2
        coolingairHorizontal_Gr = g * coolingairb * (temperature - ambientTemperature) *
coolingairHorizontal_L ^ 3 / coolingairv ^ 2
```

```
        coolingairHorizontal_C = IF coolingairHorizontal_Gr <= 8.0E6 THEN 0.54 ELSE 0.15
        coolingairHorizontal_m = IF coolingairHorizontal_Gr <= 8.0E6 THEN 1.0/4.0 ELSE 1.0/3.0
        coolingairHorizontal_hConvection = coolingairkf / coolingairHorizontal_L * coolingairHorizontal_C *
(coolingairHorizontal_Gr * coolingairPr) ^ coolingairHorizontal_m
        coolingairHorizontal_h = coolingairhRadiation + coolingairHorizontal_hConvection

        coolingairVertical_L = Cos(potTheta_Radians) / blockZ
        coolingairVertical_Gr   =   (g   *   coolingairb   *   (temperature   -   ambientTemperature)   *
coolingairVertical_L ^ 3 / coolingairv ^ 2) * (Cos(potTheta_Radians)) ^ 2
        coolingairVertical_C = IF coolingairVertical_Gr <= 1.0E9 THEN 0.59 ELSE 0.1
        coolingairVertical_m = IF coolingairVertical_Gr <= 1.0E9 THEN 1.0/4.0 ELSE 1.0/3.0
        coolingairVertical_hConvection  =  coolingairkf  /  coolingairVertical_L  *  coolingairVertical_C  *
(coolingairVertical_Gr * coolingairPr) ^ coolingairVertical_m
        coolingairVertical_h = coolingairhRadiation + coolingairVertical_hConvection

        ! Boundary Condition Schedule

!       PLANT BLOCKS LANE 1
{       endTimeCoolingStep00 = 3600*17.75                                    ! Block in pot.
        endTimeCoolingStep01 =  endTimeCoolingStep00 + 3600*0.25             ! Air cooling
        endTimeCoolingStep02 =  endTimeCoolingStep01 + 3600*6.6
        endTimeCoolingStep03 =  endTimeCoolingStep02 + 3600*0.1
        endTimeCoolingStep04 =  endTimeCoolingStep03 + 3600*75.7
        endTimeCoolingStep05 =  endTimeCoolingStep04 + 3600*0.1
        endTimeCoolingStep06 =  endTimeCoolingStep05 + 3600*0.1
        endTimeCoolingStep07 =  endTimeCoolingStep06 + 3600*58.8
        endTimeCoolingStep08 =  endTimeCoolingStep07 + 3600*0.3
        endTimeCoolingStep09 =  endTimeCoolingStep08 + 3600*7.2
        endTimeCoolingStep10 =  endTimeCoolingStep09 + 3600*0.5
        endTimeCoolingStep11 =  endTimeCoolingStep10 + 3600*145.2
        endTimeCoolingStep12 =  endTimeCoolingStep11 + 3600*0.12
        endTimeCoolingStep13 =  endTimeCoolingStep12 + 3600
        endTimeCoolingStep14 =  endTimeCoolingStep13 + 3600}

!       PLANT BLOCKS LANE 2
        endTimeCoolingStep00 = 3600*18                                               ! Block in pot.
        endTimeCoolingStep01 =  endTimeCoolingStep00 + 3600*24*15            ! Air cooling
!       endTimeCoolingStep02 = endTimeCoolingStep00 + 3600*24*15             ! Water cooling
!       endTimeCoolingStep03 = endTimeCoolingStep02 + 3600*1                 ! Air cooling

 !      TAP 42 AIR & WATER COOLING
{       endTimeCoolingStep00 = 3600*17.75 ! Block in pot.
        endTimeCoolingStep01 =  endTimeCoolingStep00 + 3600*0.25             ! Air cooling
        endTimeCoolingStep02 =  endTimeCoolingStep01 + 3600*15               ! Water cooling
        endTimeCoolingStep03 =  endTimeCoolingStep02 + 3600*0.5
        endTimeCoolingStep04 =  endTimeCoolingStep03 + 3600*1.2
        endTimeCoolingStep05 =  endTimeCoolingStep04 + 3600*0.5
        endTimeCoolingStep06 =  endTimeCoolingStep05 + 3600*1.1
        endTimeCoolingStep07 =  endTimeCoolingStep06 + 3600*0.6
        endTimeCoolingStep08 =  endTimeCoolingStep07 + 3600*1.0
        endTimeCoolingStep09 =  endTimeCoolingStep08 + 3600*0.7
        endTimeCoolingStep10 =  endTimeCoolingStep09 + 3600*1.0
        endTimeCoolingStep11 =  endTimeCoolingStep10 + 3600*1.0
        endTimeCoolingStep12 =  endTimeCoolingStep11 + 3600*1.0
        endTimeCoolingStep13 =  endTimeCoolingStep12 + 3600*1.2
        endTimeCoolingStep14 =  endTimeCoolingStep13 + 3600*1.0}


        ! Boundary Conditions
        horizontalAirCooling  =  URAMP(t  -  0.0,  t  -  1.0)  *  coolingairHorizontal_h  *  (temperature  -
ambientTemperature)
        horizontalContactCooling  =  (coolingairkf  /  (0.050)  +  coolingairhRadiation)  *  (temperature  -
ambientTemperature)
        verticalAirCooling = coolingairVertical_h * (temperature - ambientTemperature)
        verticalWaterCooling = coolingwaterh * (temperature - coolingwaterWaterTemperature )

        blockVerticalCooling =            IF       t <=endTimeCoolingStep00 THEN
                                                   0.0
                                          ELSE IF  t <=endTimeCoolingStep01 THEN
                                                   verticalAirCooling
{                                         ELSE IF  t <=endTimeCoolingStep02 THEN
                                                   verticalWaterCooling
                                          ELSE IF  t <=endTimeCoolingStep03 THEN
                                                   verticalAirCooling
                                          ELSE IF  t <=endTimeCoolingStep04 THEN
                                                   verticalWaterCooling
                                          ELSE IF  t <=endTimeCoolingStep05 THEN
                                                   verticalAirCooling
                                          ELSE IF  t <=endTimeCoolingStep06 THEN
                                                   verticalWaterCooling
                                          ELSE IF  t <=endTimeCoolingStep07 THEN
                                                   verticalAirCooling
                                          ELSE IF  t <=endTimeCoolingStep08 THEN
                                                   verticalWaterCooling
                                          ELSE IF  t <=endTimeCoolingStep09 THEN
                                                   verticalAirCooling
                                          ELSE IF  t <=endTimeCoolingStep10 THEN
                                                   verticalWaterCooling
```

```
                                           ELSE IF  t <=endTimeCoolingStep11 THEN
                                                    verticalAirCooling
                                           ELSE IF  t <=endTimeCoolingStep12 THEN
                                                    verticalWaterCooling
                                           ELSE IF  t <=endTimeCoolingStep13 THEN
                                                    verticalAirCooling
                                           ELSE IF  t <=endTimeCoolingStep14 THEN
                                                    verticalWaterCooling}
                                           ELSE     0.0

        blockHorizontalCooling =  IF       t <=endTimeCoolingStep00 THEN
                                                    horizontalAirCooling
                                           ELSE IF  t <=endTimeCoolingStep01 THEN
                                                    horizontalContactCooling
{                                          ELSE IF  t <=endTimeCoolingStep02 THEN
                                                    horizontalContactCooling
                                           ELSE IF  t <=endTimeCoolingStep03 THEN
                                                    horizontalContactCooling
                                           ELSE IF  t <=endTimeCoolingStep04 THEN
                                                    horizontalContactCooling
                                           ELSE IF  t <=endTimeCoolingStep05 THEN
                                                    horizontalContactCooling
                                           ELSE IF  t <=endTimeCoolingStep06 THEN
                                                    horizontalContactCooling
                                           ELSE IF  t <=endTimeCoolingStep07 THEN
                                                    horizontalContactCooling
                                           ELSE IF  t <=endTimeCoolingStep08 THEN
                                                    horizontalContactCooling
                                           ELSE IF  t <=endTimeCoolingStep09 THEN
                                                    horizontalContactCooling
                                           ELSE IF  t <=endTimeCoolingStep10 THEN
                                                    horizontalContactCooling
                                           ELSE IF  t <=endTimeCoolingStep11 THEN
                                                    horizontalContactCooling
                                           ELSE IF  t <=endTimeCoolingStep12 THEN
                                                    horizontalContactCooling
                                           ELSE IF  t <=endTimeCoolingStep13 THEN
                                                    horizontalContactCooling
                                           ELSE IF  t <=endTimeCoolingStep14 THEN
                                                    horizontalContactCooling}
                                           ELSE     0.0

        potVerticalCooling =               IF       t <=endTimeCoolingStep00 THEN
                                                    verticalAirCooling
                                           ELSE     verticalAirCooling

        ! Other Calculations
        liquidFraction   =   min(max((temperature   -slagSolidusTemperature_0)/(   slagLiquidusTemperature   -
slagSolidusTemperature_0),0),1)
        liquidFraction2 = max(min(liquidFraction, 1.0), 0.0)


INITIAL VALUES
        temperature = initialTemperature

EQUATIONS
        temperature:     slagDensity*cp*dt(temperature) - div(k*grad(temperature))  = 0.0

BOUNDARIES

        {REGION 1 'Block'
                initialTemperature = slagTemperature_AtTap
                initialLiquidFraction = 1.0
                k = slagk
                Cp = slagCp
                                                             START           (0.0, -blockL)
                NOBC(temperature)                    ARC(CENTER=0.0, 0.0) TO (blockrt, blockzt)
                NOBC(temperature)                    LINE     TO      (blockR, blockZ - blockL)
                NATURAL(temperature)=blockHorizontalCooling  LINE     TO      (0.0, blockZ - blockL)
                NOBC(temperature)                    LINE     TO      CLOSE}

        REGION 1 'Block'
                k = slagk
                cp = slagCp
                                                             START           (0.0, -blockL)
                NATURAL(temperature)=blockVerticalCooling  ARC(CENTER=0.0, 0.0) TO (blockrt, blockzt)
                NATURAL(temperature)=blockVerticalCooling  LINE     TO      (blockR, blockZ - blockL)
                NATURAL(temperature)=blockHorizontalCooling  LINE     TO      (0.0, blockZ - blockL)
                NOBC(temperature)                    LINE     TO      CLOSE

        {REGION 2 'Pot'
                initialTemperature = potTemperature_BeforeTap
                initialLiquidFraction = 0.0
                k = steelk
                Cp = steelCp
                                                             START           (0.0, -blockL)
                NOBC(temperature)                    ARC(CENTER=0.0, 0.0) TO (blockrt, blockzt)
                NOBC(temperature)                    LINE     TO      (blockR, blockZ - blockL)
```

```
                NATURAL(temperature)=horizontalAirCooling  LINE     TO       (blockR  +  potWallThickness  /
cos(potTheta_Radians), blockZ - blockL)
                NATURAL(temperature)=verticalAirCooling          LINE     TO       (blockrt              +
potWallThickness * sin(potPhi_Radians), blockzt - potWallThickness * cos(potPhi_Radians))
                NATURAL(temperature)=verticalAirCooling          ARC(CENTER=0.0, 0.0) TO (0.0, -blockL -
potWallThickness)
                NOBC(temperature)                          LINE     TO       CLOSE}

        FEATURE 'Block Vertical Outer Surface'
                START           (0.0, -blockL)
                ARC(CENTER=0.0, 0.0) TO (blockrt, blockzt)
                LINE    TO      (blockR, blockZ - blockL)

        FEATURE 'Block Horizontal Outer Surface'
                START           (blockR, blockZ - blockL)
                LINE    TO      (0.0, blockZ - blockL)

        FEATURE 'Block Centre Line'
                START           (0.0, -blockL)
                LINE TO  (0.0, -blockL + blockZ)

        FEATURE 'Block Roundend Radius'
                START           (0.0, 0.0)
                LINE TO  (blockrt, blockzt)

TIME
        {0.0 BY 1E-1 TO endTimeCoolingStep00}
        endTimeCoolingStep00 BY 1E-1 TO endTimeCoolingStep01


MONITORS
        FOR t= 0, 0.1, 0.5, 1, 2, 3, 4, 5, 6, 7, 8, 9, 10, 15, 20, 25, 30, 45, 60, 300, 600 BY 600 TO 3600
BY 3600 TO ENDTIME
        CONTOUR(temperature) RANGE=(0, 1700)
!       CONTOUR(temperature) PAINTED RANGE=(0, 1700)
!       CONTOUR(liquidFraction2) PAINTED RANGE=(0.0, 1.0)
!       ELEVATION(temperature) ON 'Block Vertical Outer Surface'
!       ELEVATION(verticalAirCooling) ON 'Block Vertical Outer Surface'
!       ELEVATION(temperature) ON 'Block Horizontal Outer Surface'
!       ELEVATION(horizontalAirCooling) ON 'Block Horizontal Outer Surface'

PLOTS
        FOR t=endTimeCoolingStep00 BY 3600*24 TO ENDTIME

!       CONTOUR(temperature) RANGE=(0, 1700)
!       CONTOUR(temperature) PAINTED RANGE=(0, 1700)
!       CONTOUR(max(min(liquidFraction, 1.0), 0.0)) PAINTED RANGE=(0.0, 1.0)
!       ELEVATION(temperature) ON 'Block Vertical Outer Surface'
!       ELEVATION(verticalAirCooling) ON 'Block Vertical Outer Surface'
!       ELEVATION(temperature) ON 'Block Vertical Outer Surface' EXPORT FORMAT "#d, #1"
        ELEVATION(horizontalAirCooling) ON 'Block Horizontal Outer Surface'

!       FOR t=0 BY 3600.00*24 TO ENDTIME
!       ELEVATION(temperature) ON 'Block Vertical Outer Surface' EXPORT FORMAT "#x,#y,#1"

!       PLANT BLOCK
!       FOR t = 0, 0.1, 0.5, 1, 2, 4, 6, 8, 10, 15, 20, 25, 30, 45, 60, 80, 100, 200, 300, 400, 500, 600 BY
600 TO ENDTIME
!       ELEVATION(liquidFraction) ON 'Block Centre Line' EXPORT FORMAT "#y, #1"
!       ELEVATION(temperature, coolingairvertical_h) ON 'Block Vertical Outer Surface' EXPORT FORMAT "#d,
#1, #2"
!       CONTOUR(temperature) RANGE=(0,1700) EXPORT FORMAT "#x, #y, #1"
!       ELEVATION(temperature) ON 'Block Roundend Radius' EXPORT FORMAT "#d, #1"

        SUMMARY
                REPORT potMassCapacity
                REPORT tapMass
                REPORT potR
                REPORT potTheta_Degrees
                REPORT potTheta_Radians
                REPORT potWallThickness

                REPORT potVolume
                REPORT blockVolume
                REPORT potPhi_Degrees
                REPORT potPhi_Radians
                REPORT blockL
                REPORT blockrt
                REPORT blockzt
                REPORT blockVolume_SpericalCap
                REPORT blockVolume_ConicalSection
                REPORT blockR
                REPORT blockZ
                REPORT slagSolidusTemperature_0
                REPORT slagLiquidusTemperature

        {FOR t = ENDTIME
        TRANSFER(temperature, liquidFraction) FILE="transfer.dat"}
```

```
HISTORIES
!       HISTORY(SURF_INTEGRAL(blockVerticalCooling, 'Block Vertical Outer Surface') / SURF_INTEGRAL(1,
'Block Vertical Outer Surface')) AS 'VerticalHeatLoss'
!       HISTORY(VOL_INTEGRAL(liquidFraction2, 1) / VOL_INTEGRAL(1, 1)) AS 'TotalLiquidFraction'

        {Tap 37 & 38 C10 thermocouple positions}
!       HISTORY(temperature) AT (0,0.13)  AT(0,-0.020) AT(0,-0.120)  AS 'ThermocouplePositions' EXPORT
FORMAT "#t#r,#i"
!       HISTORY(temperature, coolingairVertical_h, coolingwaterh)  AT (0.0, blockZ - blockL) AT (blockR,
blockZ - blockL) AT (blockrt, blockzt)  AT (0.0, -blockL)  AS  'Block surface temperatures' EXPORT FORMAT
"#t #r, #i"

!       TAP 42
!       HISTORY(SURF_INTEGRAL(blockHorizontalCooling, 'Block Horizontal Outer Surface')) AS 'Heatloss to
ground' EXPORT FORMAT "#t,#1"
!       HISTORY(SURF_INTEGRAL(blockVerticalCooling, 'Block Vertical Outer Surface')) AS 'Heatloss to
suroundings' EXPORT FORMAT "#t,#1"

!       PLANT TAPS
!       HISTORY(temperature, coolingairvertical_h)  AT (0.0, blockZ - blockL) AT (blockR, blockZ - blockL)
AT (blockrt, blockzt)  AT (0.0, -blockL)  AS  'Block surface temperatures' EXPORT FORMAT "#t #r, #i"


END
```

5.6 List of expressions used to calculate the heat transfer coefficient in spray cooling.[37,38]

5.7 Nomenclature

d_{32} = Sauter mean drop diameter, m

(the Sauter mean diameter is the drop diameter with a volume to surface area which is equal that of the entire water spray)

Nu =Nusselt number, dimensionless

$\Pr$ = Prandtl number, dimensionless

Re_{32} = Reynolds number based on the Sauter Mean Diameter[§§§], dimensionless

T = temperature, ˚C

Q'' =volumetric flux of the cooling water, m^3s^{-1}/m^2

q'' = heat flux, W/m^2

k = thermal conductivity, $W/m^2/°C$

σ = surface tension of water, N/m

ρ = density, kg/m^3

υ = drop speed, m/s

ϑ = kinematic viscosity of water, m^2/s

h_{fg} = latent heat of vaporisation, J/kg

Subscripts

$incip$ = point of incipient nucleate boiling

$crit$ =point of critical heat flux

$\min$ = point of minimum heat flux (Leidenfrost point)

dfb = point of departure from film boiling

s = hot surface

w = water

v = vapour

$$\mathrm{Re}_{32} = \frac{Q^{''} d_{32}}{\vartheta}$$

$$Nu_f = 2.512\,\mathrm{Re}_{32}{}^{0.76}\,\mathrm{Pr}_w{}^{0.56}$$

$$T_{incip} = 13.43\,\mathrm{Re}_{32}{}^{0.167}\,\mathrm{Pr}_w{}^{0.123}\left(\frac{k_w}{d_{32}}\right)^{0.22} + T_w$$

$$T_{crit} = 18\left(\rho_v h_{fg} Q^{''}\left(\frac{\sigma}{\rho_w Q^{''2} d_{32}}\right)^{0.198}\right)^{\frac{1}{5.55}} + T_w$$

$$T_{\min} = 204.895 Q^{''0.066}\upsilon^{0.138} d_{32}{}^{-0.035} + T_w$$

$$T_{dfb} = 280.762 Q^{''0.087}\upsilon^{0.11} d_{32}{}^{-0.035} + T_w$$

$$q^{''}{}_{dfb} = 6100300 Q^{''0.588}\upsilon^{0.244}$$

$$q^{''}{}_{\min} = 3324400 Q^{''0.544}\upsilon^{0.324}$$

$$q^{''}{}_{crit} = 122.4\rho_g h_{fg} Q^{''}\left(1 + 0.0118\left(\frac{\rho_w}{\rho_g}\right)^{0.25}\left(\frac{\rho_w Cp_w\left(T_w^{sat} - T_w\right)}{\rho_g h_{fg}}\right)\right)\left(\frac{\sigma}{\rho_w Q^{''2} d_{32}}\right)^{0.0198}$$

$$N_2 = \frac{q^{''}{}_{dfb} - q^{''}{}_{\min}}{\left(T_{dfb} - T_{\min}\right)^2}$$

$$N_1 = -2N_2\left(T_{\min}\right)$$

$$N_0 = q^{''}{}_{\min} - N_1\left(T_{\min}\right) - N_2\left(T_{\min}\right)^2$$

$$T_s > T_{dfb} \quad : \quad h = \frac{63.25\left(T_s - T_w\right)^{1.691} Q''^{0.264} d_{32}{}^{-0.062}}{\left(T_s - T_w\right)}$$

$$T_s = T_{dfb} \quad : \quad h = \frac{q''_{dfb}}{\left(T_s - T_w\right)}$$

$$T_s < T_{dfb}; T > T_{\min} \quad : \quad h = \frac{N_0 + N_1\left(T_s - T_w\right) + N_2\left(T_s - T_w\right)^2}{\left(T_s - T_w\right)}$$

$$T_s = T_{\min} \quad : \quad h = \frac{q''_{\min}}{\left(T_s - T_w\right)}$$

$$T_s < T_{\min}; T > T_{crit} \quad : \quad h = \frac{q''_{crit}}{\left(T_s - T_w\right)} - \frac{q''_{crit} - q''_{\min}}{\left(T_{crit} - T_{\min}\right)^3} \times$$

$$\frac{\left(T_{crit}{}^3 - 3T_{crit}{}^2 T_{\min} + 6T_{crit}T_{\min}\left(T_s - T_w\right) - 3\left(T_{crit} + T_{\min}\right)\left(T_s - T_w\right)^2 + 2\left(T_s - T_w\right)^3\right)}{\left(T_s - T_w\right)}$$

$$T_s = T_{crit} \quad : \quad h = \frac{q''_{crit}}{\left(T_s - T_w\right)}$$

$$T_s < T_{crit}; T > T_{incip} \quad : \quad h = \frac{0.0000187\left(T_s - T_w\right)^{5.55}}{\left(T_s - T_w\right)}$$

$$T_s < T_{incip} \quad : \quad h = \frac{Nu_w k_w}{d_{32}}$$

5.8 Tap information and composition of the two thermocouple blocks

Tap chemistry

	TiO_2	FeO	Al_2O_3	CaO	Cr_2O_3	MgO	MnO	SiO_2	V_2O_5	Total ****
Tap 37	85.42	13.25	0.71	0.04	0.11	0.89	1.51	1.01	0.45	104.02
Tap 38	84.21	13.92	0.75	0.04	0.15	1.26	1.45	0.94	0.45	102.94

Tap details

	Block mass (kg)	Tap rate (kg/min)	Tap temperature (˚C)
Tap 37	1,002	204.6	1669
Tap 38	1,365	345.7	1668

**** The total exceeds 100% because all titanium, including Ti^{3+},is reported as Ti^{4+} (TiO_2)

5.9 Cross sections water vs. air cooling

Water Air

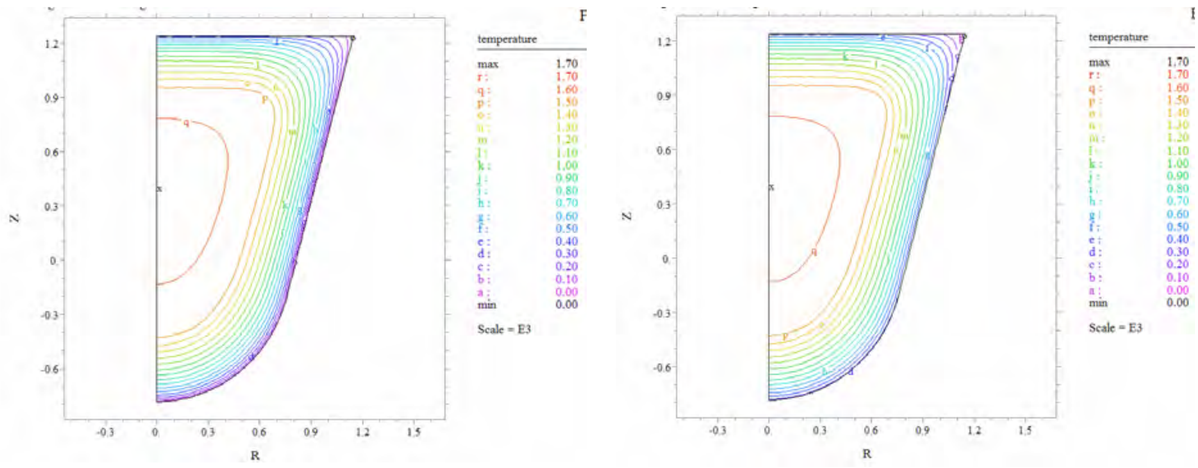

1 day

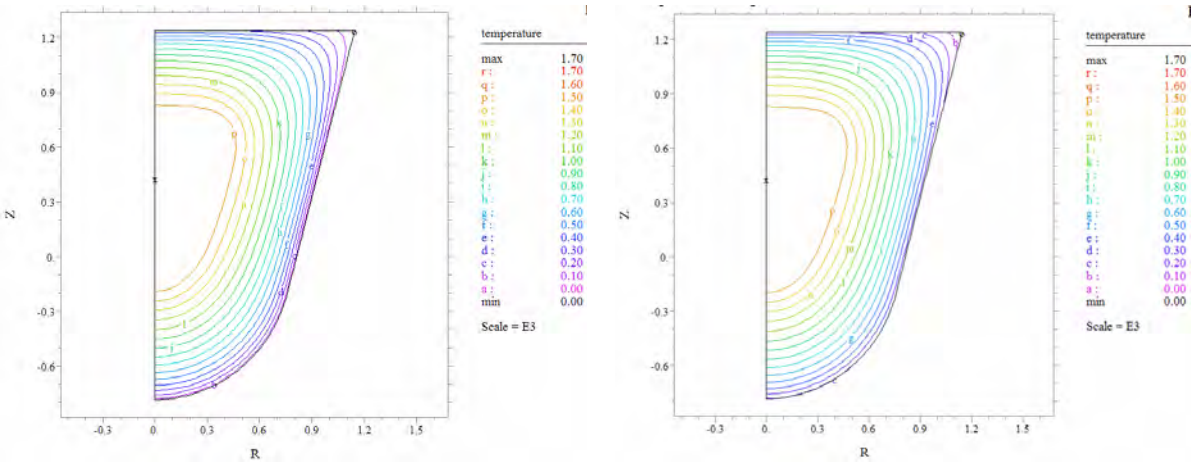

2 days

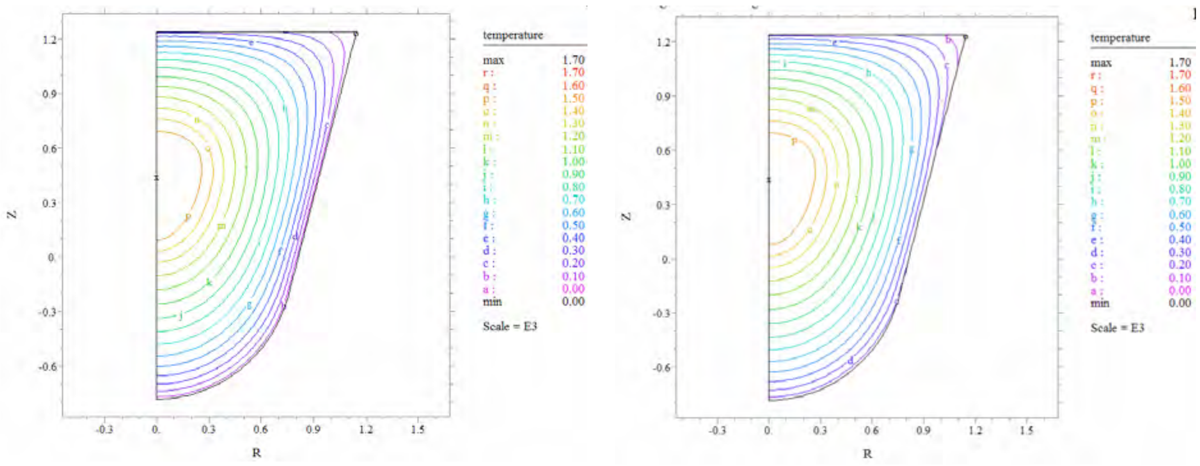

3 days

Water Air

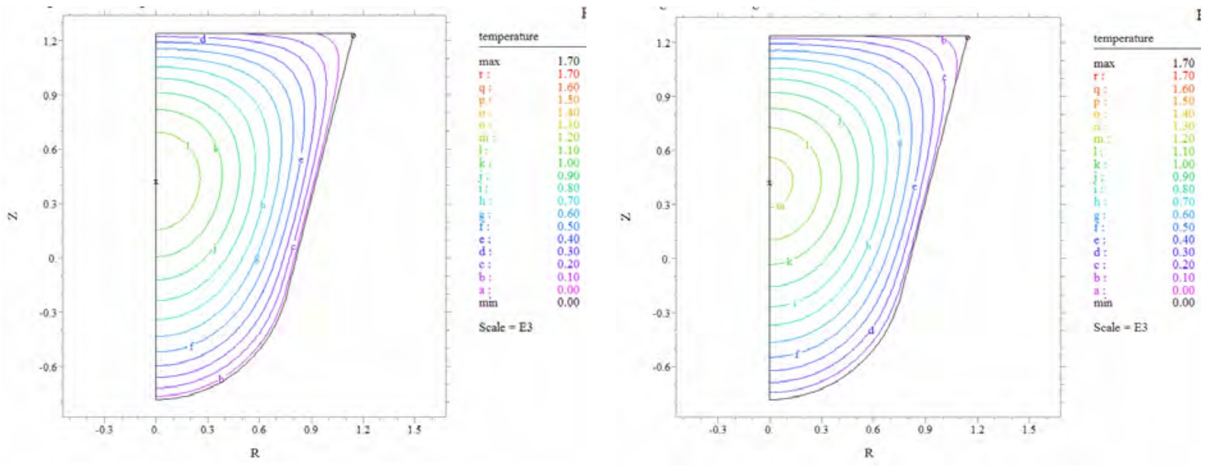

4 days

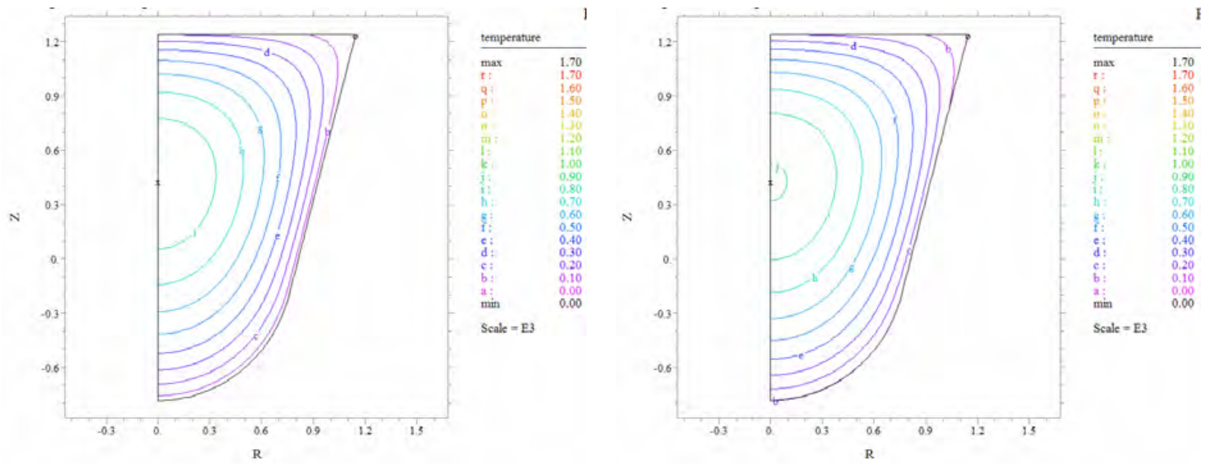

5 days

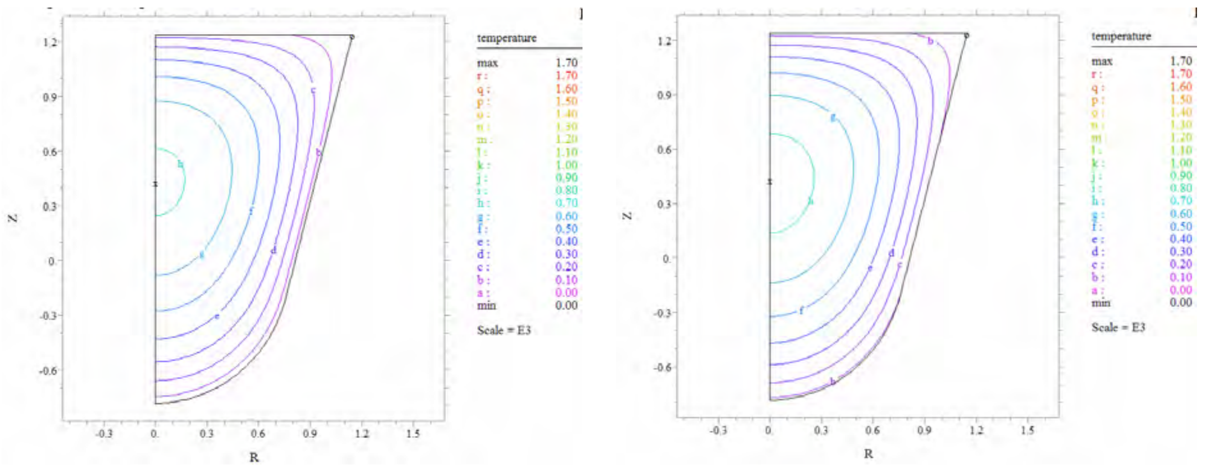

6 days

Water Air

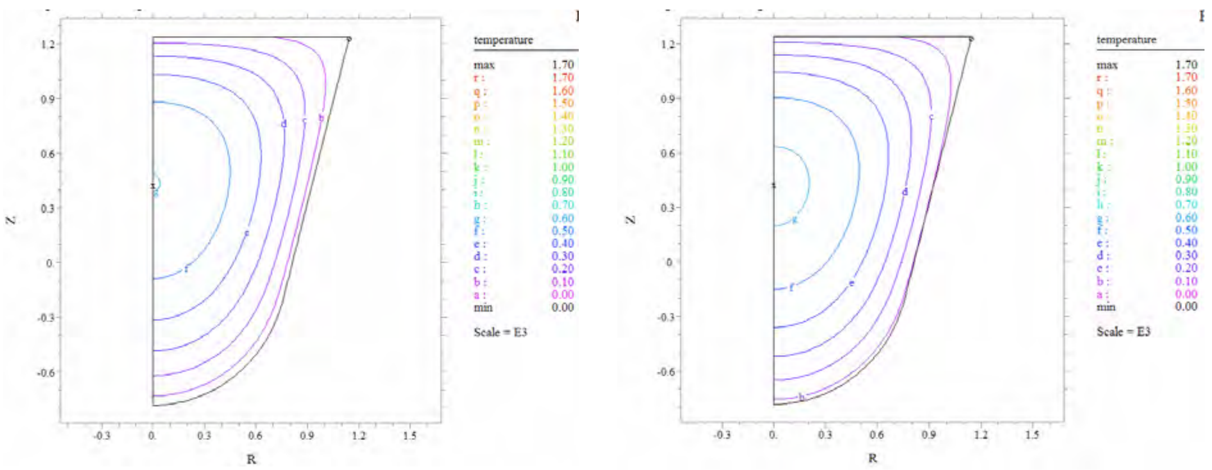

7 days

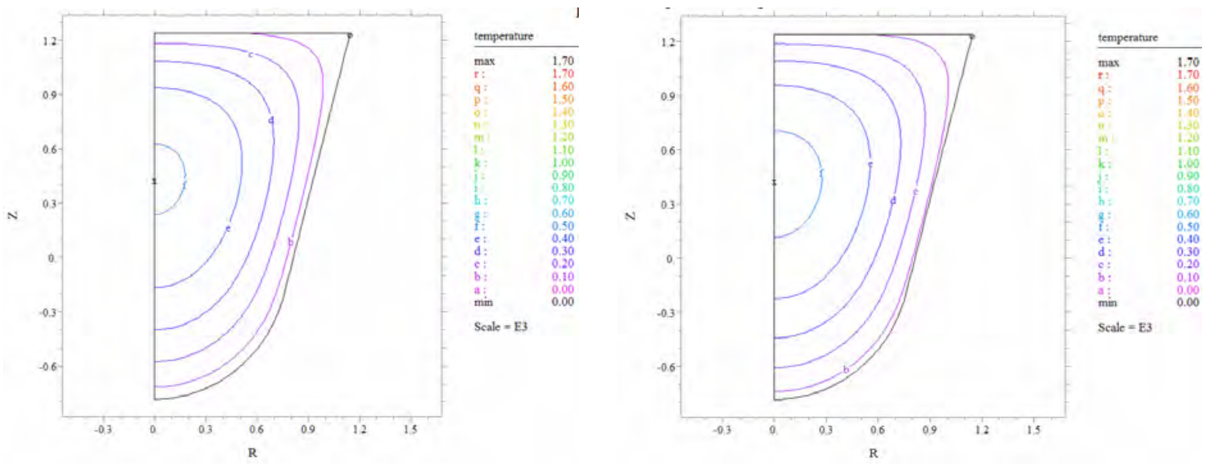

8 days

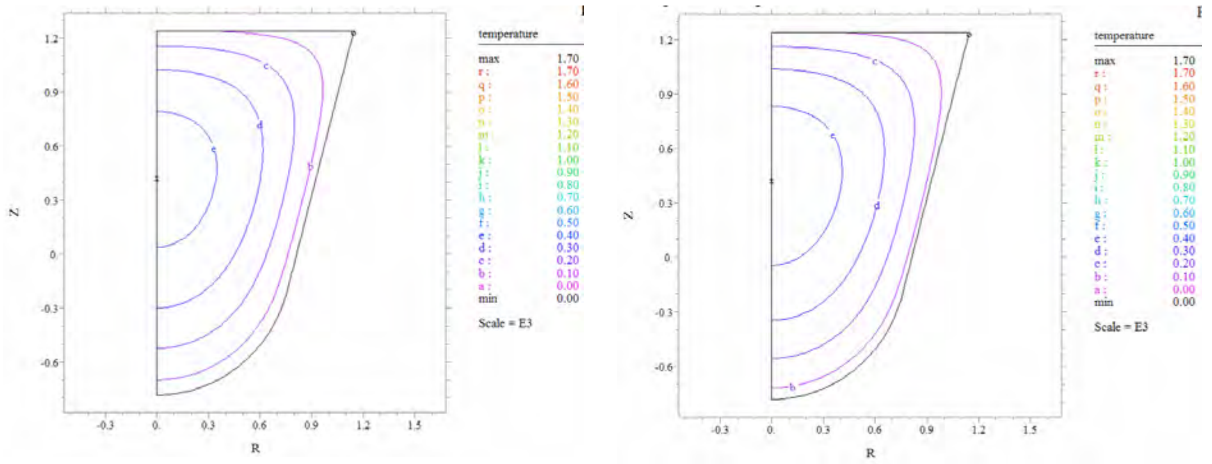

9 days

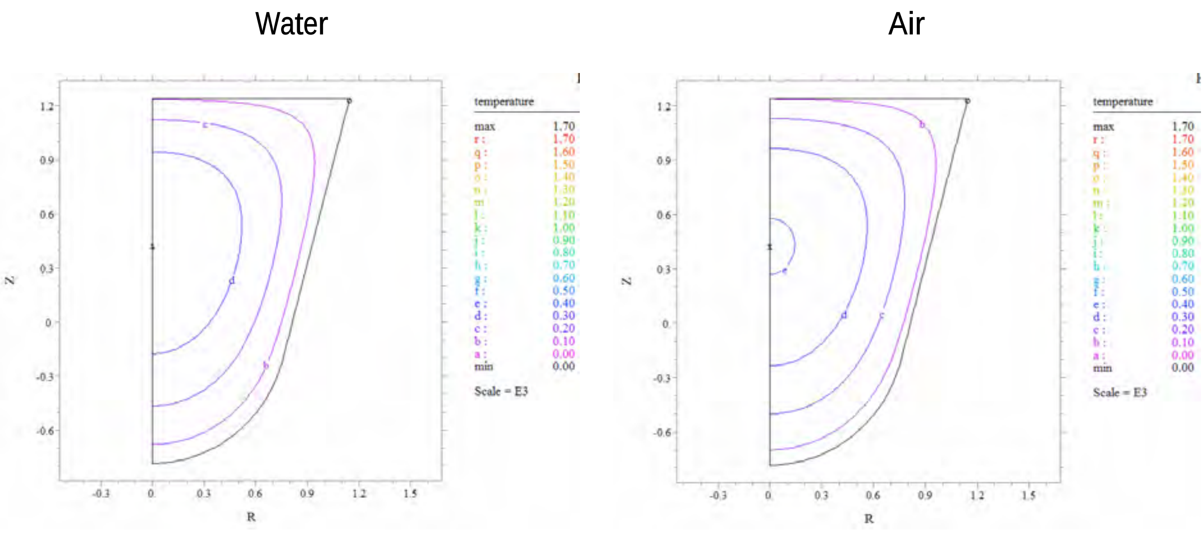
Water
Air
temperature
max 1.70
r : 1.70
q : 1.60
p : 1.50
o : 1.40
n : 1.30
m : 1.20
l : 1.10
k : 1.00
j : 0.90
i : 0.80
h : 0.70
g : 0.60
f : 0.50
e : 0.40
d : 0.30
c : 0.20
b : 0.10
a : 0.00
min 0.00
Scale = E3
Z
R
1.2
0.9
0.6
0.3
0
-0.3
-0.6
-0.3
0.3
0.6
0.9
1.2
1.5
b
c
d
e

10 days

6 References

1 http://en.wikipedia.org/wiki/Titanium_dioxide. (Accessed 15 September 2006)

2 T. P. Battle, D. Nguyen and J.W. Reeves: “The Processing of titanium-containing ores.” *The Paul E. Queneau International Symposium.* Vol. I: Fundamental Aspects., pp. 925-945, 1993.

3 H. Kotzé, D. Bessinger and J. Beukes: “Ilmenite smelting at Ticor SA.” *The Journal of the South African Institute for Mining and Metallurgy*, March 2006, vol. 106, pp. 165-170.

4 PC Pistorius and C Coetzee: "Physicochemical aspects of titanium slag production and solidification." *Metallurgical and Materials Transactions Series B*, vol. 34B, pp. 581-588B (2003).

5 Bessinger, D., Geldenhuis, J.M.A. and Pistorius P.C.: "Phase changes in the decrepitation of solidified high titania slags." *Heavy Minerals 2005*, Society for Mining, Metallurgy and Exploration, 2005. pp. 213-219.

6 Bessinger, D., Geldenhuis, J.M.A., Pistorius, P.C., Mulaba, A., Hearne, G.: "The decrepitation of solidified high titania slags." *Journal of Non-Crystalline Solids*, vol. 282, no. 1, pp. 132–142 (2001).

7 J.P.R de Villiers, J. Göske and A. Tuling: “Disintegration in high grade titania slags: low temperature oxidation reactions and associated fracture mechanics of pseudobrookite.” *Mineral Processing and Extractive Metallurgy (Trans. Inst. Min. Metall C)*, June 2005, vol. 114, pp. C73-C79.

8 M Gous: “An overview of the Namakwa Sands ilmenite smelting operations.” *The Journal of the South-African Institute of Mining and Metallurgy*, June 2006, vol. 106, pp. 379-384.

9 P.C. Pistorius: "Ilmenite smelting – the basics." *The 6th International Heavy Minerals Conference ‘Back to Basics’*. The Southern African Institute of Mining and Metallurgy, 2007. pp. 75-83.

10 J.H. Zietsman and P.C. Pistorius: "Process mechanisms in ilmenite smelting." *Journal of the South African Institute of Mining and Metallurgy*, vol. 104, pp. 653-660 (2004).

11 M. Guéguin and F. Cardarelli: "Chemistry and mineralogy of titania-rich slags. Part 1—hemo-ilmenite, sulphate, and upgraded titania slags." *Mineral processing and extractive metallurgy review*, vol. 28, pp. 1-58 (2007).

12 K. Borowiec, A.E. Grau, M. Guéguin and J.-F. Turgeon: "Method to upgrade titania slag and resulting product." United States Patent no. 5,830,420 (1998).

13 H. Elstad, J.M. Eriksen, A. Hildal, T. Rosenqvist, and S. Seim: "Equilibrium between titania slags and metallic iron." *The 6th International Heavy Minerals Conference ‘Back to Basics’*. The Southern African Institute of Mining and Metallurgy, 2007. pp. 35-42.

14 G. Eriksson and A.D. Pelton: "Critical evaluation and optimization of the thermodynamic properties and phase diagrams of the MnO-TiO_2, MgO-TiO_2, FeO-TiO_2, Ti_2O_3-TiO_2, Na_2O-TiO_2 and K_2O-TiO_2 systems." *Metallurgical Transactions B*, vol. 24B, pp. 795-805 (1993).

15 G. Eriksson, A.D. Pelton, E. Woermann and E. Ender: "Measurement and thermodynamic evaluation of phase equilibria in the Fe-Ti-O system." *Berichte der Bunsengesellschaft für physikalische Chemie*, vol. 100, pp. 1839-1849 (1996).

16 J. Pesl and R.H. Eric: "High-temperature phase relations and thermodynamics in the iron-titanium-oxygen system." *Metallurgical and Materials Transactions B*, vol. 30B, pp. 695-705 (1999).

17 C.W. Bale, P. Chartrand, S.A. Degterov, G. Eriksson, K. Hack, R. Ben Mahfoud, J. Melançon, A.D. Pelton and S. Petersen: "FactSage Thermochemical Software and Databases." *Calphad*, vol. 26, pp. 189-228 (2002).

18 S. Jahanshahi, L. Zhang and D. Bessinger: "Development of MPE package and its application in ilmenite smelting." *Heavy Minerals 2003*. South African Institute of Mining and Metallurgy, 2003. pp. 119-126.

19 D.J. Fourie, J.J. Eksteen and J.H. Zietsman: "Calculation of FeO-TiO_2-Ti_2O_3 liquidus isotherms pertaining to high titania slags." *Journal of the South African Institute of Mining and Metallurgy*, vol. 105, pp. 695-710 (2005).

20 PC Pistorius: "Fundamentals of freeze lining behaviour in ilmenite smelting." *Journal of the South African Institute of Mining and Metallurgy*, vol. 103, pp. 509-514 (2003).

21 J.M.A. Geldenhuis and P.C. Pistorius. "The use of commercial oxygen probes during the production of high titania slags." *Journal of the South African Institute of Mining and Metallurgy*, vol. 99, pp. 41-47 (1999).

22 P.C. Pistorius and T. Motlhamme: "Oxidation of high-titanium slags in the presence of water vapour." *Minerals Engineering*, vol. 19, pp. 232 236 (2006).

23 I.E. Grey, L.M.D. Cranswick, C. Li, T.J. White, and L.A. Bursill: "New M_3O_5-anatase intergrowth structures formed during low-temperature oxidation of anosovite." *Journal of Solid State Chemistry*, vol. 150, pp. 128-138 (2000).

24 J.P. van Dyk, N.M. Vegter, C.P. Visser, T. de Lange, J.D. Winter, E.A. Walpole and J. Nell: "Beneficiation of titania slag by oxidation and reduction treatment." United States patent no. 6,803,024 (2004).

25 Errol G. Kelly, David J. Spottiswood: "Introduction to mineral processing." *Australian Mineral Foundation*, pp. 461, (1995).

26 P.C. Pistorius: "The relationship between FeO and Ti_2O_3 in ilmenite smelter slags." *Scandinavian Journal of Metallurgy*, 2002, vol. 31, pp. 120-125.

27 R.M. Viljoen, J.T Smit, I. du Plessis and V.Ser: “The development and application of in-bed compression breakage principles.” *Minerals Engineering*, vol. 14, No. 5, pp. 465 – 471, 2001.

28 H Brundiek and F Poeschl: "A roller mill for cement and blast furnace slag in theory and practice." *37th IEEE Cement Industry Technical Conference*, June 1995, San Juan, Puerto Rico. pp. 197-223.

29 H.S. Carslaw and J.C. Jaeger: *Conduction of heat in solids,* second edition. Clarendon, 1959. pp. 282-286.

30 J.P. Holman. “Heat Transfer.” *McGraw-Hill Book Co*, SI Metric Edition, pp. 635, (1989).

31 A. Hamasaiid, M.S. Dargusch, C.J. Davidson, S. Tovar, T. Loulou, F. Rezaï-Aria, and G. Dour: "Effect of mold coating materials and thickness on heat transfer in permanent mold casting of aluminum alloys." *Metallurgical and Materials Transactions A*, vol. 38A, pp. 1303-1316 (2007).

32 R. Le Goff, G. Poutot, D. Delaunay, R. Fulchiron, and E. Koscher: "Study and modeling of heat transfer during the solidification of semi-crystalline polymers." *International Journal of Heat and Mass Transfer*, vol. 48, pp. 5417–5430 (2005).

33 M. Bahrami, J.R. Culham, M.M. Yananovich and G.E. Schneider: "Review of thermal joint resistance models for nonconforming solid surfaces." *Applied Mechanics Reviews*, vol. 59, pp. 1-12 (2006).

34 M.G. Cooper, B.B. Mikic and M.M. Yovanovich: "Thermal contact conductance." *International Journal of Heat and Mass Transfer*, vol. 12, pp. 279-300 (1969).

35 J.J. Salgon, F. Robbe-Valloire, J. Blouet and J. Bransier: "A mechanical and geometrical approach to thermal contact resistance." *International Journal of Heat and Mass Transfer*, vol. 40, pp. 1121-1129 (1997).

36 J.P. Holman. “Heat Transfer.” *McGraw-Hill Book Co*, SI Metric Edition, pp. 331-345, (1989).

37 W.P. Klinzing, J.C. Rozzi and I. Mudawar: “Film and transition boiling correlations for quenching of hot surfaces with water sprays.” *J. Heat Treating*, (1992) vol. 9, pp. 91-103.

38 I. Mudawar and W.S. Valentine: “Determination of the local quench curve for spray-cooled metallic surfaces.” *J. Heat Treating*, (1989), vol. 7, pp. 107-121.

39 T. Tran, C. Solnordal and C. Nexhip: “Determination of thermal conductivity of titania slags.” *Unpublished CSIRO Minerals Report*, DMR-2229, June 2003.

40 Y. Lee and D. Deming: "Evaluation of thermal conductivity temperature corrections applied in terrestrial heat flow studies." *Journal of Geophysical Research*, vol. 103, pp. 2447-2454 (1998).

41 J.R. Smyth and T.C. McCormick: "Crystallographic data for Minerals", in *Mineral Physics and Crystallography, a handbook of physical constants*. American Geophysical Union, 1995. p. 3.

42 M.D. Lind and R.M. Housley: "Crystallization Studies of Lunar Igneous Rocks: Crystal Structure of Synthetic Armalcolite." *Science*, vol. 175, no. 4021, pp. 521-523 (1972).

43 W.D. Kingery, H.K. Bowen and D.R. Uhlmann: *Introduction to ceramics*, second edition. John Wiley & Sons, 1976. pp. 612-643.

44 H.J. Siebeneck, D.P.H. Hasselman, J.J. Cleveland and R.C. Bradt: "Effects of grain size and microcracking on the thermal diffusivity of $MgTi_2O_5$." *Journal of the American Ceramic Society*, vol. 60, pp. 336-338 (1977).

45 H.J. Siebeneck, D.P.H. Hasselman, J.J. Cleveland and R.C. Bradt: "Effects of microcracking on the thermal diffusivity of Fe_2TiO_5." *Journal of the American Ceramic Society*, vol. 59, pp. 241-244 (1976).